WRITING OF HOLOGRAPHIC DIFFRACTION GRATINGS OF UNRESTRICTED LENGTH

Bruce Napier; April 1998.

Submitted in partial fulfilment of the requirements of the degree of Ph.D. awarded by De Montfort University.

SYNOPSIS

The aim of this work was to find a method of writing continuous Bragg diffraction gratings in optical fibres; either written directly into the fibre or transferred into fibre via illumination through a phase mask. Chapter 1 describes why these devices are of such interest and Chapter 2 tells of some of the methods which have been adopted for their manufacture in recent years.

Chapter 3 describes an initial grating writing method which was investigated which used two scanning holographic beams. This was successful in that it did provide a method of writing gratings longer than the diameter of the writing beams, but was abandoned since it could not give the unlimited length grating which was desired. Chapter 4 describes the thought processes which led to the final solution: the stitching together of any number of weak gratings in a seamless manner. The precision of position required for this superposition is obtained by analysing the interference pattern formed between the diffracted beam from the latent image grating and a fringe locked reference. Thus the process essentially looks at what has already been written and adds to it in a self-replicating feedback procedure. Chapter 5 gives a discussion of a modelling of the growth of latent image in AZ1350 photoresist, the medium chosen for these trials, and chapter 6 gives details of the fringe-locking Michelson interferometer which was used to maintain the position of the workpiece.

The experimental procedure and preliminary results are described in chapter 7. Continuous gratings of a length 2 cm were written with beams of approximate diameter 3 mm using this stitching method. The grating length was only limited by the travel of the micropositioning stage: longer stages will yield longer gratings. The cosmetic quality of these gratings was limited by the quality of optics available when this work was carried out and lack of spatial filtering on the beams. However, there is no fundamental limitation on the length or quality of gratings which may be written with this method.

Following the successful work described herein a purpose-built rig is under construction and an extension to the project is under way, funded by Nortel. Further results will be published in due course.

This work has produced a paper ("Use of real time latent images to write long holographic diffraction gratings in photoresist"; SPIE Vol. **3011**, 182-193 (1997)) and a patent has been applied for by the sponsors, Nortel ("Writing gratings": US Patent Application No. 08-788-615).

ACKNOWLEDGEMENTS

This work was fulfilled as a CASE award sponsored by Nortel. I would like to thank everyone who has been involved at the Harlow end, especially Steve Clements, Kevin Byron and Howard Rourke.

The biggest thankyou must go to Prof. Nick Phillips whose support over the last few years has been total and uncompromising. Quite where Nick gets his unfailing enthusiasm or his seemingly endless knowledge and experience from I shall never know, but I do know that I could not wish for a better "boss".

Thanks to Dr. Chris Barnett for showing me the wonders of Excel, but more for the evenings of encouragement over a quiet malt. Thanks also to Jo and the Julies for helping me through the hardest part of the Ph.D.: the forms. I congratulate Brian at Ventra Engineering for doing a wonderful job of making the various bits of kit over the years. I must also acknowledge the important contribution of the R&D Friday evening meetings, particularly that of the founder members: Adi, Allan, Ben, Claire, David, Martin, Stuart, Ursula and Zane. It is an institution which I am proud to have helped instigate.

Finally I thank Mum, Dad, John and Louise for unceasing support throughout.

CONTENTS

Chapter 1

IN-FIBRE BRAGG GRATINGS

1.1 INTRODUCTION

In recent years the field of in-fibre Bragg diffraction gratings has become one of intense interest and activity in the telecommunications and optoelectronics industries. These optical components have become a hot topic in the popular scientific literature (e.g. [1.1]. [1.2], [1.3]) because of their huge potential in a broad range of applications in the fibre-optics networks of the future: chiefly in the areas of wavelength division multiplexing (WDM), optical amplification and dispersion compensation.

The first in-fibre grating was reported by Hill in 1978 [1.4] following an experiment in which radiation from a 488 nm argon ion laser travelling in a germanium-doped silica fibre was reflected from the polished end of the fibre so that an optical standing wave was formed within the core. It was noted that the fibre exhibited a permanent photosensitive refractive index change, resulting in a weak Bragg grating. The exciting feature of such a grating is that it acts as a highly wavelength-sensitive mirror.

Although the exact nature of the photosensitive reaction is still not well understood (see section 1.2), a coupled wave analysis reveals that this process is one which "pulls itself up by its own bootstraps": the standing wave leads to a periodic refractive index change in the fibre with a pitch equal to the wavelength of the interfering light. This grating acts as a distributed reflector for that particular wavelength, reinforcing the standing wave and hence the reflectivity of the fibre increases leading to further index change, up to a maximum of around 90% for this standing wave method [1.5].

The basic mechanism of these gratings is a straightforward Bragg diffraction: radiation travelling along the fibre impinges on the planes of periodically varying index, and radiation which has a wavelength (in the waveguide) equal to twice the grating pitch will be reflected according to the Bragg condition. Hence if the mean refractive index over the grating period

in the fibre is $\tilde{n}$, then the Bragg wavelength reflected from a grating of pitch Λ at some point z is given by:

$$\lambda_B(z) = 2\tilde{n}(z)\Lambda(z) \qquad (1.1)$$

The problem with this original writing method is obviously that it is very limited as regards the period of the gratings that may be written, and hence the wavelength that may be reflected. The next step in fibre gratings technology came from Meltz et al. who succeeded in writing a fibre grating by a transverse holographic method [1.6]. Essentially the experiment conducted was to illuminate a germanium-doped silica fibre with two coincident laser beams to form a traditional holographic diffraction grating at the fibre core. It was found once again that this led to the formation of a permanent grating in the fibre, only in this case the growth does not rely on the weak Fresnel reflection from the fibre end and subsequent increase in reflection due to grating growth: the pitch and contrast of the pattern may be externally controlled.

Using this method fibre gratings could be written with a range of periods including those that reflect the important regions of the spectrum used in optical fibre communications systems: 1.3 μm and more recently 1.55 μm (see section 1.3.4.1). Furthermore, if a grating is written with a pitch that is not uniform across its length, then other forms of filter may be written; this broadens the possible applications tremendously and gives fibre gratings the potential to be used as made-to-measure optical filters [1.7].

1.2 PHOTOSENSITIVITY IN OPTICAL FIBRES FOR BRAGG GRATINGS

The discovery by Hill of the growth of the gratings in the germanium doped fibres was quite accidental and the physical mechanism for the refractive index change is still, almost twenty years later, not well understood. Various studies on the UV absorption of both fibres and preforms have been carried out with some conflicting results. However, the refractive index change seems to be due to the bleaching of an absorption peak at around 242 nm, which is associated with a positive charged oxygen vacancy known as a Ge *E'* defect [1.8]. Hence the wavelengths used to write these gratings are in the hard ultra-violet region of the spectrum, typically using radiation from frequency doubled argon ion (244 nm) or Kr-F excimer (248 nm) lasers.

One early suggestion for the change in index was that photoexcited electrons diffuse away from the regions of high electric field in the fibre leading to a periodic space charge in the fibre and consequently a change in refractive index due to Pockel's effect [1.9]. A second proposal was that the breaking of Ge-Si bonds leads to the creation of Ge[1] and Ge[2] defects (other forms of oxygen vacancy defect in GeO_2) [1.10]. However further studies seemed to point to a bleaching of the Ge *E'* defect band at 242 nm [1.11], [1.12], [1.13] by means of a two photon absorption process [1.14], [1.15]. Such a theory has been modelled mathematically, and the experimental observation of real-time growth of gratings in fibres is in reasonable agreement with the bleaching theory [1.16], [1.17]. More recent work has actually observed UV-induced corrugations in Ge-doped preform slices and assigns the index change to a combination of permanent and elastic strains within the core [1.18], [1.19].

The difficulties in describing the process of grating growth are now thought to be due to the fact that there are two forms of reaction leading to index change involving all the Ge[1], Ge[2] and GeE' oxygen deficiencies. There is a fast-acting change leading to an increase in refractive index and the formation of a Type I grating which occurs simultaneously with a slower negative index change associated with the formation of a Type II grating [1.20], [1.21]. Thus if the exposure is continued past the point of maximum efficiency, then instead of a simple decay to zero as the grating is washed out, there is a slight decay but there follows the growth of a second grating, accompanied with a red shift in the Bragg wavelength [1.22], [1.23], [1.24].

In short, the microscopic processes leading to the formation of the optical elements are not yet fully understood, and there are still question marks as to the long term stability of these gratings. Since the growth process has not yet been satisfactorily described, the decay cannot be reliably predicted. There is some evidence that the index change has a stable component and an unstable component and that long term stability can be increased with a pre-annealing process [1.25]. However, concrete conclusions as to the precise nature of the growth and stability of these gratings must await the outcome of future studies.

It should be mentioned that germanium-doped fibres are not the only forms of optically sensitive waveguide. Other dopants which have been reported that lead to gratings include

germanium-free tin-doped fibre [1.26] and cerium-doped fluorozirconate glass [1.27]. However it is Ge-doped fibres which have received most attention and considerable effort has been applied to find methods of increasing the photosensitivity of this material.

In high quality silica fibres the defects which lead to photosensitivity are very scarce. In order to increase the refractive index change the number of defects may be increased, e.g. by heating the fibre (up to 1700°C) in the region in which the grating is to be written: a technique known as flame brushing [1.28]. Another common technique used to increase the sensitivity is "hydrogen loading" in which the fibre is kept for several days in an atmosphere of high pressure H_2 before exposure [1.29]; large changes have also been reported with D_2 [1.30]. The mechanism of this process is not well understood, but it is thought to involve the diffusion of the hydrogen into the glass defects. After exposure there is a shift in the grating wavelength with time after exposure as the hydrogen diffuses out of the fibre [1.31].

1.3 APPLICATIONS OF LINEAR IN-FIBRE BRAGG GRATINGS

Fibre gratings have found many applications in recent years. Although the range of uses is broad, they can roughly be classed into three main groups: optical filters, fibre lasers and sensing elements for both strain and temperature. These three categories are discussed in more detail below: the description is not exhaustive since the area is expanding rapidly, and there are numerous other specialist fields in which their use has been reported, e.g. [1.32] [1.33], [1.34]. Furthermore there are long-period gratings (Λ of the order of millimetres) which are applied in areas such as mode conversion [1.35], [1.36] and rocking filters [1.37], [1.38] for polarisation rotation; this family of gratings is not described here.

1.3.1 Fibre gratings for strain and temperature measurement

As has been discussed above, the wavelength reflected from a Bragg grating is proportional to the pitch of the grating according to (1.1). Perhaps, then, the most obvious application of a fibre grating is to measure length changes, for instance those due to a thermal expansion or an applied strain. As the physical length of the fibre changes, the pitch of the in-fibre grating will also change and the reflected wavelength will vary correspondingly.

However, the physics of an expanded grating is rather more complicated than may first appear: consider a grating which has been subjected to some arbitrary longitudinal and transverse strain. Obviously the physical size of the grating will be effected directly and this will change the reflected wavelength in a manner which depends on both the Young's modulus and the Poisson's ratio of the fibre [1.39]. Concurrent with this change the refractive index of the silica is itself a function of strain and the index ellipsoid is effected by the strain via the photo-elastic effect [1.40]. In a similar fashion when the grating is subjected to a temperature change there are changes due to both the thermal expansion of the grating itself and also the change in refractive index due to the thermo-optic effect [1.40].

Nevertheless fibre gratings offer an attractive option as strain measurement devices. They provide a robust long-term implementable device which may be incorporated into structures during construction and which may be used to monitor the stresses within the structure throughout its lifetime. The information from such gratings gives an absolute value to the strain at that particular part of the structure which is independent of any variations in the amplitude of the light intensity used to interrogate the gratings. This is in contrast with interferometric fibre methods (e.g. [1.41] and [1.42]), in which the information obtained suffers from the disadvantages of being both a relative, not an absolute, phase signal and also of being dependent on the intensity of the interrogating light. Already fibre gratings have found many uses in this field, for example in high temperature sensing (up to 800°C) [1.43], cryogenic temperature sensing (down to 80 K) [1.44] engineering strain sensing [1.45], [1.46] and strain measurement in aerospace structures [1.47]. Various methods of measuring the reflected Bragg wavelength by passive [1.48] and active [1.49], [1.50], [1.51] demodulation methods have been reported.

The chief problem associated with the use of Bragg gratings as either strain or temperature sensors is that the grating will be affected by both these variables and it is impossible to separate them using only a single measurement of Bragg wavelength shift. Thus when measuring the strain on a grating, the temperature must be kept constant and vica versa otherwise the information is useless. Naturally to keep the temperature or strain constant is not convenient in many applications and so numerous techniques have been investigated to discriminate between the two effects.

The wavelength changes due to temperature, $\Delta\lambda_T$, and strain, $\Delta\lambda_\varepsilon$, may be written:

$$\Delta\lambda_T = K_T\Delta T \qquad \text{and} \qquad \Delta\lambda_\varepsilon = K_\varepsilon\Delta\varepsilon \tag{1.2}$$

Here K_T is a constant related to the thermal expansion coefficient and the thermo-optic coefficient of the fibre and K_ε is another constant dependent on its Young's modulus, Poisson ratio and photoelastic coefficient. For small changes the strain and temperature response of the fibre have been found to be independent [1.52]; thus in general the shift in Bragg wavelength due to changes in both temperature and strain may be written:

$$\Delta\lambda_B = K_T\Delta T + K_\varepsilon\Delta\varepsilon \tag{1.3}$$

Since the Bragg wavelength shift depends on two variables, temperature and strain, at least two measurements are required in order to distinguish between them. Various techniques have been examined. One method is to have a second grating in a different material of known characteristics: armed with two separate sets of data the variations due to temperature may be compensated for [1.52]. It is also possible to write two gratings superimposed on each other, e.g. one with a Bragg wavelength of ~1300 nm and the other ~800 nm. Assuming the linear approximation (1.3) by applying known temperatures and strains the K_ε and K_T values (both wavelength dependent and so different for each grating) may be deduced and from there the sensor characterised [1.53]. Alternatively it is possible to measure the second order of diffraction simultaneously with the first order and obtain the necessary information to deduce both temperature and strain [1.54].

A further suggestion is to use the fact that in a linear grating, although the wavelength shift depends on both strain and temperature the bandwidth is essentially unaffected. In contrast to this in a chirped grating (i.e. one which has a pitch which varies along its length: see section 2.5) subject to a strain gradient the bandwidth is strain dependent, but is independent of uniform temperature change [1.55]. Thus by measuring the bandwidth it is possible to obtain a direct measurement of the strain [1.56].

1.3.2 Bragg gratings as optical filters

In 1974 Hill described how aperiodic refractive index structures could theoretically be used to perform a role as optical filters with a pre-determined spectral response [1.57]. Four years later he himself was to report on the first in-fibre grating. Such structures have been investigated in integrated optics applications, and now with the introduction of Bragg gratings

they may be put directly into the fibres themselves. An important area of interest for uniform gratings is that of wavelength division multiplexers. Aperiodic gratings are under investigation as dispersion compensators in long-haul telecommunications lines (see section 1.3.4). There is also considerable promise for their use as made-to-measure filters and DFB laser applications.

1.3.2.1 Wavelength division multiplexing (WDM)

The role of wavelength division multiplexing (WDM) devices in fibre-optics technology is to put signals from different peak wavelength sources into the same fibre with as little crosstalk between the signals as possible. Wavelength division de-multiplexing is the process by which the signals are separated at the end of the transmission line [1.58]. The various methods which have been investigated to obtain a passive device to perform this task may be classified into three main groups: directional coupler, angularly dispersive and filter. The first approach yields a surface interaction device and the other two methods utilise a core interaction for operation [1.59]. For comparison with the methods using Bragg gratings, these other methods are briefly discussed here: a more detailed discussion may be found in [1.58].

Directional coupler devices exploit the fact that optical power transfer between neighbouring single-mode fibres is periodic and highly wavelength-dependent. Two fibre cores are brought together in close proximity over a certain "interaction length" along which light of one wavelength is efficiently coupled from one fibre into the other. This close interaction of fibre cores may be achieved by fixing the curved fibres within quartz blocks, grinding the blocks to expose the fibre cores and then bringing the two blocks together [1.60]. A second method involves fusing the fibres together at around 1500°C during fibre-pulling in a process known as the fused biconical taper technique [1.61], [1.62]. Working devices have been demonstrated using both these techniques, but the devices are difficult to fabricate and each coupler can only separate two channels: further (de)multiplexing requires cascaded couplers.

The first type of core interaction device are those which use the difference in angular dispersion between the wavelengths in order to separate them: the device may use a prism to obtain this dispersion, but it is more common to use a diffraction grating. The type of grating is usually a blazed silicon grating (i.e. one obtained from the anisotropic etching of a single

crystal of silicon) in either a Littrow device or a concave grating. In the Littrow type mount the face of the blazed grating elements is almost normal to the incident light and so the efficiency of the grating is maximised and the diffracted beams are directed to the required destination using a lens which may be a conventional optic [1.63] or a GRIN lens [1.64]. In a concave grating the grating performs both the diffraction and focusing operations. In either case the incident light from the input fibre impinges onto the grating and the various components are diffracted through a certain angle depending on their particular wavelength. These diffracted beams are then guided by the lens into the output fibres of the device. Although this means that a single device may be used to separate numerous signals of a similar wavelength, there are high insertion losses associated with such devices.

The final type of WDM devices to be discussed utilise optical filters, both of the interference and absorption varieties. Interference filters, for example quarter wave stack filters, are generally manufactured using a series of layers of material with alternating high and low refractive index which give rise to filters which act as high pass, low pass or bandpass depending on which layer structures are used [1.65]. Absorption filters rely on the absorptive properties of the material from which they are constructed to give highly efficient edge filters and they may be combined with interference filters to give a more flexible design.

One direct approach used with these WDM filters is to cleave a fibre and insert an edge filter in the gap: the incident mixture of wavelengths (in the demultiplexing regime) has one component transmitted through the filter, whilst the other component will be reflected into an appropriately aligned fibre [1.66]. An alternative in-line geometry uses two graded index (GRIN) lenses between which is sandwiched a band-pass filter: the lenses channel the transmitted and reflected signals into their respective fibres [1.67]. More than two channels may be separated by cascading the filters but at the cost of insertion losses for each filter element. Such filters work well, but are somewhat prone to moisture absorption which may be a problem for their long-term stability.

It is this optical filter class of WDM device that the in-fibre Bragg grating best fits. Although it consists of a diffraction grating it is not a plane grating and it does not rely for its operation on the dependence of diffraction angle on wavelength; rather the Bragg grating acts as a very

neat and efficient in-fibre band rejection (in transmission) or band-pass (in reflection) optical filter.

1.3.2.2 Bragg gratings in WDM applications

The first proposed use of Bragg gratings in a WDM application was a design concept optical "tap and combiner" or "drop and insert" filter [1.68]. The role of these devices is to take a signal comprising of several different wavelengths travelling in a fibre and to either tap off or add a single wavelength channel without effecting any of the other components of the signal. The filter consists of Mach-Zender interferometer formed from two 3dB couplers with an identical Bragg grating written into each arm; a sketch of the device is shown in Fig. 1.1.

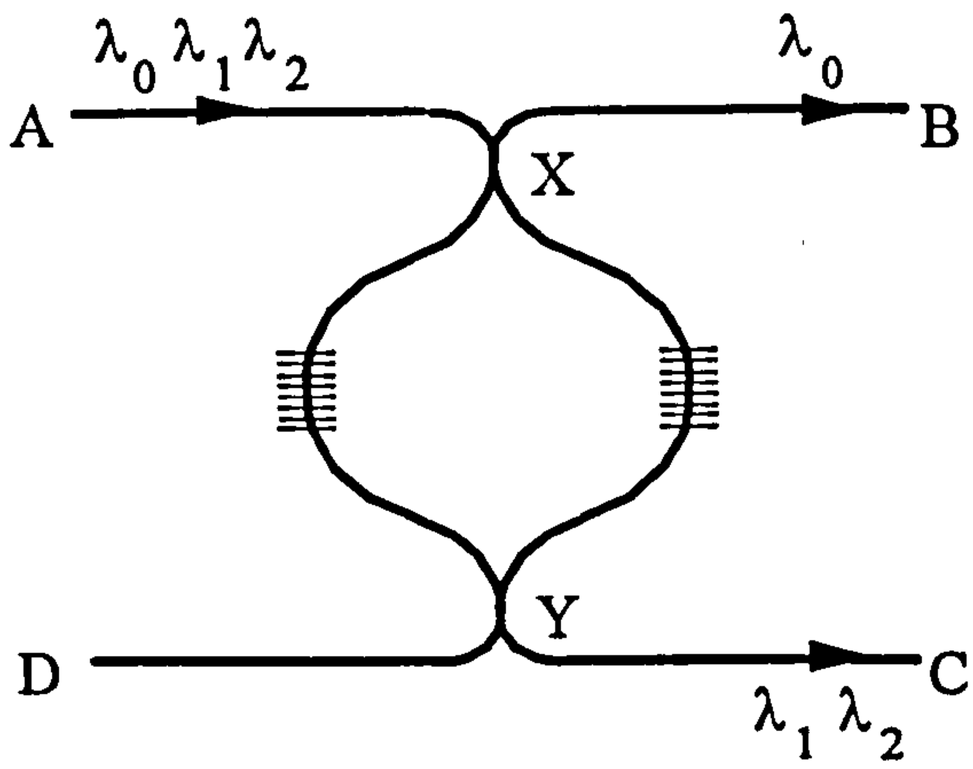

Fig. 1.1: *A sketch of the drop-and-insert filter formed from two Bragg gratings on an all-fibre Mach-Zender interferometer being used in "drop" mode.*

The filter has two input arms *A* and *D* and two output arms *B* and *C*: which arms are used depends on whether components are to be added or removed from the signal. Consider the case where the input signal at *A* has three discrete wavelength components: λ_0, λ_1 and λ_2, and where the two Bragg gratings are written so as to reflect the wavelength λ_0. The Mach-Zender interferometer is assumed to be wavelength insensitive and perfectly balanced, so the wavelengths λ_1 and λ_2 are equally split at the coupler *X* and the two components travel through the separate arms of the interferometer and pass unaffected through the gratings. Since the two interferometer arms are perfectly balanced the beams then recombine at the coupler *Y* and exit through port *C*.

The λ_0 component is also split equally between the two arms, however both signals will be reflected from the gratings back to coupler *X* where they interfere constructively and exit through port *B*. [N.B. No light will be coupled back down the input fibre *A* because of the $\pi/2$ phase shift associated with the 3dB coupler. Any light travelling back down *A* must have been coupled twice or not at all, so there will be a phase difference of π between the waves and destructive interference will occur.]

Thus the interferometer has acted as an optical tap on the input signal at *A*, tapping off a single wavelength whilst permitting the remainder of the signal to continue uninterrupted. The use of the filter as an insertion device is very similar: the signal to be added (which must be of the wavelength reflected by the grating, i.e. λ_0) is input at *D* whilst the remainder of the signal is input at *A* as before. The main signal passes through the filter and exits through port *C* in the manner described above. The λ_0 signal is reflected from the gratings, recombines at coupler *Y* and joins the rest of the signal exiting at port *C*.

Since the conception of this design in 1987 [1.68] there have been several practical realisations as well as numerous other filters based on a similar system. A planar waveguide filter using Bragg gratings in Ge-doped planar silica rather than fibre was first reported in 1993 with a central wavelength of 1555.8 nm and an insertion loss of ~1.4 dB [1.69]. An all-fibre narrowband bandpass filter which is essentially the filter illustrated in Fig. 1.1 without the second coupler was reported in 1994 which had a passband at 1535 nm with a full width half maximum of 0.25 nm and an insertion loss of 1.2 dB [1.70].

A working prototype filter using the scheme described above was first reported by Cullen et al. [1.71] in 1994 with a central wavelength of 1558.7 nm and an insertion loss of less than 1.0 dB. The use of Bragg gratings in large scale communications systems in which optical circulators are used to direct signals to the grating has also been studied [1.72] and compared with the use of Fabry-Perot structures [1.73]. The results suggest that the fibre gratings have significant advantages over Fabry-Perot structures in terms of crosstalk, network capacity and bit error rate.

1.3.2.3 Other in-fibre filters using Bragg gratings

Although WDM is perhaps the area of most interest for linear fibre gratings, there are numerous other types of filter to which they may be adapted. Some of these are outlined here in brief as an indication of the broad range of potential uses.

Several types of filter resembling a Fabry-Perot resonator using Bragg gratings have been reported both with linear and chirped gratings. If two linear Bragg gratings are written adjacent to one another on a piece of fibre then the response of the filter depends crucially on the gap between the two gratings. By post processing using UV trimming the bulk refractive index of the silica between the two gratings may be adjusted so that the optical path separation results in a phase shift of π, forming a high finesse Fabry-Perot etalon-like filter which may be used as the basis for an all-fibre laser (see section 1.3.3) [1.74].

In a different form of filter two low reflectivity gratings chirped in the same direction are used to form a wide band Fabry-Perot resonator with a bandwidth dependent on the reflectivity of the gratings giving a filter similar to that formed between two partially transmissive plane mirrors except for a quadratic phase shift [1.75]. A further type of filter similar to the previous one described may be written by having only a slight shift in the position of the second grating to create a moiré rather than a Fabry-Perot structure with a single narrow passband in the middle of the broad stopband [1.76].

1.3.3 Bragg gratings for fibre lasers

Distributed feedback lasers have been under investigation in planar semiconductor waveguides for some years, the theory first described by Kogelnik [1.77] in an adaptation of his now classic work on coupled wave theory describing diffraction from thick holograms [1.78]. Without going into any mathematical detail, a wave travelling in a medium with optical gain with a periodically varying refractive index will be partially reflected from the index ripples, giving rise to a smaller wave travelling in the opposite direction, which in turn will grow and give rise to further reflected waves which in turn are amplified and so on [1.79].

In terms of semi-conductor lasers, there are two main types of operation: the distributed feedback laser (DFB), which consists of a single region of periodic index in an active medium

and the distributed Bragg reflector (DBR) laser which consists of two Bragg reflectors at either end of a region of material which has optical gain [1.58], [1.80]. One refinement to improve the performance of the DFB laser is to modify the centre of the grating so as to provide an optical phase shift of an integer multiple of $\pi/4$. This has the effect of reducing the threshold gain of the system and improving the single-mode stability since the gain difference between the central and side modes is increased [1.81].

Both these types of lasers from semi-conductor technology have now been implemented into fibre lasers. A convenient method of obtaining an in-fibre optically amplifying medium is to dope the silica fibre with erbium. By putting two Bragg gratings on the same piece of erbium-doped fibre it is possible to achieve a DBR laser and several were reported in the early 1990's with gradually decreasing length: 50 cm [1.82], 10 cm [1.83] and 1 cm [1.84]. One interesting feature of such lasers is that the output wavelength may be tuned by varying the grating pitch by either stretching or heating the reflectors. Numerous DFB lasers written into erbium-doped fibre have also been reported with phase steps introduced by, for instance, heating the centre of the grating [1.85] or UV trimming after grating formation [1.74], [1.86], [1.87]. More recently all-fibre lasers with a pump conversion efficiency of almost 10% have been reported using Sn/Er/Yb doping [1.88].

1.3.4 In-fibre Bragg gratings for dispersion compensation

One of the most promising applications of in-fibre gratings, which has received much study over recent years, is the application of chirped gratings to the compensation of chromatic dispersion in long-haul single-mode optical fibres. Chromatic dispersion arises due to the dependence of refractive index, and hence wave velocity, on wavelength. Since all spectral sources have a finite spectral linewidth, the spectral components of any transmitted signal will be subject to this form of dispersion resulting in pulse broadening and signal degradation.

1.3.4.1 Chromatic dispersion in single-mode fibres

Any pulse travelling in an optical fibre has a certain finite bandwidth. In any dielectric media, the refractive index, n, is frequency dependent and hence so is the group velocity, v_g: consequently each frequency component of the pulse will travel at a different velocity. As the pulse propagates along the waveguide its shape is distorted as the order of the frequency

components changes: this is chromatic dispersion. Using the fact that $\upsilon = c/\lambda n(\lambda)$ the group velocity v_g may be written [1.89]:

$$v_g = -\lambda^2 \frac{d\upsilon}{d\lambda} = \frac{c}{n(\lambda)}\left(1+\frac{\lambda}{n(\lambda)}\frac{dn}{d\lambda}\right) \qquad (1.4)$$

Thus the dispersion in the group velocity arises from the wavelength dependence of the refractive index. It may be shown, assuming a perfectly uniform fibre diameter and refractive index, that the temporal spreading, $\Delta\tau$ of the pulse having travelled a distance L is approximately given by [1.89]:

$$\Delta\tau = \left|-\frac{L\lambda}{c}\left(\frac{d^2n}{d\lambda^2}\right)\Delta\lambda\right| \qquad (1.5)$$

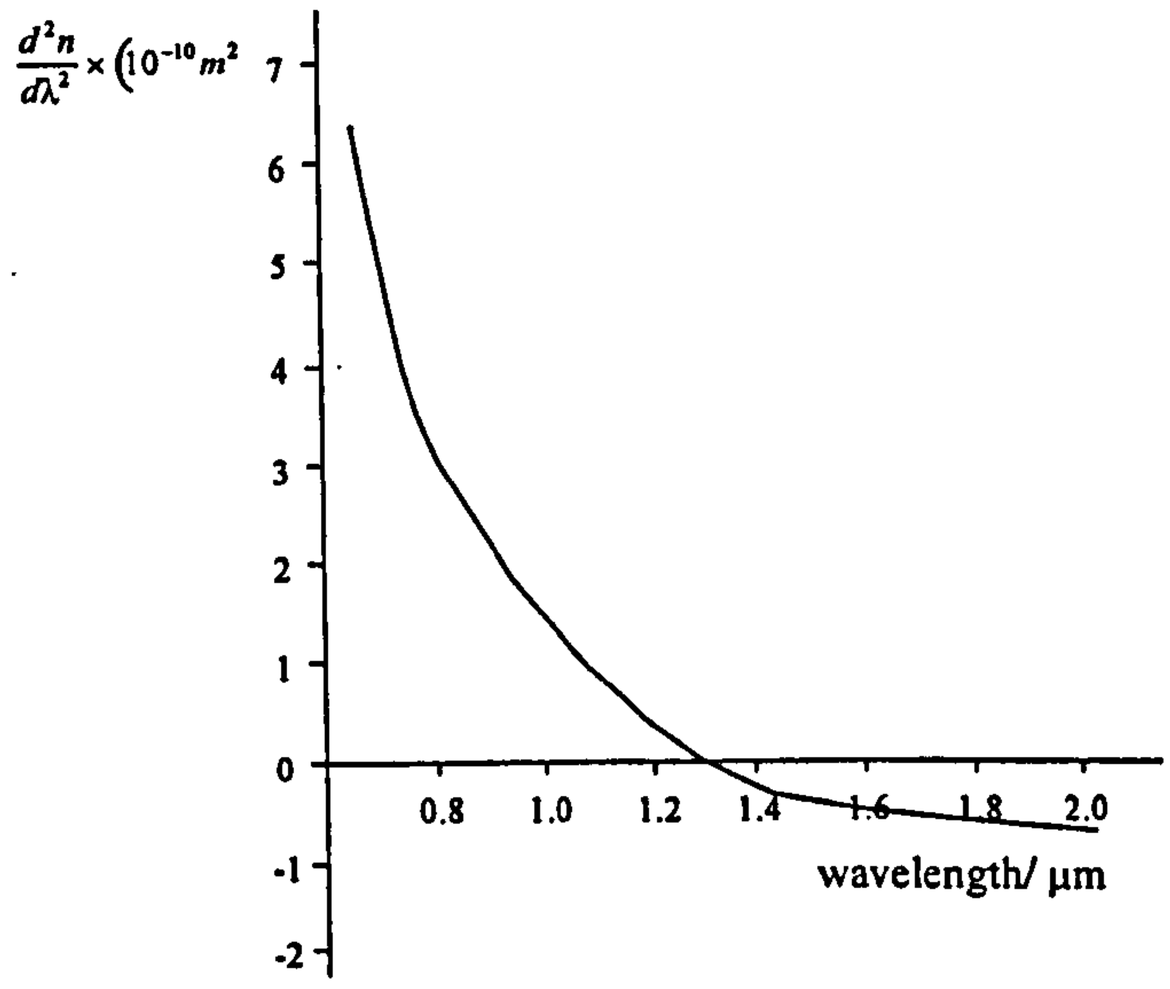

Fig. 1.2: *Showing the variation of $d^2n/d\lambda^2$ for pure silica (from [1.89]) The zero point may be shifted by the appropriate addition of dopants.*

From (1.5) it can be seen that the pulse spreading is approximately proportional to $d^2n/d\lambda^2$. Fig. 1.2, which shows this quantity for pure silica, shows that the value of $d^2n/d\lambda^2$ goes to zero around 1.3 μm, and consequently this is known as the zero material dispersion (ZMD) point for pure silica. However, a second vital variable in determining signal propagation in a waveguide is the absorption of the medium from which the waveguide is composed: Fig. 1.3 shows the absorption of silica as a function of wavelength. Furthermore in addition to the material chromatic dispersion due to the waveguide medium, there is also the waveguide dispersion and the profile dispersion which are not considered in the simple derivation of (1.5) Thus although the ZMD point occurs at 1.3 μm for pure silica, the situation in a fibre is more

complicated and it is possible to vary it by up to ~ ±2 nm by adjusting the fibre core diameter, profile and composition [1.90].

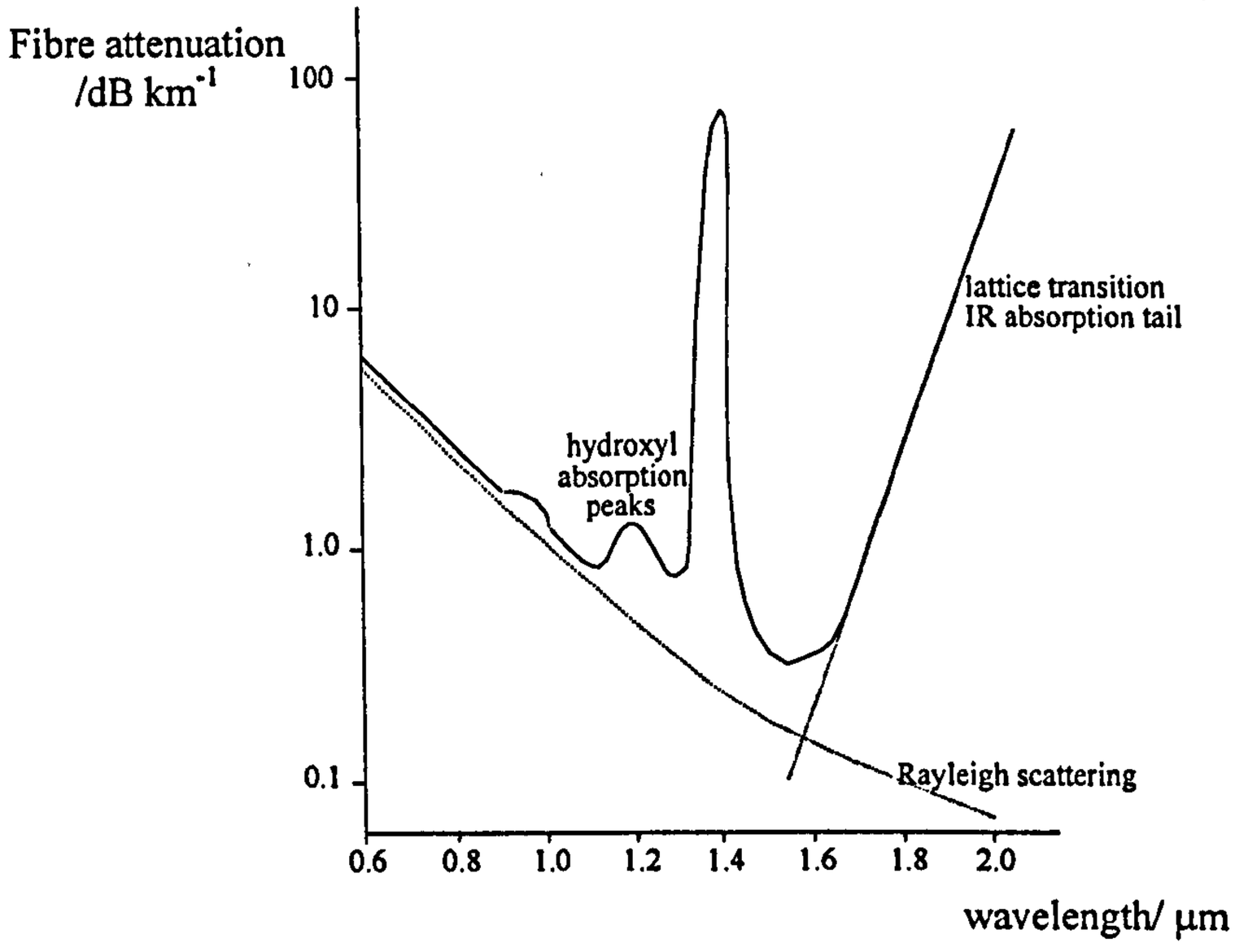

Fig. 1.3: *Sketch graph showing the attenuation versus wavelength of a typical pure silica fibre. [From 1.89.]*

The absorption spectrum shape arises from three main sources: fundamental Rayleigh scattering losses, absorption from hydroxyl ions and infrared absorption from lattice transitions. Fig. 1.3 shows there are three dips in the absorption spectrum at 1.1, 1.3 and 1.55 μm. Initial efforts at fibre waveguides concentrated on the 1.3 μm transmission wavelength because this coincided with the bulk silica ZMD point. The important breakthrough came in 1970 with the first transmission with losses less than 20 dB km^{-1}, which was seen as the minimum loss for optical fibres to be economically viable [1.91].

However, the absorption at 1.55 μm is far lower than at 1.3 μm (~0.2 dB compared with ~0.8 dB) and it is now possible to obtain fibres which can achieve virtually the Rayleigh limit of ~0.2 dB [1.92]. Thus the modern approach is to use transmission wavelengths around the 1.55 μm window and reduce chromatic dispersion by varying the fibre characteristics (which results in an increase in attenuation). Due to the practicalities of achieving fibre uniformity the best that has been achieved to date is a few ps $km^{-1}nm^{-1}$, and so in long-haul systems it is necessary to employ separate dispersion compensation devices, such as those from Bragg gratings.

1.3.4.2 Chirped in-fibre Bragg gratings for dispersion compensation

It was suggested as long ago as 1974 [1.57] that by varying the pitch along a fibre grating, in a so-called "chirped" grating, it can be made to reflect a broader band of wavelengths and furthermore that different wavelengths are reflected from different points on the grating. Naturally this phenomenon suggests a method for the compensation of chromatic dispersion in optical fibres, as is illustrated schematically in Fig. 1.4.

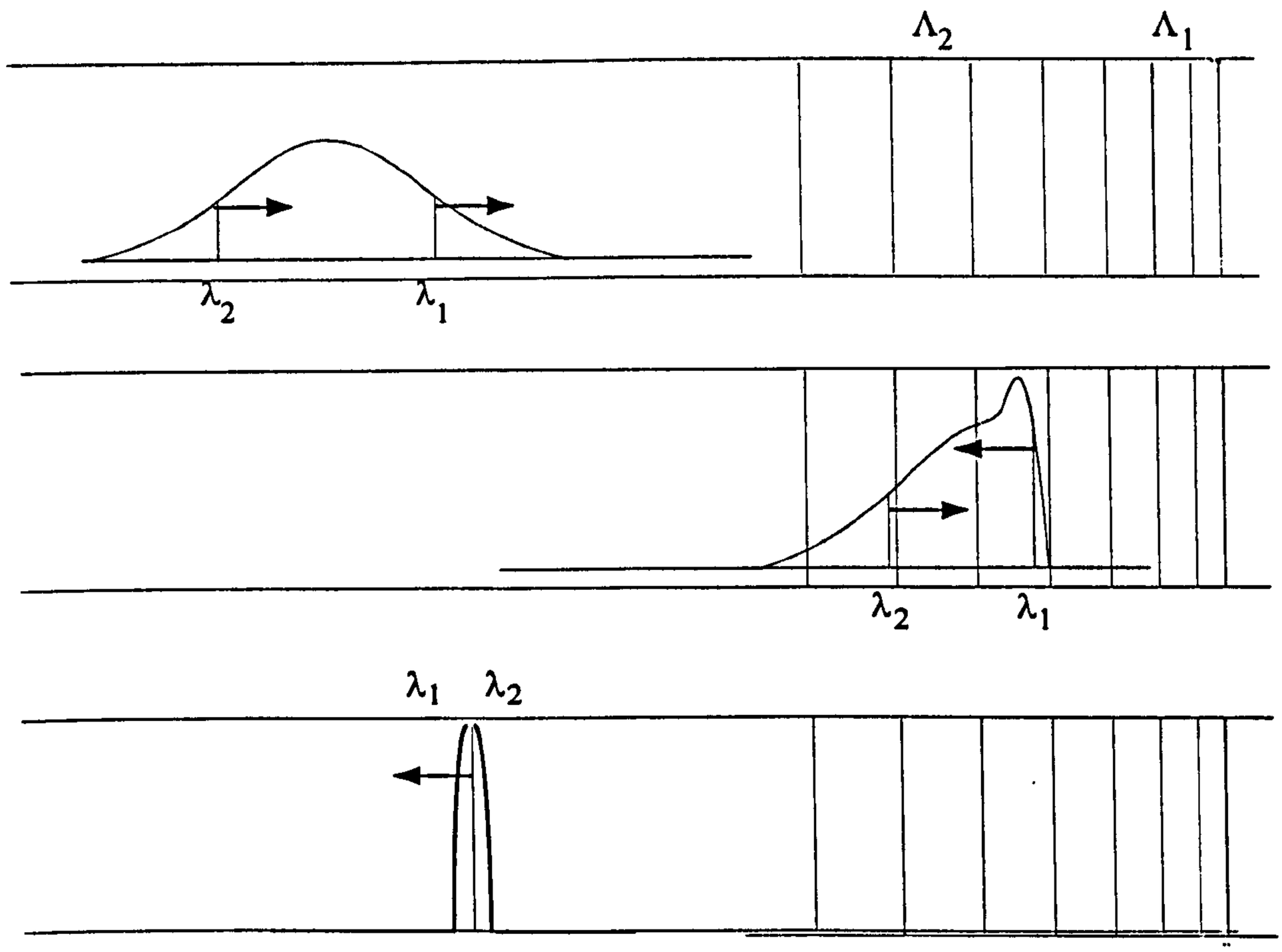

Fig. 1.4: *A schematic showing the compression of a pulse by a chirped Bragg grating. The shorter wavelength (λ_1) travels further along the grating before it reaches the region where it is Bragg reflected (Λ_1). The longer wavelength λ_2 is reflected from the region Λ_2 and so travels less distance in the grating, resulting in a compression of the pulse.*

The central Bragg wavelength of the filter is designed to coincide with the central wavelength of the dispersed pulse. The grating is chirped in such a way that the longer pitch grating elements are at the front of the filter, and there is a gradual decrease in pitch along the filter. The shorter wavelength (λ_1) travels further along the grating before it reaches the region where it is Bragg reflected from Λ_1. The longer wavelength λ_2 is reflected from the region Λ_2 and so travels less distance in the grating. Hence, if the chirp is calculated correctly, the optical path difference introduced by the grating chirp can be made to compensate for the

chromatic dispersion introduced by the fibre, and the pulse is compressed back to its original shape.

Simplistically, the optimum length of fibre that may be compensated by a linearly chirped grating may be roughly deduced from the following analysis. If a signal of linewidth $\Delta\lambda$ has travelled along a fibre of length L_f with a dispersion given by D then an initially very narrow pulse will have broadened to a width τ_{DISP} given by:

$$\tau_{DISP} = DL_f \Delta\lambda \approx -DL_f \Delta f \frac{\lambda^2}{c} \tag{1.6}$$

Now if the grating is of length L_g and is linearly chirped with a bandwidth Δf then the time delay imposed, τ_{GRAT} is given by:

$$\tau_{GRAT} = \frac{2L_g n}{c} \tag{1.7}$$

For perfect compensation the resultant time delay should be zero:

$$\tau_{GRAT} + \tau_{DISP} = 0$$

$$\Rightarrow L_f = \frac{2n}{D\lambda^2}\left(\frac{\Delta f}{L_g}\right)^{-1} \tag{1.8}$$

Putting in some numbers for a typical modest chirped Bragg grating: $L_g \sim 10$ cm and a typical strain chirp might be 0.03%, giving a bandwidth of ~50 GHz; thus for 1.55 μm transmission along non-dispersion shifted fibre (typical dispersion perhaps 18 ps $km^{-1}nm^{-1}$) gives a possible link compensation of:

$$L_g = \frac{2 \times 1.5}{(1550\text{nm})^2.(18\text{ps km}^{-1}\text{ nm}^{-1})}\left(\frac{50\text{ GHz}}{0.1\text{ m}}\right)^{-1} > 400\text{ km.}$$

Such a grating was modelled theoretically and the results were favourable, paving the way for experimental trials [1.93]. By mid-1995 dispersion compensation for fibre lengths of up to 100 km had been reported with a wide variety of methods employed to obtain chirp including velocity controlled phase mask scanning [1.94], exposure profile chirping [1.95], offset-core chirping [1.96], strain chirping using a tapered cantilevered beam [1.97] and chirp applied using a temperature gradient [1.98]. These and more recent methods of writing chirped gratings are discussed in more detail in section 2.5.

Although it is not proposed to give details here, the performance of chirped gratings as dispersion compensators is much improved by the apodisation of the ends of the gratings, so that there is a smooth blending of the index modulation with the rest of the fibre. Good results have been achieved using various profiles including cosine [1.99], cosine squared [1.100] and Gaussian [1.101] profiles, although theory suggests that a sinc apodisation function is optimum [1.102]. Using such terminations on the gratings the group delay is made both more linear and free from ripples and their performance has been improved to compensate for reported lengths of standard monomode fibre up to 400 km [1.103] and 540 km [1.104].

1.4 CONCLUSIONS

This discussion has demonstrated the broad range of applications of in-fibre Bragg gratings in both sensing and communications technology. The following section describes methods of writing such gratings and their limitations in such factors as length, pitch consistency, stitch errors and apodisation. Most gratings in use at the moment are limited in length to less than 10 cm; one of the main thrusts of current research is to write very long (>1m) gratings because of the huge potential of such structures for dispersion compensation over very long distances. This is one of the prime motivations for this work, which is an attempt to find a novel method of writing a diffraction grating which is essentially unlimited in length.

REFERENCES

1.1 S.K. Juma: "Fibre Bragg gratings: ready to drive markets": Lasers and Optronics: **15**, 5, 41 (1996).

1.2 S.K. Juma: "Fibre gratings reinforce the bandwidth explosion"; Opto and Laser Europe: **34**, 25 (1996).

1.3 T. Erdogan: "Fibre gratings - provide keys to future optical networks"; Photonics Spectra (January 1998).

1.4 K.O. Hill et al.: "Photosensitivity in optical fibre waveguides: applications to reflection filter fabrication"; Appl. Phys. Lett. **32**, 647 (1978).

1.5 J. Bures, L Lapierré and D. Pascale: "Photosensitivity effect in optical fibres: a model for the growth of an interference filter"; Appl. Phys. Lett. **37** (10), 860 (1980).

1.6 G. Meltz, W.W. Morey and W.H. Glenn: "Formation of Bragg gratings in optical fibres by a transverse holographic method"; Opt. Lett. **14**, 823 (1989).

1.7 M. Froggatt: "Distributed measurement of the complex modulation of a photoinduced Bragg grating in an optical fibre"; Appl. Opt. **35**, 5162 (1996).

1.8 M. Rothschild, D.J. Ehrlich and D.C. Shaver: "Effects of excimer laser irradiation on the transmission, index of refraction and density of ultraviolet grade fused silica"; Appl. Phys. Lett. **55**, 13, 1276 (1989).

1.9 F.P. Payne: "Photorefractive gratings in single-mode optical fibres"; Elec. Lett. **25**, 8, 498 (1989).

1.10 O.P. Hand and St. J. J. Russell; Opt. Lett. **15**, 102 (1990).

1.11 T.E. Tsai, C.G. Askins and E.J. Friebele: "Photoinduced grating and intensity dependence of defect generation in Ge-doped silica optical fibre"; Appl. Phys. Lett. **61**, 4, 390 (1992).

1.12 L. Dong et al.: "A study of UV photosensitivity in germanosilicate preforms and fibres"; Colloquium on Fibre Gratings, IEEE, January 1995.

1.13 D.L. Williams et al.: "Direct observation of UV induced bleaching of 240 nm absorption band in photosensitive germanosilicate glass fibres"; Elec. Lett. **28**, 4, 369 (1992).

1.14 D.K.W. Lam and B.K. Garside: "Characterisation of single mode optical fibre filters"; App. Opt. **20**, 3, 440 (1981).

1.15 J. Albert, B. Malo et al.: "Comparison of one-photon and two-photon effects in the photosensitivity of germanium doped silica optical fibres exposed to intense ArF excimer laser pulses"; Appl. Phys. Lett. **67**, 24, 3529 (1995).

1.16 S. LaRochelle, V. Mizrahi and G.I. Stegeman: "Growth dynamics of photosensitive gratings in optical fibres"; Appl. Phys. Lett. **57**, 8, 747 (1990).

1.17 B. Guo and D.Z. Anderson: "Undepleted pump regime of Hill grating formation in optical fibres"; Appl. Phys. Lett. **60**, 6, 741 (1992).

1.18 B. Poumellec, P. Niay et al.: "The UV-induced refractive index grating in Ge:SiO_2 preforms: additional CW experiments and the macroscopic origin of the change in index"; J Phys. D: Appl. Phys. **29**, 1842 (1996).

1.19 H.G. Limberger, P.-Y. Fonjallaz et al.: "Compaction and photo-elastic-induced index changes in fibre Bragg gratings"; Appl. Phys. Lett. **68**, 3069 (1996).

1.20 J. Albert, B. Malo et al.: "Comparison of one-photon and two-photon effects in the photosensitivity of germanium-doped silica optical fibres exposed to intense ArF excimer laser pulses"; Appl. Phys. Lett. **67**, 3529 (1995)..

1.21 W. X. Xie, P. Niay et al.: "Experimental evidence of two types of photorefractive effects occurring during photoinscriptions of Bragg gratings within germanosilicate fibres"; Opt. Comm. **104**, 185 (1993).

1.22 L. Reekie and L. Dong: "Material considerations for Bragg fibre gratings"; Proc. SPIE **2998**, 2, (1997).

1.23 J. Hubner, M. Svalgaard: "Phenomenological model of UV-induced Bragg grating growth in germanosilicate fibres"; Proc. SPIE **2998**, 11 (1997).

1.24 P. Niay, P. Bernage et al.: "Behaviour of spectral transmissions of Bragg gratings written in germania-doped fibres: writing and erasing experiments using pulsed or CW UV exposure"; Opt. Comm. **113**, 176 (1994).

1.25 T. Erdogan, V. Mizrahi et al.: "Decay of ultraviolet-induced fibre Bragg gratings"; J. Appl. Phys. **76**, 73 (1994).

1.26 L. Dong, J.L. Cruz et al.: "Strong photosensitive gratings in tin-doped phosphosilicate optical fibres"; Opt. Lett. **20**, 1982 (1995).

1.27 H, Poignant, S. Boj, E. Delevaque et al.: "Efficiency and thermal behaviour of cerium-doped flourozirconate glass fibre Bragg gratings"; Elec. Lett. **30**, 1339 (1994).

1.28. F. Bilodeau, B. Malo et al.: "Photosensitisation of optical fibre and silica on silica waveguides"; Opt. Lett. **18**, 12, 953 (1993).

1.29 P.J. Lemaire et al.: "High pressure H_2 loading as a technique for achieving ultrahigh UV photosensitivity and thermal sensitivity in GeO_2 doped optical fibres"; Elec. Lett. **29**, 1191 (1993).

1.30 V. Mazrahi, P.J. Lamaire et al.: "Ultraviolet fabrication of ultrastrong optical fibre gratings and of germania-doped channel waveguides"; Appl. Phys. Lett. **63**, 1727 (1993).

1.31 B. Malo et al.: "Effective index drift from molecular hydrogen diffusion in H_2 loaded optical fibres and its effect on Bragg grating fabrication"; Elec. Lett. **30**, 5, 442 (1994).

1.32 P.A. Morton, V. Mizrahi et al.: "Mode-locked hybrid soliton pulse source with extremely wide operating frequency range"; IEEE Phot. Tech. Lett. **5**, 28 (1993).

1.33 M.C. Farries, C.M. Ragdale and D.C.J. Reid: "Broadband chirped fibre Bragg filters for pump rejection and recycling in erbium doped fibre amplifiers"; Elec. Lett. **28**, 487 (1992).

1.34 A. Molony, C. Edge and I. Bennion: "Fibre grating time delay element for phased array antennas"; Elec. Lett. **31**, 1485 (1995).

1.35 K.O. Hill, B. Malo et al.: "Efficient mode conversion in telecommunication fibre using externally written gratings"; Elec. Lett. **26**, 1270 (1990).

1.36 S.E. Kanellopoulos, V. A. Handereck and J. Rogers: "Photo-induced polarisation couplers in elliptical core of optical fibres written using 532 nm and 266 nm sources"; Elec. Lett. **28**, 1559 (1992).

1.37 Hill, F. Bilodeau: "Birefringent photosensitivity in monomode optical fibre: application to external writing of rocking filters"; Elec. Lett. **27**, 1548 (1991).

1.38 Johnson, F. Bilodeau et al.: "Long-length, long-period rocking filter fabricated from conventional monomode telecommunications optical fibre"; Opt. Lett. **17**, 1635 (1992).

1.39 H. Courtney: "Mechanical behaviour of materials"; McGraw-Hill (1990).

1.40 M. Born and E. Wolf: "Principles of Optics"; Sixth edition, Pergamon Press (1993).

1.41 D.A. Flavin, R. McBride and J.C. Jones: "Interferometric fibre-optic sensing based on the modulation of group delay and first order dispersion: application to strain-temperature measurand"; J. Lightwave Tech. **13**, 7, 1314 (1995).

1.42 A.S. Gerges, F. Farahi et al.: "An interferometric fibre optic sensor using a short coherence source"; Elec. Lett. **23**, 1110 (1987).

1.43 G. Meltz and W.W. Morey: "Bragg grating formation and germanosilicate fibre photosensitivity"; Proc. SPIE **1516**, 185 (1991).

1.44 S. Gupta, T. Mizunami et al.: "Fibre Bragg grating cryogenic temperature sensors"; Appl. Opt. **35**, 25, 5202 (1996).

1.45 J.D.Prohaska, E. Snitzer et al.: "Fibre optic Bragg grating strain sensor in large scale concrete structures"; Proc. SPIE **1798**, 286 (1992).

1.46 R.M. Measures, A.T. Alavie et al.: "Bragg grating structural sensing system... for bridge monitoring"; SPIE **2294** 53 (1994).

1.47 P.D. Foote: "Optical fibre Bragg grating sensors for aerospace smart structures"; Colloquium on Fibre Gratings, IEEE, January 1995.

1.48 S.M. Melle, K. Liu and R.M. Measures: "A passive wavelength demodulation system for guided-wave Bragg grating sensors"; IEEE Phot. Tech. Lett. **4**, 516 (1992).

1.49 M.G. Xu, H. Geiger et al.: "Novel interrogating system for fibre Bragg grating sensors using an acousto-optic tuneable filter"; Elec. Lett. **29**, 510 (1993).

1.50 T. Corey, P.J. Ellerbrock et al.: "Active wavelength demodulation of Bragg fibre-optic strain sensor using acousto-optic tuneable filter"; Elec. Lett. **31**, 1602 (1995).

1.51 Y.J. Rao, K. Kalli et al.: "Spatially multiplexed fibre-optic Bragg grating strain and temperature sensor system based on interferometric wavelength shift detection"; Elec. Lett. **31**, 1009 (1995).

1.52 W.W. Morey, G. Meltz and W.H. Glenn: "Fibre optic Bragg grating sensors"; Proc. SPIE **1169**, 98 (1989).

1.53 M.G. Xu et al.: "Discrimination between strain and temperature effects using dual wavelength fibre grating sensors"; Elec. Lett. **30**, 13, 1085 (1994).

1.54 K. Kalli et al.: " Possible approach for the simultaneous measurement of temperature and strain via first and second order diffraction from Bragg grating filters"; Colloquium on Fibre Gratings, IEEE, January 1995.

1.55 S. Huang, M.M. Ohn et al.: "Fibre-optic intragrating distributed strain sensor"; Proc. SPIE **2294**, 81 (1994).

1.56 M.G. Xu, L. Dong et al.: "Temperature-independent strain sensor using a chirped Bragg grating in a tapered optical fibre"; Elec. Lett. **31**, 10, 823 (1995).

1.57 K.O. Hill: "Aperiodic distributed-parameter waveguides for integrated optics"; Appl. Opt. **13**, 1853 (1974).

1.58 J.M. Senior: "Optical fibre communications: principles and practice"; 2nd edition, Prentice Hall (1992).

1.59 J.M. Senior and S.D. Cusworth: "Devices for wavelength multiplexing and demultiplexing"; Proc. IEE, **136**, 3, 183 (1989).

1.60 M.J.F. Digonnet and H.J. Shaw: "Wavelength multiplexing in single mode fibre couplers"; Appl. Opt. **22**, 484 (1983).

1.61 T. Brichendo and A Fielding: "Stable low-loss single mode couplers"; Elec. Lett. **20**, 230 (1984).

1.62 K.O. Hill, D.C. Johnson and R.G. Lamont: "Optical fibre directional couplers: biconical taper technology and device applications"; Proc. SPIE, **574**, 92 (1985).

1.63 Y. Fujii, K. Aoyama and J. Minowa: "Optical demultiplexer using a silicon echette grating"; IEEE J. Quan. Elec. **QE16**, 165 (1980).

1.64 R. Erdmann: " Prism gratings for fibre-optic multiplexing"; Proc. SPIE **417**, 12 (1983).

1.65 S.G. Lipson, H. Lipson and D.S. Tannhauser: "Optical physics"; 3rd edition, Cambridge University Press (1995).

1.66 G. Winzer, H.F. Mahlein and A. Reichelt: "Single-mode and multimode all- fibre directional couplers or WDM"; Appl. Opt. **20**, 3128 (1981).

1.67 Y. Fujii, J. Minowa and H. Tanada: "Practical two-wavelength multiplexer and demultiplexer : design and performance"; Appl. Opt. **22**, 3090 (1983).

1.68 D.C. Johnson, K.O. Hill et al.: "New design concept for a narrowband wavelength-selective optical tap and combiner"; Elec. Lett. **23**, 13, 668 (1987).

1.69 R. Kashyap, G.D. Maxwell and B.J. Ainslie: "Laser-trimmed four-port bandpass filter fabricated in single-mode photosensitive Ge-doped planar waveguide"; IEEE Phot. Tech. Lett. **5**, 2, 191 (1993).

1.70 F. Bilodeau, K.O. Hill et al.: "High-return-loss narrowband all-fibre bandpass Bragg transmission filter"; IEEE Phot. Tech. Lett. **6**, 1, 80 (1994).

1.71 T.J. Cullen, H.N. Rourke et al.: "Compact all-fibre wavelength drop and insert filter"; Elec. Lett. **30**, 25, 2160 (1994).

1.72 D. Pastor, J. Marti, J. Capmany: "Fibre gratings as demultiplexing filters for WDMA networks"; Colloquium on Fibre Gratings, IEEE, January 1995.

1.73 P.A. Humblet and W.M. Hamdy: "Crosstalk analysis and filter optimisation of single- and double- cavity Fabry-Perot filters"; IEEE J. Sel. Ar. in Comm. **8**, 6, 1095 (1990).

1.74 J. Canning and M.G. Skeats: " π-phase-shifted periodic distributed structures in optical fibres by UV post-processing"; Elec. Lett. **30**, 16, 1344 (1994).

1.75 G.E. Town, K. Sugden et al.: "Wide-band Fabry-Perot-like filters in optical fibres"; IEEE Phot. Tech. Lett. **7**, 1, 78 (1995).

1.76 L. Zhang, K. Sugden et al.: "Wide-band chirped fibre moiré grating transmission filters"; Elec. Lett. **31**, 6, 477 (1995).

1.77 H. Kogelnik and C.V. Shank: "Coupled-wave theory of distributed feedback lasers"; J. Appl. Phys. **43**, 5, 2327 (1972).

1.78 H. Kogelnik: "Coupled wave theory for thick hologram gratings"; Bell Syst. Tech. J. **48**, 2909 (1969).

1.79 J.T. Verdeyen: "Laser electronics"; 2nd edition, Prentice-Hall (1989).

1.80 G.A. Ball and W.H. Glenn: "Design of a single-mode linear-cavity erbium fibre laser utilising Bragg reflectors"; J. Lightwave Tech. **10**, 1338 (1992).

1.81 K. Utaka, S. Akiba et al.: "λ/4-shifted InGaAsP/InP DFB lasers"; IEEE J. Quan. Elec. **QE-22**, 1042 (1986).

1.82 G.A. Ball, W.W. Morey and W.H. Glenn: "Standing-wave multimode erbium fibre laser"; IEEE Phot. Tech. Lett. **3**, 613 (1991).

1.83 G. A. Ball and W.W. Morey: "Continuously tuneable single-mode erbium fibre laser"; Opt. Lett. **17**, 6, 420 (1992).

1.84 J.L. Zyskind, V. Mizrahi et al.: "Short single frequency erbium-doped fibre laser"; Elec. Lett. **28**, 15, 1385 (1992).

1.85 J.T. Kringlebotn, D.J. Archambault et al.: "Er^{3+}:Yb^{3+}-co-doped fibre distributed-feedback laser"; Opt. Lett. **19**, 24, 2101 (1994).

1.86 M Sejka, P. Varming et al.: "Distributed feedback Er^{3+}-doped fibre laser"; Elec. Lett. **31**, 17, 1445 (1995).

1.87 W.H. Loh and R.I. Laming: "1.55 μm phase-shifted distributed feedback fibre laser"; Elec. Lett. **31**, 17, 1440 (1995).

1.88 W.H. Loh, L. Dong and J.E. Caplen: "Single-sided output Sn/Er/Yb distributed feedback fibre laser"; Appl. Phys. Lett. **69**, 15, 2151(1996).

1.89 J. Wilson and J.F.B. Hawkes: "Optoelectronics"; 2nd edition, Prentice Hall (1989).

1.90 W.A. Gambling, H. Matsumura and C.M Ragdale: "Mode dispersion, material dispersion and profile dispersion in graded index single-mode fibres"; IEE J. Mic., Opt. and Ac. (GB) **3**, 6, 239 (1979).

1.91 F.P. Kapron, D.B. Keck and R.D. Maurer: "Radiation losses in optical waveguides"; Appl. Phys. Lett., **10**, 423 (1970).

1.92 T. Miya et al.: "Ultimate low-loss single mode fibre at 1.55μm"; Elec. Lett. **15**, 4, 106 (1979).

1.93 P.L. Mason, R.V. Penty and I.H. White: "Multiple stage dispersion compensation in long haul optical fibre systems using chirped fibre Bragg gratings"; Elec. Lett. **30**, 15, 1244 (1994).

1.94 K. Takiguchi: "Chirped in-fibre Bragg gratings for compensation of optical-fibre dispersion"; Opt. Lett. **19**, 17, 1314 (1994).

1.95 K.A. Ahned and H. Liu: "Experimental demonstration of compression of dispersed optical pulses by reflection from self-chirped optical fibre Bragg gratings"; Opt. Lett. **19**, 12, 877 (1994).

1.96 P.A. Krug, T. Stephens et al.: "Dispersion compensation over 270 km at 10 Gbit/s using an offset-core chirped fibre Bragg grating"; Elec. Lett **31**, 13, 1091 (1995).

1.97 M. Le Blanc, S.Y. Huang et al.: "Tuneable chirping of a fibre Bragg grating using a cantilevered beam"; Elec. Lett. **31**, 13, 1093 (1995).

1.98 D. Taverner, D.J. Richardson et al.: "Dispersion compensation of 16 ps pulses over 100 km of step-index fibre using cascaded chirped fibre gratings"; Elec. Lett. **31**, 12, 1004 (1995).

1.99 R. Kashyap, A. Swanton and D.J. Armes: "Simple technique for apodising chirped and unchirped fibre Bragg gratings"; Elec. Lett. **32**, 1226 (1996).

1.100 B. Malo, S Thériault, D.C. Johnson et al.: "Apodised in-fibre grating reflectors photoimprinted using a phase mask"; Elec. Lett. **31**, 223 (1995).

1.101 J. Albert, K.O. Hill, B. Malo et al.: "Apodisation of the spectral response of fibre Bragg gratings using a phase mask with variable diffraction efficiency"; Elec. Lett. **31**, 222 (1995).

1.102 Pastor, J. Capmany et al.: "Design of apodised linearly chirped fibre gratings for dispersion compensation"; J. Lightwave Tech. **14**, 11, 2581 (1996).

1.103 W.H. Loh, R.I. Laming et al.: "10 cm chirped fibre Bragg grating for dispersion compensation at 10 Gbit/s over 400 km of non-dispersion shifted fibre"; Elec. Lett. **31**, 25, 2203 (1995).

1.104 P.L. Mason, R.V. Penty and I.H. White: "Extending the transmission distance of a directly modulated laser source using Bragg grating dispersion compensators"; IEEE Colloquium on fibre gratings (1995).

Chapter 2

ESTABLISHED METHODS OF WRITING IN-FIBRE BRAGG GRATINGS

2.1 INTRODUCTION

The technique by which fibre gratings were discovered in 1978 by Hill et al., i.e. the formation of an optical standing wave in the fibre core by interfering light with its reflection from a cleaved end [1.4], is of limited use for writing a grating with a specified pitch. There was a gap in the development of fibre gratings of almost a decade before Meltz et al. developed a holographic technique of writing gratings with any desired pitch, by varying the angle between two coherent UV laser beams incident on the fibre [1.6]. Once the interest in fibre gratings was reawakened by this advance, methods were investigated for writing them in a commercially viable manner.

A breakthrough came with the use of phase masks: relief gratings etched in fused silica which may be transferred into fibre by illumination with hard UV radiation. These phase gratings are designed to diffract UV radiation into two first order beams whilst the zero order is suppressed. The fibre is positioned in the region of overlap of the diffracted beams which form an interference pattern that is recorded in the photosensitive fibre. Phase masks may be written holographically or using e^- beam lithography. Once a phase mask has been written it is possible to write as many "fibre copies" as desired with good consistency between gratings.

However, these masks do have problems associated with them, and any errors in the mask will lead to imperfections in the grating recorded in the fibre. Specifically so-called "stitch errors" between patches on e^- beam written gratings lead to sidelobes on the response of the fibre gratings [2.1], [2.2]. Furthermore the fibre gratings are limited in length by the dimensions of the phase mask used to write them, and current research into chirped gratings for dispersion compensation indicates the need for very long (>1m) fibre gratings.

2.2 DIRECTLY WRITTEN HOLOGRAPHIC IN-FIBRE GRATINGS

The holographic technique for writing in-fibre Bragg gratings is a straightforward two beam interference process which was first demonstrated by Meltz and his co-workers in 1989 [1.6]. Two UV laser beams of wavelength λ are brought together at the fibre at an angle 2θ; the resulting interference pattern has a pitch d given by [2.3]:

$$d = \frac{\lambda}{2 \sin \theta} \tag{2.1}$$

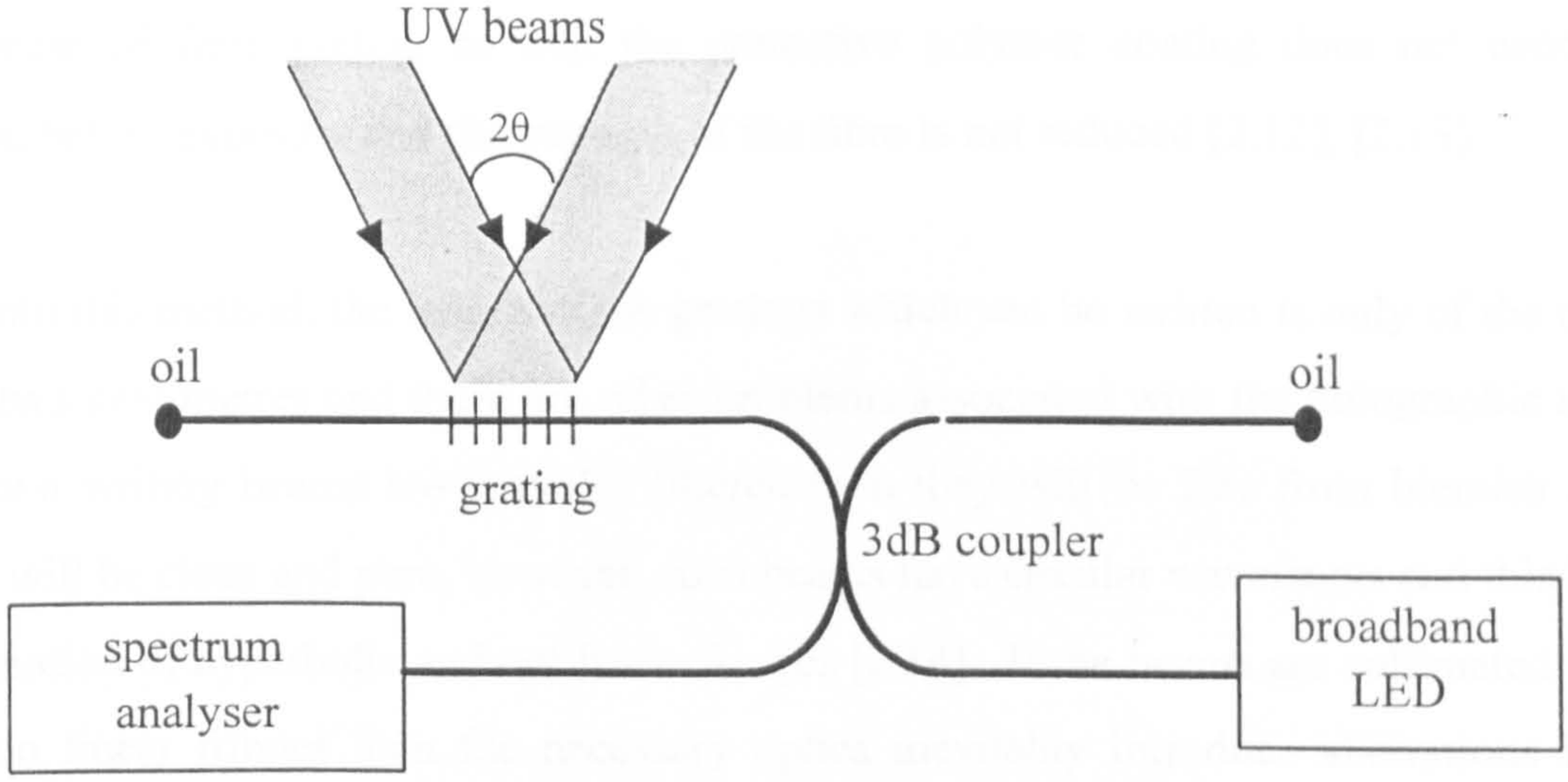

Fig. 2.1: *Typical holographic method for writing in-fibre Bragg gratings similar to that devised by Meltz et al.*

Fig. 2.1 shows a typical exposure and measurement apparatus: a broadband LED source is used to input a signal to a 50/50 fibre coupler. One arm of the fibre coupler, which has the external protective plastic coating of the fibre removed so as to expose the cladding, is exposed to the interfering UV beams and consequently a grating will begin to grow. To increase the exposure efficiency a cylindrical lens may be used to focus the beams into a line focus along the fibre axis. Part of the input spectrum from the LED will be reflected from the grating back towards the coupler and into the spectrum analyser. Thus as the exposure progresses and the grating grows, the strength of the reflected signal varies and the growth of the grating may be monitored in real time. The other two ends of the fibre have a drop of index-matching oil applied in order to reduce the Fresnel reflection from the ends.

Several other exposure geometries utilising prisms in order to bring the beams to interference at the desired angle have been reported using frequency-doubled argon ion laser radiation with continuous wave powers of up to 100 mW at 244 nm [2.4], [2.5], [2.6], [2.7]. One problem

with using continuous wave radiation at around this wavelength is that because the laser power is rather low the exposure times required are several minutes and this can cause problems with stability and hence fringe contrast that are typical in holographic work. One method of improving on this situation is to use pulsed lasers; for instance the KrF excimer laser at 248 nm may be used to write very high reflectance gratings with a single pulse with a duration of only a few tens of nanoseconds [2.8], [2.9], [2.10], [2.11]. A further innovation, directed towards a more commercial method of manufacture is to expose the gratings during the process of fibre pulling so that the protective polymer coating does not need to be removed before exposure and the strength of the fibre is not reduced [2.12], [2.13].

Even with this method, the length of the gratings which can be written is only of the order of one or two centimetres and there are other problems associated with the holographic method. If the two writing beams are spatially filtered then they will be free from blemish and the grating will be clean and pure, however, such beams have circular wavefronts and this leads to the formation of hyperbolic and not linear fringes [2.14]. If the beams are collimated in order to obtain linear fringes then the necessary optics inevitably introduce aberrations into the writing beams and these will show up in the spectrum reflected from the grating. A further difficulty is that the grating pitch is a sensitive function of the inter-beam angle and to control it to the extent that is required for the demands of the telecommunications industry is extremely difficult. In order to try to combat these problems, a more pragmatic and robust method of fabrication was attempted: the use of the phase mask.

2.3 PHASE MASK WRITTEN IN-FIBRE GRATINGS

The phase mask technique for writing in-fibre gratings was first reported by Hill et al. in 1993 [2.15]. This is a proximity phase mask method in which the fibre is positioned in contact or near-contact with the mask, in a method similar to one which had been used previously to write gratings in planar substrates for use in DFB lasers [2.16]. The mask itself consists of an optically flat piece of high quality fused silica which has a surface-relief structure written into one of its surfaces, usually using electron beam lithography. Silica is necessary since it is one of the few materials transparent to hard UV radiation.

The pattern etched on the mask consists of a series of lines which are approximately rectangular in profile, with a depth chosen to give a phase difference of π between a wavelet incident on the "mark" of an element compared with one emerging from a "space", resulting in destructive interference between the directly transmitted radiation and a suppression of the straight-through beam. Thus the depth of the grooves is designed to be $\lambda/2(n\text{-}1)$ where λ is the laser wavelength and n is the refractive index of the silica. By this method the zero order (i.e. transmitted) beam is nulled (typical transmitted output <5% input radiation) and typically 80% of the incident light is present in the two first order diffracted beams.

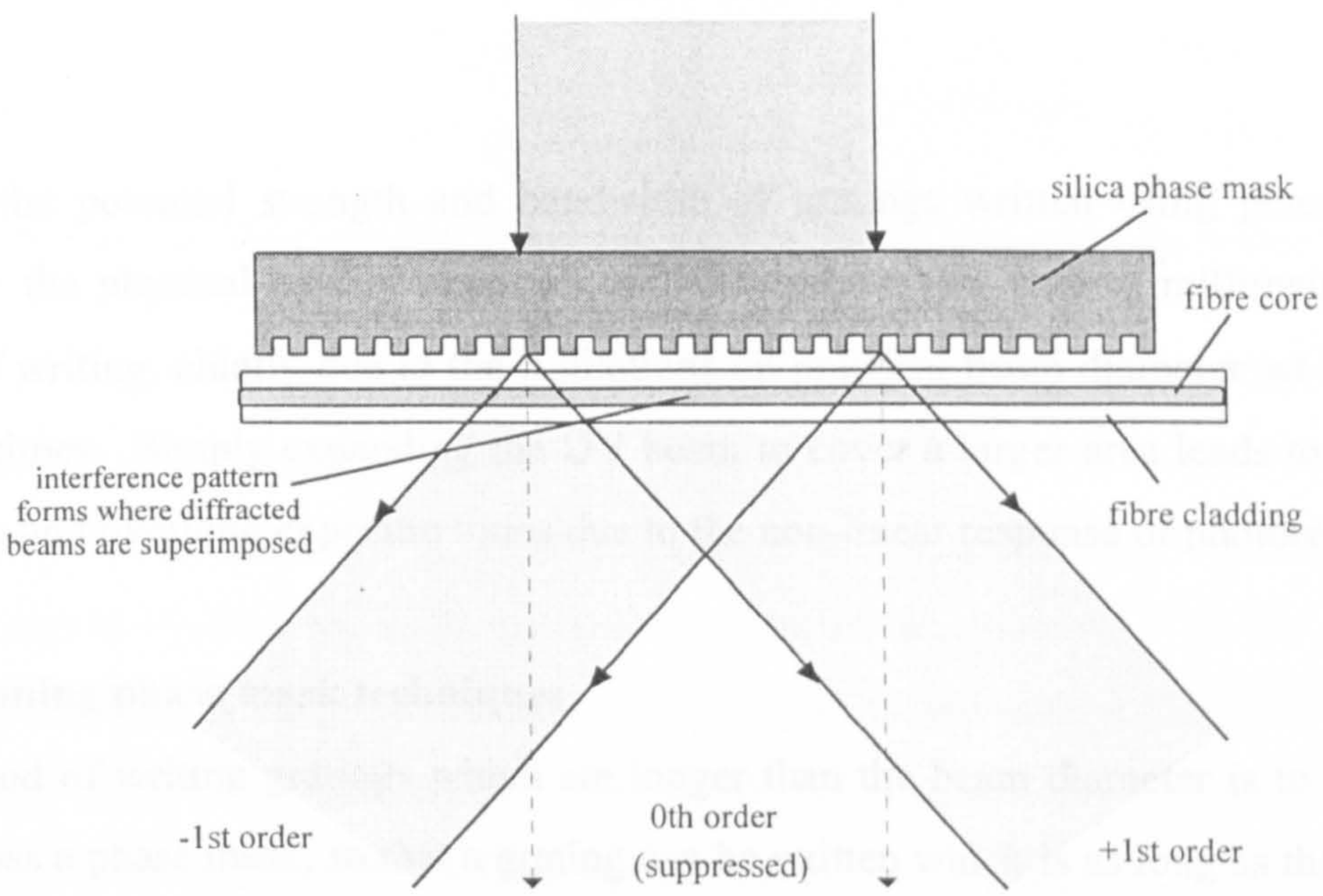

Fig. 2.2: *A schematic showing the apparatus used to write an in-fibre Bragg grating using a silica phase mask.*

A typical exposure set up is sketched in Fig. 2.2: the phase mask is placed in close proximity to a germanium doped photosensitive fibre and KrF (249 nm) pulsed beam is incident on the fibre through the mask. Because the fibre is so close to the mask the coherence length of the laser may be small. Most of the incident light forms the +1 and -1 diffracted orders and these interfere where they overlap to give a Fresnel diffraction pattern which is self-image of the grating at regular intervals from the phase mask [2.17]. If the pitch of the phase mask is p then the pitch of the recorded pattern will be given by $p/2$ [2.1].

This method has been used to write gratings [2.18] and there have been some variations on this basic method, for instance by using the zeroth and first order beams to give the necessary

interference using a tripled NdYAG-pumped frequency-doubled dye laser tuned to 242 nm [2.19]. Phase masks can also be made more flexible in the pitch that can be written by projecting an image of the phase mask using high quality optics onto the fibre [2.20], [2.21], [2.22]. Another advantage of e^- beam written phase masks is that because of the programmable nature of the lithographic process the phase steps in the grating necessary for DFB lasers and some optical filtering applications (e.g. band pass filters) may be written directly [2.23] or the masks may be UV-trimmed to change the refractive index so as to give the correct phase step [2.24]. Furthermore, if a laser with extended coherence is used then the grating pitch may be tuned by adjusting the angle of the fibre in the region of interference [2.25].

However the potential strength and bandwidth of gratings written using phase masks are limited by the physical area of exposure, which means a few tens of millimetres with this method of writing, chiefly due to the limitations on practical beam diameter set by excessive exposure times. Simply expanding the UV beam to cover a larger area leads to problems of uniformity and overlong exposure times due to the non-linear response of photoresist [2.26].

2.3.1 Scanning phase mask techniques

One method of writing gratings which are longer than the beam diameter is to scan the UV beam across a phase mask, so that a grating can be written which is as long as the mask itself, independent of beam size. Provided that the mask does not move relative to the fibre, and that the incident angle of the grating is not changed, then the grating which is written into the fibre will be continuous [2.27]. One sketch of such an apparatus is shown in Fig. 2.3.

Using this technique the bandwidth and reflectivity of the in-fibre gratings may be increased, and by changing the intensity envelope other types of filter, such as comb filters may be fabricated [2.28]. By monitoring the response of the written gratings it is possible to determine systematic errors due to imperfect phase masks, and it has been shown that by changing the scan speed during exposure it is possible to compensate for this error [2.29]. Yet another variation on this method, which may be used to obtain different pitches from the same phase mask, is to move the fibre whilst the writing beam is scanning: uniform motion results in a linear shift of the pitch of the recorded grating [2.30].

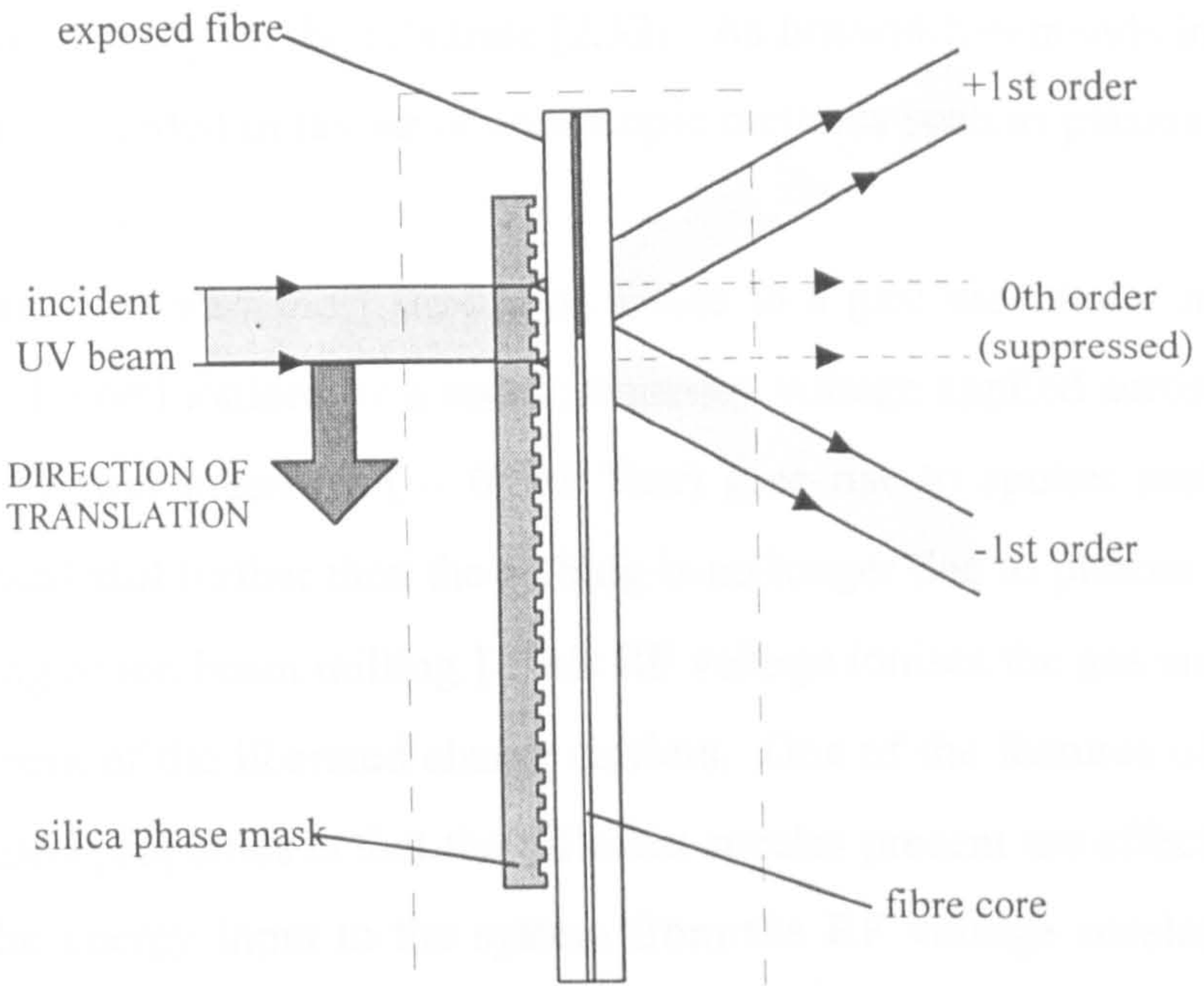

Fig. 2.3: *Schematic showing a method of writing long in-fibre gratings by scanning the writing beam along a phase mask.*

2.3.2 Manufacture of phase masks

Phase masks are manufactured by a process known as plasma etching: a technology which was kick-started by the revolution in the microelectronics industry. In the explosion of interest and activity in computer technology, chiefly since the early 1970's, the demands on the size and complexity of integrated circuit boards has increased in an unprecedented manner. It is in the manufacture of these boards that plasma etching has shown itself to be the best available technology, and the subsequent investment in its development has yielded a whole new technology [2.31]. This technology, having been developed for the computer industry, has also found important niches in optoelectronics, and more recently in the fibreoptics and telecommunications industries.

In the early years of this technology, the etching process was carried out using a "wet" chemical etch: the mask was placed in a chemical (usually a liquid) which would remove the areas not covered by the resist. However, the chemical process is, by nature, isotropic, and the etchant attacks exposed areas of the film with no preferred direction, leading to an undercutting of the resist features. Consequently in order to etch a 1 μm line into a 1 μm film, for instance, the feature cross-section will have a width of ~ 3 μm at the top of the resist,

which limits the line density on the substrate [2.32]. As linewidth demands increased, the wet etch technique was discarded in favour of anisotropic methods such as plasma etching.

A plasma is a state of matter most similar in nature to a gas: essentially it is a gas at low pressure (~ 0.01 - 1 Torr) ionised by a radio frequency voltage applied across it between two electrodes. [N.B. Lower pressures (~ 0.001 Torr) give rise to sputter methods, and if the pressure is decreased still further then the etching is no longer due to plasma processes, but to reactive ion etching or ion beam milling.] This RF voltage ionises the gas and a current flows due to the movement of the liberated charge carriers. One of the features of a plasma which gives it such unusual properties is that the different species present are effectively at different temperatures. The energy input to the system from the RF voltage accelerates the charged species. Since the mass of the electrons is several orders of magnitude less than that of the positive species and energy transfer between the two is inefficient (due to this mass difference). Thus the electrons reach much greater speeds than the heavier particles and are therefore effectively at a higher temperature.

The key feature of plasma etching is that these high temperature electrons can *inelastically* collide with other plasma particles leading to the presence of species such as free radicals and excited states which are normally only present at much higher temperatures which would melt the resist. Thus high temperature reactions can take place in a low temperature environment. In the ion-enhanced chemical plasma etch process a flux of reactive ions impinges vertically on the substrate. The chemicals are chosen so that the resulting reaction product is volatile and so is removed from the etch site, resulting in a highly anisotropic etch with sharp sided features.

The manufacture of phase masks is a fairly simple example of the use of plasma etching: in the manufacture of a typical integrated circuit containing MOSFETs there are many stages of lithography, coating and selective etching in order that the various layers of oxides, resists and metals may be built up into the complex structures required for modern computer hardware. In the manufacture of phase masks there are just two layers above the quartz substrate: a thin layer (250 Å) of chrome lying beneath a 0.5 μm layer of spin- or dip-coated positive photoresist.

The plate is exposed and developed using an e^- beam or optical exposure process, and the resist above the areas of quartz to be etched is removed. The developed plates need to have the chrome removed first in a plasma etch process so as to expose the silica. The silica itself is then etched to give the necessary phase grating depth. Finally the excess resist and chrome is removed leaving just the silica phase mask. The particular process used in this project is a standardised one that has been reached after many experimental trials by Nortel. The gas ratios and pressures, the RF frequencies and power and all the other relevant experimental parameters are all computer-controlled.

The first part of the process is known as descumming: this is a short etch with pure oxygen carried out to clean up the resist before the chrome etch. Pure oxygen etches will attack unexposed as well as exposed resist so it is only a short process, otherwise too much resist will be removed and some feature definition will be lost. One of the most common chemicals used as an etchant gas is chlorine, however, chromium chloride is not volatile and so is of little use for the plasma etching of chrome. Nevertheless chrome does have a highly volatile oxychloride and thus etch rates increase sharply if oxygen is added to the chlorine [2.33]. As mentioned above, one problem with the use of oxygen is that it will attack the unexposed resist and so the ion energies are limited in order to prevent excessive resist removal.

The method used to find the end-point during the etch process is to monitor the reflectivity of the plate surface during etching. As the chrome is removed and the silica uncovered, the reflectance changes. Once the laser and detector have been aligned the reflectance and its time derivative are monitored until there is a sharp rate of change in the reflected power, signalling the breakthrough of the plasma to the silica. A standard over-etch is then allowed to "clear" the troughs in the pattern.

The silica etch etchant gas is C_3H_8: the reaction mechanism for this process is not well understood and there are several proposed reaction schemes [2.33]. It has been found experimentally that the RF power required is quite high and so the plate needs to be kept cool (10°C). In this case the end point is deduced from a calibration curve of etch depth against etch time. Next the etched plates are given a pure oxygen etch to remove any remaining resist, and then dipped in a strong chemical chrome etch (perchloric acid with ammonium

ceric nitrate) to remove any remaining chrome. Finally they are washed in purified water and dried with filtered nitrogen.

2.3.3 Drawbacks of the phase mask technique

The phase mask technique works well for a limited size of grating. It has been shown in other fields that electron beam lithography may be used to write extremely precise phase steps and variable grating periods, for instance in the manufacture of DFB lasers [2.34]. However, there are important problems with phase masks which show up in their application to the writing of in-fibre gratings. One of these is the limit on the physical size that gratings can be manufactured, chiefly due to the requirement of the electron lithography technique for a high vacuum chamber. A 5 cm mask is unusually long [2.35] and at present the longest e^- beam masks are of the order of 10 cm. However, dispersion compensation applications for the future will require in-fibre Bragg gratings with lengths of the order of metres, not centimetres, and e^- beam written masks cannot give such lengths.

A further important problem associated with e^- beam written phase masks is that of stitch errors. In the process of e^- beam lithography, the electron beam itself can write a patch of the order of 0.5 x 0.5 mm^2 onto the substrate. The base plate on which the substrate rests is then translated to a neighbouring position on the substrate for the writing of the next patch. Despite the incredible (sub-nanometre) accuracy of these amazing machines, there are serious problems with so called "stitching errors" associated with the joining together of these patches [2.1], [2.2]. These errors are extremely tiny and are difficult to observe, even when using special moiré techniques designed to show up the phase steps [2.36]. Despite the smallness of these stitch errors, they have been shown to lead to side lobes in the reflection spectrum from in-fibre gratings made from such phase masks which make them unsuitable for high performance telecommunications applications.

2.4 OTHER TECHNIQUES FOR THE MANUFACTURE OF IN-FIBRE GRATINGS

The third main method of writing in-fibre Bragg gratings is the point-by-point method, in which grating elements are written sequentially and individually. This method was first reported with reference to large pitch gratings (Λ of an order between tens of microns to tens of centimetres) which are used for in-fibre mode converters [2.37] and polarisation mode

converters [2.38]. These long-period gratings were written using exposure through a slit and a straightforward step-and-repeat method. This technique was then extended to gratings with a pitch of 1-1.5 μm which act as second or third order Bragg reflectors for radiation in the 1500 nm region [2.39]. As with conventional optical lithographic techniques the non-linearity of the recording process means that features may be recorded which have a size smaller than the beam used to write them. However, the precision and versatility of such techniques is not comparable with either holographic or phase masking methods.

It was mentioned in section 2.3.1 that the phase mask may be adapted to remove unwanted chirping errors by moving the grating during exposure and also that phase steps can be introduced to linear masks by UV-trimming. It should be mentioned that there are also techniques which have been reported whereby the characteristics of individual gratings may be modified to suit requirements. In one technique, a weak seed grating written with 248 nm excimer laser radiation is amplified using a uniform 193 nm ArF laser pulse, as a result of what is thought to be a type II damage mechanism (see section 1.2) [2.40].

In addition to this increase in reflectivity it is also possible to introduce permanent phase steps in fibre gratings after the writing process by both UV-trimming [2.41] and localised heat treatment, e.g. using a laboratory fusion splicer [2.42]. In both these methods a part of the grating is subjected to a process which causes a bulk change in the refractive index of a region of the grating, which may be controlled by monitoring the reflected spectrum in real time. Another type of post-writing manipulation is that of chirping which is discussed more thoroughly in section 2.5.

It was mentioned in section 1.3.4.2 that the reflection spectrum of Bragg gratings is strongly dependent on the manner in which the ends of the grating are blended into the fibre: an abrupt end to the variation in refractive index causes severe side lobes to appear in the filter response. In holographically written gratings there is a natural apodisation due to the Gaussian profile of the writing beams, but this is non-ideal and although there is a suppression of the side lobes, there is still fine structure, especially in the high-reflectivity gratings, because the grating pitch varies with a Gaussian profile, setting up a form of Fabry-Perot device within the grating [2.43].

An improved technique is to use a double exposure: the first is a blanket exposure through a shadow mask to change the bulk index across the grating, followed by a cos^2 shadow mask exposure through a phase mask [2.44]. Another alternative is to expose the fibre twice with the fibre length stretched by $\pm\Lambda/2$ between exposures: in this way the grating is almost rubbed out at each end but is strong in the central region, resulting in a smooth cosinusoidal apodisation [2.45]. In an even more recent development, exploiting the latest advances in electron beam techniques, phase masks may be written which have a zero nulling efficiency which varies along the mask length, giving an in-built apodisation with a single exposure [2.46], [2.47].

2.5 METHODS OF CHIRPING IN-FIBRE GRATINGS

A chirped grating is one in which the pitch is varied, usually linearly, along its length, as was described in the discussion on WDM applications in section 1.3.2.2. It was also mentioned that the Bragg wavelength of a grating at a point z along a fibre where the grating pitch is $\Lambda(z)$ and the mean refractive index $\tilde{n}(z)$ is given by:

$$\lambda_B = 2\tilde{n}(z)\Lambda(z) \qquad (2.2)$$

Hence in order to introduce a chirp into the grating, there must be a variation in either (or both) the average refractive index of the fibre core or in the grating pitch. Some of the many reported methods for achieving this result are briefly discussed below.

An interesting method of characterising a chirped grating involves a small heat probe which heats a very tiny region of the grating. By monitoring the reflected spectrum and comparing it with that from the unheated grating, that part responsible for each component of the reflected spectrum may be deduced [2.48]. Another characterisation technique uses low coherence reflectometry to measure the time delay and a tuneable source to scan the grating and obtain the filter response [2.49].

2.5.1 Chirping by fibre manipulation

The most obvious method of obtaining a variable chirp on a grating is surely to stretch it; this has been reported in several different forms. Chirping may be achieved by direct holographic exposure of a fibre which is subjected to a strain gradient [2.50]: during the holographic

exposure the fibre is bent into a shallow arc so that the fringes formed have a gradually changing spatial frequency along the fibre. This method is very simple and effective but it does result in a blazed grating resulting in some loss through coupling to the radiation modes of the fibre if the bending is too severe [2.51]. Methods which avoid fibre bending include the use of a form of soft glue which imposes a strain gradient on the fibre when under tension [2.52] and a stepped exposure through a phase grating with a uniform strain which was varied for each grating patch [2.53].

Techniques have also been demonstrated which bend a uniform grating using a cantilever [2.54] and in one version this provides a method of obtaining a variable chirp and hence more flexible compensation [2.55]. A more sophisticated version uses a fibre cemented to a stack of piezoelectric segments which may be programmed to give a variety of strain gradients along the fibre [2.56]. However, straining the fibre, whether before or after exposure, is a rather crude method which is difficult to implement in a serious large scale commercial fashion.

A second form of fibre manipulation is to vary the core diameter and hence the effective refractive index of the fibre: a so-called "fibre taper". This can be done by sophisticated fibre drawing techniques [2.57] or by HF etching of the core before exposure [2.58], [2.59]. Other techniques have also been reported which apply a temperature gradient along a grating in order to vary the refractive index and length, but it is generally recognised that this rather cumbersome method has limited practical use due to the inconvenience of maintaining the high temperatures which are required to obtain useful chirps [2.60], [2.61].

2.5.2 Chirping using phase masks

Chirping using a phase mask may be obtained by either directly writing a chirp into the mask itself or by varying the scan speed whilst the grating is being transferred into the fibre. If the chirp is directly written, then it is a so-called "step-chirped" mask in which small blocks of grating are written next to each other, each one having a slightly different pitch to its neighbour, resulting in a gradual grading of the pitch along the mask [2.51].

The second method is to vary the scan speed during exposure; the slower the speed the higher the exposure and the greater the change in refractive index. This method is very flexible since any profile exposure may be written simply by varying the scan speed accordingly [2.62].

2.5.3 Optical methods of achieving chirping

It may be shown (see section 3.1) that two coincident spherical waves will interfere to form hyperbolic fringes, which to first order may be approximated to linear fringes. If wavefronts with dissimilar curvature are interfered then the periodicity of the pattern will vary and chirped gratings may be written using either direct holographic exposure [2.63], [2.64] or an optical element to produce the hyperbolic fringes [2.65]. Another method utilises the intensity profile of the recording beam, which is intrinsically Gaussian, and hence has a "built in" gradient [2.66].

Some of the other numerous optical techniques which have been adopted include the use of a shadow mask [2.67], a lens positioned before the phase mask so as to deform the plane wavefront [2.68] and double exposure photoimprinting similar to that described in section 2.4.3 for apodising masks [2.69].

2.6 CONCLUSIONS

From this brief summary it is clear that over the past decade numerous methods have been adopted to write fibre gratings of both uniform and varying pitch. Some other, more recent techniques are discussed in a special volume on fibre gratings [2.70]. Mainly by using either the holographic method or the phase mask method, good highly efficient gratings have been manufactured. However, both these methods are limited in the length of grating that may be written to around ten centimetres: in the case of the holographic gratings this is due to the limitations on beam size and with gratings written using phase masks this is because of the restricted size of the vacuum chamber on the e^- beam writing machine. This grating length restriction dictates a limitation on the potential performance of the gratings, especially in the important application of dispersion compensation, in which gratings of several metres in length are desirable.

Some other, more recent techniques are discussed in a special volume on fibre gratings [2.70]. Of particular relevance to this work is a recently reported method which uses an interferometer to assess the position of a moving grating and superposes many pulses to form a continuous grating [2.71]. This work, which is similar in nature to that discussed here but completely independent of this project has been used to write gratings up to 20 cm long.

The aim of this project is to devise a method of writing longer in-fibre Bragg diffraction gratings. The ideal aim of Nortel, the project sponsors, was set out at the beginning of the work: to find a method of writing continuous gratings. Thus one reel of fibre may be imagined to spool onto a second reel and between the reels there occurs some process which is capable of writing a single continuous stitch-free grating of unlimited length. This, then, was taken as the fundamental aim of the project.

REFERENCES

2.1 J.A.R. Williams, X. Liu et al.: "The effects of phase steps in E-beam written phase-masks used for fibre grating fabrication by near-field holography"; ECOC 97 IEE Conference Publication No. **448**, 187 (1997).

2.2 T. Kjellberg and R. Schatz: "The effect of stitching errors on the spectral characteristics of DFB lasers fabricated using electron beam lithography"; J. Lightwave Tech. **10**, 1256 (1992).

2.3 R.J. Collier, C.B. Burckhardt and L.H. Lin: "Optical holography"; Academic Press (1971).

2.4 R. Kashyap, J. R. Armitage, R Wyatt et al.: "All-fibre narrowband reflection gratings at 1500 nm"; Elec. Lett. **26**, 730 (1990).

2.5 H. Patrick and S.L Gilbert: "Growth of Bragg gratings produced by continuous-wave ultraviolet light in optical fibre"; Opt. Lett. **18**, 1484 (1993).

2.6 Q. Zhang, D.A. Brown et al.: "Simple prism-based scheme for fabricating Bragg gratings in optical fibres"; Opt. Lett. **19**, 2030 (1994).

2.7 N.H. Rizvi and M.C. Gower: "Production of Bragg gratings in optical fibres by holographic and mask projection methods"; IEEE Colloquium on Fibre Gratings (1995).

2.8 C.G. Askins, T.-E. Tsai, G.M. Williams et al.: "Fibre Bragg reflectors prepared by a single excimer pulse"; Opt. Lett. **17**, 833 (1992).

2.9 J.-L. Archambault, L. Reekie and P. St.J. Russel: "High reflectivity and narrow bandwidth fibre gratings written by single excimer pulse"; Elec. Lett. **29**, 28 (1993).

2.10 J.-L. Archambault, L. Reekie and P. St.J. Russel: "100% reflectivity Bragg reflectors produced in optical fibres by single excimer laser pulses"; Elec. Lett. **29**, 453 (1993).

2.11 A. Putnam, C.G. Askins, G.M. Williams et al.: "Single pulse fabrication of fibre Bragg gratings using a phase-conjugated KrF excimer laser"; Elec. Lett. **31**, 885 (1995).

2.12 C.G. Askins, M.A. Putnam et al.: "Stepped-wavelength optical-fibre Bragg grating arrays formed in line on a draw tower"; Opt. Lett. **19**, 147 (1994).

2.13 L. Dong, J.-L. Archambault et al.: "Single pulse Bragg gratings written during fibre drawing"; Elec. Lett. **29**, 1577 (1993).

2.14 E.K. Popov, L.V. Tsonev and M.L. Sabeva: "Technological problems in holographic recording of plane gratings"; Opt. Eng. **31**, 2168 (1992).

2.15 K.O. Hill, B. Malo et al.: "Bragg gratings fabricated in monomode photosensitive optical fibre by UV exposure through a phase mask"; Appl. Phys. Lett. **62**, 1035 (1993).

2.16 G. Pakulski, R Moore, C. Maritan et al.: "Fused masks for printing uniform and phase adjusted gratings for distributed feedback lasers"; Appl. Phys. Lett. **62**, 222 (1993).

2.17 J.D. Prohaska, E. Snitzer and J. Winthrop: "Theoretical description of fibre Bragg reflectors prepared by Fresnel diffraction images"; App. Opt. **33**, 3896 (1994).

2.18 B. Malo, D.C. Johnson et al.: "Single-excimer-pulse writing of fibre gratings by use of a zero-order nulled phase mask: grating spectral response and visualisation of index perturbations"; Opt. Lett. **18**, 1277 (1993).

2.19 D.Z. Anderson, V. Mizrahi et al.: "Production of in-fibre gratings using a diffractive optical element"; Elec. Lett. **29**, 566 (1993).

2.20 J.D. Prohaska, E. Snitzer et al.: "Magnification of mask fabricated fibre Bragg gratings"; Elec. Lett. **29**, 1614 (1993).

2.21 S.J. Mihailov and M.C. Gower: "Recording of efficient high-order Bragg reflectors in optical fibres by mask image projection and single pulse exposure with an excimer laser"; Elec. Lett. **30**, 707 (1994).

2.22 H. Rizvi, M.C. Gower et al.: "Excimer laser writing of sub-micrometre period fibre Bragg gratings using phase shifting mask projection"; Elec. Lett. **31**, 901 (1995)

2.23 R. Kashyap, P.F. McKee and D. Armes: "UV written reflection grating structures in photosensitive optical fibres using phase-shifted phase masks"; Elec. Lett. **30**, 1977 (1994).

2.24 R. Kashyap, P.F. McKee and D.J. Armes: "Replication of phase-shifted DFB grating structures in photosensitive germania and rare-earth-doped optical fibres"; IEEE Colloquium on Fibre Gratings, January 1995.

2.25 A. Othonos and X. Lee: "Novel and improved methods of writing Bragg gratings with phase masks"; Phot. Tech. Lett. **7**, 1183 (1995).

2.26 F. Iwata and J. Tsuijiuchi: "Characteristics of a photoresist hologram and its replica"; Appl. Opt. **13**, 1327 (1974).

2.27 J. Martin and F. Ouellette: "Novel writing technique of long and highly reflective in-fibre gratings"; Elec. Lett. **30**, 811 (1994).

2.28 B.J. Eggleton, P.A. King et al.: "Long periodic superstructure Bragg gratings in optical fibres"; Elec. Lett. **30**, 1620 (1994).

2.29 W.H. Loh, M.J. Cole et al.: "Compensation of imperfect phase mask with moving fibre-scanning beam technique for production of fibre gratings"; Elec. Lett. **31**, 1483 (1995).

2.30 M.J. Cole, W.H. Loh, R.I. Laming et al.: "Moving fibre/phase mask-scanning beam technique for enhanced flexibility in producing fibre gratings with uniform phase mask"; Elec. Lett. **31**, 1488 (1995).

2.31 D. Elliot: "Microlithography: process technology for IC fabrication"; McGraw-Hill (1986).

2.32 D.M. Manos and D.L. Flamm: "Plasma etching: an introduction"; Academic Press (1989).

2.33 S.S. Rossnagel, J.J. Cuomo and W.D. Westwood: "Handbook of plasma processing technology"; Noyes Publications (1990).

2.34 C. Kaden, U. Griesinger et al.: "Fabrication of non-conventional distributed feedback lasers with variable grating periods and phase shifts by electron beam lithography"; J. Vac. Sci. Tech. **B10**, 2970 (1992).

2.35 H.N. Rourke, S. R. Baker, K.C. Byron et al.: "Fabrication and characterisation of long, narrowband fibre gratings by phase mask scanning"; Elec. Lett. **30**, 1341 (1994).

2.36 F. Barnier: "Assessing phase mask stitching errors"; Nortel Opt. Com. Mini-forum (1997).

2.37 K.O. Hill, F. Bilodeau et al.: "Efficient mode conversion in telecommunication fibre using externally written gratings"; Elec. Lett. **26**, 1270 (1990).

2.38 D. Johnson, F. Bilodeau et al.: "Long-length, long-period rocking filters fabricated from conventional monomode telecommunications optical fibre"; Opt. Lett. **17**, 1635 (1992).

2.39 B. Malo, K.O. Hill et al.: "Point-by-point fabrication of micro-Bragg gratings in photosensitive fibre using single excimer pulse refractive index modification techniques"; Elec. Lett. **29**, 1668 (1993).

2.40 P.E. Dyer, R.J. Farley et al.: "Amplification of fibre Bragg grating reflectivity by post-writing exposure with a 193 nm ArF laser"; Elec. Lett. **30**, 1133 (1994).

2.41 M. Sejka, P. Varming et al.: "Distributed feedback Er^{3+}-doped fibre laser"; Elec. Lett. **31**, 1445 (1995).

2.42 D. Uttamchandani and A. Othonos: "Phase shifted Bragg gratings formed in optical fibres by post-fabrication thermal processing"; Opt. Comm. **127**, 200 (1996).

2.43 V. Mizrahi and J.E. Sipe: "Optical properties of photosensitive gratings"; J. Lightwave Tech. **LT-11**, 823 (1993).

2.44 B. Malo, S. Thériault et al.: "Apodised in-fibre Bragg grating reflectors photo-imprinted using a phase mask"; Elec. Lett. **31**, 223 (1995).

2.45 R. Kashyap, A. Swanton and D.J. Armes: "Simple technique for apodising chirped and unchirped fibre Bragg gratings"; Elec. Lett. **32**, 1226 (1996).

2.46 J. Albert, K.O. Hill et al.: "Apodisation of the spectral response of fibre Brag gratings using a phase mask with variable diffraction efficiency"; Elec. Lett. **31**, 222 (1995).

2.47 J. Albert, K.O. Hill et al.: "Moiré phase masks for automatic pure apodisation of fibre Bragg gratings"; Elec. Lett. **32**, 2260 (1996).

2.48 S. Sandgren, B Sahlgen et al.: "Characterisation of Bragg gratings in fibres using the heat scan technique"; Elec. Lett. **31**, 665 (1995).

2.49 M. Volanthen, H. Geiger et al.: "Low-coherence technique to characterise reflectivity and time delay as a function of wavelength within a long fibre grating"; Elec. Lett. **32,** 757 (1996).

2.50 K. Sugden, I. Bennion et al.: "Chirped gratings produced in photosensitive optical fibres by fibre deformation during exposure"; Elec. Lett. **30,** 440 (1994).

2.51 R Kashyap et al.: "Novel method of producing all-fibre photoinduced gratings"; Elec. Lett. **30,** 996 (1994).

2.52 M.A. Putnam, G.M. Williams and E.J. Friebele: "Fabrication of tapered, strain-gradient chirped fibre Bragg gratings"; Elec. Lett. **31,** 309 (1995).

2.53 K.C. Byron and H.N. Rourke: "Fabrication of chirped fibre gratings by novel stretch and write technique"; Elec. Lett. **31,** 60 (1995).

2.54 D. Garthe, W.S. Lee, R.E. Epworth et al.: "Practical dispersion equaliser based on fibre gratings with a bit rate length product of 1.6 Tbit s km"; Proc. 20th ECOC **4,** 11 (1994).

2.55 D. Garthe, M.J. Stewart and R.E. Epworth: "Applications of fibre gratings to high capacity transmission systems"; IEEE Colloquium on fibre gratings, January 1995.

2.56 M.M. Ohn, A.T. Alavie et al.: "Dispersion variable fibre Bragg grating using piezoelectric stack"; Elec. Lett. **32,** 2000 (1996).

2.57 K.C. Byron, K. Sugden et al.: "Fabrication of chirped Bragg gratings in photosensitive fibre"; Elec. Lett. **29,** 1659 (1993).

2.58 L. Dong, J.L. Cruz et al.: "Fabrication of chirped fibre gratings using etched tapers"; Elec. Lett. **31,** 908 (1995).

2.59 L. Cruz, L. Dong et al.: "Fibre Bragg gratings with various chirp profiles made in etched tapers"; Appl. Opt. **35,** 6781 (1996).

2.60 J. Lauzon, S. Thibault et al.: "Implementation and characterisation of fibre Bragg gratings linearly chirped by a temperature gradient"; Opt. Lett. **19,** 2027 (1994).

2.61 Laming et al.: "Dispersion tuneable grating in a 10 Gbit/s 100-220 km step index fibre link"; Proc. ECOC **2,** WE.B.1.7, 585 (1995).

2.62 D. Garthe et al.: "Adjustable dispersion compensators for 10 and 20 Gbit/s over distances up to 160 km"; Elec. Lett. **30,** 2159 (1994).

2.63 J.A.R. Williams et al.: "Fibre dispersion compensation using a chirped in-fibre Bragg grating"; Elec. Lett. **30,** 985 (1994).

2.64 M.C. Farries, C.M. Ragdale and D.C.J. Reid: "Broadband chirped fibre Bragg filters for pump rejection and recycling in erbium doped fibre amplifiers"; Elec. Lett. **28**, 487 (1992).

2.65 K. Hibino: "Method of fabricating diffraction grating using hyperbolic gratings and an apparatus for carrying out the method"; Appl. Opt. **34**, 5569 (1995).

2.66 B.J. Eggleton et al.: "Experimental demonstration of compression of dispersed pulses by reflection from self-chirped optical fibre Bragg gratings"; Opt. Lett. **19**, 877 (1994).

2.67 M.C. Farries, K. Sugden et al.: "Very broadband reflection bandwidth (44 nm) chirped fibre gratings and narrow bandpass filters produced by the use of an amplitude mask"; Elec. Lett. **30**, 891 (1994).

2.68 Y. Painchaud, A. Chandonnet and J. Lauzon: "Chirped fibre gratings produced by tilting fibre"; Elec. Lett. **31**, 171 (1995).

2.69 K.O. Hill, S. Thériault et al.: "Chirped in-fibre grating dispersion compensators: linearisation of dispersion characteristic and demonstration of dispersion compensation in 100 km, 10 bit/s optical fibre link"; Elec. Lett. **30**, 1755 (1994).

2.70 J. Lightwave Tech. **15**, 8 (August 1997).

2.71 A. Asseh, H. Storøy et al.: "A writing technique for long fibre gratings with complex reflectivity profiles"; J. Lightwave Tech. **15**, 1419 (1997).

Chapter 3

SCANNING METHOD FOR WRITING LONG HOLOGRAPHIC DIFFRACTION GRATINGS

3.1 INTRODUCTION

Some of the methods which have been devised for the writing of in-fibre Bragg gratings have been described in chapter 2. One of the most commercially viable methods is the transfer of a pattern written using electron beam lithography from a phase mask into the fibre itself. However, there are some serious problems associated with the use of e^- beam written phase masks, particularly those of limited grating length and the presence of stitch errors between grating fields. The aim of this project was to investigate methods of writing long holographic phase masks, which would be free from these stitch errors. However, there are different problems associated with holographic diffraction gratings including the uniformity of illumination and pitch along the length of the grating and the lack of precision in the grating pitch arising due to the limited accuracy in the alignment of the beam angle [3.1].

The standard method of writing a plane holographic diffraction grating has been described in many places [e.g. 3.2]. Essentially two coherent beams of light are coincident in a region on some recording medium which records the resulting interference pattern. The beams may be collimated, but in practice it is good procedure to avoid the presence of any optical surfaces between the spatial filter and the recording medium for either beam, and so the interfering wavefronts are spherical. Here it is shown that to a first order approximation the interference of two divergent spherical wavefronts will yield linear fringes.

Consider a point source as illustrated in Fig. 3.1. From Pythagoras it is clear that:

$$r^2 = D^2 + s'^2 = D^2 + x'^2 + y'^2 \tag{3.1}$$

Using the Fraunhofer approximation: $r \sim D + \frac{(x'^2 + y'^2)}{2D}$ (3.2)

Hence the amplitude, A_T at the observation plane, Σ', resulting from the interference of waves from two perfectly coherent point sources in Σ separated by a distance $2d$ in the y direction is simply the sum of the two amplitudes:

$$A_T = A\exp\left[ik\left\{D+\frac{\left(x'^2+(y'-d)^2\right)}{2D}\right\}\right]+A\exp\left[ik\left\{D+\frac{\left(x'^2+(y'+d)^2\right)}{2D}\right\}\right] \qquad (3.3)$$

The D term in each exponential term may be neglected, since it is just a constant phase factor. The intensity at Σ', $A_T A_T^*$, is now calculated; simplification yields:

$$I = 2A^2 + A^2\left[\exp\left(\frac{-i2ky'd}{D}\right)+\exp\left(\frac{+i2ky'd}{D}\right)\right]$$

$$\therefore I = = 2A^2\left[1+\cos\left(\frac{2ky'd}{D}\right)\right] \qquad (3.4)$$

Since there are only linear terms in the argument of the cosine function, it follows that the form of the intensity variation is simply sinusoidal . Hence the fringes of the interference pattern formed from two spherical waves are the Young's fringes obtained from collimated sources to a first order approximation.

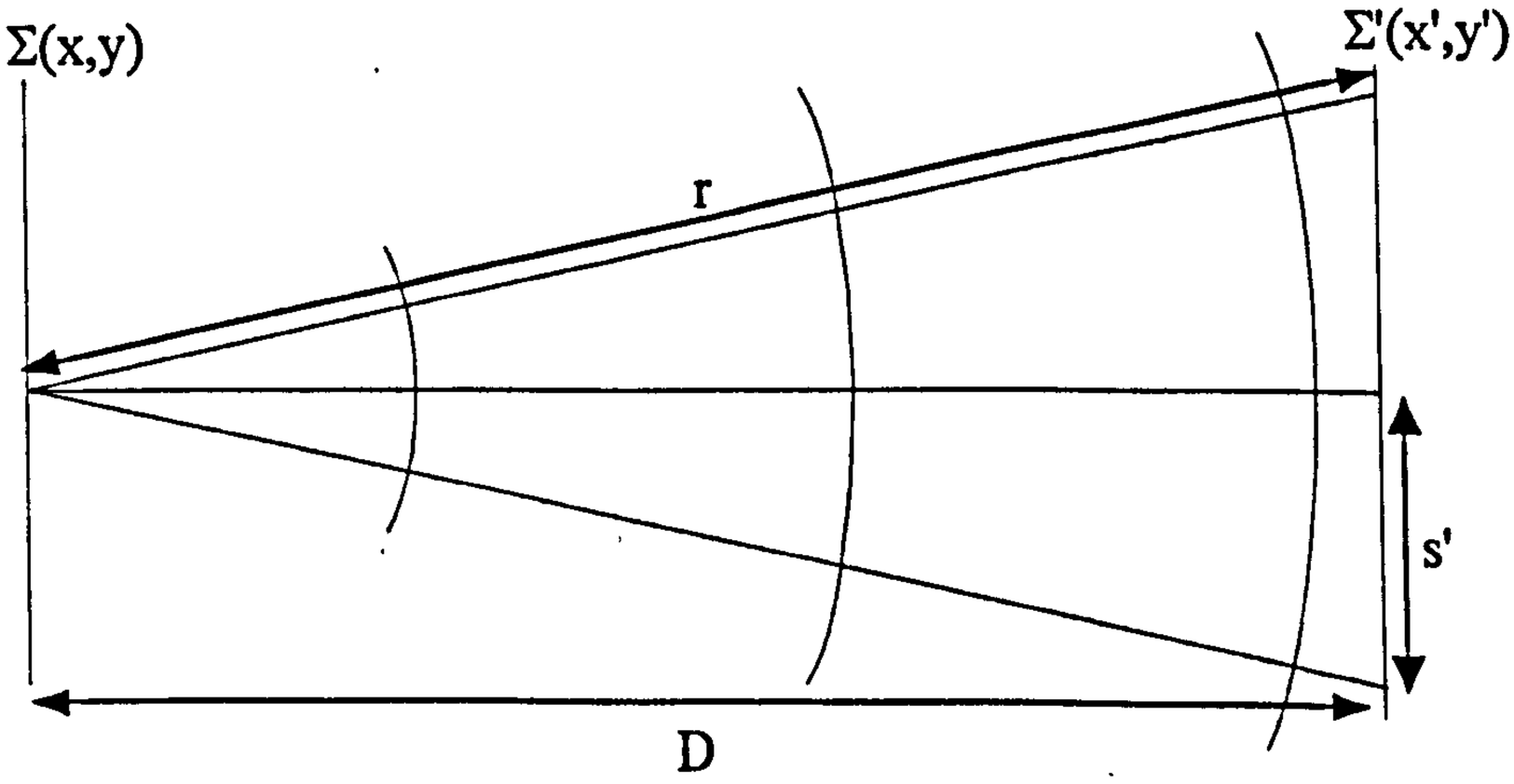

Fig. 3.1: *To illustrate the geometry of a point source.*

3.2 NOVEL SCANNING METHOD FOR HOLOGRAPHIC GRATINGS

The length of a traditional holographic grating is limited by the diameter of the writing beams, which is constrained by the available beam power if realistic exposure times are to be achieved. However, it is possible to write gratings larger than the writing beams themselves by scanning them across the recording medium. It is interesting that it is possible to move both the writing beams across the medium simultaneously and yet maintain a single uninterrupted grating.

The apparatus to be discussed is depicted in Fig. 3.2: for illustrative purposes it is assumed that the mirrors *M1, M4* and the beam splitter are at exactly 45° to the beam, and that *M2* and *M3* are precisely symmetric. The key to the method is in the movement of mirror *M1*, which shifts the point where the beam from the laser hits the beam splitter. Since all the mirrors are plane, the angle of intersection of the beams at the recording plate remains 2θ and so the pitch of the grating is constant. However the point of illumination on the plate is shifted as the mirror *M1* is moved.

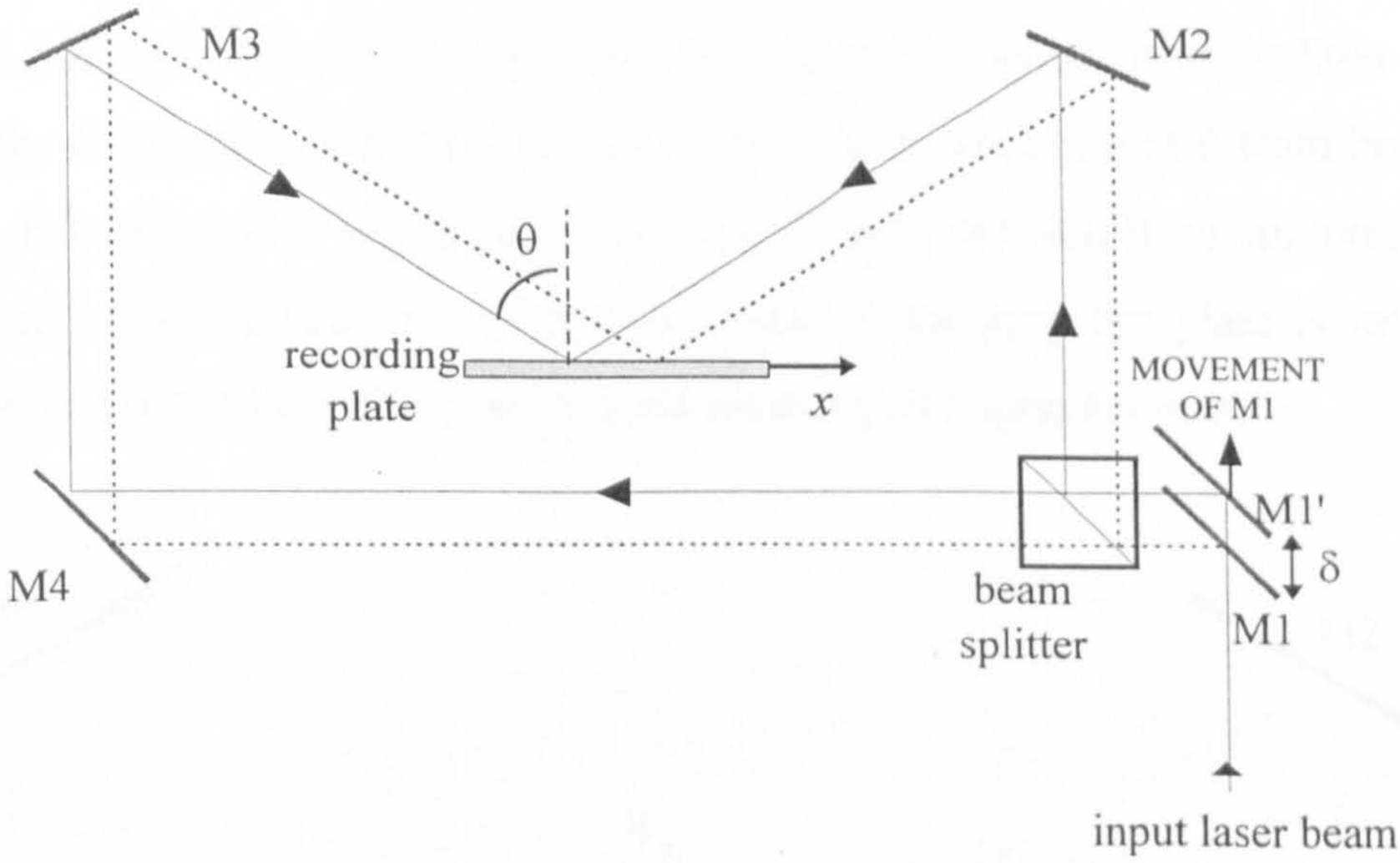

Fig. 3.2: *A sketch of an experimental apparatus to write long holographic gratings using a scanning method. For illustrative purposes mirrors M1 and M4 as well as the beam splitter are at exactly 45° to the beam, and M2 and M3 are precisely symmetric.*

The interference pattern formed on the recording medium will have a pitch determined by the inter-beam angle and a particular phase dependent on the absolute path difference between the two beams. The movement of the mirror *M1* will not effect this pitch since the inter-beam angle is unchanged. On the other hand the path

difference between the beams will change, and so the phase of the grating relative to the beams is shifted. However, it can be shown that the fringes do not move relative to the plate and the pattern is not wiped out: the beams sweep across the recording material and write a single continuous grating.

Consider the particular phase of the grating at the beginning of the exposure before *M1* has shifted from its initial position. If the phase difference between the two waves, each of amplitude A, is ϕ then by the principle of superposition the resultant electric field in the region of interference, A_{T1}, may be represented by:

$$A_{T1} = A\exp(ikx\sin\theta + i\phi) + A\exp(-ikx\sin\theta) \qquad (3.5)$$

Now consider the mirror *M1* moving a distance δ. The point of incidence on the beam splitter will be different and this results in a shift in the path of both the recording beams such that they coincide at a different point on the recording plate: x'. From Fig. 3.3 it can be seen that there is an distance $\delta tan\theta$ added to the path of beam A and reduced from that of beam B. [Because the mirror *M4* and the beam splitter are both at exactly 45° to the beam there is also a path length reduction of δ from both of the beams, but since this is identical in each it will not result in an optical path difference.] Consequently the light from beam A reaching the plate is retarded in phase by $k\delta tan\ \theta$, whilst that from B is advanced by the same amount.

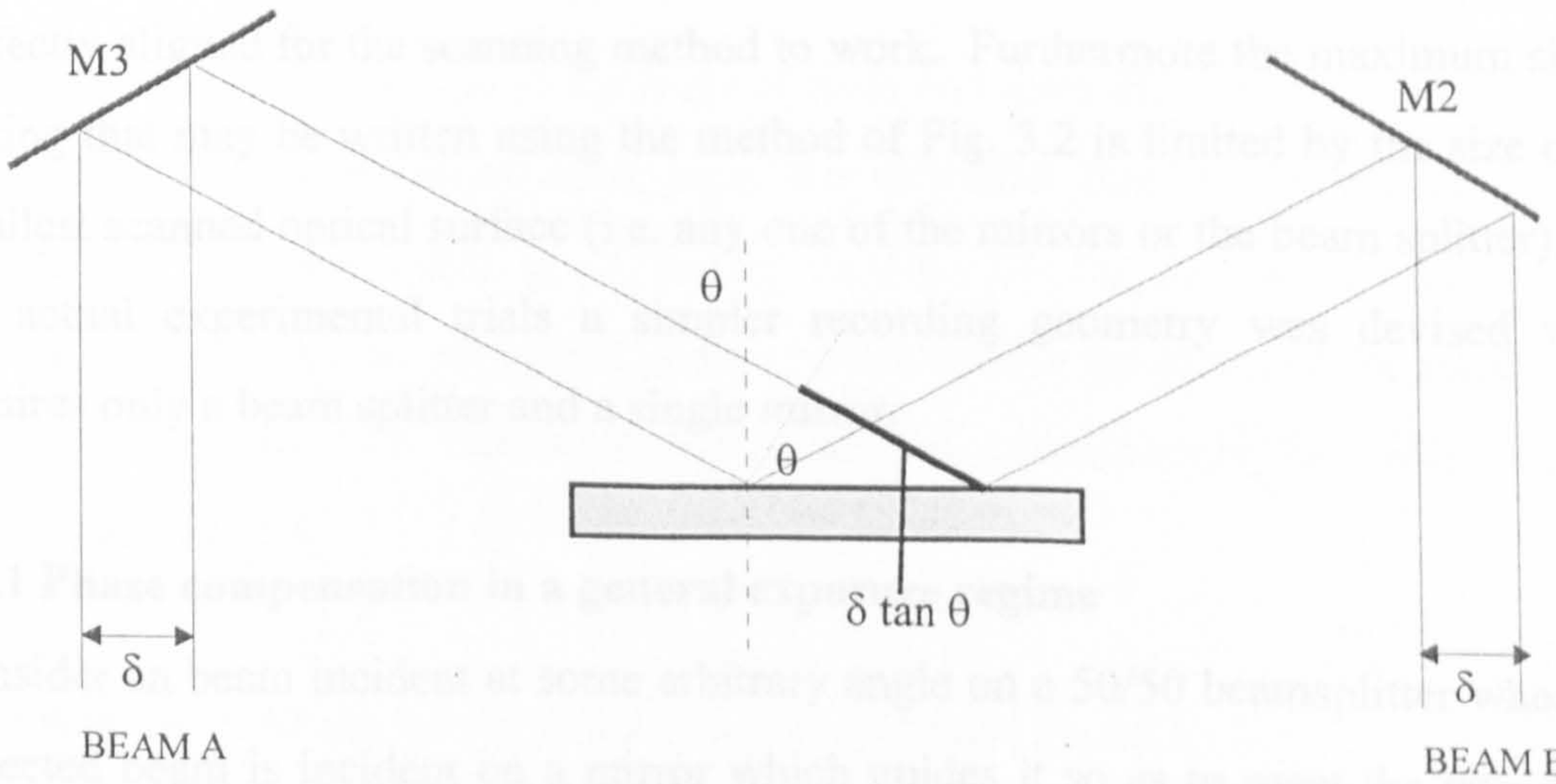

Fig. 3.3: *Showing the geometry of the path length changes.*

Substituting these new phases into (3.5) yields:

$$A_{T2} = A\exp\left(ikx'\sin\theta + i(\phi - k\delta\tan\theta)\right) + A\exp\left(-ikx'\sin\theta + ik\delta\tan\theta\right) \qquad (3.6)$$

The effect of the scan is to move the interference pattern a distance $\delta/cos\ \theta$ along the plate to x', hence (3.6) becomes:

$$A_{T2} = A\exp\left(ik(x+\frac{\delta}{\cos\theta})\sin\theta + i(\phi - k\delta\tan\theta)\right) + A\exp\left(-ik(x+\frac{\delta}{\cos\theta})\sin\theta) + ik\delta\tan\theta\right)$$

$$\therefore A_{T2} = A\exp\left(ikx\sin\theta + i\phi\right) + A\exp\left(-ikx\sin\theta\right) \qquad (3.7)$$

But this is identical to (3.5): the pattern is unchanged: thus the pattern is not shifted by the scanning of the beams.

3.3 EXPOSURE GEOMETRIES IN THE SCANNING REGIME

The experimental arrangement shown in Fig. 3.2 for writing scanned gratings is an idealised example of the method to illustrate the ideas behind the technique. In this stylised model all the angles are assumed to be perfectly precise for the sake of simplicity. In a practical realisation of such a set up there will be finite errors in the alignment of the optical components: here it is shown that the beam need not be perfectly aligned for the scanning method to work. Furthermore the maximum size of grating that may be written using the method of Fig. 3.2 is limited by the size of the smallest scanned optical surface (i.e. any one of the mirrors or the beam splitter). For the actual experimental trials a simpler recording geometry was devised which requires only a beam splitter and a single mirror.

3.3.1 Phase compensation in a general exposure regime

Consider an beam incident at some arbitrary angle on a 50/50 beamsplitter where the reflected beam is incident on a mirror which guides it so as to meet the transmitted beam such that the angle between the two interfering beams is 2θ. In this more general case the incident beam will be inclined with respect to the beamsplitter face,

i.e. it is no longer at exactly 45° to the beamsplitting plane. Consider the geometry as the beam scans some distance Δx across the face of the beamsplitter, as illustrated in Fig. 3.4. Since the angle of incidence with the mirror is unchanged the angle between the beams at the new point of intersection will also be unchanged and the rays will trace out two similar triangles.

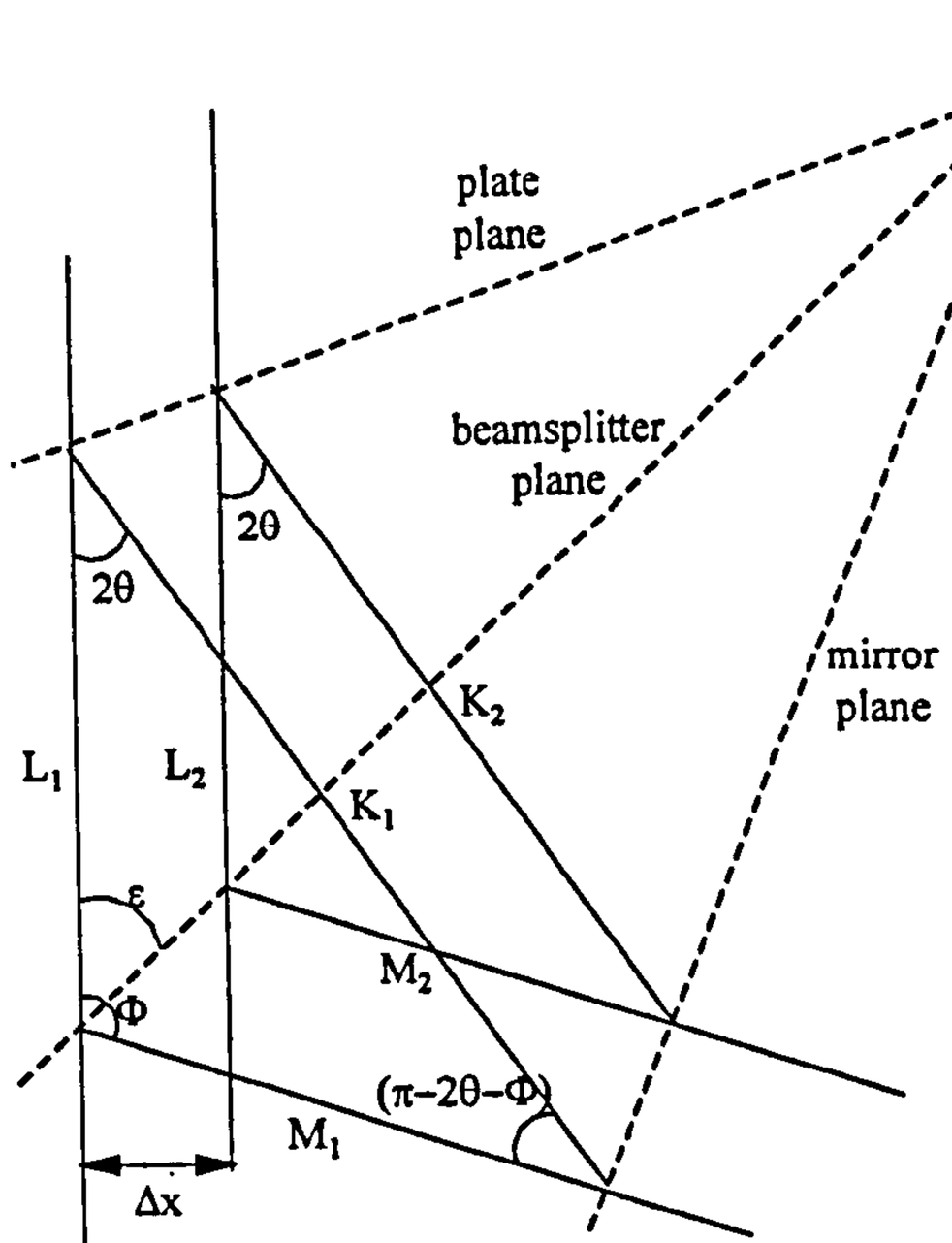

Fig. 3.4: *A diagram of the geometry of a scanned exposure with a beamsplitter inclined at an arbitrary angle to the initial beam.*

Since the ratio of the lengths of the sides of these triangles must be constant, the locus of this point of intersection must meet the extended line of the mirror and the beamsplitter at some point Q as shown in Fig. 3.4: in the actual exposure the recording plate is placed along this plane. Now consider the effect of the scanning on the phases of the two beams at the plate and consequently the effect on the interference pattern.

For a scan distance Δx, let the side K_1 change in length by ΔK to K_2:

$$K_2 = K_1 + \Delta K \tag{3.8}$$

Similarly for L_1 and M_1. To find path differences introduced by this scanning consider the sine rule for the two similar triangles $K_1L_1M_1$ and $K_2L_2M_2$:

$$\frac{K_1}{\sin\Phi} = \frac{L_1}{\sin(\pi-\Phi-2\theta)} = \frac{M_1}{\sin 2\theta} \tag{3.9}$$

and:

$$\frac{K_2}{\sin\Phi} = \frac{L_2}{\sin(\pi-\Phi-2\theta)} = \frac{M_2}{\sin 2\theta} \tag{3.10}$$

Hence:

$$\Delta M = M_2 - M_1 = L_2 \frac{\sin 2\theta}{\sin(\Phi+2\theta)} - L_1 \frac{\sin 2\theta}{\sin(\Phi+2\theta)}$$

$$\Delta M = \Delta L \frac{\sin 2\theta}{\sin(\Phi+2\theta)} \tag{3.11}$$

Similarly:

$$\Delta K = \Delta L \frac{\sin\Phi}{\sin(\Phi+2\theta)} \tag{3.12}$$

Hence the total path differences introduced by the scan are given by:

Straight through beam:

$$\Delta L \tag{3.13}$$

Reflected beam:

$$\Delta K + \Delta M = \frac{\Delta L}{\sin(\Phi+2\theta)}(\sin\Phi + \sin 2\theta)$$

Or equivalently

$$\Delta K + \Delta M = \Delta L \frac{\cos(\Phi/2-\theta)}{\cos(\Phi/2+\theta)} \tag{3.14}$$

Next an expression for each of ΔL, ΔM and ΔK in terms of Δx, Φ and θ is derived and hence an expression for the total optical path difference.

First an expression for ΔL: from Fig. 3.5 it can be seen that the change in length of the straight through beam may be considered to be the difference between the lengths ΔL_2 which is effectively added to the path, and ΔL_1, which is subtracted. Hence:

$$\Delta L = \Delta L_2 - \Delta L_1 = \Delta x\left(\tan\theta - \frac{1}{\tan\varepsilon}\right) \tag{3.15}$$

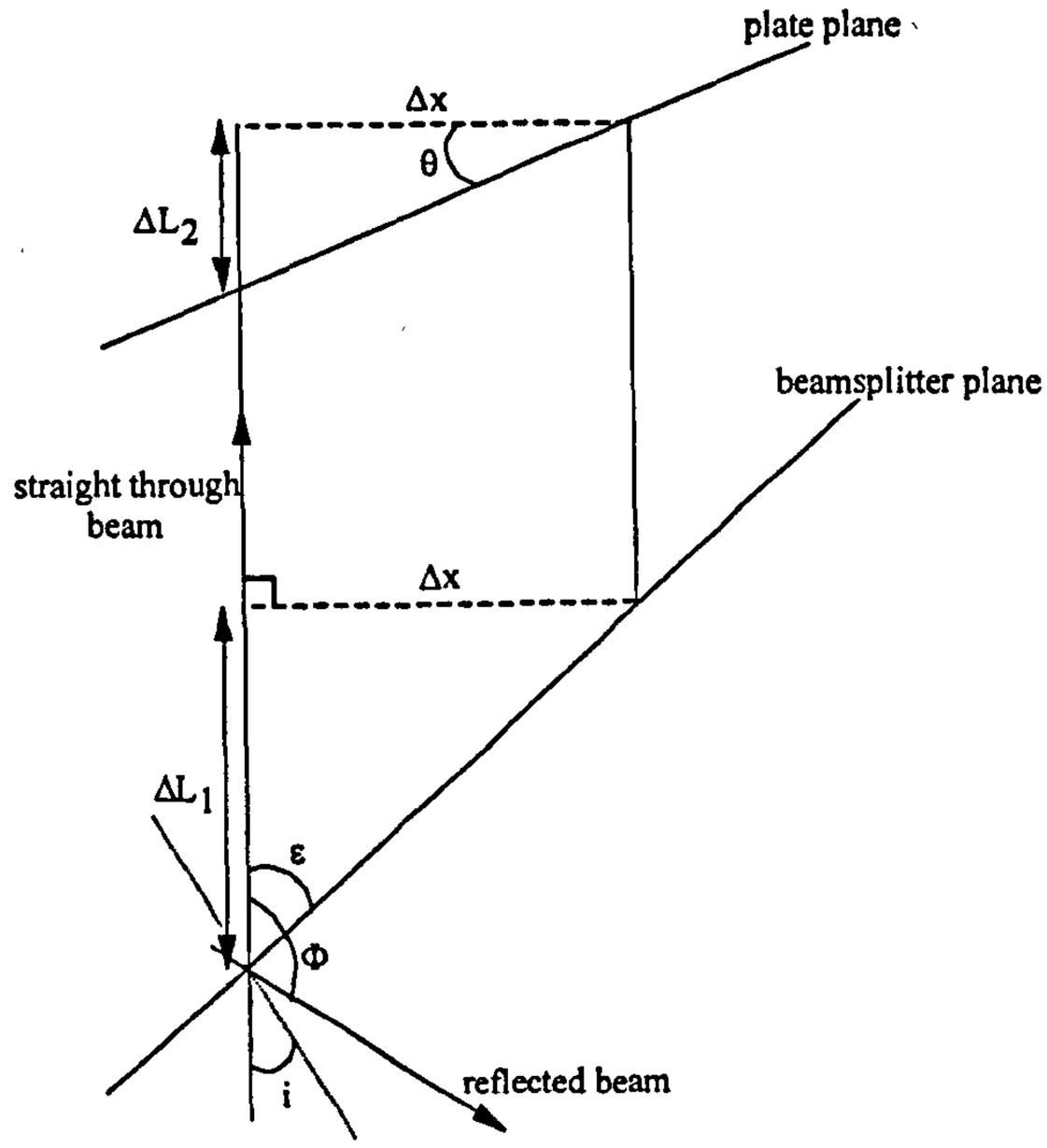

Fig. 3.5: *Showing more detailed geometry for calculation of ΔL.*

But from the symmetry of Fig. 3.5: $\varepsilon = \Phi/2$

Thus the total path length change for the straight through beam may be written:

$$\Delta L = \Delta x \left(\tan\theta - \frac{1}{\tan \Phi/2} \right) \tag{3.16}$$

Rearranging:

$$\Delta L = -\Delta x \left(\frac{\cos(\Phi/2 + \theta)}{\cos\theta \sin(\Phi/2)} \right) \tag{3.17}$$

Substituting (3.17) into (3.14) yields:

$$\Delta K + \Delta M = \Delta x \left(-\frac{\cos(\Phi/2 + \theta)}{\cos\theta \sin \Phi/2} \right) \left(\frac{\cos(\Phi/2 - \theta)}{\cos(\Phi/2 + \theta)} \right)$$

$$\Delta K + \Delta M = \Delta x \left(-\tan\theta - \frac{1}{\tan \Phi/2} \right) \tag{3.18}$$

Hence the path difference introduced by the scanning of the incident beam is simply the difference between (3.16) and (3.18): $2\Delta x tan\theta$, identical to the result for the perfectly aligned beamsplitter.

3.3.2 Discussion of rolling fringes and phase compensation

An examination of Fig. 3.4 shows that the mirror plane must be inclined at an angle θ to the beamsplitter plane at Q if the interference angle at the plate is to be 2θ. Hence as the beamsplitter is rotated, the mirror must also be rotated through the same angle. The effect on the path lengths is that a distance $\Delta x \cot(\Phi/2)$ is added to or subtracted from (depending on the scan direction) each of the two beams, resulting in no net effect on the phase difference at the plate. The other term, $\pm\Delta x \tan\theta$ is the same as in the idealised example described in section 3.2, and so the same rolling fringe effect will result for a more general beamsplitter angle and exposure geometry. This is an important result since it shows that the calculation is not simply a quirk arising from an expedient choice of beamsplitter angle.

The rolling fringe effect arises from the addition of a path length to one beam and the simultaneous subtraction of the same path length from the other so as to "take up the slack". Thus the path length variations alter the phase and spatial position of each beam such that the phase of the interference pattern at the plate changes by an amount opposite to the change due to the movement in the beam positions. Thus the pattern itself remains stationary as the beams scan across, as if the pattern were there all the time and the beams were simply illuminating it as they sweep past.

It is tempting to imagine each beam as a series of parallel rays: as they scan, in each beam rays are removed from one side and added to the other. This will not effect the pattern in the middle of the beams but will simply extend the grating in the direction of the scan. Such a visualisation can be misleading since the scanning method only works in regimes in which the path differences arise as a result of the angle of the beams relative to the plate.

At first glance a scheme such as that depicted in Fig. 3.6 seems ideal, since the grating is not limited by the size of any of the components and so large mirrors or beamsplitters are not required. However, consider the phase compensation at the plate.

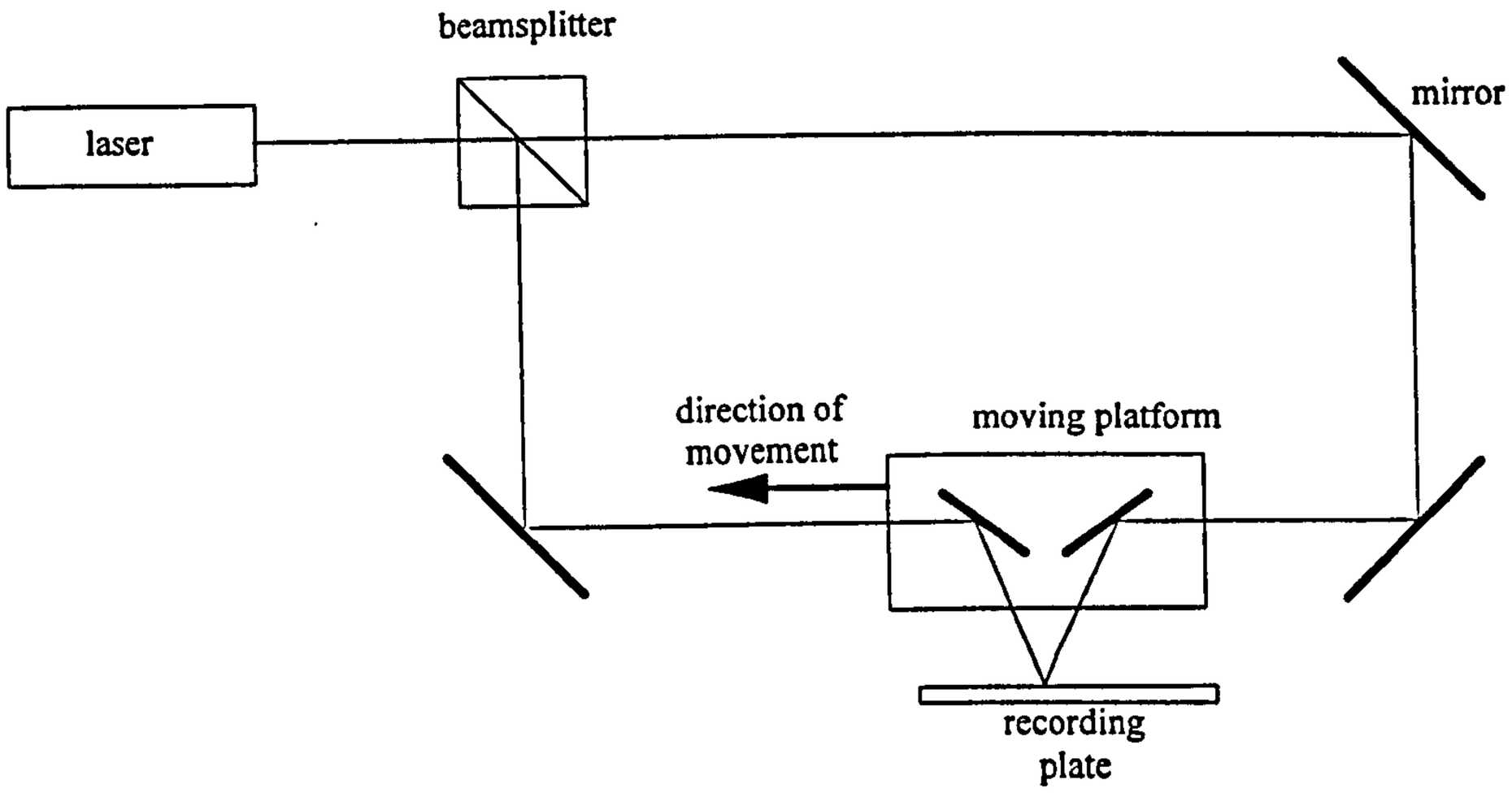

Fig. 3.6: *A flawed scanning regime.*

As before let the initial phase of the interference pattern be due to the sum of amplitudes:

$$A_{T1}^{F} = A\exp\left(ikx\sin\theta + i\phi\right) + A\exp\left(-ikx\sin\theta\right) \tag{3.19}$$

If the mirrors move some distance Δx then the pattern itself will also be shifted by this distance. However in this case the grating phase is dependent on the angle θ, whilst the path difference is not:

$$\begin{aligned} A_{T2}^{F} = A\exp\left(ik\left(x+\Delta x\right)\sin\theta + i\left(\phi + k\Delta x\right)\right) \\ + A\exp\left(-ik\left(x+\Delta x\right)\sin\theta - ik\Delta x\right) \end{aligned} \tag{3.20}$$

Thus there is not the tidy cancellation of terms exhibited in (3.7) and the scanning will rub out the grating. From the geometry of Fig. 3.6 it can be seen that there is no change in the sum of the two beam paths. This is in contrast to the analysis given in 3.3, which is based on path length changes between similar triangles which are intrinsically different sizes. By extending the mirror and beam splitter planes the illustrative example of Fig. 3.3 can be shown to be a special case of the more general analysis of section 3.3, with an extra identical path length introduced to both beams due to the use of the two extra mirrors.

A second flawed exposure regime (which was tried experimentally) is sketched in Fig. 3.7. Again, it would seem that this arrangement offers a significant improvement on that described in section 3.3.1 since the length of the beamsplitter plane is no longer a

restriction on the length of grating that may be written. The key difference is that the beamsplitter itself is moved, so that it needs only to be a little bigger than the beam diameter itself. In this method the only optical components that limit the size of the grating that can be written are the mirror and the recording plate itself.

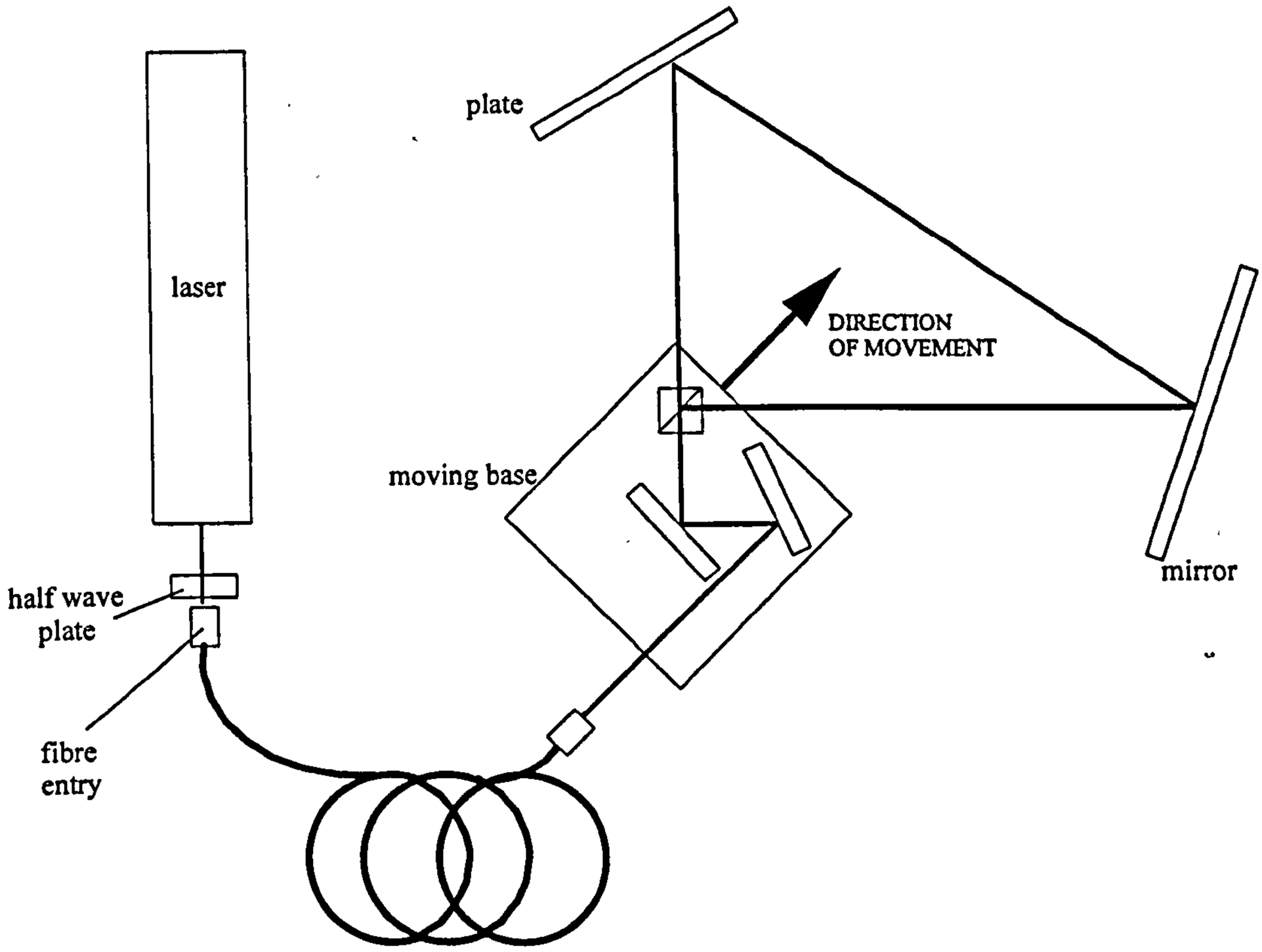

Fig. 3.7: *A sketch of a flawed experimental set up in which the beamsplitter itself is moved. Theoretically this is an preferable option, but in practice, vibrations in spatial location of the splitter result in insufficient stability to write fine diffraction gratings.*

The stability and the alignment of fibre was vital in order to obtain constant output power and hence it was considered undesirable to move the output of the fibre. This was avoided by using the two mirrors on the moving bed. It may be seen from Fig. 3.7 that as the bed moves in a direction parallel to the beamsplitting plane the point of division of amplitude of the two beams is shifted in the same way as for the method outlined in section 3.3.1. Since the phase differences occur only after the point of splitting, all the mathematics derived for the original method also hold for this moving beam splitter arrangement without the need for the large splitter.

However, there is a fundamental difference between this method and the original experiment. In the method described in 3.3.1 vibrations from the micropositioner will

be transmitted to the mirror *M1* in Fig. 3.2 and this will produce vibrations in the beam incident on the beamsplitter. However, the pattern formed at the plate is dependent only on the phase *differences* between the two beams. Hence any spatial variations on the input beam will have an identical effect on each beam and so will not effect the interference pattern. It has already been shown that a beam that scans across the beamsplitter in this set up will not change the pattern at the plate, only extend the existing pattern. These vibrations may be regarded as a form of scanning and consequently will not cause any problems to the pattern formation, only in the uniformity of exposure of the grating.

The situation in the moving beamsplitter case, however, is very different. The vibrations are transmitted from the base plate to the beamsplitter; the point of splitting is moved along with the two split beams. As has been described, this will not change the pattern formed, but in moving the point of splitting a distance δ, the whole pattern will be shifted on the plate by a distance $(\delta/\cos\theta)$, since it is effectively a shifting of the origin of co-ordinates. Thus the whole pattern will be smeared about on the plate across an distance comparable with the vibrational amplitude of the beamsplitter. Since the grating pitch is of the order of one micron, the pattern will be rubbed out for any vibrations with a similar or greater magnitude.

In conclusion this moving-beamsplitter method is fine theoretically, but in order to write efficient gratings of pitch p, a micropositioning device is required which has a maximum error in position, ε, in three dimensions, where $\varepsilon << p$. The original moving mirror method is far less stringent on its stability demands, but does have the disadvantage that the grating size is limited by the beamsplitter.

3.4 FLUENCE CALCULATION IN THE SCANNING REGIME

Any point M on the recording medium will receive radiation from the whole of one cross section of the beam during the exposure. Thus the incident power at M is not constant during the exposure, but will vary as the beam is scanned across the plate. In a normal static exposure the fluence is simply the product of the intensity, I, and the

exposure time, τ. In the scanning case τ depends on the speed of the travelling beam and I depends on the position within the Gaussian profile of the beam at any particular time.

There follow two models for this fluence calculation. In the first the intensity is considered to be constant across the beam: the so called "top hat" intensity profile. An example of such a profile would that from a laser beam which had been passed through an anti-Gaussian filter. The second model assumes a Gaussian beam profile; i.e. the profile of a typical TEM_{oo} laser beam.

3.4.1 Fluence calculation using a top hat approximation for the beam profile

Consider a beam of circular cross section with radius a being scanned across a mirror with a speed v. This beam has a uniform intensity profile and it impinges on the plate with some angle of incidence θ as shown in Fig. 3.8.

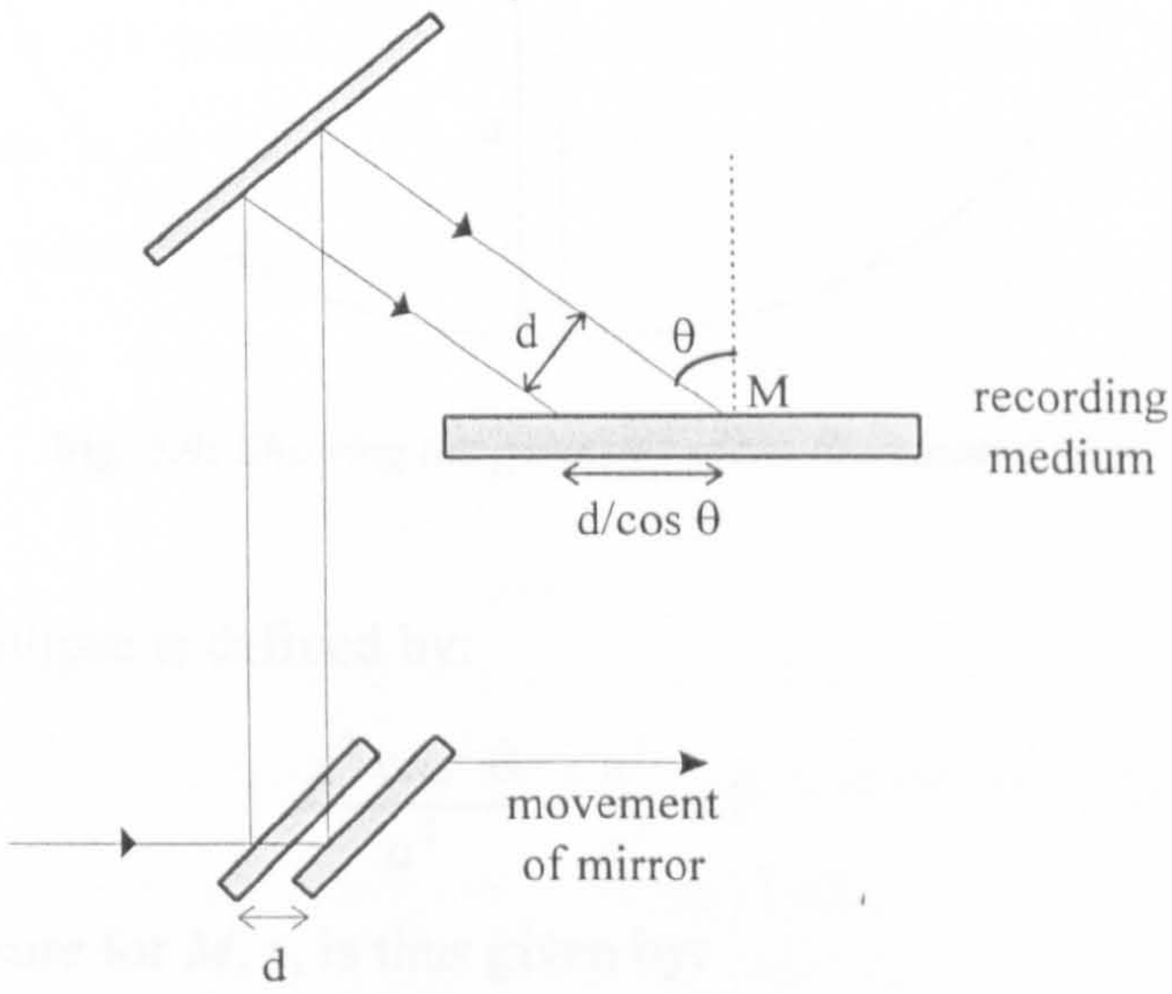

Fig. 3.8: *Showing the geometry of the scanning beam.*

Consider the point M on the plate which is illuminated by the beam. The fluence received at M is given by $I\tau$, the product of the intensity and the exposure time. In this simple model, where the light flux is assumed to be constant across the beam area, if the total beam power is P then the intensity per unit area impinging on a plane at some angle θ to the beam, I, is given by:

$$I = \frac{P\cos\theta}{\pi a^2} \tag{3.21}$$

The exposure time for this arbitrary point M is dependent both on the speed at which the beam scans across the plate, the intensity of the beam and the position of the point relative to the centre of the beam. A circular beam intersecting a plane at angle of incidence θ will give an ellipsoidal region of illumination. Suppose that M is a perpendicular distance c from the centre of the beam, as shown in Fig. 3.9. The period for which this point is illuminated for a given scan speed depends on the length of the chord X. Hence points nearer to the centre of the beam will receive a greater exposure because they are passed over by a greater part of the beam.

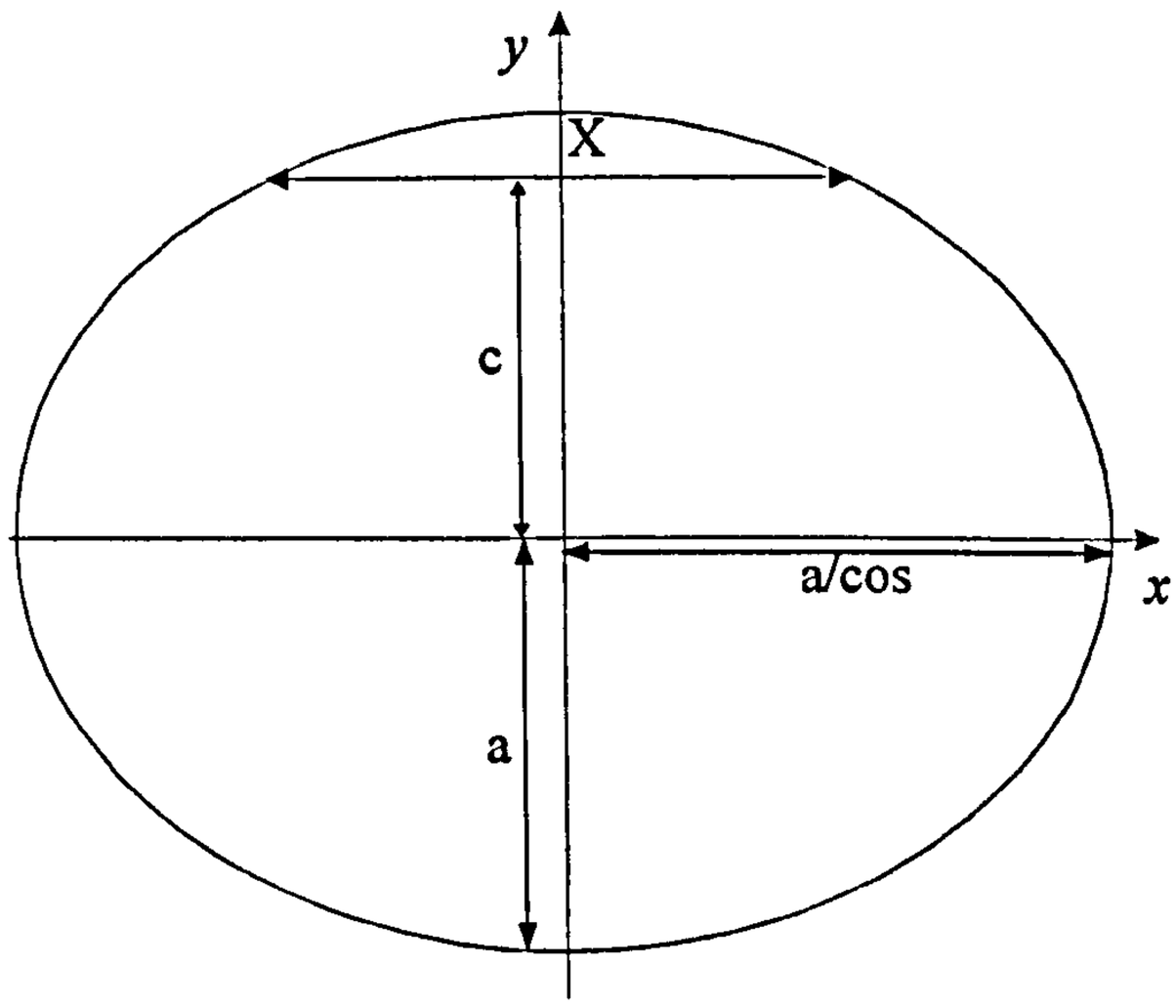

Fig. 3.9: *Showing the geometry of the illuminated area.*

The curve of the ellipse is defined by:

$$\frac{x^2 \cos^2\theta}{a^2} + \frac{y^2}{a^2} = 1 \tag{3.22}$$

The time of exposure for M, τ, is thus given by:

$$\tau = \frac{X}{v} = \frac{2}{v}.x\Big|_{y=c} = \frac{2\sqrt{a^2 - c^2}}{\upsilon \cos\theta} \tag{3.23}$$

The fluence, $I\tau$ of any point is thus the product of (3.21) and (3.23).

$$E = \left(\frac{2P}{\pi v a^2}\right)\sqrt{\left(a^2 - c^2\right)} \tag{3.24}$$

Thus the effect of the angle of incidence on the exposure is cancelled. This is expected since the energy in the beam is fixed regardless of θ: as the beam is tilted the intensity is reduced by the same factor as the exposure time is increased.

3.4.2 Fluence calculation using a Gaussian beam profile

In a typical TEM_{oo} laser beam the electric field vector amplitude, A, at a distance x from the centre of the beam follows a Gaussian profile [3.3].

$$A = A_O \exp\left(\frac{-x^2}{\omega_o^2}\right) \tag{3.25}$$

where A_0 is the amplitude at the centre of the beam and ω_0 is the "spot size", defined as the radius for which the field has decreased to e^{-1} of its maximum value. Thus the intensity profile may be written:

$$I = |A|^2 = I_o \exp\left(\frac{-x^2}{a^2}\right) \tag{3.26}$$

where $I_o\left(=|A_o|^2\right.$ is the intensity at the centre of the beam, and $a\ \left(=\omega_o/\sqrt{2}\right)$ is the radius for which the intensity has decreased to e^{-1} of its maximum value .

Consider a point on the recording medium which is illuminated by the centre of the beam scanning in the x direction. The instantaneous exposure of any point is given by $I(t)dt$: as the beam scans across the plate the resultant exposure is found by integrating over the whole beam.

$$E = \int_{scan} I(t)dt = \int_{beam} I_o \exp\left(\frac{-x^2}{a^2}\right)\frac{dx}{v} \tag{3.27}$$

where the substitution $dt=dx/v$ has been used. This integral can be converted to a standard form using the substitution $\beta = x/a$. Thus using the standard result for the integration of a Gaussian between infinite limits [3.4]:

$$E = \frac{aI_o}{v}\int_{-\infty}^{+\infty}\exp\left(-\beta^2\right)d\beta = \frac{aI_o}{v}\sqrt{\pi} \tag{3.28}$$

Evaluation of E from this equation requires the value of the peak intensity of the beam, I_o, which would require a precise beam profile. However, the total power of the beam, P, can be easily measured using a light meter. This value of P is the total energy flux of the beam given by:

$$P = \iint_{whole\ beam} I_o \exp\left(-\frac{\left(x^2+y^2\right)}{a^2}\right)dxdy \tag{3.29}$$

This double integral may be evaluated using the same substitution method described above for both co-ordinates, giving:

$$P = I_o \pi a^2 \tag{3.30}$$

[N.B. Comparison with (3.21) reveals why a rather than ω_0 was used as the normalising parameter: the Gaussian beam of width a, and peak intensity I_O has the same total energy flux as the top hat beam with the same parameters.]

Substituting (3.30) into (3.28) yields the energy incident at a point illuminated by the centre of a single beam as it scans:

$$E = \frac{1}{\sqrt{\pi}}\left(\frac{P}{av}\right) \tag{3.31}$$

The intensity profile of the circular Gaussian beam in two dimensions may be represented by:

$$I = I_o \exp\left(-\frac{\left(x^2 + y^2\right)}{a^2}\right) \tag{3.32}$$

Since the beam scans in the x direction, for any point on the plate the y co-ordinate is constant. Hence for a point a distance c from the centre of the beam,

$$I = I_o \exp\left(-\frac{\left(x^2 + c^2\right)}{a^2}\right) = I_o \exp\left(\frac{-c^2}{a^2}\right) \exp\left(\frac{-x^2}{a^2}\right) \tag{3.33}$$

Including this factor in (3.31) gives the exposure energy impinging on an arbitrary point on the plate as a single beam scans:

$$E = \frac{1}{\sqrt{\pi}} \exp\left(\frac{-c^2}{a^2}\right)\left(\frac{P}{av}\right) \tag{3.34}$$

3.4.3 Comparison of the two models

From these two models, then, we have two similar equations.

$$E = \left(\frac{2}{\pi}\right)\frac{\sqrt{\left(a^2 - c^2\right)}}{a}\left(\frac{P}{av}\right)$$ Fluence from top hat intensity profile model (3.24).

$$E = \left(\frac{1}{\sqrt{\pi}}\right)\exp\left(\frac{-c^2}{a^2}\right)\left(\frac{P}{av}\right)$$ Fluence from Gaussian intensity profile model (3.34).

The two models can be shown to be equivalent by the conservation of energy, since as mentioned above, the two beams have the same total energy flux. Consequently, for a scan of unit length, the total energy incident on the plate, F, should be the same for both models. First consider the top hat model: integrating across the y cross-section of the beam:

$$F = 2\left(\frac{2P}{\pi v a^2}\right)\int_{y=0}^{y=a}\sqrt{\left(a^2 - y^2\right)}dy \qquad (3.35)$$

Using the substitution $y = a\sin\phi$

$$F = 2\left(\frac{2P}{\pi v a^2}\right)\int_{\phi=0}^{\phi=\frac{\pi}{2}} a^2\cos^2\phi.d\phi = \left(\frac{4P}{\pi v}\right)\left[\tfrac{1}{2}\left(\phi + \tfrac{1}{2}\sin 2\phi\right)\right]_0^{\frac{\pi}{2}}$$

$$\Rightarrow F = \frac{P}{v} \qquad (3.36)$$

Similarly to find the total energy from the Gaussian model (3.34) is integrated across a complete y profile (which in this case will involve integrating across all of space): the energy per unit length of scan, F, is given by:

$$F = \frac{1}{\sqrt{\pi}}\left(\frac{P}{av}\right)\int_{-\infty}^{\infty}\exp\left(\frac{-y^2}{a^2}\right)dy \qquad (3.37)$$

$$\Rightarrow F = \frac{P}{v} \qquad (3.38)$$

A sketch of the two equations (3.24) and (3.34) illustrates the exposure profiles obtained from the two beam intensity profiles.

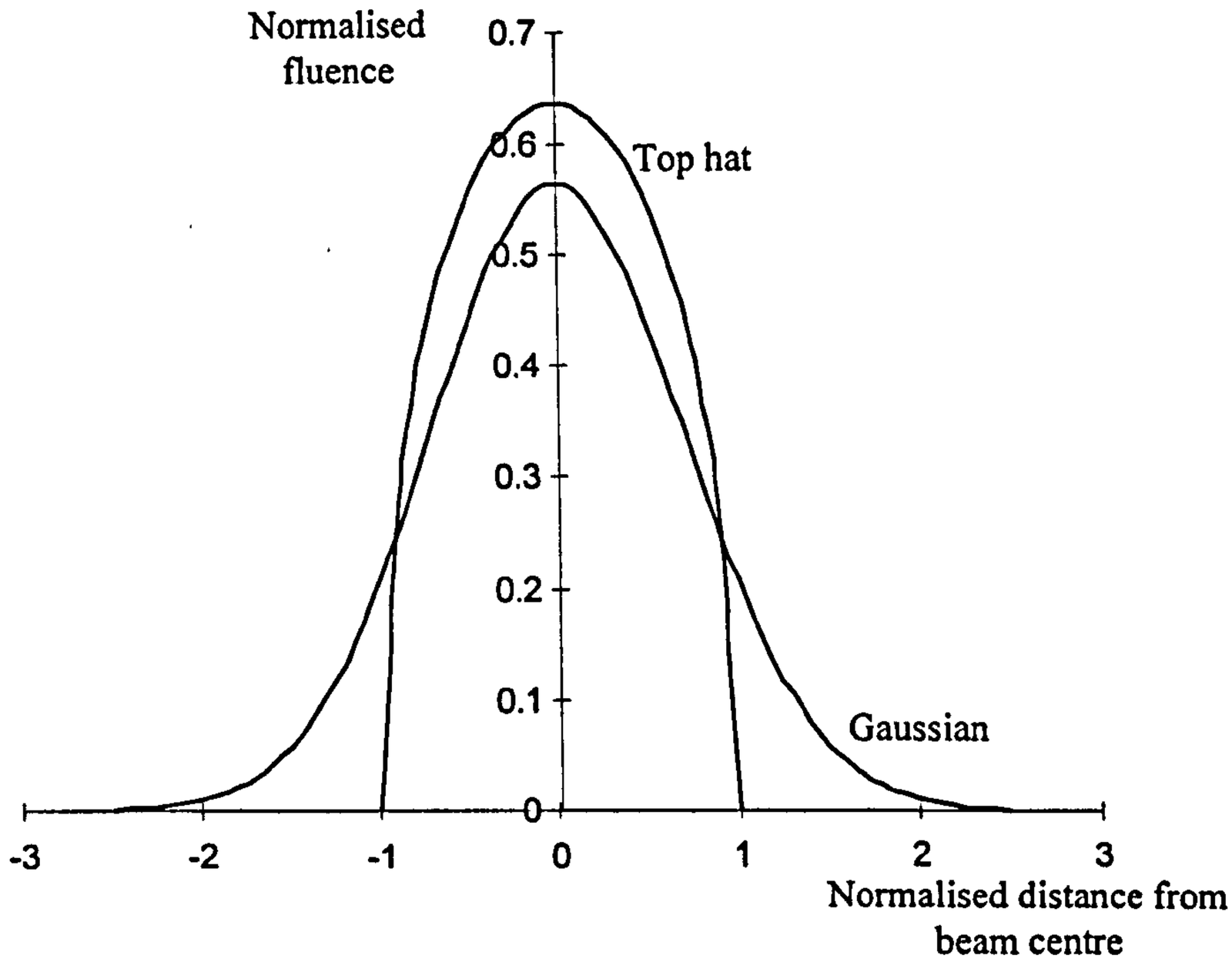

Fig. 3.10: *A sketch of the two exposure profiles for the top hat and Gaussian models.*

3.5 EFFECT OF PLATE MISALIGNMENT ON GRATING CONTRAST

Since the mirror and the beamsplitter may be considered as fixed planes, then the path followed by the point of interference will be a straight line. Obviously for the best results the plate must be placed with the plane of the resist co-linear with this line so that the normal to the plate is the bisector of the two interfering beams. Naturally if the plate is misaligned, there will be a decrease in the contrast of the pattern.

Fig. 3.11 shows the geometry of illumination for an arbitrary point P some perpendicular distance δ from the locus. Qualitatively it is obvious that the contrast is maximum along the locus and dies away asymptotically and symmetrically with perpendicular distance from this line as δ increases.

If the electric field vectors of the two beams at the point P are written as A_1 and A_2 and if there is a phase difference of ϕ between the two wavefronts, then the resultant intensity, I, at the point P will be given by:

$$I = A_1^2 + A_2^2 + 2A_1A_2\cos\phi \qquad (3.39)$$

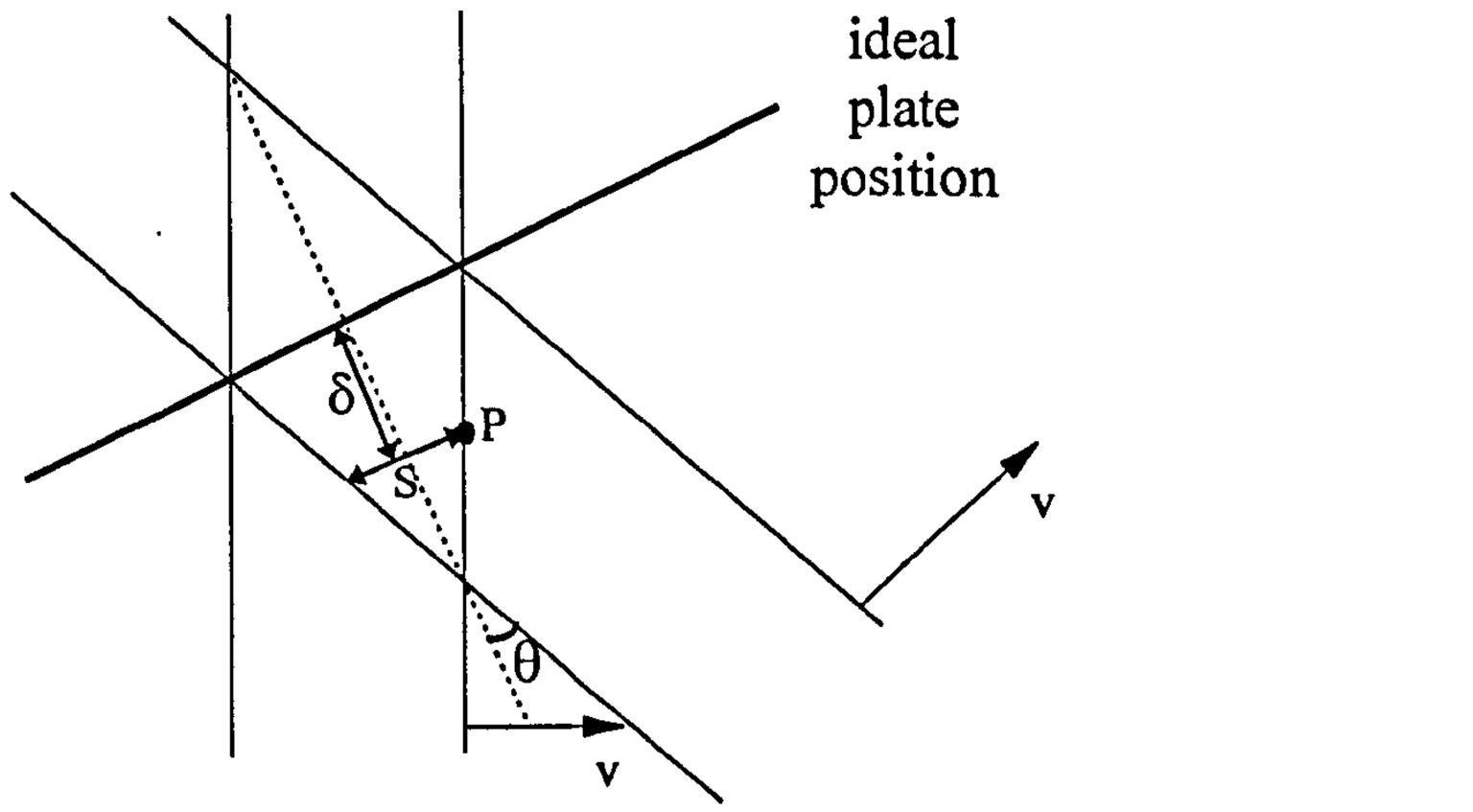

Fig. 3.11: *A sketch showing the two beams passing over a point P during the scan.*

Now the two beams are assumed to have a Gaussian profile with a spot size (electric field e^{-1} radius) of ω_0. Considering the geometry of Fig. 3.11, the effective spot size of both the beams at the point P is $b=\omega_0/\cos\theta$; however the component of the electric field vector of each beam is decreased by a factor $\cos\theta$ and so the beam may be considered to be one of width ω_0. Hence if the separation of the two beams is as indicated in Fig. 3.11, then the instantaneous intensity at P at some point in time during the scan is sketched in Fig. 3.12.

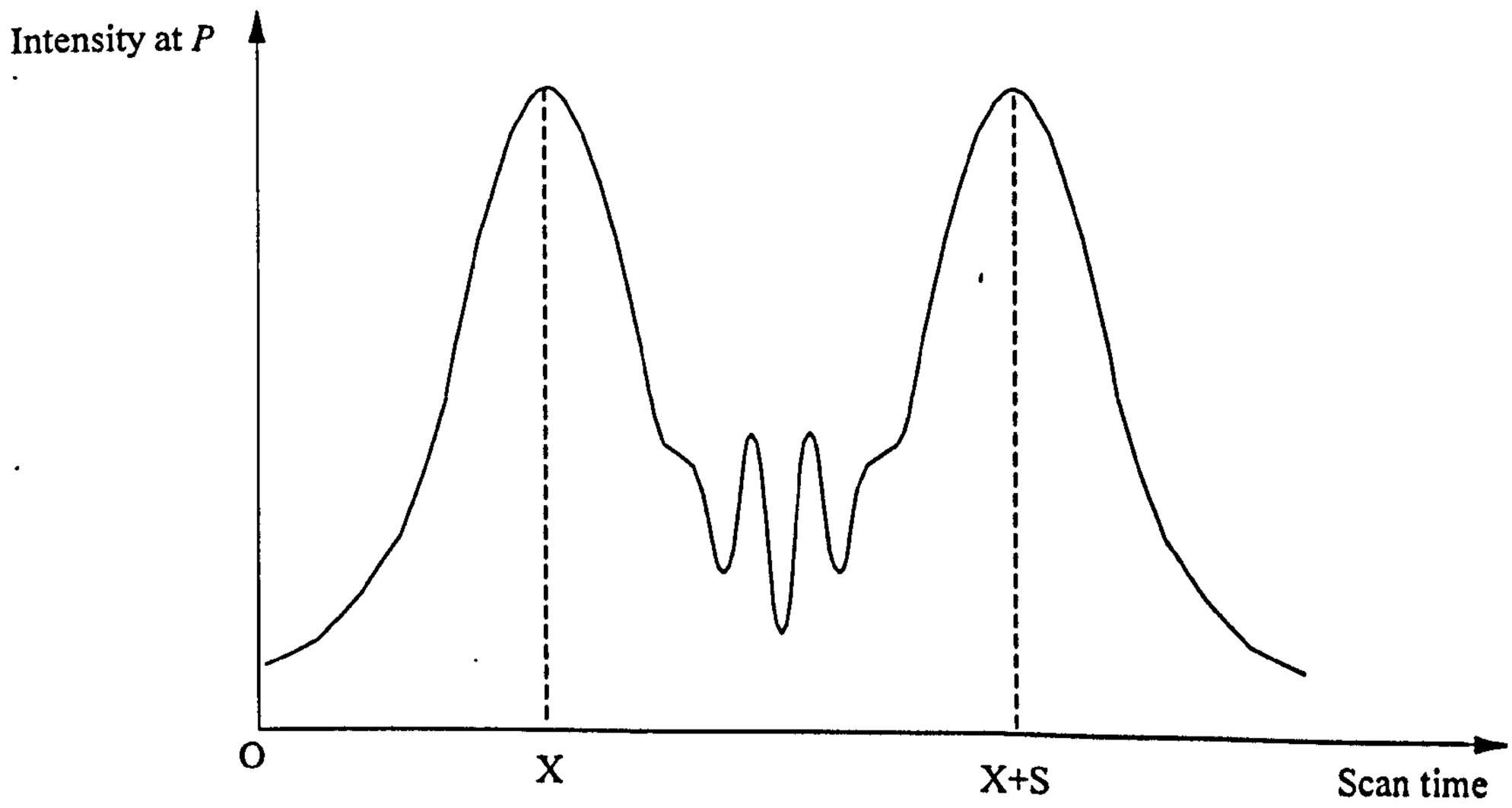

Fig. 3.12: *Schematic of the variation in intensity incident on point P during a scan.*

As the beams pass over the plate the intensity passes through two maxima corresponding to the peak intensity of each of the individual beams; as δ approaches zero, so does S and the two peaks coalesce into the usual two beam recording geometry. There will only be significant interference at points at which the intensity of the two beams is similar giving an intensity profile as sketched in Fig. 3.12. Assuming perfect coherence the intensity at P at some point during the exposure may be represented using the usual notation by:

$$I_P = \left[A_1 \exp\left(-\frac{(x-X)^2}{\omega_o^2}\right)\right]^2 + \left[A_2 \exp\left(-\frac{(x-(X+S))^2}{\omega_o^2}\right)\right]^2 + 2\cos\phi\left[A_1 A_2 \exp\left(-\frac{(x-X)^2}{\omega_o^2}\right)\exp\left(-\frac{(x-(X+S))^2}{\omega_o^2}\right)\right] \tag{3.40}$$

To find the total exposure for the point P if the whole pattern passes over the point during the scan, ζ, it is necessary to integrate the instantaneous exposure over all time, or equivalently in this case, over all space:

$$\zeta = \int_{-\infty}^{\infty} I(t)dt = \int_{-\infty}^{\infty} I(x)\frac{dx}{v} \tag{3.41}$$

The integration of the first two terms of this expression, ζ_1, is straightforward using the standard integral:

$$\int_{-\infty}^{\infty} \exp\left(-\frac{(z-D)^2}{C^2}\right)dz = C\sqrt{\pi}$$

Hence:
$$\zeta_1 = \frac{1}{v}\int_{-\infty}^{\infty} A_1^2 \exp\left(-\frac{2(x-X)^2}{\omega_o^2}\right) + A_2^2 \exp\left(-\frac{2(x-(X+S))^2}{\omega_o^2}\right)dx$$

$$\zeta_1 = \left(A_1^2 + A_2^2\right)\frac{\omega_o}{v}\sqrt{\frac{\pi}{2}} \tag{3.42}$$

The third part of the expression, ζ_2, may be re-written as a quadratic exponential: a standard integral involving the error function [3.4].

$$\zeta_2 = 2\cos\phi A_1 A_2 \int_{-\infty}^{\infty} \exp\left[-\left(\frac{2x^2 - (4X+2S)x + \left(2X^2 + 2XS + S^2\right)}{\omega_o^2}\right)\right]\frac{dx}{v} \tag{3.43}$$

$$\zeta_2 = 2\cos\phi\, A_1 A_2 \times \frac{\omega_o}{v}\sqrt{\frac{\pi}{2}}\exp\left(-\frac{S^2}{2\omega_o^2}\right) erfc\left(-\frac{(2X+S)}{\sqrt{2}\omega_o}\right) \tag{3.44}$$

The complementary error function, *erfc*, is involved in this function in order to account for the small intensity to the left of x=0 neglected in the integration. In the limit as $X \rightarrow \infty$ this light becomes negligible and the expression simplifies down to:

$$\zeta_2 = 2\cos\phi\, A_1 A_2 \frac{\omega_o}{v}\sqrt{\frac{\pi}{2}}\exp\left(-\frac{S^2}{2\omega_o^2}\right) \qquad (3.45)$$

Adding in the other two terms from (3.42) yields:

$$\zeta = \zeta_1 + \zeta_2 = \frac{\omega_o}{v}\sqrt{\frac{\pi}{2}}\left(\left(A_1^2 + A_2^2\right) + 2\cos\phi\, A_1 A_2 \exp\left(-\frac{S^2}{2\omega_o^2}\right)\right) \qquad (3.46)$$

For simplicity assume the intensities are balanced, i.e. $A_1 = A_2$, and also substitute in $a = \omega_0/\sqrt{2}$, $S = 2\delta\tan\theta$ from Fig. 3.11 and P from (3.30) to give:

$$\zeta = \frac{2P}{av\sqrt{\pi}}\left(1 + \cos\phi\exp\left(-\frac{\delta^2\tan^2\theta}{a^2}\right)\right) \qquad (3.47)$$

[Note that if δ=0, i.e. the plate is correctly aligned, then the average exposure (*cos* ϕ=0) is twice the value of (3.34), i.e. that which would be expected for two beams.] Using the measure of contrast defined by Michelson [see e.g. 3.5], the *visibility* of the fringes is given by:

$$V = \frac{I_{max} - I_{min}}{I_{max} + I_{min}} \qquad (3.48)$$

Substituting in the maximum and minimum values (*cos* ϕ = ±1) gives a visibility:

$$V = \exp\left(-\frac{\delta^2\tan^2\theta}{a^2}\right) \qquad (3.49)$$

This relationship suggests, as may be expected, that there is a line in space along which (assuming perfect coherence and power matching) the pattern recorded has perfect contrast, which falls away in a Gaussian fashion on either side. The angle of interference is important, since this is a factor in the spatial contrast function. Beams having a small angular separation will overlap in a longer region of space and so will have higher efficiencies than wider separated beams at a given distance. Thus if a plate is orientated as shown in Fig. 3.13 where there is some angle ε between the plate and the locus of optimum contrast, then the grating will have a diffraction efficiency as indicated, i.e. a highly efficient region with a symmetrical tail-off in efficiency of the grating towards each end of the grating.

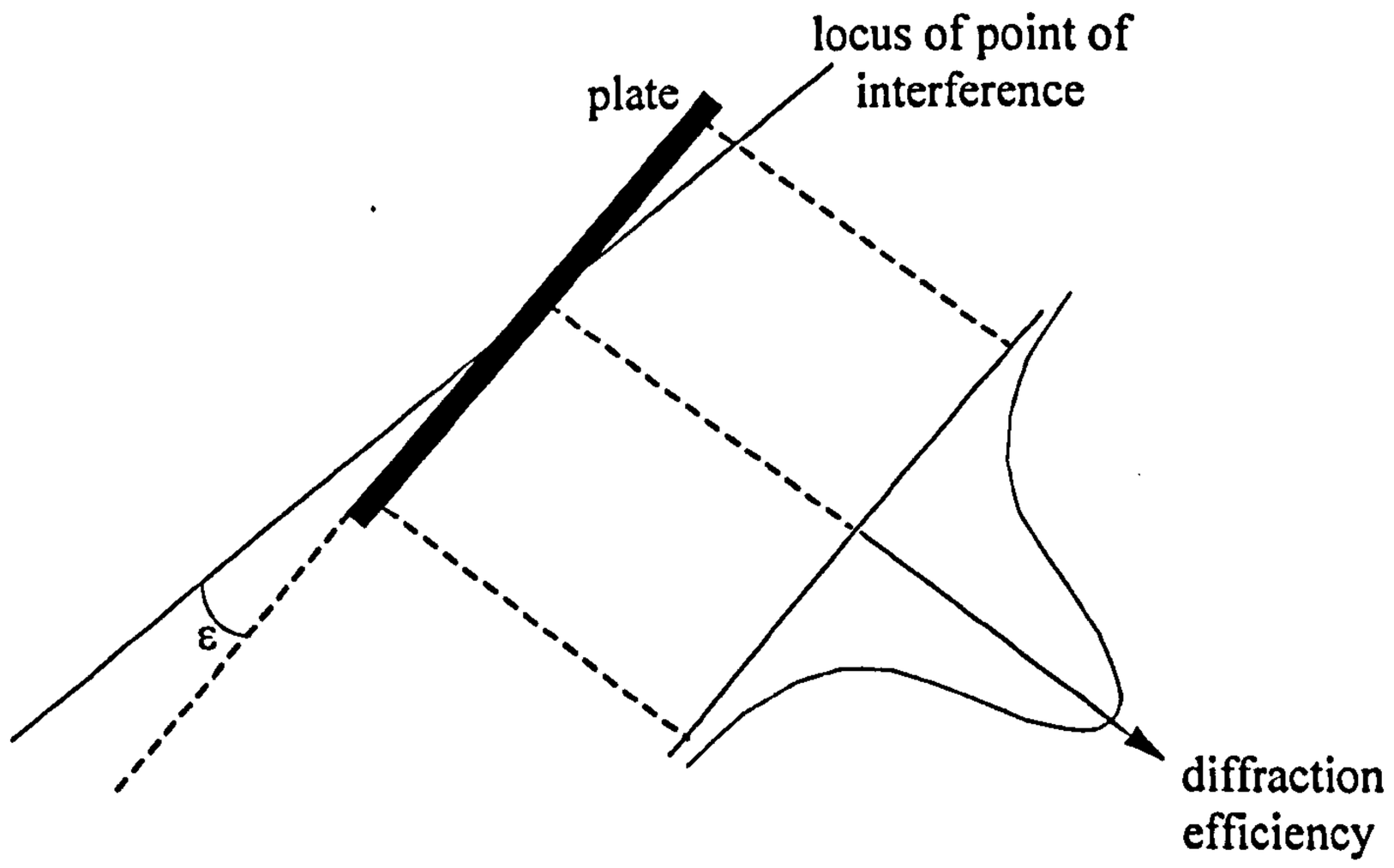

Fig. 3.13: *A sketch of the variation of diffraction efficiency for a misaligned plate.*

3.6 EXPERIMENTAL TRIALS

The experimental outline discussed in 3.3 was set up and exposures carried out as described in 3.4. For details on the actual experimental parameters the reader is referred to section 7.1.1 for information on the experimental apparatus used to obtain the holographic interference pattern and the appendix for the resist processing method, adapted for the 458 nm exposure wavelength.

3.6.1 Adoption of step and repeat exposure method

Several different micropositioning devices have been used in these experiments: chiefly an Oriel model 18009 motormike and a Time and Precision Digiplan UR3 stepper motor with a control signal derived from an Acorn 3000 microcomputer. It was observed that both micropositioners were rather coarse: vibrations in the apparatus mounted on the moving beds were obvious while the apparatus was in motion, and indeed with the stepper motor the bed vibrated even when the motor was off, as the device "hunted" to maintain its position. Because of these contrast-reducing vibrations, a step and repeat exposure method was adopted, whereby the laser was not incident on the plate while the mirror was actually moving. Thus the mirror moves a small distance, pauses to allow the apparatus to settle, and then a laser pulse is delivered, and the mirror moves again.

The micropositioner and shutter were controlled by a simple piece of electronics fabricated in the laboratory. Using a square wave input signal from a frequency generator the micropositioner was activated and the mirror moved for the duration of high part of the square wave. When the signal went low the movement ceased and the shutter opened, after a delay from a variable resistor/capacitor combination. When the pulse next went high, the shutter was closed and another shorter pause was introduced from a second variable *RC* combination to ensure that the shutter was fully closed before the next movement begins.

The total exposure resulting from this method at a single point consists of a series of flashes of length τ, with the beam itself moving some distance δx between flashes. Fig. 3.14 shows the exposure received by a point on the plate as the beam scans. The resultant exposure is essentially a sum of rectangles:

$$E_{pulse} \cong 2\left(I(t)\big|_{t=0}\Delta t + I\big|_{t=\Delta t}\Delta t + I\big|_{t=2\Delta t}\Delta t + \ldots \right. \qquad (3.50)$$

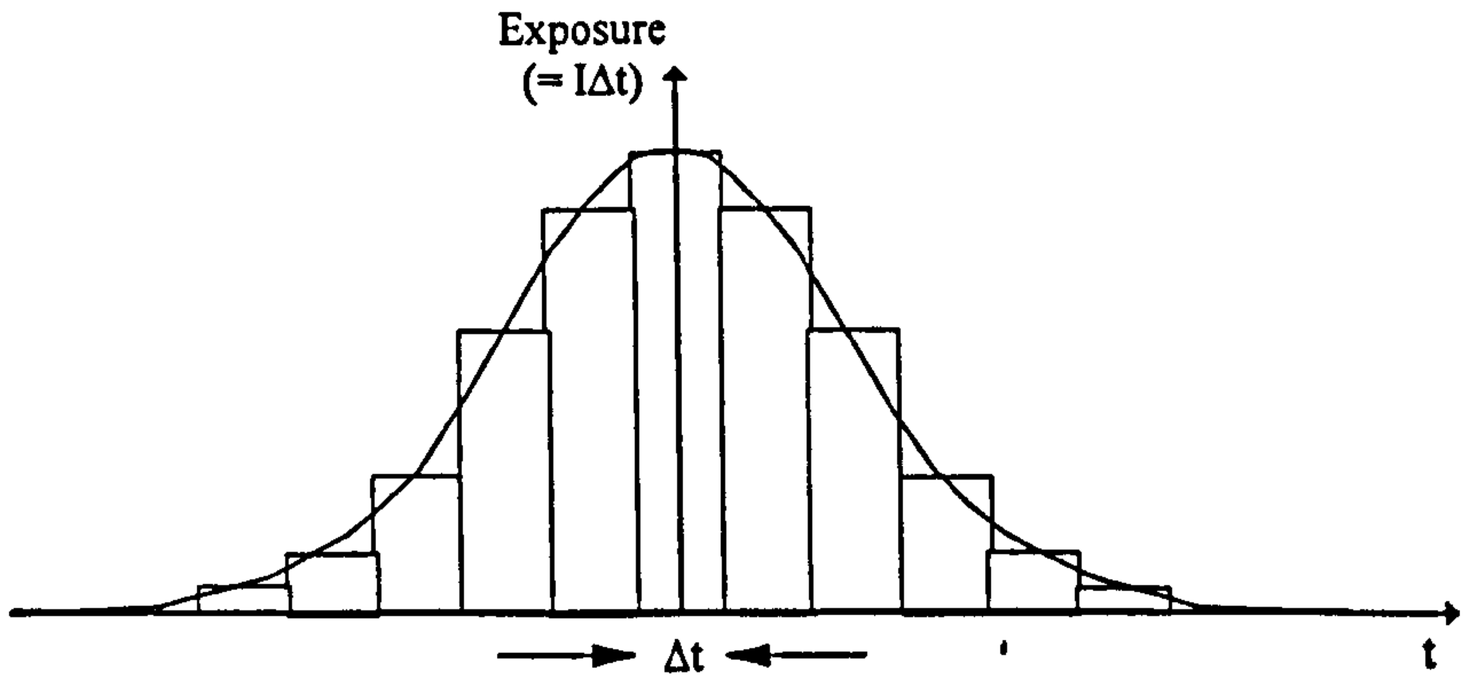

Fig. 3.14: *Showing the total exposure of the step and repeat process as a sum of rectangles. Here the spaces between pulses have been ignored since they are unimportant to the exposure calculation.*

The smaller the steps, the closer the exposure approximates a Gaussian. Naturally in the limit, as Δt tends to zero, the profile becomes that of a continuously scanned grating [3.5]. Fig. 3.14 is a schematic of the actual exposure in which the spaces between pulses have been compressed to zero. The quantity τ is a parameter related to the length of the exposure flash equivalent to a/v in (3.28).

Naturally as the exposure pulse time increases the overall exposure increases proportionately just as the inverse of the scan speed effects the total exposure.

$$E_{total} = \lim_{\Delta t \to 0} \left\{ 2 \sum_{n=0}^{\infty} I(t)\big|_{t=n\Delta t} \Delta t \right\} = \int_{-\infty}^{\infty} I_o \exp\left(-\frac{t^2}{\tau^2}\right) dt$$

$$E_{total} = \int_{-\infty}^{\infty} I_o \exp\left(-\frac{x^2}{a^2}\right) \frac{dx}{v} = \frac{I_o a}{v} \sqrt{\pi} \qquad (3.51)$$

3.6.2 Results

The step and repeat scanning method was used to expose a large number of gratings and was shown to be successful. The results using the step and repeat method look generally much tidier and more uniform than the continuously scanned gratings. However, because the micropositioner devices are rather coarse and crude, and also due to the highly non-linear nature of the resist exposure process the gratings are not very uniform along their length. Nevertheless, continuous diffraction gratings of a lengths up to 25 mm (the limit of the micropositioner movement range) were written using writing beams with $a \sim 0.5$ mm. Plate 3.1 shows an electron micrograph showing the individual grating lines.

Although in some ways this is an elegant method, there are important problems associated with it. There are two key difficulties which have been identified: firstly the length of the grating is limited by the size and perfection of the mirror and beamsplitter. Thus any grating that may be written with this method is limited in precision by the flatness of the mirror and beamsplitter (which will have a direct bearing on the recording beam wavefronts) and in length by the size of these optics. Also the method is an open loop process: once the run has started there is no way of assessing how it is progressing and so problems such as non-uniformities in exposure cannot be corrected for. Thus a different, more flexible method was sought, which would yield continuous unlimited grating.

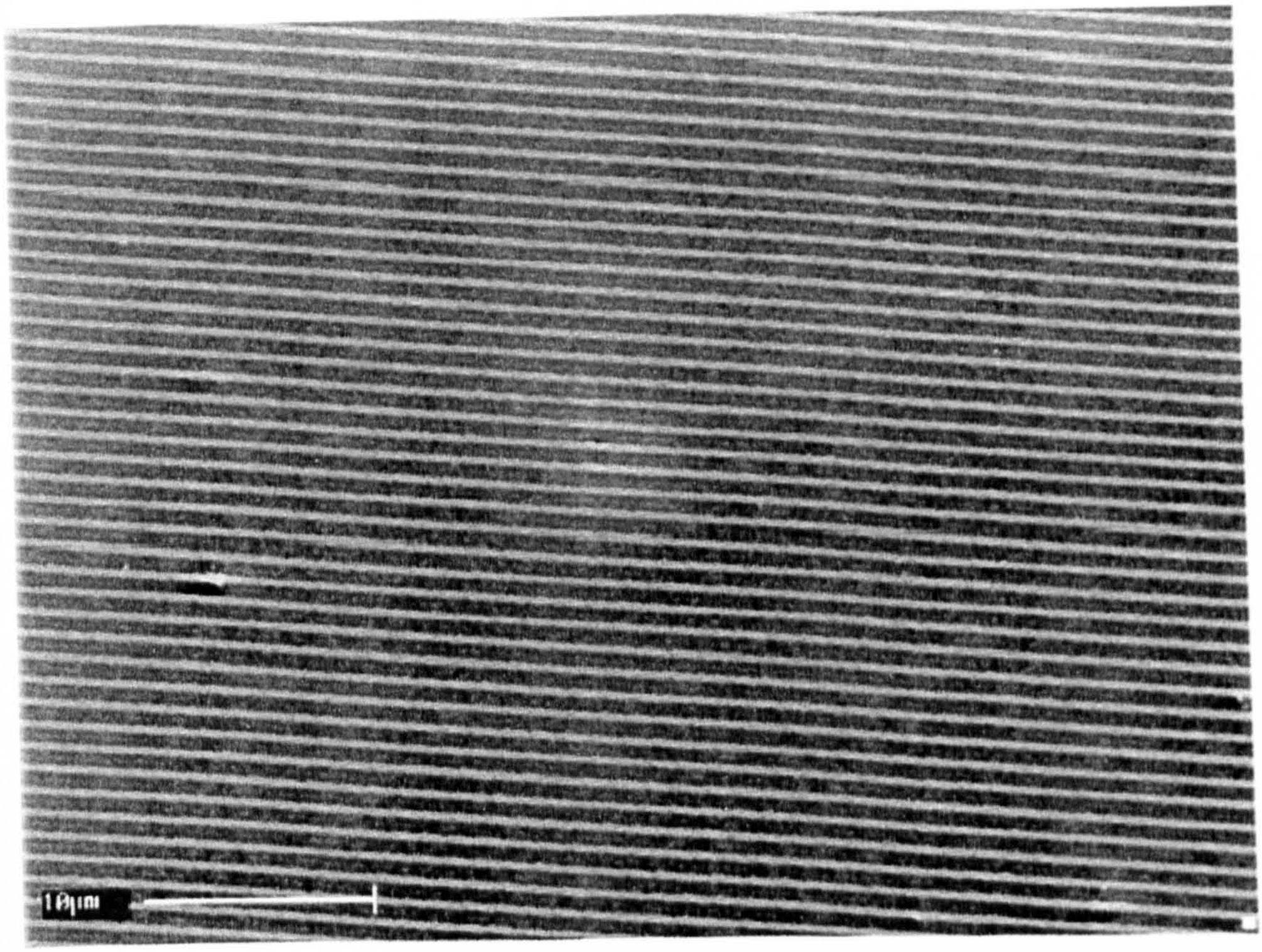

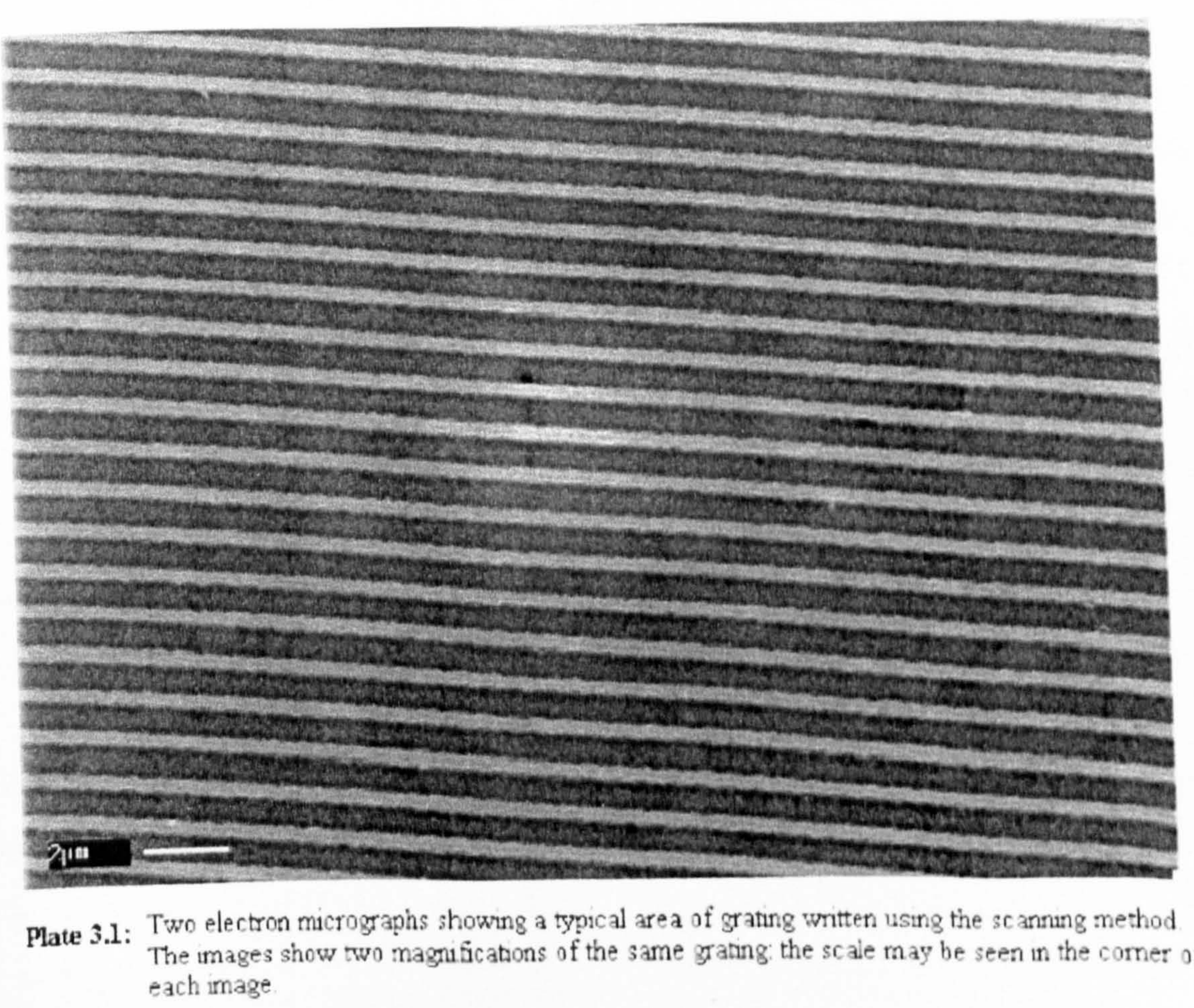

Plate 3.1: Two electron micrographs showing a typical area of grating written using the scanning method. The images show two magnifications of the same grating: the scale may be seen in the corner of each image.

REFERENCES

3.1 E.K. Popov, L.V. Tsonev and M.L. Sabeva: "Technological problems in holographic recording of plane gratings": Opt. Eng. **31**, 10, 2168 (10/92).

3.2 G. Schmahl and D. Rudolph: "Holographic diffraction gratings"; from "Progress in Optics XIV" ed. E. Wolf, North Holland (1976).

3.3 J.T. Verdeyen: "Laser electronics"; ch. 3, 2nd edition, Prentice Hall (1989).

3.4 M. Abramowitz and I.A. Stegun: "Handbook of mathematical functions"; Dover Publications (1964).

3.5 G. Stephenson: "Mathematical methods for science students"; 2nd edition, Longman (1973).

Chapter 4

METHOD FOR WRITING CONTINUOUS DIFFRACTION GRATINGS

4.1 INTRODUCTION

4.1.1 Chapter outline

The aim of this research is to find a method of writing continuous, unlimited seamless diffraction gratings in photoresist, ideally with the facility to adapt the method to write direct into optical fibre. This chapter sets out to describe the thought processes and experimentation that led to the final solution to this problem and to describe the principles behind the adopted method.

The initial work on scanned holographic gratings, described in chapter 3, was successful to an extent, but such methods will always be limited by the size and precision of the optics (i.e. the mirrors and beamsplitters) used in the apparatus. A method was sought which would use the intrinsic periodicity of the grating to replicate itself in a seamless manner and hence provide a method of writing a continuous diffraction grating: i.e. one having a length unrestricted by either the beam diameter or by any of the optics in the apparatus.

The solution arrived at uses the latent image in photoresist to derive a signal from which the position of the grating may be deduced as it is moved slowly in its own plane. This data is used to deliver an exposure pulse each time the grating has moved exactly one pitch. In this way many thousands of weak pulses are delivered, each shifted by a single pitch and the grating is extended *ad infinitum*.

In arriving at this successful method, several strategies were attempted. This chapter is intended to give an insight to these preliminary ideas and show how their development led to the final technique.

4.1.2 Two relevant phenomena

It is well known that photoresist undergoes a chemical change on exposure which results in a variation in its refractive index. In the recording of diffraction gratings this index change leads to a detectable phase grating before development: the so-called latent image. The growth of the grating may be observed in real-time by monitoring the intensity of the diffracted beams from this latent image.

If a diffraction grating is moved in its own plane in a direction perpendicular to its elements then the phase front of the nth order diffracted beam will shift by $2n\pi$ for each pitch travelled by the grating. If this diffracted beam is interfered with some isolated coherent reference beam then the relative position of the grating elements may be deduced from the interference pattern formed. It was envisaged that this positional information could be used as a trigger for an exposure pulse. Any number of weak gratings could be superimposed, each displaced by precisely one pitch so as to form a strong grating with a length independent of the size of the writing beams.

4.2 SOME THOUGHTS ON THE WAY TO A SOLUTION

In arriving at the proposed scheme, several constraining factors had to be taken into consideration. From knowledge of stitch errors in e^- beam lithography it is clear that even with state-of-the-art apparatus there are unresolved difficulties in achieving the precision required for in-fibre gratings [2.1], [2.2]. Problems arise when the absolute precision of a micropositioning device is relied on to give the sub-nanometre accuracy and uniformity which must be maintained uninterrupted along the whole length of the grating. After some thought this led to the idea that the method should involve a form of feedback in which the characteristics of the laser light and the diffraction grating itself are used in a self-governing manner, avoiding the need for ultra-precise control of the grating speed or position.

An ideal solution might be envisaged as consisting of a drum of fibre spooling onto a second drum; in doing so the fibre is moved through a region in which the core is exposed in some fashion that leads to a single continuous grating in a process which may be continued *ad infinitum*. In order for such a method to avoid the problem of stitch errors, the exposure

technique needs to have a symmetry such that there is never any step in the procedure that is not identical for every grating element. This is where the e^- beam techniques fail: despite their incredible accuracy in the determining the grating pitch for each grating field, the stitch errors between fields, although they are almost immeasurably small, lead to distinct side lobes in the grating characteristic.

Initial thoughts were thus concentrated towards somehow introducing a circular aspect to the scanning regime which was discussed in the previous chapter. Instead of a linear scan across a plane mirror, the movement (or perhaps the mirror) would be circular and so keep the size of the optics within a given limit. A length of grating would be written and then as the process continued the scanning optic would end up back where it started, but a length of grating would be written and fresh recording medium would have moved to the point of interference in a continuous process. However, even if such a geometry were conceived, this would imply a stitch error where the system completes a cycle: *unless the cycle were completed for every single element of the grating.*

A famous experiment suggested a method of grating writing in which the exposure consists of a large number of pulses which are triggered at times when the grating is correctly aligned with the exposure pattern. In this classic experiment in 1849 Fizeau measured the speed of light using a spinning toothed wheel to generate a series of pulses of light, which were reflected back to the wheel from a distant mirror [4.1]. The reflected pulse would only be observed if it returned to the wheel at a time when there was a notch rather then a cog at the point of observation. By varying the frequencies of rotation he deduced the time taken for the light to traverse the path and hence arrived at a value for c.

Consider a process in which the recording media moves past some given point where a pulsed interference pattern is formed which may be switched on and off as rapidly as required. If it were possible to give pulses of exposure at intervals such that the grating being written moves exactly one pitch between pulses then the exposing lines and spaces of the exposure pattern would overlap with those that had already been written. The exposure would reinforce the existing grating and extend it by one pitch. In this way it can be conceived that a continuous uniform and seamless grating may be written.

Naturally, the difficulty with such a method would be the very accurate control required on the delivery of the exposure flashes. As has been mentioned, the micropositioner itself cannot be relied on for such precision of either speed or position; in other words it is not sufficiently precise to trigger the exposure pulses by independently monitoring the absolute grating position. However it is well known that gratings lend themselves to high precision measurements, for instance utilising the moiré effect of two or more crossed gratings (see e.g. [4.2], [4.3]). An ideal solution would seem to be *to use the grating itself to govern its own writing* via some form of optical feedback.

It has been known for many years that recording media which require a development process, such as silver halide or photoresist, possess an undeveloped or "latent" image once they have been exposed. This phenomenon has been associated with the presence of four grain developable clusters of silver in silver halide emulsions [4.4] which lead to a measurable image, albeit a very tiny one: typical diffraction efficiencies are only around 10^{-8} [4.5]. Once the emulsion is developed, however, the amplification of these tiny seed regions of silver can exceed 10^{9} [4.6], leading to the tiny observable black specks which make up the image in a photograph.

In DQN photoresist the latent image is associated with the destruction of the DQ inhibitor molecule, which leads to a measurable change in refractive index of the medium (see section 5.1). It was proposed to use the latent image of the recorded grating in photoresist, in which the effect is several orders of magnitude greater than is found with silver halide, to assess the relative grating position.

When a beam of light is diffracted from a grating, the phase of the wavefront of the beam is dependent on the exact spatial position of the grating elements. If the grating is moved uniformly a distance of one pitch, then the phase front of the nth order diffracted beam will be uniformly changed by $2n\pi$: i.e. when the grating is back where it started so is the phase of the diffracted beam.

Fig. 4.1 shows the usual elementary method of visualising the formation of the diffracted beam; for clarity only one set of first order diffracted wavefronts are shown. In this model,

each of the elementary slits in the diffraction grating acts as a source of Huygens-Fresnel secondary wavelets, emitting spherical wavefronts coherently in the forward direction. In certain directions these wavelets interfere constructively and give rise to the diffracted beams.

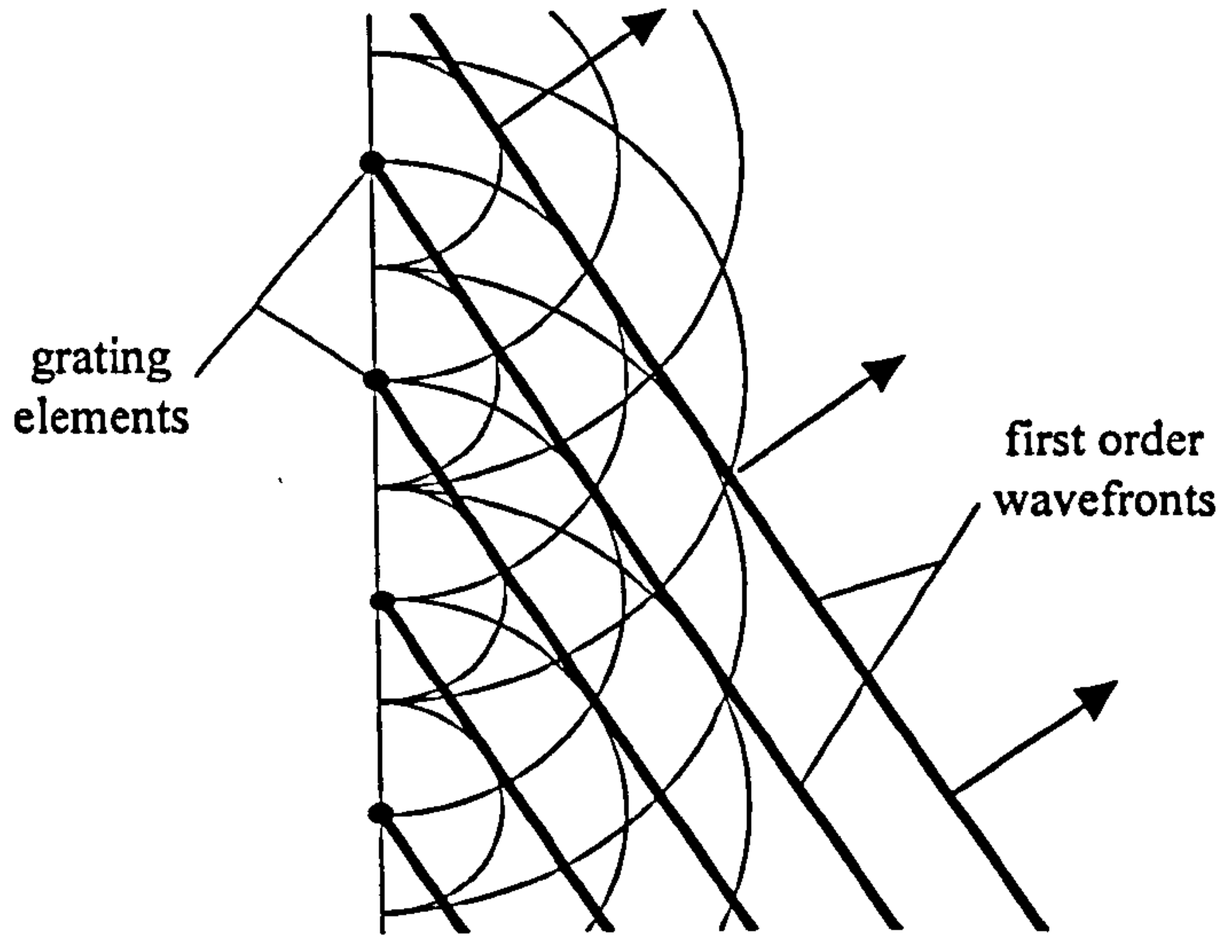

Fig. 4.1: *A sketch showing an elementary method of visualising the formation of diffracted beams. The dots represent the grating elements and the circles the Huygens secondary wavelets. These interfere constructively in certain directions to give a diffracted beam: the thick straight lines represent the first order wavefronts.*

If the grating is then moved some distance x in its own plane in a direction normal to its elements, then the sources of these wavelets will be shifted, as shown in Fig. 4.2. This diagram shows the original diffracted wavefronts as the thick black lines. Neglecting relativistic effects, the position of the sources of these diffracted wavefronts will be shifted by a distance x.

It can be seen that this lateral shift in position will result in the wavefronts being "dragged" forward by a distance p in the direction of the diffracted beam. At a distance far from the grating this will be seen as a change in phase of:

$$\Delta\phi = \frac{2\pi}{\lambda} p = \frac{2\pi}{\lambda} x \sin\theta \qquad (4.1)$$

But from the elementary grating equation: $m\lambda = d\sin\theta$ (4.2)

Hence for the first order beam (m =1): $$\Delta\phi = 2\pi \frac{x}{d} \qquad (4.3)$$

This simple result is the basis of the proposed method.

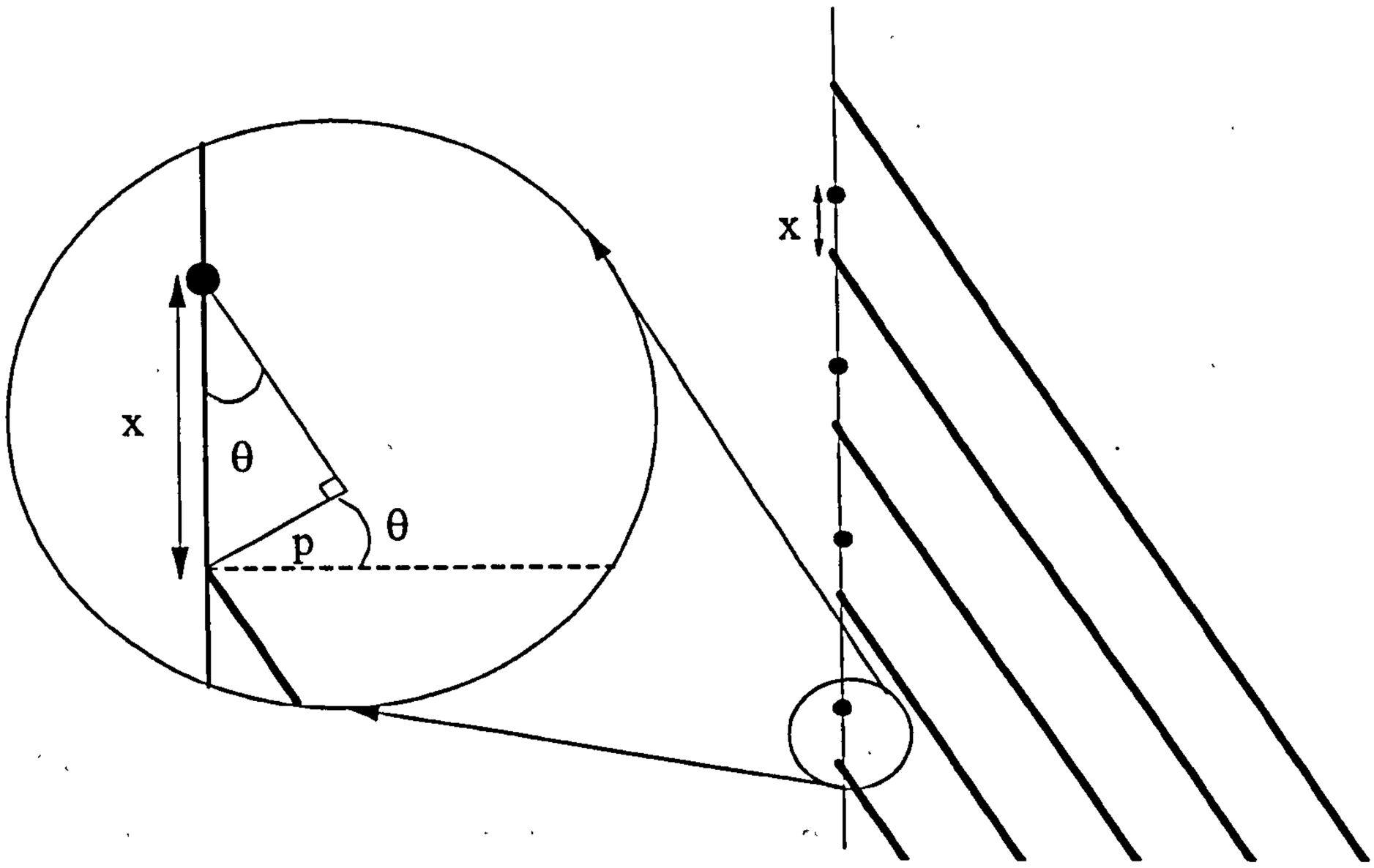

Fig. 4.2: *Showing the geometry of the wavefronts when the grating is moved. The thick black lines show the wavefronts of the diffracted beam before the movement occurs. The grating is then moved a distance* **x**. *The wavefronts will be "dragged" with the grating, with the result that the phase will change due to the change in optical path, p.*

4.3 INITIAL EXPERIMENTS USING MOIRE PATTERNS

4.3.1 Moiré patterns and their use in metrology

The moiré effect is observed frequently in everyday life in situations where periodic structures of alternate opaque and transparent zones (i.e. transmission gratings) of the same or similar pitch are overlapped. The effect is commonly seen, for instance, in neighbouring picket fences or overlapping nets or cloths; indeed the word "moiré" comes from a type of silk in which these patterns may be observed when it is folded. These striking patterns are caused by the partial overlapping of the threads and spaces within the material. In the more general case of the overlap of periodic structures it is apparent that in some regions the dark portions may overlap, and the result is a medium with a transmissivity similar to that of a single grating

structure. In other areas the transparent regions could be obscured to some extent by the opaque ones and the result is a more opaque medium. If the media are not plane or parallel then this gives rise to a series of light and dark bands which constitute the moiré pattern.

The first scientific study of the effect was given by Lord Rayleigh in 1874 [4.7] and since then moiré patterns have found applications in areas such as metrology and interferometry. Naturally the coarse patterns described above have analogies in smaller periodic structures such as diffraction gratings. Similarly light itself is a periodic entity and interference effects may be argued to be a phase analogue of moiré patterns [4.8]. Furthermore these patterns are not restricted to amplitude absorption gratings: a phase analogue of moiré may be observed using two overlapping phase gratings. It is just such a pattern that was considered for use in this initial proposal for a continuous grating writing method.

In metrology moiré patterns are used to obtain information on positional displacement. A typical example is the case in which two identical absorption gratings are overlapped; radiation from a light source on one side of the grating pair is received by a detector placed on the opposite side. If one grating is moved relative to the other then the intensity received at the detector passes through a series of maxima and minima corresponding to the variation in the overlap of the transparent and opaque regions of the gratings. The number of cycles measured gives the number of pitches which the grating has moved and hence its spatial displacement may be calculated.

Interpolative techniques can be used to accurately estimate the fraction of a pitch moved, giving precision above that of the grating pitch; a technique used very effectively, for instance, on the Anorad CNC-2000 micropositioner to obtain positional control to ~0.1 μm from two gratings of pitch 10 μm. By using a quadrature signal method it is also possible to deduce the direction of movement giving a versatile spatial position measurement device [4.9]. The gratings used in such micropositioners tend to be absorption gratings of a relatively coarse pitch; a typical working example might be two identical 10 μm absorption gratings with 100 μm spacing between them. Once the pitch of the grating gets much smaller than 8-10 μm diffraction effects begin to obscure the "pure" moiré patterns [4.2].

4.3.2 The use of moiré phase analogue for writing a continuous grating

In one of the first trials in this phase of work the method adopted was as follows. The first order diffracted beam from the latent image of a grating undergoing exposure is aligned with the first order beam from a control grating with the same pitch and efficiency, forming the characteristic "bull's eye" pattern in the observation plane. If the grating which is being written is then moved in its own plane in a direction normal to its elements, then the phase shift described by (4.3) will be imposed on the first order beam. However, the control grating will be unaffected by this movement, and consequently the interference pattern will change according to the phase change imposed by the movement.

If first order beams are used to form the interference pattern then the change will be a shift of one fringe for each pitch that the grating is moved. If, for instance, there happened to be a maximum at the centre of the pattern before the movement began then the circular fringes would be observed to collapse into the centre (or emerge outwards, depending on the direction of movement) to give a central dark fringe, and return to a bright again for each pitch moved by the grating. Thus if the intensity of a small portion of the central fringe of the pattern were to be measured then it would vary sinusoidally if the grating moved uniformly.

The crux of this method is to trigger very brief pulses of exposure at points in the cycle corresponding to displacements of an integer number of pitches from the initial grating position. Unlike the scanning method discussed in the previous chapter, this method is free from the constraints of the size of the optical components, indeed the two beam holographic method of forming the interference pattern is non-essential. Several of the methods described in chapter 2 could be used to form the pattern including the use of a phase mask or prism instead of the traditional holographic set up. Furthermore, although this experimental work used photoresist, any recording medium which forms some type of image during the writing process may be adopted so that direct in-fibre writing could be possible.

The essence of this method is that it uses the grating itself, that is the undeveloped latent image in the photoresist, to assess its own position relative to the second grating. This positional information can be used to detect when the gratings are exactly aligned as one grating is moved relative to the other, and this can be used as the trigger for a laser exposure

pulse. In this way a grating of theoretically unlimited length may be written by the superposition of a great number of weak exposure pulses with each pulse displaced by exactly one grating pitch.

One early experimental set up which was tried is sketched in Fig. 4.3: the grating is illuminated with laser radiation of a wavelength at which the recording media is insensitive, e.g. for AZ1350 photoresist HeNe at 632.8 nm would be an obvious choice. A phase grating is written, in this case using a two beam holographic method, and the phase analogue moiré pattern is incident on a detector which feeds its data into some form of analysis electronics. Then the grating is moved and the output from the electronics is used to control an acousto-optic modulator, which fires and exposes the grating at points when the phase of the pattern is the same as before the grating was moved.

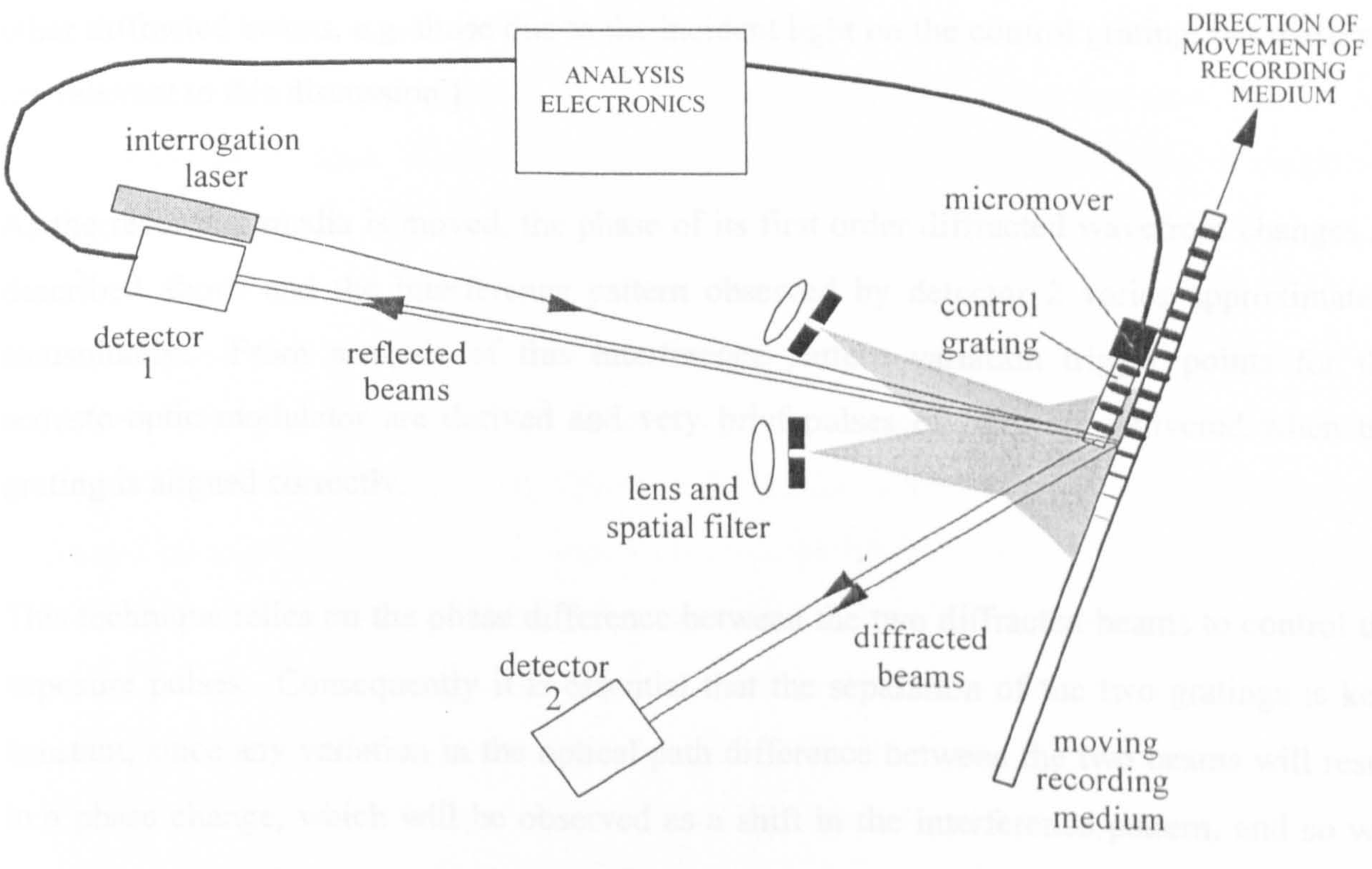

Fig. 4.3: *An example of a proposed experimental set up using the ideas described in the text. Only relevant diffracted and reflected beams are shown.*

The set up consists of three main parts: the apparatus to provide the interference pattern to be imprinted on the fibre, apparatus to detect the interference pattern and to trigger the exposure pulses and a fringe locker, to ensure that the distance between the two gratings is kept constant. The fringe locker is key to the success of the method, since variations in grating spacing will effect the phase of the triggering pattern; this is discussed in some detail in chapter 6.

The interrogation laser beam is almost normally incident on the gratings. Most of the incident light passes directly through the control grating and onto the grating being written: some of this light is diffracted from the latent image towards detector 2. The remainder of the incident light is reflected back from the recording medium substrate (in this case chrome) and is diffracted towards detector 2 by the control grating, which is designed to have a similar efficiency to the latent grating in the recording media and so result in a good contrast interference pattern when these two diffracted beams are brought together. [There will be other diffracted beams, e.g. those due to the incident light on the control grating, but these are not relevant to this discussion.]

As the recording media is moved, the phase of its first order diffracted wavefront changes as described above and the interference pattern observed by detector 2 varies approximately sinusoidally. From analysis of this interference pattern variation trigger points for the acousto-optic modulator are derived and very brief pulses of light are delivered when the grating is aligned correctly.

This technique relies on the phase difference between the two diffracted beams to control the exposure pulses. Consequently it is essential that the separation of the two gratings is kept constant, since any variation in the optical path difference between the two beams will result in a phase change, which will be observed as a shift in the interference pattern, and so will cause exposure pulses to be put down in the wrong position. To guard against this, the beams reflected specularly from the two gratings are brought together to form a second interference pattern. This pattern is monitored by detector 1, and a second set of analysis electronics is used to control a micropositioning device, for instance a piezo electric actuator, which adjusts

the separation of the gratings by moving the small control grating and thus keeps the fringe pattern stable.

In these initial experimental trials this fringe locker was not constructed since the work advanced onto the next phase. Consequently no gratings were written using this early design. However, the remainder of the apparatus was assembled and the trigger pattern that was predicted was observed.

4.4 IMPROVED METHOD TO WRITE CONTINUOUS GRATINGS

The method described in the previous section was conceived whilst pursuing the possibility of using moiré patterns to monitor the grating position. It was this idea of moiré which led to the adoption of the control grating to derive the moiré phase analogue signal. However if one takes a step back it is apparent that the only purpose of the second grating is to provide a reference signal with which to compare the diffracted beam. This function could just as well be provided by a beam diverted from the incident interrogation beam in a simplified arrangement.

This simplified method relies on the interference pattern formed by the superposition of the diffracted first order beam from the latent image grating being written and a fringe locked reference beam. Fig. 4.4 shows an prototype design for monitoring the grating position: the diffracted beam is brought to interference with a reference beam diverted from a beam splitter. The central circular fringe observed at the detector will have a phase dependent on both the grating phase (i.e. the grating fringe position) and on the difference between the diffracted beam path, *ABC*, and the reference beam path *AC*. If the grating moves with a constant speed, the intensity of this central fringe varies sinusoidally with a frequency dependent on the speed of the movement.

However, in a practical realisation of such a set up, the effects of the finite precision of alignment of the system must be taken into consideration just as with the moiré method. If the recording medium has any component of movement perpendicular to that indicated in Fig.

4.4 then there will be a path length change imposed onto path *ABC*, and consequently a phase change in the pattern at the detector. This phase change would be indistinguishable from that due to the moving grating fringes.

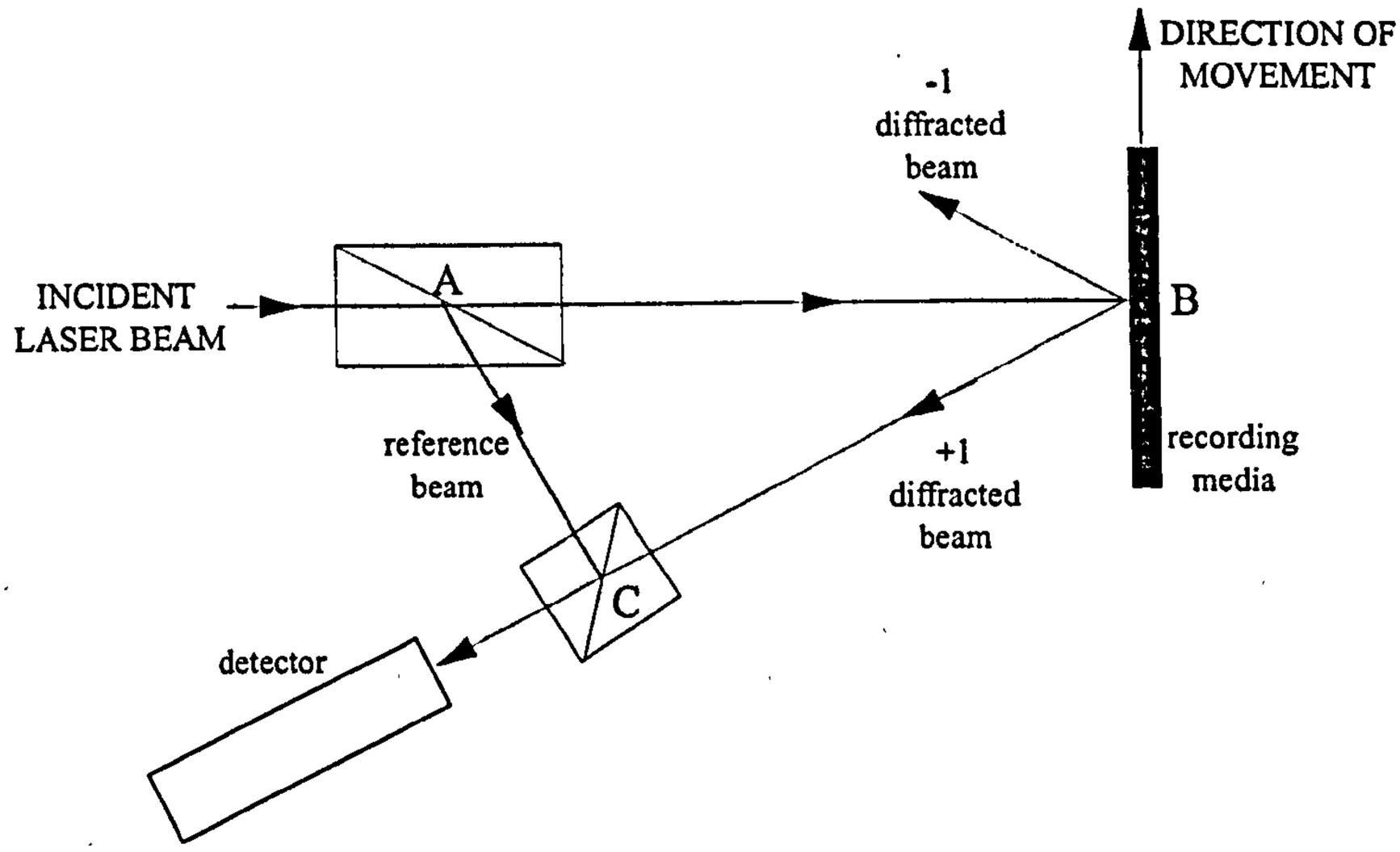

Fig. 4.4: *A basic design for triggering the exposure pulses.*

This has very serious consequences for the grating writing process and indicates the major weakness of using a single *relative* phase signal to determine position: there is no *absolute* information. If the transverse movement of the plate approaches $\lambda/4$ then the path difference is changed by $\sim\lambda/2$: an error of $\sim\pi$ is introduced into the detected signal and the exposure pulses will be put down in exactly the wrong place. The grating will be erased.

Thus with HeNe light, a transverse error of ~160 nm is sufficient to render the phase information worse than useless. Clearly some form of active positional control device was required to keep the recording medium in the same plane during the exposure, and so the design of an appropriate feed back fringe locker was investigated: this successful work is discussed in chapter 6.

4.5 FRINGE CONTRAST GIVEN FINITE ERROR IN PULSE TRIGGERING

It is a well known result that the intensity of the interference pattern *I(x)* due to two collimated beams with electric field vector a_o and Ba_o (i.e. with a beam ratio of B) interfering at some angle 2θ may be written:

$$I(x) = a_o^2\left[\left(1+B^2\right)+2B\cos\left(\frac{2\pi x}{\Lambda}\right)\right] \tag{4.4}$$

where Λ, the grating pitch, is given by : $$\Lambda = \frac{\lambda}{2\sin\theta} \tag{4.5}$$

In the exposure technique proposed above, the resulting pattern at the plate will be an incoherent sum of many such pulses superimposed upon one other. Given that there will be some error in the trigger position of the exposure pulses, it is assumed that there will be a clustering of the pulses around the correct position. This random error in triggering position may be approximated by assuming the pulses are put down in a Gaussian distribution around the correct position.

The probability density function for the Gaussian distribution with variance σ^2 and mean m is given by [4.10]:

$$P(t) = \frac{1}{\sigma\sqrt{2\pi}}\exp\left[-\frac{(t-m)^2}{2\sigma^2}\right] \tag{4.6}$$

Thus the pattern recorded in the plate will be a weighted sum of all the exposure pulses:

$$I_T(x) = \sum_n P_n I_n(x) \tag{4.7}$$

If the error in position is ξ, then from (4.4):

$$I_\xi(x) = a_o^2\left\{\left(1+B^2\right)+2B\cos\left[\frac{2\pi}{\Lambda}(x+\xi)\right]\right\} \tag{4.8}$$

and from (4.6): $$P_\xi = \frac{1}{\sigma\sqrt{2\pi}}\exp\left(-\frac{(\xi-m)^2}{2\sigma^2}\right) \tag{4.9}$$

In the limit as $n\to\infty$ and substituting in (4.8) and (4.9), (4.7) becomes:

$$I(x) = \frac{a_o^2}{\sigma\sqrt{2\pi}}\int_{-\infty}^{\infty}\exp\left[-\frac{(\xi-m)^2}{2\sigma^2}\right]\left\{\left(1+B^2\right)+2B\cos\left[\frac{2\pi}{\Lambda}(x+\xi)\right]\right\}d\xi \tag{4.10}$$

It is assumed that the mean of the distribution is zero ($m = 0$), i.e. the pulses are distributed equally around the correct trigger position, leading to:

$$I(x)=\frac{a_o^2}{\sigma\sqrt{2\pi}}\int_{-\infty}^{\infty}\left\{\begin{array}{c}\left(1+B^2\right)\exp\left(-\frac{\xi^2}{2\sigma^2}\right)\\ +2B\cos\left(\frac{2\pi x}{\Lambda}\right)\exp\left(-\frac{\xi^2}{2\sigma^2}\right)\cos\left(\frac{2\pi\xi}{\Lambda}\right)\\ -2B\sin\left(\frac{2\pi x}{\Lambda}\right)\exp\left(-\frac{\xi^2}{2\sigma^2}\right)\sin\left(\frac{2\pi\xi}{\Lambda}\right)\end{array}\right\}d\xi \tag{4.11}$$

This equation may be solved using the following standard results [4.10]:

$$\int_0^{\infty}\exp\left(-at^2\right)dt=\frac{1}{2}\sqrt{\frac{\pi}{a}} \tag{4.12}$$

$$\int_0^{\infty}\exp\left(-at^2\right)\cos(2bt)dt=\frac{1}{2}\sqrt{\frac{\pi}{a}}\exp\left(-\frac{b^2}{a}\right) \tag{4.13}$$

$$\int_0^{\infty}\exp\left(-at^2\right)\sin(2bt)dt=\frac{1}{\sqrt{a}}\exp\left(-\frac{b^2}{a}\right)\int_0^{b/\sqrt{a}}\exp\left(t^2\right)dt \tag{4.14}$$

The first two terms to be integrated in (4.11) are symmetrical about the origin whilst the third is anti-symmetric, and totals zero when integrated over all space, leaving:

$$I(x)=a_o^2\left\{\left(1+B^2\right)+2B\exp\left(-2\left(\frac{\sigma\pi}{\Lambda}\right)^2\right)\cos\left(\frac{2\pi x}{\Lambda}\right)\right\} \tag{4.15}$$

Thus on the assumption that the pulses, on average, are triggered at the correct position, the recorded pattern will be a cosinusoidal grating of pitch Λ with fringe visibility (as defined in (3.48)):

$$V=\left(\frac{2B}{1+B^2}\right)\exp\left[-2\left(\frac{\sigma\pi}{\Lambda}\right)^2\right] \tag{4.16}$$

This makes physical sense: the contrast is reduced as the standard deviation, σ, increases and also as the grating pitch Λ is reduced, i.e. the pattern becomes more sensitive to error as the pitch is made finer. Fig. 4.5 shows a graph of the visibility of the fringes as a function of σ for three beam ratios and Fig. 4.6 shows a few grating profiles for different values of σ.

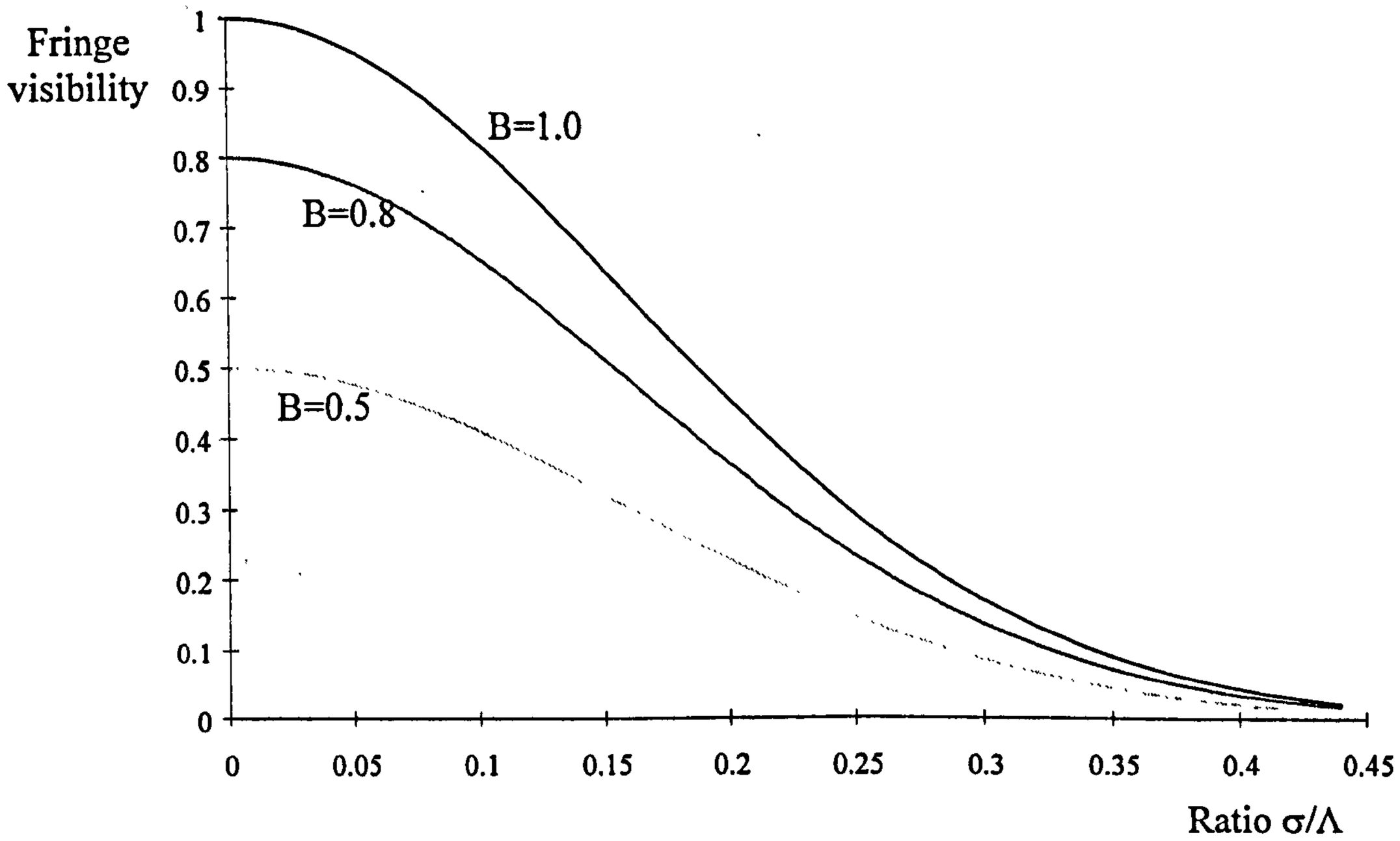

Fig. 4.5: *A graph of fringe visibility versus standard deviation of pulse position in the multiple exposure regime for beam ratios 1.0, 0.8 and 0.5.*

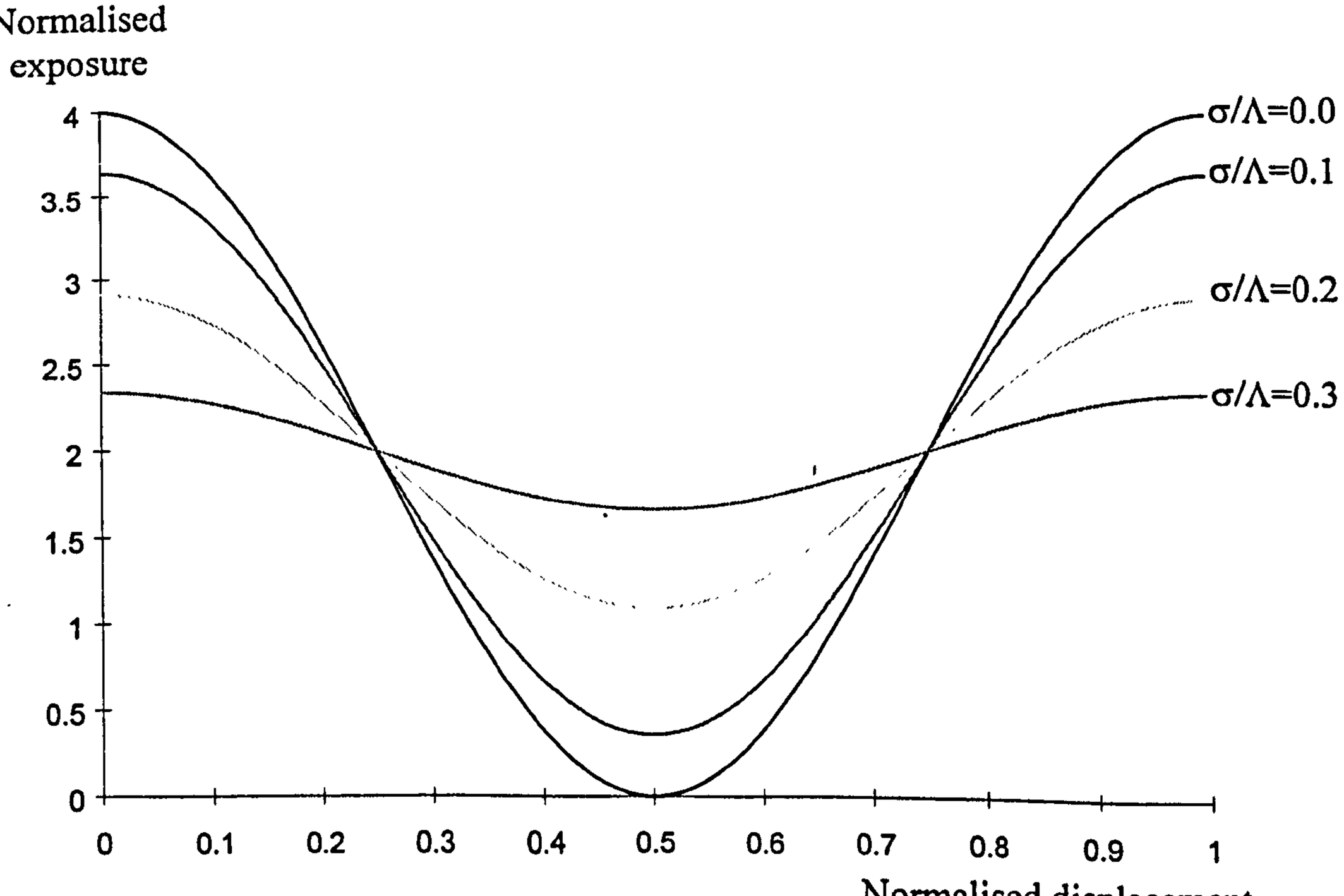

Fig. 4.6: *Some theoretical grating profiles using the above model for the multiple exposure regime. The beam ratio, B, is taken as unity .*

REFERENCES

4.1 R.M. Eisberg: "Fundamentals of modern physics"; Wiley (1961).

4.2 A.J. Durelli and V.J. Parks: "Moiré analysis of strain"; Prentice Hall (1970).

4.3 D.C. Williams: "Optical methods in engineering metrology"; Chapman and Hall (1993).

4.4 L.P. Clerc: "Photography: theory and practice"; 2nd ed., Pitman (1937).

4.5 A.A. Benken and D. I. Stasel'ko: "Light in the formation of a latent image by pulsed laser radiation"; Sov. Phys. Tech. Phys. **27** (7), 896, July 1982.

4.6 H.I. Bjelkhagen: "Silver-halide recording materials for holography and their processing"; Springer-Verlag Vol. 66 (1995).

4.7 Lord Rayleigh: "On the manufacture and theory of diffraction gratings"; Scientific Papers **1**, 209: Phil Mag. **47** 81-93 and 193-205 (1874).

4.8 N. Abramson: "Light in flight *or* the holodiagram"; SPIE Opt. Eng. Press (1996).

4.9 A. Ernst: "Digital linear and angular metrology"; Verlag Moderne Industrie.

4.10 M. Abramowitz and I. Stegun: "Handbook of mathematical functions"; Dover Publications (1965).

Chapter 5

A STUDY OF LATENT IMAGE GROWTH IN AZ1350 PHOTORESIST

5.1 LATENT IMAGE FORMATION IN AZ1350 PHOTORESIST

When photoresist is exposed to electromagnetic radiation within a certain frequency range, a photochemical reaction occurs which results in a change in its refractive index. This physical change in the resist composition leads to the formation of a weak exposure pattern in the resist before it is developed: this is known as the latent image.

The presence of a latent image is well known in other holographic recording media. In silver halide emulsions it is due to the formation of "developable clusters" in the exposed material consisting of a few silver atoms [5.1]. Such clusters act as catalytic centres for the conversion of silver halide to silver by the action of a reducing agent (the developer) forming a grain of silver. The resulting grain may be up to 10^9 times as large as the original cluster, which can initially be as small as four silver atoms [4.6]. Despite the minuteness of the effect, important and useful information has been deduced from studies of the latent image in silver halide, including an examination of the different stages in the mechanism of photolytic silver formation [4.5], [5.2] and assessment the quality of a recording material [5.3].

In photoresist the latent image is rather stronger: when a resist plate is exposed to a diffraction grating pattern, for instance that formed from the overlap of two coherent laser beams, the sinusoidal intensity pattern results in a corresponding similar refractive index profile in the resist. This periodic index variation acts as a weak diffraction grating: the so-called latent image, and it is this weak grating, which exists *before development* that is exploited in this method of diffraction grating recording. It is proposed to use the weak diffracted beam from the latent image to deduce the relative position of the grating being written, as has been described in the previous chapter.

The photoresist used in these experiments was Shipley AZ1350 resist; both spin coated onto Hoya chromoplates and dip coated onto Towne Technologies ferroxoplate. This resist is one

of the family of DQN resists which are formed from two main components: an alkali-soluble phenolic-formaldehyde resin (known as a "novolak" or "N" resin), throughout which is dispersed a smaller photoactive diazoquinone (DQ) ester [5.4].

The presence of the hydrophobic DQ molecule in the alkali-soluble novolak resin dramatically reduces its dissolution rate from ~15 nm s^{-1} to ~0.1-0.2 nm s^{-1} (using a typical development technique) [5.5]. However, once exposed to light with a wavelength between ~300 - 460 nm the DQ inhibitor is destroyed in a photolytic reaction releasing nitrogen gas and generating a carbene through Wolff rearrangement, which rapidly rearranges itself to form a ketene. This molecule reacts with adsorbed moisture, thought to be held within the resin by hydrogen bonds [5.6], to form an indene acid: the reaction mechanism is sketched in Fig. 5.1.

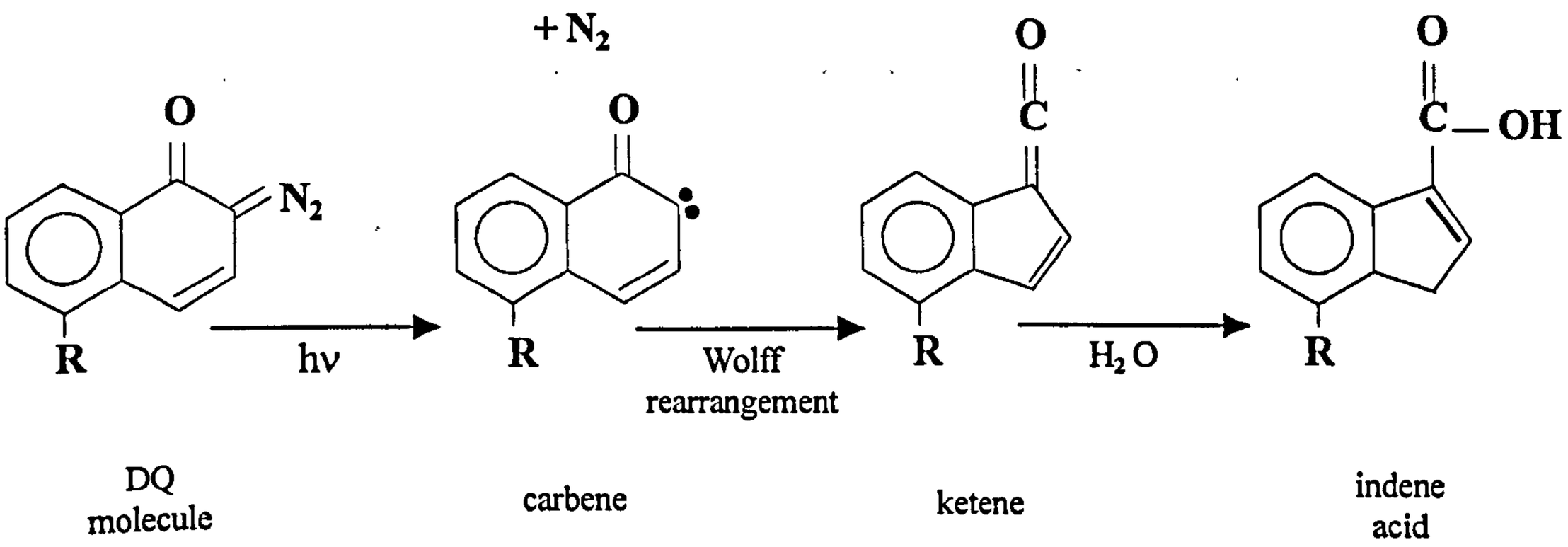

Fig. 5.1: *Showing the three stages in the chemical change of DQN photoresist on exposure [5.4].*

Once the DQ molecules have been destroyed in this way, the alkaline solubility of the exposed resin is increased to ~100 - 200 nm s^{-1}. It is this large difference in solubility between the exposed and unexposed material that makes photoresist of such use as a recording medium in lithography and holography.

As well as the dramatic change in alkaline solubility there is another important result of this photolytic reaction: the refractive index of the resist is changed. Fig. 5.2 shows a sketch graph of the refractive index of a typical DQN resist before and after exposure: it is clear that there is a significant change in the refractive index right across the visible spectrum.

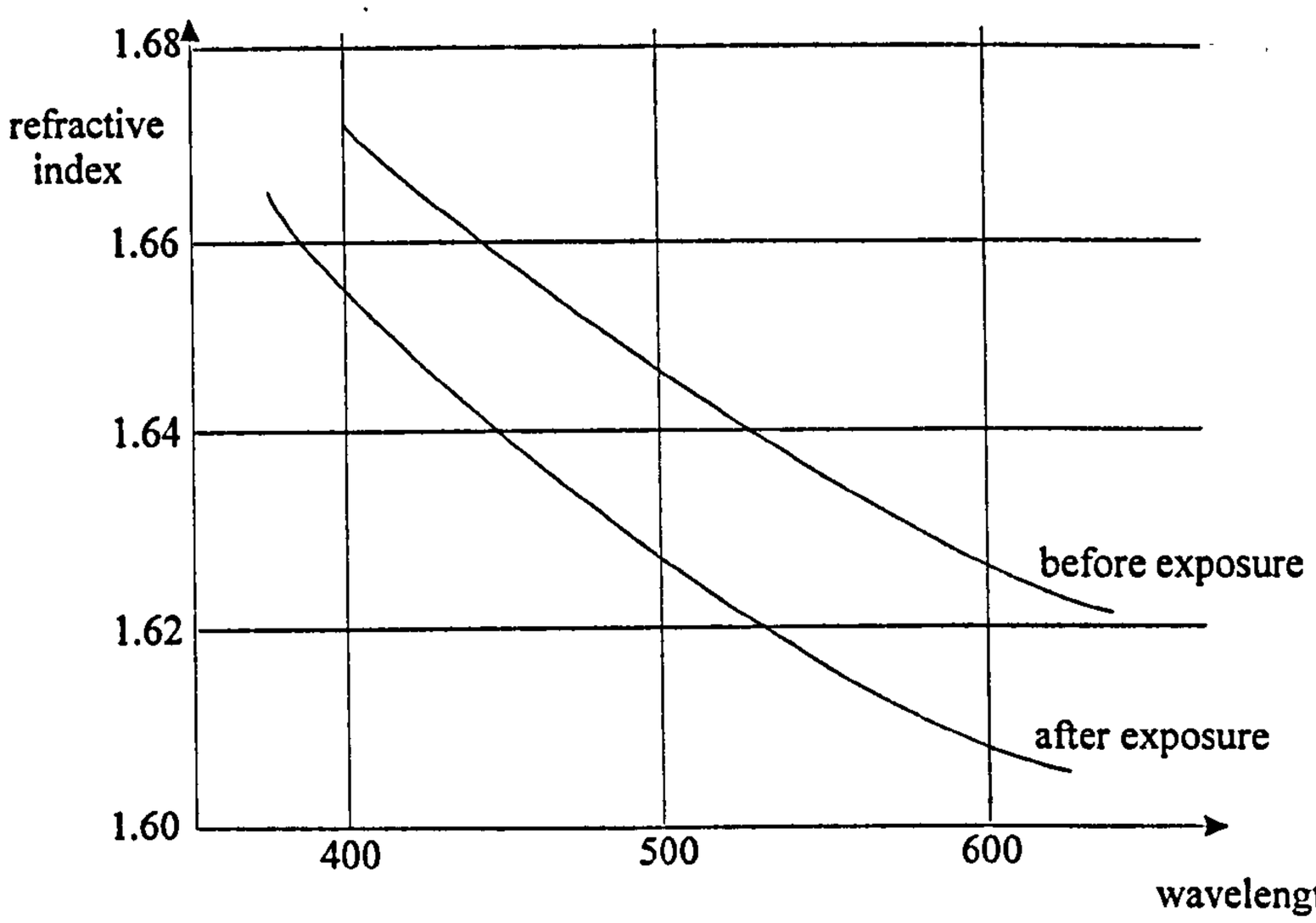

Fig. 5.2: *A sketch graph showing the variation of refractive index with wavelength of a typical DQN resist before and after exposure [5.4].*

5.2 A SIMPLE RATE EQUATION MODEL OF LATENT IMAGE GROWTH

5.2.1 Efficiency of latent image gratings

As a consequence of this refractive index change, when a resist plate is exposed to a pattern of high spatial frequency, such as those used in the manufacture of holographic phase gratings, a very weak phase hologram is produced *before development.* This pre-development or latent image may be used for the non-invasive monitoring of the grating growth and the progress of exposure.

Accompanying the refractive index variation there is also a tiny change in the absorption of the resist with exposure, but this is negligible at 458 nm, which is on the edge of the sensitivity of AZ1350 [5.7]. Neglecting this very small absorption variation, the grating may be considered a pure phase grating. The thickness of the resist layer on all the plates used in these experiments was 0.5 μm. In cases such as this, where the medium thickness is comparable with the wavelength of the incident radiation, it is acceptable to consider the grating as a plane hologram (see, e.g. [5.8]).

Consider the intensity pattern formed by two beams of wavelength λ with amplitude a and r which are symmetrically incident on a layer of recording material. If the half angle between

the beams is θ, and the wave vector $k = 2\pi/\lambda$ then the resulting pattern may be written in the form:

$$I(x) = a^2 + r^2 + 2ar\cos(2kx\sin\theta) \qquad (5.1)$$

It may be shown that the nth order diffraction efficiency of a plane sinusoidal pure phase grating is given by [5.8]:

$$\eta = \left[J_n\left(\frac{\phi}{2}\right)\right]^2 \qquad (5.2)$$

where J_n is the Bessel function of the first kind and nth order and ϕ is the maximum phase change imposed between different points on the same wavefront, which is incident normally on the grating.

Here for simplicity it is assumed that the recording material is linear (a reasonable approximation for photoresist, especially if a blanket pre-exposure is given [5.9]), that the amplitude ratio of the interfering beams is unity (i.e. $a = r$ in (5.1)) and that the maximum refractive index change induced by the exposure is Δn. In such a grating recording then, the change in refractive index at a point, $\delta n(x)$, is simply given by:

$$\delta n(x) = gI(x)t\Delta n \qquad [\delta n(x) \le \Delta n] \qquad (5.3)$$

where g is a constant of proportionality dependent on the exposure required for the recording media and t is the exposure time.

Thus from (5.1) and (5.3), an idealised exposure (i.e. maximum contrast and perfect exposure time) will yield an exposure profile given by:

$$n(x) = n_o + [1 + \cos(2kx\sin\theta)]\frac{\Delta n}{2} \qquad (5.4)$$

where n_o is the initial refractive index of the material. If the thickness of the recording medium is d then ϕ, the maximum phase change, is given by:

$$\phi = \frac{2\pi}{\lambda} d\Delta n \qquad (5.5)$$

Thus, from (5.2), the maximum efficiency in the first order is given by:

$$\eta_{max} = \left[J_1\left(\frac{\pi d\Delta n}{\lambda}\right)\right]^2 \qquad (5.6)$$

Using the approximation: $J_1(\alpha) \approx \frac{\alpha}{2}$ for $\alpha << 1$ gives:

$$\eta_{max} \approx \left(\frac{\pi d \Delta n}{2\lambda}\right)^2 \qquad (5.7)$$

For HeNe light ($\lambda = 632.8$ nm), 0.5 μm resist thickness and a Δn of ~ -0.015 (from Fig. 5.2):

$$\eta_{max} = 0.035\ \%$$

5.2.2 Justification for the rate equation model

From the laws of photochemistry it may be stated that only light that is absorbed by a molecule can be effective in producing photochemical change in that molecule [5.10]. Furthermore, the absorption of light is a quantum process and so probability is key in determining the nature of the photochemical reaction. Consequently it seems reasonable to assume that the probability of a particular DQ molecule absorbing a photon and changing its form will be a constant (the quantum efficiency) and so the rate of change of refractive index of a region in the material will be dependent on the concentration of DQ molecules in that area and on the incident light intensity. This suggests a simple rate equation model for the grating growth.

If the number density of unreacted DQ molecules in the resist is *N*, then the rate of decrease of concentration with time at any point is assumed to be proportional both to *N* and to the intensity *I(x)* at that point. Hence:

$$\frac{\partial N(x,t)}{\partial t} = -CI(x)N(x,t) \Rightarrow \frac{dN(t)}{dt} = -C\,IN(t) \qquad (5.8)$$

where *C* is a constant of proportionality dependent on the exposure required by the material. Solution of (5.8) leads to the usual exponential decrease of unreacted DQ concentration with time, or equivalently with exposure $E(x)=I(x)t$. Thus:

$$N = N_o \exp\left(-\frac{E}{E_o}\right) \qquad (5.9)$$

where N_O is the initial number of DQ molecules per unit volume, E is the exposure given to the sample and E_O is the characteristic exposure for the material.

5.2.3 Approximate diffraction efficiency of plane phase gratings

It has been shown that it is reasonable to approximate the latent image grating by a pure plane phase grating. The efficiency of such gratings may be modelled by considering the distortion introduced to the phase fronts of a normally incident plane wave of unit amplitude using the Huygens-Fresnel principle [5.11], as illustrated in Fig. 5.3. It is assumed that during the exposure there is a homogeneous mixture of exposed and unexposed material and that the resulting medium has a refractive index somewhere between that of the unexposed resist (n_O) and that of the fully exposed resist (n_1). Hence when the resist is exposed to the characteristic sinusoidal grating pattern from two overlapping beams, there is some form of periodic refractive index variation, $n(x)$, represented schematically in Fig. 5.3 by two layers of material with indices n_O and n_1.

Whatever the precise shape of the grating profile, the direction of propagation of the mth order diffracted beam is determined by the pitch, d, of the grating according to:

$$\sin\theta_m = \frac{m\lambda}{d} \tag{5.10}$$

where θ_m is the direction of propagation measured from the y axis and λ is the wavelength of the light *in vacuo*.

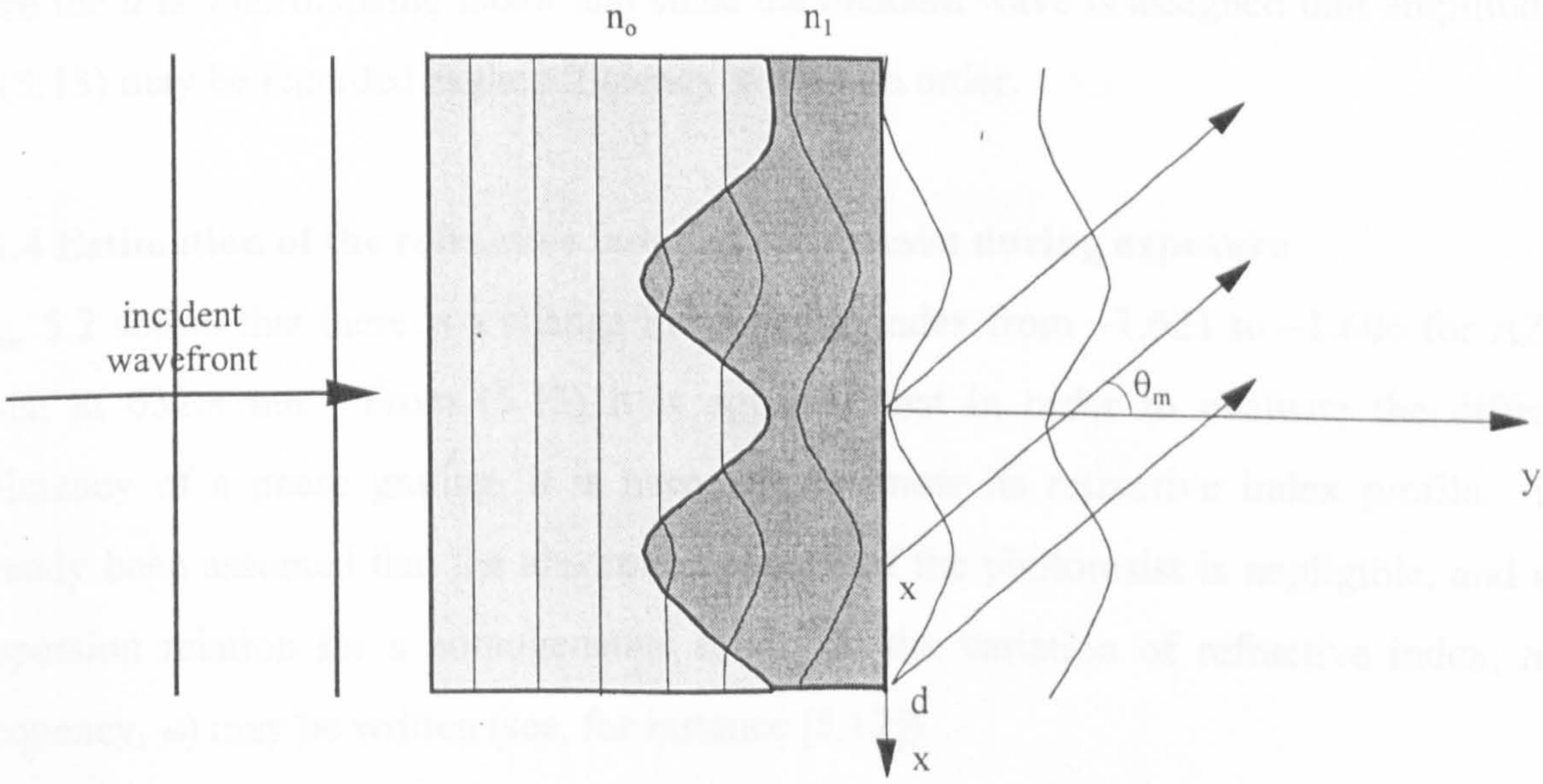

Fig. 5.3: *A schematic representation of the effect of a pure plane phase grating on incident plane wavefronts.*

The intensity of the diffracted beam in the far-field may be found using the Kirchoff approximation. That is to assume that at a point far from the grating in the direction of propagation of the *m*th order diffracted ray the phase of the Huygens-Fresnel secondary wavelet from some point x in Fig. 5.3, relative to the phase at $x = 0$ is approximately equal to [5.11]:

$$\Phi(x)\exp\left(\frac{2\pi i}{\lambda}x\sin\theta_m\right) = \Phi(x)\exp\left(\frac{2\pi imx}{d}\right) \qquad (5.11)$$

Here $\Phi(x)$ is a function describing the phase shift imposed by the varying refractive index of the phase grating on the incident wave. Essentially this formula approximates the distance to the point of observation to a constant plus the extra distance, $x\sin\theta$, travelled by the wavelets from x compared with those from $x=0$. The function $\Phi(x)$ represents the phase change due to the optical path in the grating medium, thickness T, and may be written:

$$\Phi(x) = \exp\left(2\pi i\frac{n(x)T}{\lambda}\right) \qquad (5.12)$$

Following Gale [5.11] the resultant intensity of the *m*th diffracted beam may be calculated by summing the amplitudes of all wavelets and squaring:

$$\eta_m = \left|\frac{1}{d}\int_0^d \exp\left\{2\pi i\left[\frac{n(x)T}{\lambda} - \frac{mx}{d}\right]\right\}\right|^2 \qquad (5.13)$$

Here the d is a normalising factor and since the incident wave is assigned unit amplitude η_m in (5.13) may be regarded as the efficiency in the *m*th order.

5.2.4 Estimation of the refractive index of photoresist during exposure

Fig. 5.2 shows that there is a change in refractive index from ~1.621 to ~1.606 for AZ1350 resist at 632.8 nm. From (5.13) it is apparent that in order to evaluate the diffraction efficiency of a phase grating, it is necessary to know its refractive index profile. It has already been assumed that the absorption change of the photoresist is negligible, and so the dispersion relation for a homogeneous solid (i.e. the variation of refractive index, n with frequency, ω) may be written (see, for instance [5.12]).

$$\frac{n^2-1}{n^2+2} = \frac{Nq_e^2}{3\varepsilon_o m_e}\sum_j \frac{f_j}{\omega_{oj}^2-\omega^2} \qquad (5.14)$$

Here N is the number of molecules of per unit volume, q_e is the electronic charge, ε_o the permittivity of free space, m_e the electronic mass and f_j is the transition probability for a particular resonant frequency ${\omega_{0j}}^2$.

For the case in hand, i.e. that of finding the refractive index of a homogeneous mixture of exposed and unexposed material, this equation may be simplified by observing that for a given material in any homogeneous mixture, most of the terms on the right hand side may be combined into a single constant K:

$$\frac{n^2-1}{n^2+2} = KN \tag{5.15}$$

Using this simplification, if the total number of molecules per unit volume is N_O, then the initial index of the resist, n_O, and the fully exposed refractive index, n_1 , have the dispersion relations:

$$\frac{{n_0}^2-1}{{n_0}^2+2} = K_0 N_0 \tag{5.16}$$

and

$$\frac{{n_1}^2-1}{{n_1}^2+2} = K_1 N_0 \tag{5.17}$$

In the rate equation model the number of unexposed molecules per unit volume decreases exponentially from this value N_O. Hence at some arbitrary point during the exposure, when the number of unexposed molecules is N, the refractive index, n, of the mixture may be written:

$$\frac{n^2-1}{n^2+2} = K_1(N_0-N)+K_0 N = K_1 N_0 + (K_0-K_1)N \tag{5.18}$$

Substituting in N from the rate equation, (5.9), (5.18) becomes:

$$\frac{n^2-1}{n^2+2} = K_1 N_0 + (K_0 N_0 - K_1 N_0)\exp\left(-\frac{E}{E_0}\right) \tag{5.19}$$

Substituting (5.16) and (5.17) into (5.19) gives:

$$\frac{n^2-1}{n^2+2} = \frac{{n_1}^2-1}{{n_1}^2+2} + \left(\left(\frac{{n_0}^2-1}{{n_0}^2+2}\right) - \left(\frac{{n_1}^2-1}{{n_1}^2+2}\right)\right)\exp\left(-\frac{E}{E_0}\right) \tag{5.20}$$

Since $n \approx n_0 \approx n_1$, the denominators in this equation are approximately equal, and (5.20) may be simplified to give:

$$n^2 = n_1^2 + \left(n_0^2 - n_1^2\right)\exp\left(-\frac{E}{E_0}\right) \tag{5.21}$$

If the difference in refractive index between the two states of resist is Δn, and Δn is small compared with n_0 and n_1 then:

$$n_1 = n_0 + \Delta n$$

$$\therefore n_0^2 - n_1^2 = n_0^2 - \left(n_0^2 + 2n_0\Delta n + \Delta n^2\right) \approx -2n_0\Delta n$$

Thus (5.21) becomes:

$$n^2 = n_1^2\left(1 - 2\frac{n_0}{n_1^2}\Delta n \exp\left(-\frac{E}{E_0}\right)\right) \tag{5.22}$$

This may be simplified once more using the binomial approximation:

$$n = n_1\left(1 - \frac{n_0}{n_1^2}\Delta n \exp\left(-\frac{E}{E_0}\right)\right) \approx n_1 - \Delta n \exp\left(-\frac{E}{E_0}\right) \tag{5.23}$$

Thus the, perhaps intuitive, exponential variation of refractive index with exposure does indeed follow from a rate equation model using the dispersion relation and these simple approximations.

5.2.5 Diffraction efficiency of latent image during exposure

In a typical holographic two beam diffraction grating set up, if the amplitudes of the interfering beams are a_o and r_o and the half angle between the two beams is θ, then the resulting exposure profile may be written (adapted from [5.8]):

$$E(x,t) = I(x)t = \left[a_o^2 + r_o^2 + 2a_o r_o \cos\left(\frac{2\pi}{\lambda}x\sin\theta\right)\right]t \tag{5.24}$$

If (5.24) is substituted into (5.23), then the refractive index profile as a function of time is obtained. Fig. 5.4 shows a series of profiles of a grating element for a series of normalised exposures, with the beam ratio, B, chosen as 0.7 for illustrative purposes. As the resist is exposed the index drops (Δn is negative in AZ1350 resist), naturally more rapidly in the

brighter areas than in the dark. In the dark areas (the centre of Fig. 5.4) the drop is slower, but since the beam ratio is less than one, there is a finite intensity even at the centre and the grating slowly washes out, eventually yielding a uniform material of index n_1 as $t \to \infty$.

Having found the index profile from (5.23) and (5.24), it may be substituted into (5.13) to obtain an equation describing the diffraction efficiency at particular times during the exposure. Fig. 5.5 shows how the diffraction efficiency changes as the exposure increases for several beam ratios $\left(B = {}^{a_o}/_{r_o}\right)$. The exposure is normalised, and typical values for AZ1350 photoresist are used (Δn = -0.015, resist thickness T = 0.5 μm).

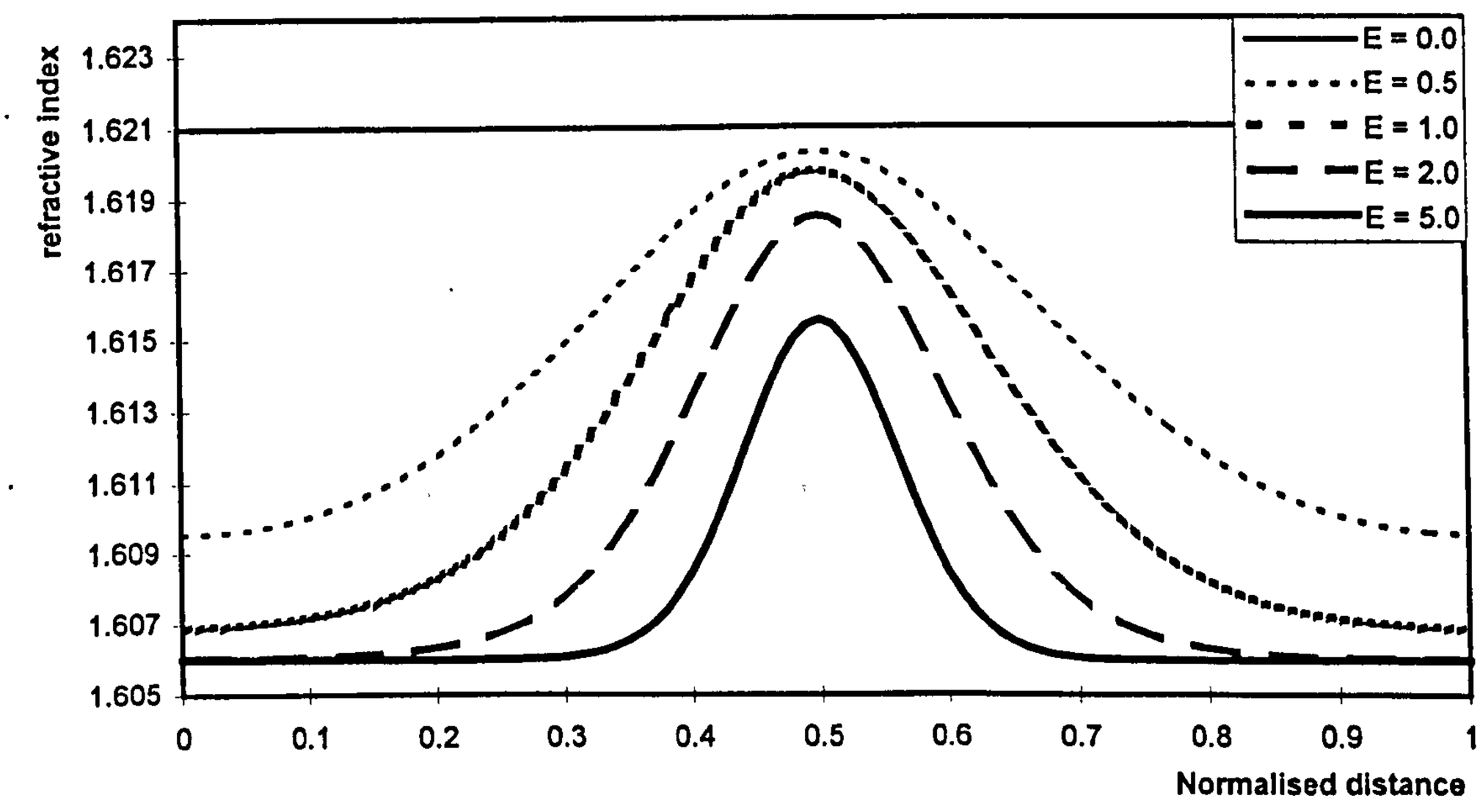

Fig. 5.4: *Showing the refractive index profiles of a single pitch on a grating recorded with a beam ratio of 0.7 for a range of normalised exposures.*

[Note that the efficiency never reaches the theoretical maximum for a perfect sinusoidal grating (0.0346 %) as discussed in section 5.2.1, even for a grating formed with perfect beam ratios. If a pure sinusoidal profile obtained from a perfect linear response is put into this model, it yields this same maximum value of 0.0346%, corresponding to a refractive index profile of a sine wave with amplitude $\Delta n/2$. However, this model becomes unrealistic, since n then continues to decrease below 1.60 (the minimum index achieved in the real material). If

the profile is curtailed (i.e. all values <1.60 are defined as 1.60) then the efficiency continues to rise up to 0.05 %, before sharply dropping.]

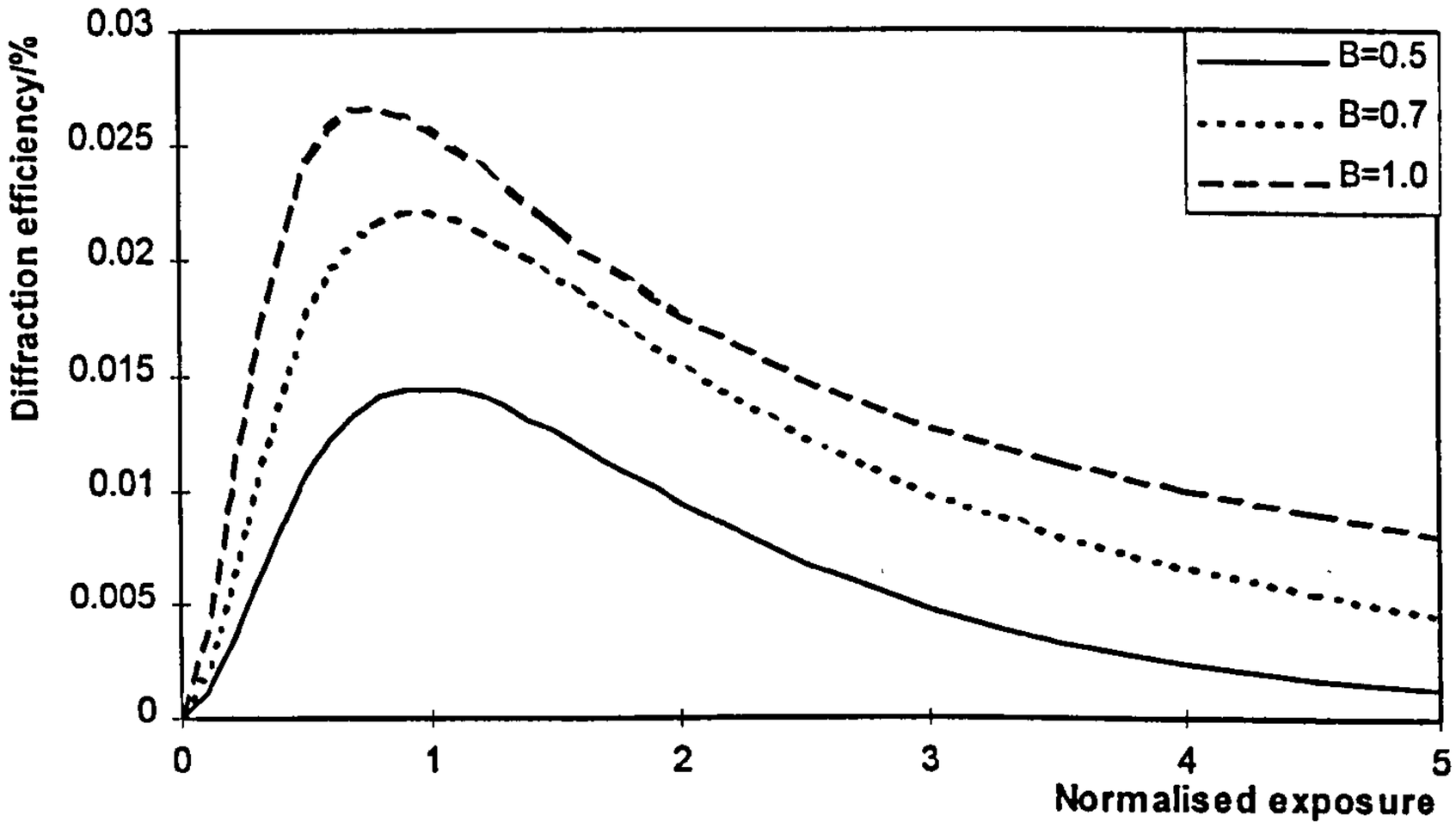

Fig. 5.5: *A graph showing the variation of diffraction efficiency (in %) during the exposure process for several different beam ratios, B, obtained using a rate equation model for the exposure profile. Here the exposure has been normalised and the predicted efficiency is for a Δn of -0.015.*

5.2.6 Recognised shortcomings of the rate equation model

The formulae derived in the previous section for the efficiency of the phase hologram are rather idealised. In practice the exposure pattern itself, $E(x)$, is more complicated than a pure sinusoid for several reasons. If spatially filtered beams with spherical wavefronts are used to write the grating then the period of the recorded grating varies continuously across the area of interference, but if collimated beams are used then inevitably there are aberrations and noise from the collimating optics [5.13]. Another distortion to the pattern, albeit a tiny one, is that due to diffraction from the latent grating on the writing beams.

Similarly the effect of absorption, which has been neglected in the above analysis, will result in a variation of refractive index in the z direction, that is perpendicular to the plane of the resist layer, since the intensity at some depth z in the resist layer will be smaller than that at the surface. This will have an effect on the refractive index profile and consequently on the diffraction efficiency of the grating.

One further important effect which has been ignored is the formation of standing waves due to interference between the incident and reflected waves [5.14], [5.15]. The reflected waves undergo a phase change upon reflection at the chrome/resist interface which is dependent on factors such as the angle of incidence, the reflection coefficient and the polarisation [5.16] (and is not, in general, π as assumed in [5.15]). These standing waves lead to nodes in the z intensity profile, and consequently instead of a smooth sinusoid, the resist profile after development has several steps: each step corresponding to a node in the standing wave pattern.

In the various exotic mathematical models which have been used to study grating growth, one practice is to consider the grating as a lamellar structure and to use a coupled wave theory to treat the interactions of the diffracted and incident waves ([5.17], [5.18]). In the studies presented here, such techniques were discarded in favour of the simple plane grating model because the resist layer thickness (0.50 μm) is comparable with the wavelength of the light in the medium (632 nm/1.6 ~ 0.4 μm). This compares well with a rule of thumb devised by Klein [5.19] to determine the validity of coupled wave theory using the parameter Q, where:

$$Q = \frac{2\pi T\lambda_a}{n d^2} \qquad (5.25)$$

In these experiments: T = 0.5 μm, λ_a = 633 nm, n ~ 1.6 and the grating pitch d = 1 μm, giving a Q of ~ 1.2. The coupled wave theory begins to give good results when $Q \geq 10$, and so these gratings are well below this accepted "thick hologram standard".

5.3 REAL–TIME OBSERVATION OF LATENT IMAGE GRATING GROWTH

5.3.1 Experimental method to observe latent image grating growth

A holographic grating is recorded using 458 nm argon ion radiation on a resist plate upon which a 632.8 nm HeNe beam is simultaneously incident. Because the resist is insensitive to the HeNe radiation, it does not effect the recording of the grating, but this red light will be diffracted by the latent image grating into an appropriately aligned photomultiplier fitted with a HeNe filter across its entrance aperture to prevent the blue light from swamping the signal. The photocurrent resulting from this beam is approximately proportional to the diffracted intensity and hence to the efficiency of the grating.

Because the Δn for the resist is fairly large, the diffracted signal from the latent image is reasonably strong and thus the photomultiplier can be used on a low voltage (~ 1 kV). [Indeed the diffracted light may be observed with the naked eye by looking along the beam.] The grating writing procedure was fairly standard: the beam powers at the plate were balanced and the polarisations were both made vertical using two half wave plates in conjunction with the polarisation sensitive beam splitter. Since reasonably long exposure times were envisaged, the stability of the grating writing process was also under investigation. For this reason low powers were used at the monitoring position: a typical exposure would be in the region of two minutes.

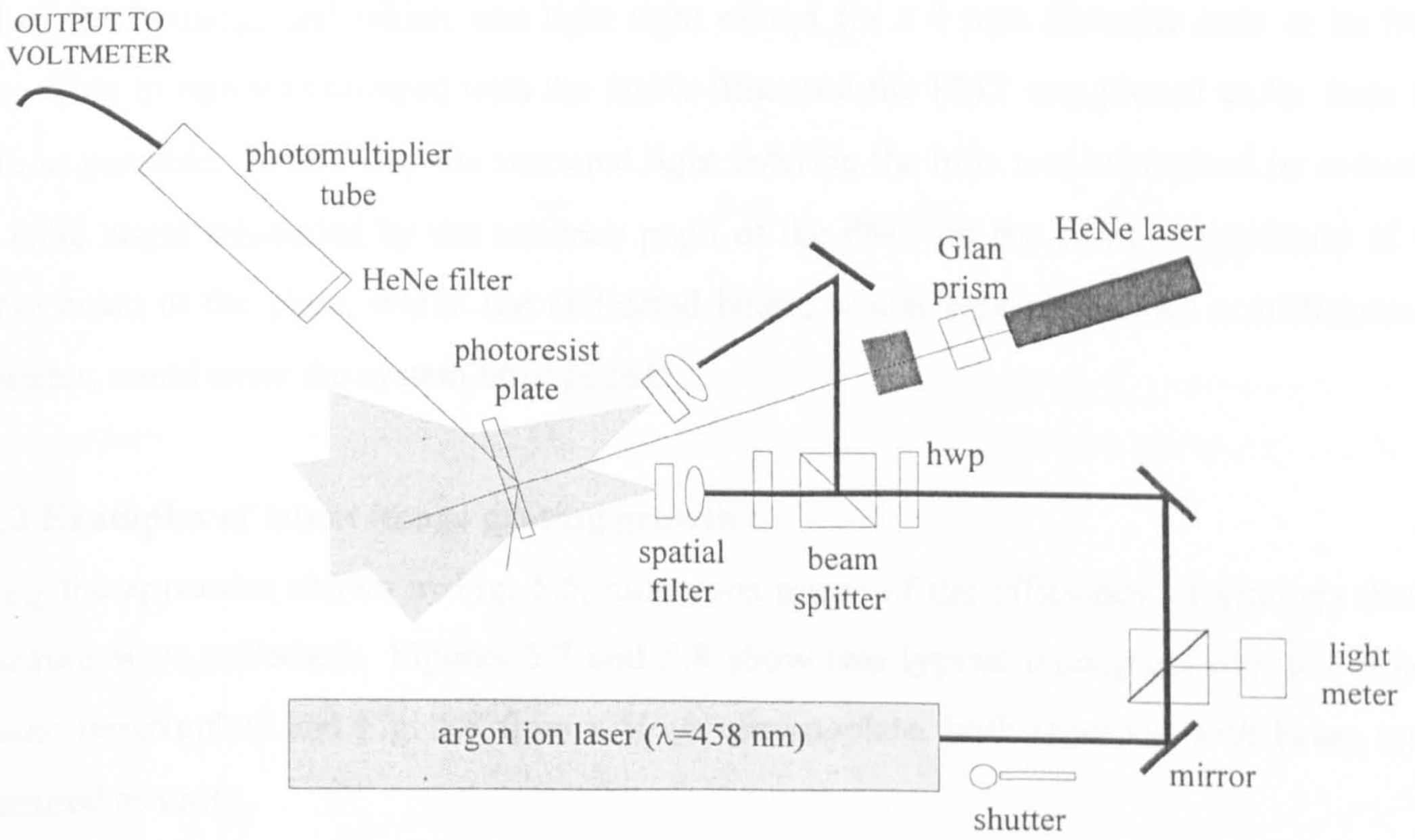

Fig. 5.6: *A sketch showing the experimental apparatus used to write a diffraction grating in the photoresist whilst simultaneously monitoring its growth. [N.B. This arrangement is for a ferroxoplate which is transparent to the red. If chrome plates were used then the diffracted beam would be reflected and the PMT aligned appropriately.*

The PMT used in these experiments is an Electron Tubes 9124B: this is a linearly focused tube containing eleven dynodes with a rubidium bialkali (Sb-Rb-Cs) photocathode. This photocathode is most sensitive in the blue and UV parts of the electromagnetic spectrum, and tails off in the red. However, there is still significant response (~ 12 mAW^{-1}) at the HeNe wavelength, 632.8 nm. It should be noted that the tube is extremely sensitive to the grating

writing wavelength ($R_{\lambda=458nm} \sim 80$ mAW^{-1}) and so it was important to shield the photocathode from as much of the background radiation as possible.

The tube was mounted in its own housing which was light tight and electrostatically and magnetically screened; this housing also contained the voltage divider for the dynodes. A second housing was engineered which bolted onto the manufacturer's housing and allowed the PMT to be fitted to the standard optical mounts used in the laboratory.

The entrance to this housing was a circular aperture 40 mm in diameter. A cover for the entrance aperture of the housing was made from black plastic which fitted snugly over the end of the housing, and which was light tight except for a 4 mm diameter hole in its front face. This in turn was covered with the HeNe filter and the PMT was placed as far from the plate as possible. In this way the scattered light entering the tube was minimised by reducing the solid angle subtended by the entrance pupil of the PMT on the point of incidence of the HeNe beam at the plate, whilst the diffracted beam, which was only about a millimetre in diameter, could enter the system unimpeded.

5.3.2 Examples of latent image grating growth

Using the apparatus shown in Fig. 5.6, numerous traces of the efficiency of gratings during exposure were collected. Figures 5.7 and 5.8 show two typical examples: Fig. 5.7 from a Towne ferroxoplate and Fig. 5.8 from a Hoya chromoplate, both recorded with beam ratios measured as unity.

The photocathode in the photomultiplier was not accurately calibrated and so no attempt has been made to calculate absolute diffraction efficiencies. Calculations based on an approximate radiant sensitivity for the photocathode indicate maximum efficiencies of ~ 0.020 % to ~ 0.025 %: values in reasonable agreement with those predicted from Fig. 5.5.

The theoretical graphs in Fig.s 5.7 and 5.8 have been plotted using the same parameters as in Fig. 5.5, with a beam ratio of 1.0, fitting the parameter E_o so that the maxima coincide and then scaling the graph to account for the uncalibrated photomultiplier output. The theory predicts fairly well the efficiency in the first stages of the grating growth and in practice it is

this part of the graph which will be of interest. As the exposure continues the experimental curve dies away more rapidly than the theory predicts.

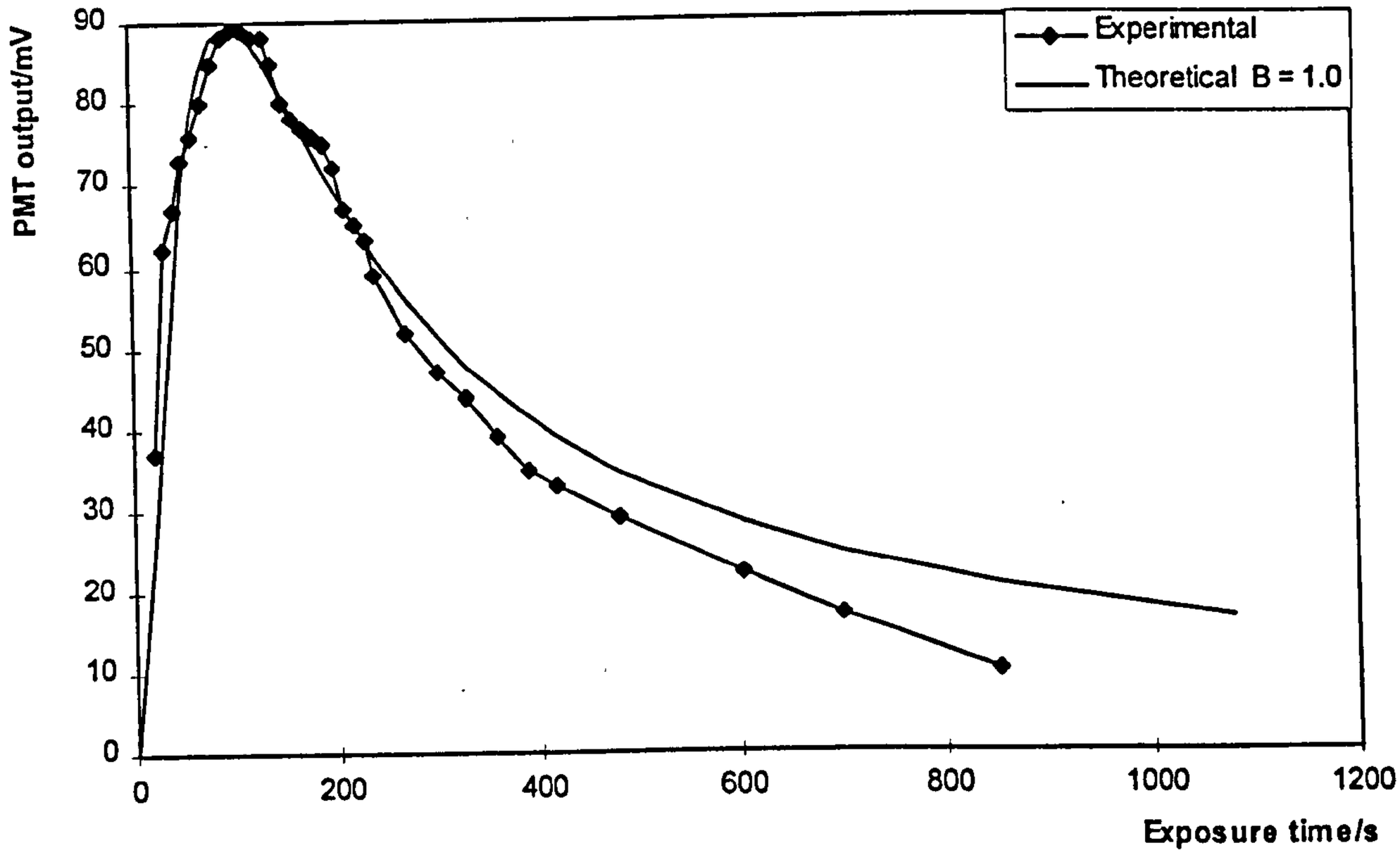

Fig. 5.7: *A graph showing the growth and decay in efficiency of a typical latent image grating written on a Towne ferroxoplate. The smooth curve shows the theoretical efficiency (for a beam ratio of 1.0), and the diamonds show the actual values measured.*

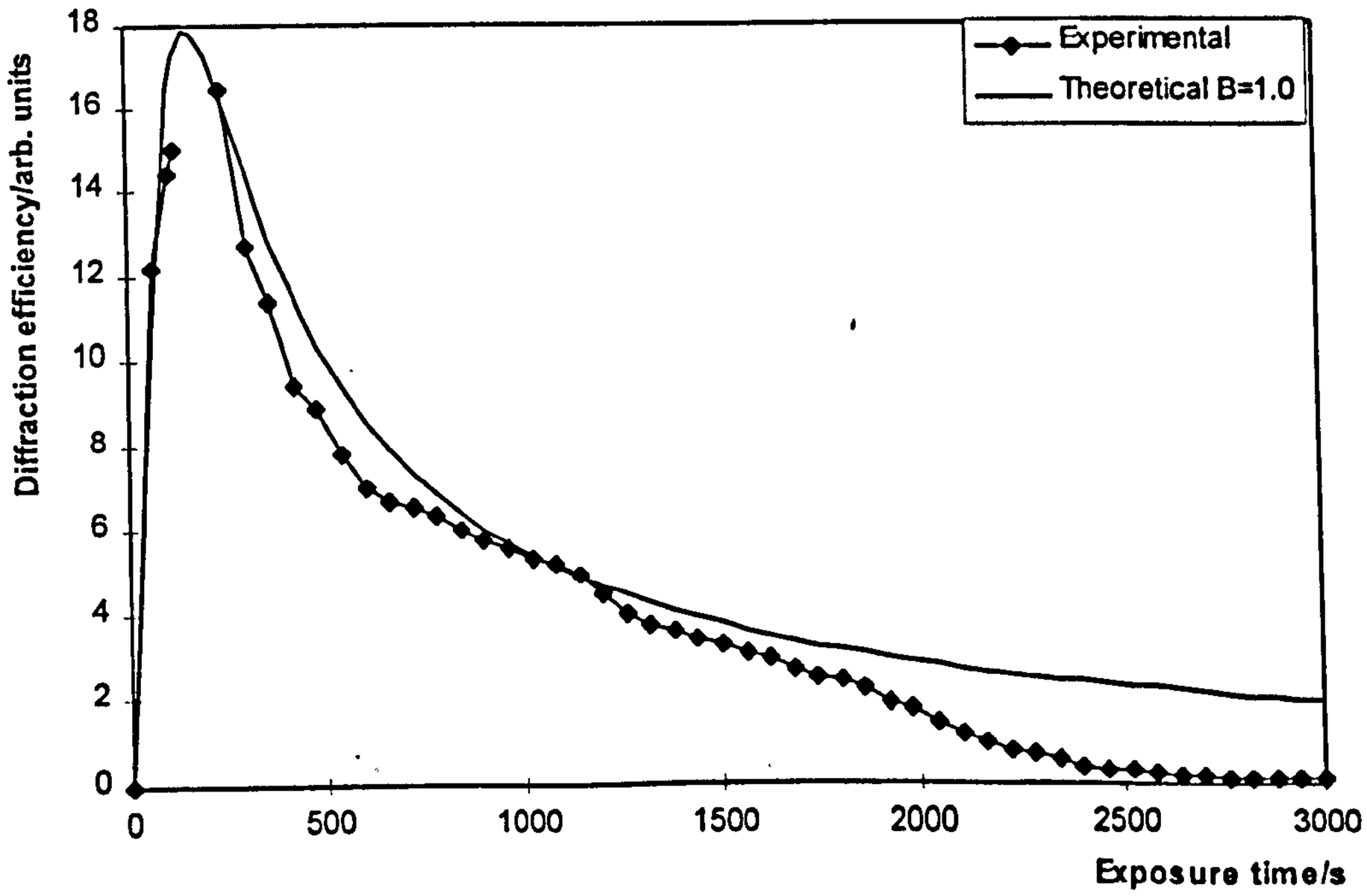

Fig. 5.8: *A graph showing the growth and decay in efficiency of a typical latent image grating written on a Hoya chromoplate. The smooth curve shows the theoretical efficiency (for a beam ratio of 1.0), and the diamonds show the actual values measured.*

This is fairly unsurprising, since the beam ratio will be less than unity in practice, and so the dark regions in the resist will actually be receiving some light: consequently the grating would be expected to rub out faster than the theory predicts. It is also suggested that in the later stages of exposure, when the plate has been illuminated for several tens of minutes, the cumulative effect of any vibrations and instabilities in the optical set up will be observed as a gradual washing out of the grating: this would also tie in with the two traces illustrated.

5.3.3 Double peaks with dip-coated plates

An experimental mystery was experienced in the initial trials with Towne ferroxo plates. Traces of diffraction efficiency against time such as that illustrated in Fig. 5.9 were observed in which the grating grew and faded as predicted but then there was a re-growth of the grating during which there was a definite rise in the efficiency before it decayed back to zero. Such behaviour was not predicted by the theory outlined above and could not initially be explained.

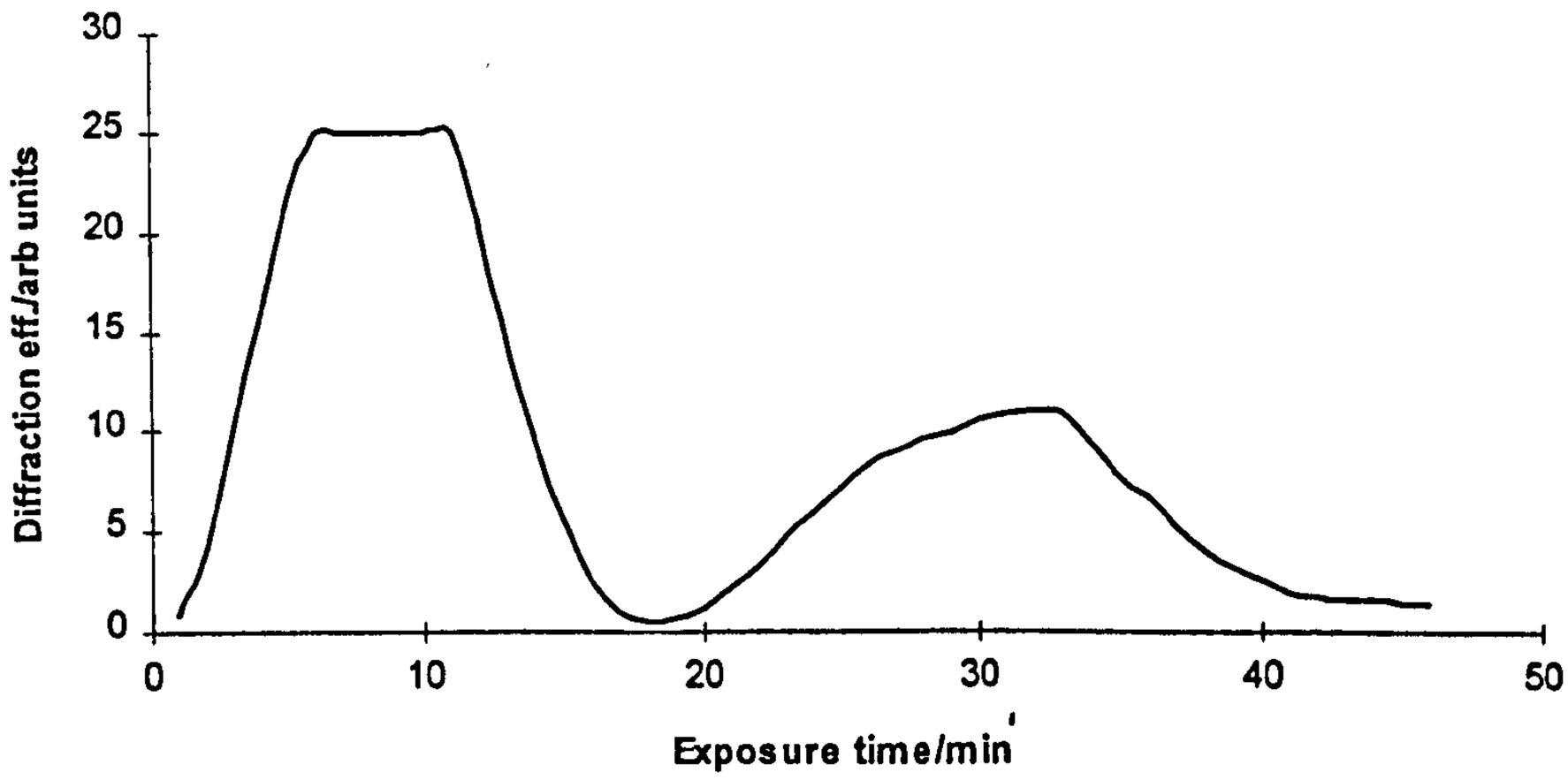

Fig. 5.9: *Showing a typical two-peak trace. The second peak was significantly smaller than the first and the PMT went off-scale at the maximum of the first peak in order to give better definition of the second peak*

Observations showed that such gratings gave rise to two separate diffracted beams, and it was this that led to the explanation: two parallel beams suggested two separate gratings of the same pitch. The plates used in these experiments are ~ 60×70 cm^2 and they are cut down to size for the exposures. Such plates are too large for spin coating and so they have to be dip coated with resist. As the plates are slowly drawn out of the baths a layer of resist adheres to the ferroxo substrate; however there is also a second layer of resist which adheres to the back

of the glass plate. Naturally when these plates are exposed, the second resist layer will respond to the radiation and a second latent image grating will form.

Because the ferroxo layer is fairly strongly absorbing in the blue, the intensity on the back of the plate is much less, and so it takes longer for the grating to grow. Also, because the ferroxo is strongly scattering, there will be much lower contrast fringes due to the high background blue light level, which explains why the second grating has a much lower efficiency than the first. Thus if dip-coated ferroxo plates are to be used in this work then the resist layer on the back of the plates must be removed, for instance with an organic solvent such as dichloromethane.

5.4 LATENT IMAGE MEASUREMENT AS A PROCESS CONTROL METHOD

The efficiency of the latent grating may be used as an indicator of the extent of the exposure and hence as a method for exposure end-point detection ([5.20], [5.21], [5.22]). The purpose of the experiments in these references was purely as a monitoring method for determining the optimum exposure for gratings in resist. Most industrial gratings are written using an "upstream" or "open loop" monitoring process in which there is no feedback or direct control. Such processes use a calibration test to find the exposure characteristic for a particular feature size, or critical dimension, and then rely on statistical methods for process control. A closed loop system is advantageous for several reasons.

The grating profile depends on the variables in the exposure and development of the plate. Theoretically by controlling these variables: exposure time and power, polarisation, developer concentration and temperature etc., it should be possible to obtain identical gratings for each exposure. However, there are tiny variations between resist plates and there is unavoidably some error in the control of the various experimental parameters. Due to the highly non-linear nature of the resist exposure and development processes these small variations between processing conditions can lead to significant differences between individual gratings.

The real time monitoring of the diffracted image, whether during exposure using the latent image, or during the development process as the relief grating grows, is a closed loop form of control, and each exposure/development can be adjusted for each grating, giving a higher yield of gratings ([5.23], [5.24]). It also allows less restriction on the experimental conditions, leading to advantages such as re-use of developer chemicals.

REFERENCES

5.1 L.P.Clerc: "Photography: Theory and Practice": 2nd Edition, Pitman and Sons (1937).

5.2 I.O. Starobogatov and S.D. Nicholaev: "Research of fast stages of latent image formation in holographic photoemulsions influenced by ultrashort radiation pulses": SPIE Vol. 1238: Three-Dimensional Holography: Science, Culture, Education (1989), pg. 153.

5.3 M.G. Girina and G.A. Sobolev: "Estimation of quality of a holographic material using a latent image": Opt. Spektrosk. **32**, 216 (1972).

5.4 W. M. Moreau: "Semiconductor lithography: principles, practice and materials"; Plenum Press (1988).

5.5 F. H. Hill et al.: "Characterisation of positive photoresist": IEEE Trans. Elec. Dev. **22**, 7 (1975).

5.6 J. Pacansky: Polym Eng. Sci. **20**, 1049 (1980).

5.7 L. Mashev and S. Tonchev: "Formation of holographic diffraction gratings in photoresist": Appl. Phys. **A26**, 143 (1981).

5.8 R. J. Collier, C. B. Burckhardt and L. H. Lin: "Optical holography": Academic Press (1971).

5.9 M. J. Beesley and J. G. Cassadine: "The use of photoresist as a holographic recording media": Appl. Opt. **9**, 2720 (1970).

5.10 J. Guillet: "Polymer photophysics and photochemistry"; Cambridge University Press (1985).

5.11 M.T. Gale and K. Knop: "Surface-relief images for colour reproduction"; Focal Press, London (1985).

5.12 E. Hecht: "Optics"; 2nd edition, Addision-Wesley (1987).

5.13 E. K. Popov, L. V. Tsonev and M. L. Sabeva: "Technological problems in holographic recording of plane gratings": Opt. Eng. **31**, 2168 (1992).

5.14 S. Austin and F. T. Stone: "Fabrication of thin periodic structures in photoresist: a model": Appl. Opt. **15**, 1071 (1976).

5.15 L.F. Johnson, G. W. Kammlott and K. A. Ingersoll: "Generation of periodic surface corrugations": Appl. Opt. **17**, 1165 (1978).

5.16 M. Born and E. Wolf: "Principles of Optics": ch. 13.4.2, 4th Ed., Pergamon Press (1970).

5.17 Lifeng Li: "Multilayer modal method for diffraction gratings of arbitrary profile, depth and permittivity"; Opt. Soc. Am. A, **10**, 2581 (1993).

5.18 R Petit: "Electromagnetic theory of gratings": Springer-Verlag (1980).

5.19 W. R. Klein: "Theoretical efficiency of Bragg devices"; Proc. IEEE **54**, 803 (1966).

5.20 J. A. Gregus et al.: "Real-time latent image monitoring during holographic fabrication of sub-micron gratings": J. Vac. Sci. Tech. B **11**, 2468 (1993).

5.21 E. Yoon et al.: "Latent image diffraction from sub-micron photoresist gratings": J. Vac. Sci. Tech. **B10**, 2230 (1992).

5.22 K. C. Hickman et al.: "Use of diffracted light from latent images to improve lithography control": J. Vac. Sci. Tech. **B10**, 2259 (1992).

5.23 J. A. Britten, R. D. Boyd, B. W. Shore: "*In situ* end-point detection during development of submicrometer grating structures in photoresist": Opt. Eng. **34**, 474 (1995).

5.24 W. Tsang and S. Wang: "Simultaneous exposure and development technique for making gratings on positive photoresist": Appl. Phys. Lett. **24**, 196 (1974).

Chapter 6

DESIGN AND OPERATION OF A FRINGE LOCKING DEVICE

6.1 THE NEED FOR A FRINGE LOCKER

6.1.1 The effect of transverse plate movement

In any practical experimental arrangement of the apparatus discussed in the chapter 4 there will be some finite error in the alignment of the plane of the recording medium with its direction of movement. This will lead to a tiny lateral displacement of the plate as it travels. In addition to this systematic error due to the finite precision of alignment, there is also a random error due to imperfections in the quality of the micropositioning device, system vibrations, thermal expansions and other environmental effects.

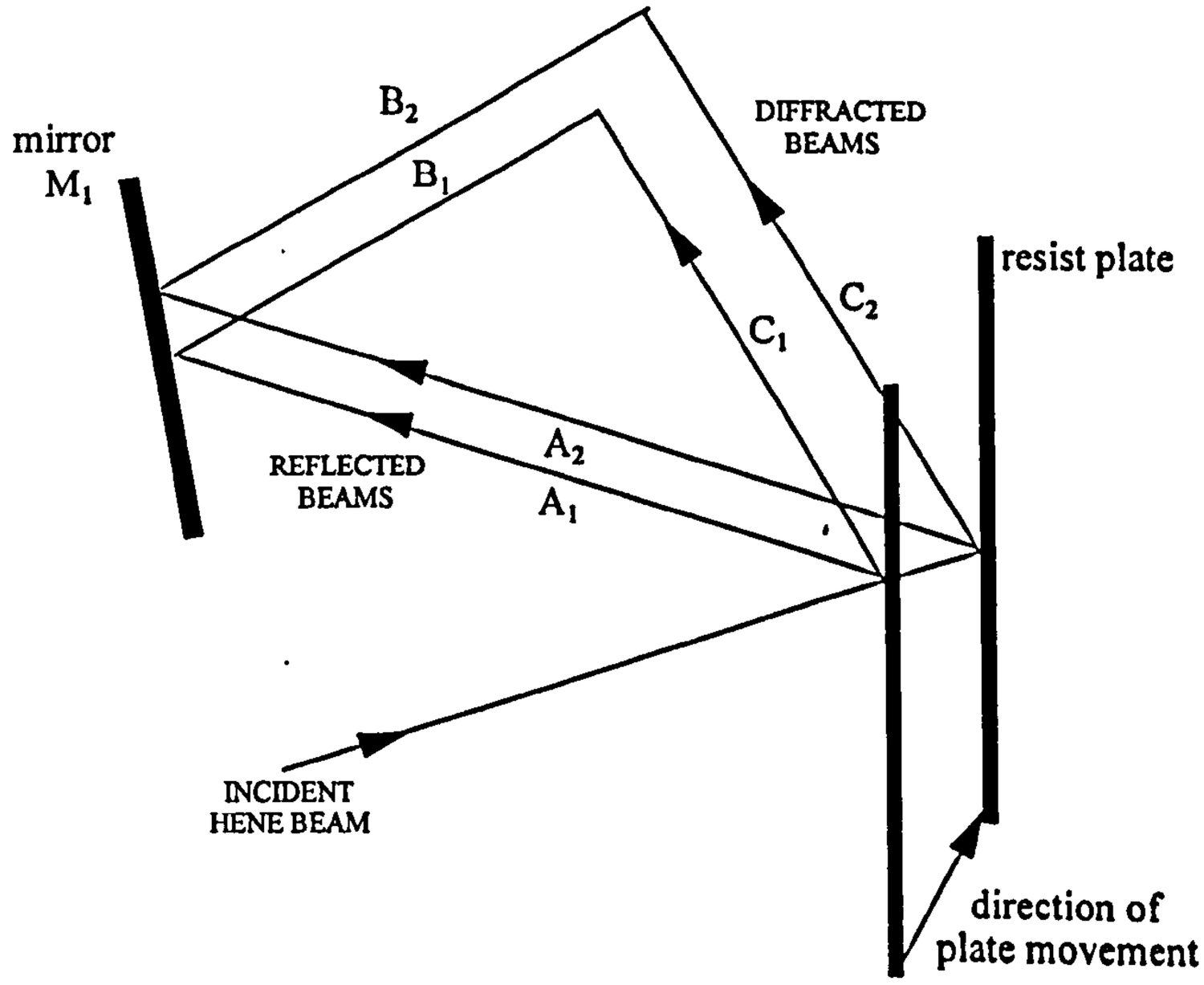

Fig. 6.1: *Showing the change in beam paths due to transverse plate movement.*

It can be seen from Fig. 6.1 that this transverse movement will change the triangle formed by the reflected and diffracted beams used to analyse the plate position. Since the angle made by the plate and the incident beam is unchanged, the triangles $A_1B_1C_1$ and $A_2B_2C_2$ are similar

but they are not congruent hence the path difference between the interfering beams will be different. [In fact this path difference calculation is similar to that examined in chapter 3; however in this case because the angles and wavelengths are different there is no phase compensation.] Obviously in Fig. 6.1 this misalignment is greatly exaggerated, but it must be remembered that a path difference error of just half a wavelength of the interrogating light (i.e. ~ 300 nm) will result in the exposure pulses being put down π radians out of phase: i.e. in exactly the wrong position.

There will be another change in the phase at the detector because as the plate moves transversely the incident HeNe beam will effectively be hitting a different point on the grating unless it is perfectly normal to the plate. The geometry is illustrated in Fig. 6.2.

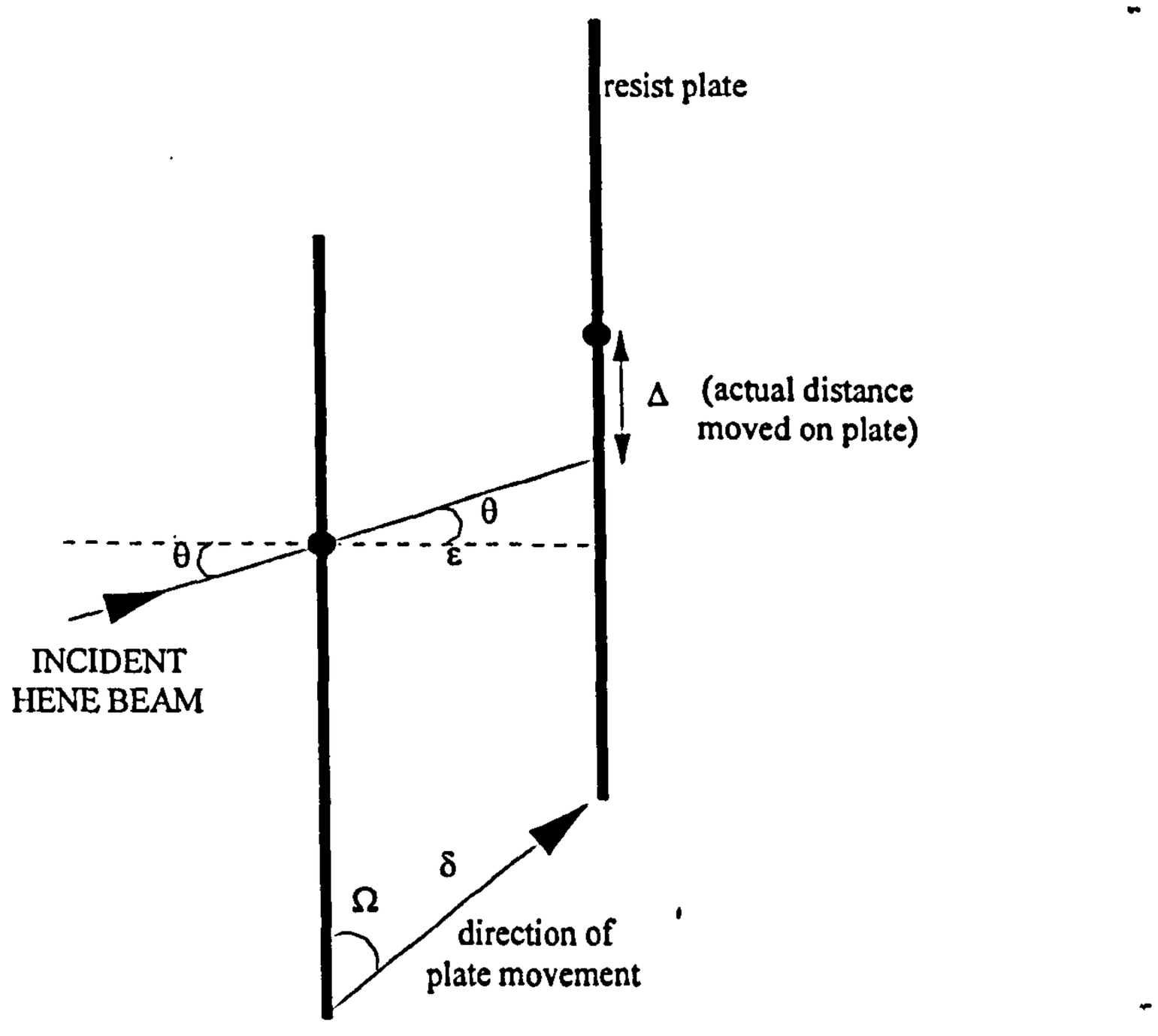

Fig. 6.2: *Showing the error due to the transverse displacement* ε *of the plate.*

From Fig. 6.2 it can be seen that the HeNe beam is incident on a different position than if the plate axis and the direction of movement were co-linear. If the plate is misaligned from its direction of motion by some angle Ω and travels some distance δ in this direction then let the lateral displacement be ε. For a beam incident at an angle θ, the point of incidence on the plate will shift by a distance:

$$\Delta = \delta\cos\Omega - \varepsilon\tan\theta$$

$$\Delta = \delta\left[\cos\Omega - \sin\Omega\tan\theta\right] \qquad (6.1)$$

If the grating has a pitch Λ then this will be observed as a change in phase of the interference pattern of:

$$\phi_{shift} = \frac{2\pi}{\Lambda}\delta[\cos\Omega - \sin\Omega\tan\theta] \tag{6.2}$$

The other component of the phase change is due to the change in size of the triangle ABC. As mentioned above, triangles $A_1B_1C_1$ and $A_2B_2C_2$ are similar, hence:

$$\frac{\Delta A}{A_1} = \frac{\Delta B}{B_1} = \frac{\Delta C}{C_1} \tag{6.3}$$

Now the phase change ϕ_{OPD} at the detector due to this path difference is given by:

$$\phi_{OPD} = \frac{2\pi}{\lambda}(\Delta A + \Delta B - \Delta C)$$

From (6.3):

$$\phi_{OPD} = \frac{2\pi}{\lambda}\left(\Delta A + \frac{B_1}{A_1}\Delta A - \frac{C_1}{A_1}\Delta A\right)$$

$$\phi_{OPD} = \frac{2\pi}{\lambda}\left(\frac{\Delta A}{A_1}\right)(A_1 + B_1 - C_1)$$

$$\phi_{OPD} \propto \Delta A \tag{6.4}$$

But from Fig. 6.1 it is obvious that ΔA depends on the angle of the mirror M_1. However, the phase change from (6.2), due to the shifting of the grating is independent of this angle, and consequently there is no way that for a general case the two functions can compensate for each other. The implications of this extra phase term are grave since it means that the pattern observed at the detector is not purely a function of the grating fringe position, but also of its lateral displacement. Consequently a transverse movement will lead to an unpredictable phase change at the observation point, rendering the phase information useless as a method of determining the grating spatial phase position.

The crux of the problem is that the information obtained at the detector is from the relative phases of the two interfering beams: there is no data on the actual position of the grating fringes. Once the plate has moved from its initial position, the two components of movement: i.e. parallel and perpendicular to the plate axis, each provide a phase term and the resultant phase is a combination of these terms. There is no way to distinguish between the two components of the plate displacement from a single observation of this resultant phase and consequently no way of determining the absolute fringe position.

Thus the transverse position of the plate must be held constant if any meaningful information is to be extracted from the interference pattern formed by the reflected and diffracted beams. Several ideas which proved fruitless were investigated including moving beam geometries and passive methods of plate levelling, such as floating the resist plate in a bath of mercury. The method finally adopted was to use active control of the grating position in a feedback controlled loop: a method known as fringe locking.

6.1.2 Initial proposals for fringe locker design

Traditional fringe lockers work by adjusting the position of a small mirror in one of the beam paths so as to keep the interference pattern stationary relative to the workpiece. This classic fringe locker arrangement is not quite suited to the requirements of this experiment since here the plate is deliberately being moved relative to the pattern. This case differs because it is not the pattern that must be kept fixed relative to the plate, but the transverse position of the plate in space as it moves in its own plane.

As the plate moves, there will inevitably be some transverse movement due to finite precision of both experimental alignment and of the precision of the workpiece micropositioner itself. Assuming that the rotation of the plate during the movement is negligible, the angle of incidence of the beam on the plate will be constant, and consequently so will the angles of the diffracted and reflected beams. Thus the triangle made by the two beams will be geometrically similar to that of the initial triangle. In order to compensate for the transverse displacement the movement of the mirror must be such as to keep this triangle congruent so that the path difference between the two arms of the interferometer is constant.

To this end it was proposed to use an interferometer arrangement with the reflected beam (the diffracted beam is no use in this respect since the phase will be changing as a result of the movement of the grating) as one arm and a direct reference as the other. As the plate moves transversely the path difference between these two beams will effect the interference pattern. Several initial suggestions for an interferometer in which such a corrective optic is used were made: one example is that sketched in Fig. 6.3.

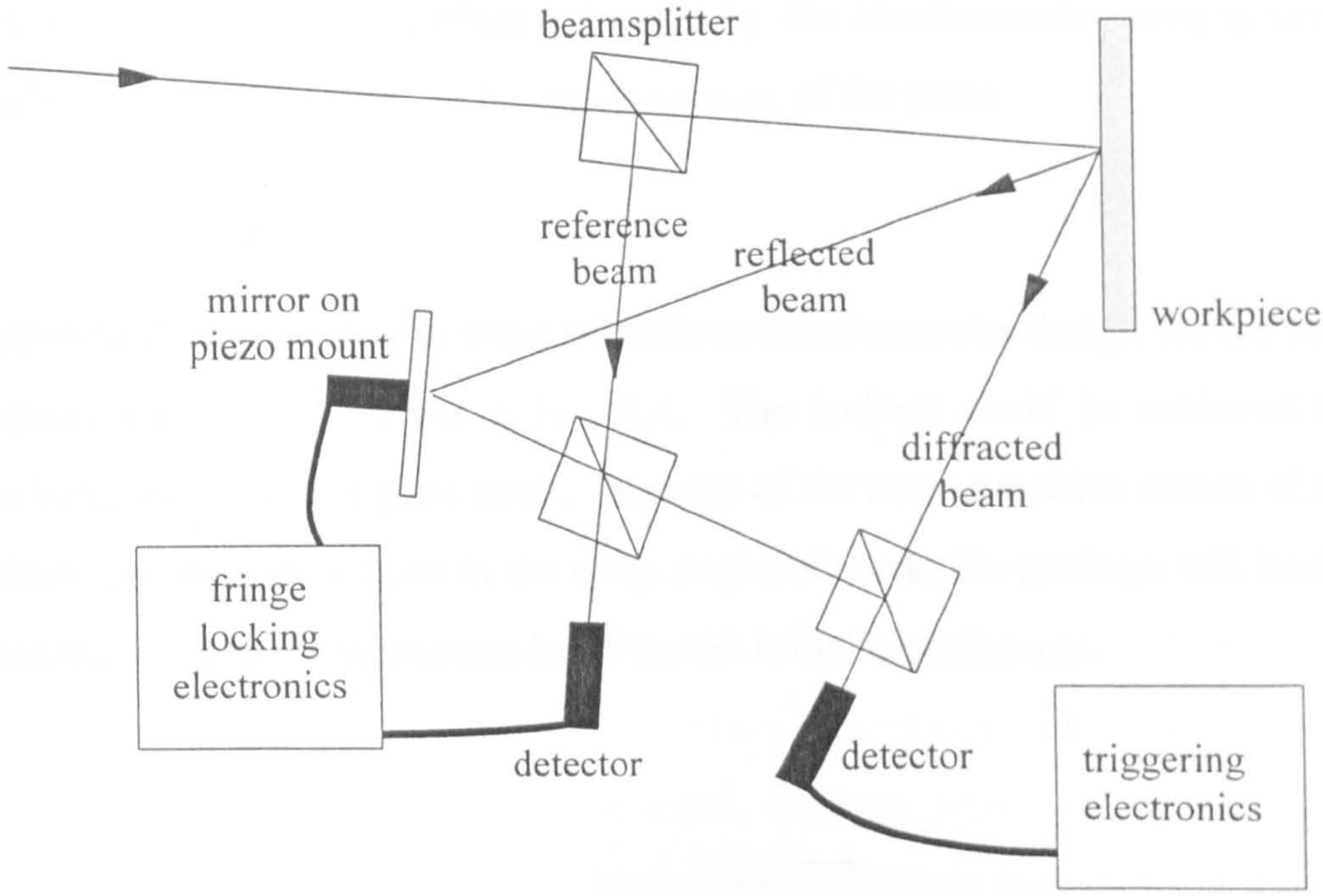

Fig. 6.3: *Showing one initial proposed interferometer arrangement for fringe locking to compensate for transverse movement of the plate. Such methods are flawed because the important path difference is that between the reflected and diffracted beams, and this differs from the corrected path by some arbitrary factor depending on the particular geometry of the beams.*

However, after some thought it was realised that such arrangements will not measure the path difference between the interfering beams: it will measure another path difference (that between the reflected beam and the reference beam) which is proportional to the required length, where the constant of proportionality is dependent on the exact geometry of the interferometer. As the plate moves, the mirror is moved in sympathy so as to keep the pattern at the detector stationary: this imposes several path length changes on the beams:

(a.) As the plate moves transversely the reflected beam path is changed by an amount dependent on the angle of incidence.

(b.) The change to the path length of the diffracted beam is related to the sum of the angle of incidence and the angle of diffraction.

(c.) As the piezo-controlled mirror is moved to compensate, the path of the reference beam may be changed by some amount depending on the geometry of the set up.

These changes are not related to each other in an easily measurable way, and in order to have the desired path compensation it would be necessary to use some form of analogue multiplier between the detector and the input to the piezo driver. Further contemplation revealed that a

system is required in which the triangle formed by the interferometer arms is kept constant using a reference that is unchanged by the movement of the piezo.

One solution to this problem is to use a Michelson interferometer design for the formation of the interference pattern as shown in Fig. 6.4. The locking could be achieved by shifting either the beamsplitter or the plate itself. Because of the more sensitive nature of moving the beamsplitter and because, at least in the early stages of work, the gratings will be fairly small it was decided to move the workpiece itself for the initial experiments.

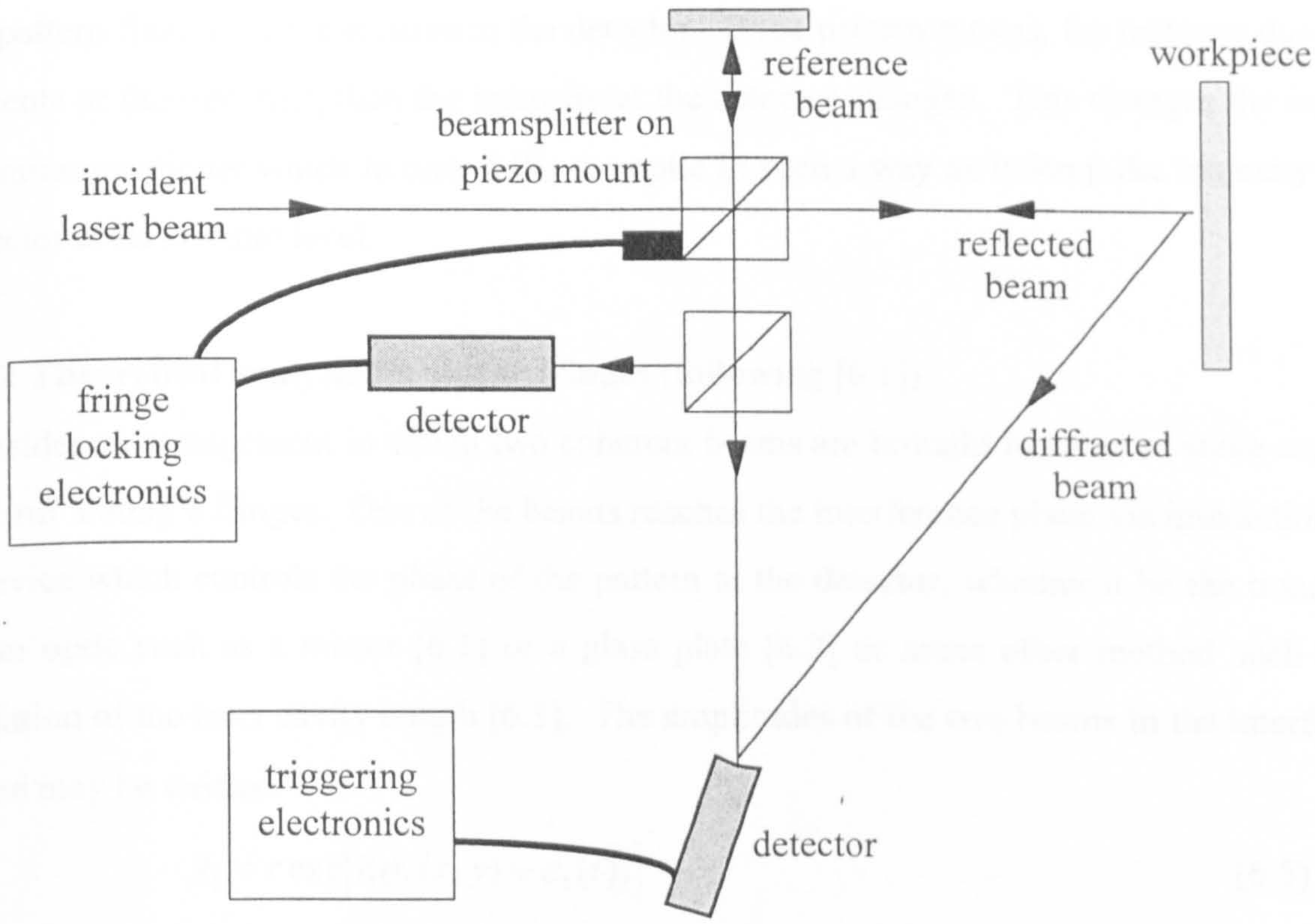

Fig. 6.4: *A sketch showing an improved interferometer set up in which the beamsplitter is moved in sympathy with any transverse movement of the recording media. Thus the whole triangle made by the beams of the interferometer is moved so as to maintain constant separation of the beam splitter and the plate.*

6.2 BRIEF THEORY OF A FRINGE LOCKING MICHELSON INTERFEROMETER

6.2.1 Fringe lockers in holography

Fringe lockers are used in holography in order to increase the stability of fringe patterns. The basic method of operation is to position a light detector so as to measure the intensity at some point in the holographic fringe pattern which is to be stabilised. This detector may observe the pattern direct [6.1] or use a moiré pattern to increase the sensitivity [6.2]. One of the optics used to form the holographic pattern is fitted to a micropositioning device and the position of this component, and hence the spatial position of the pattern, is dependent on the intensity at the detector. In this way the detector and the micropositioner are fixed together in a feedback loop which, when correctly balanced, will lock onto a certain intensity and hold the pattern fixed in space relative to the detector. If the pattern moves, for instance due to air currents or thermal drift, then the intensity at the detector changes. This changes the input to the micropositioner which in turn shifts the optic in such a way as to keep the intensity at the detector at its original level.

6.2.2 Theoretical analysis for linear fringes (following [6.1])

Consider an arrangement in which two coherent beams are brought together at some angle 2θ to form Young's fringes. One of the beams reaches the interference plane via interaction with a device which controls the phase of the pattern at the detector, whether it be the translation of an optic such as a mirror [6.1] or a glass plate [6.2] or some other method such as the variation of the laser cavity length [6.3]. The amplitudes of the two beams in the interference plane may be written:

$$A_1 = r\exp\left[i\left(\phi_1(x,y)+\varepsilon_1(t)\right)\right] \tag{6.5}$$

$$A_2 = a\exp\left[i\left(\phi_2(x,y)+\varepsilon_2(t)-\Phi(t)\right)\right] \tag{6.6}$$

Here a and r are the amplitudes of the two waves, $\phi_{1,2}(x,y)$ are the phases at some point in the interference plane due to the unperturbed optical path of the two beams, $\varepsilon_{1,2}(t)$ are the errors in phase at the interference plane due to any unwanted phase shifts in the system and $\Phi(t)$ is the phase component due to the movement of the piezo actuator-controlled optic. The resulting interference pattern may be written:

$$I = a^2 + r^2 + 2ar\cos\left[\left(\phi_1(x,y)-\phi_2(x,y)+\varepsilon_1(t)-\varepsilon_2(t)+\Phi(t)\right)\right] \tag{6.7}$$

If a photodetector observes a small point of the pattern or a line parallel to the fringes, then the sum of the $\phi(x,y)$ terms will simplify to some constant ϕ_o and the $\varepsilon_{1,2}(t)$ terms may be replaced by their sum $\varepsilon(t)$:

$$I(t) = a^2 + r^2 + 2ar\cos\left[(\phi_o + \varepsilon(t) + \Phi(t)\right] \tag{6.8}$$

Assuming that the photodetector amplifier supplies a voltage V_{amp} which is proportional to the intensity at the slit, and that the micropositioner gives a movement, Δ, which is proportional to the applied voltage, then:

$$V_{amp} = PI(t) \tag{6.9}$$

$$\Delta = MV_{amp} \tag{6.10}$$

$$\Rightarrow \Delta = MP\left[a^2 + r^2 + 2ar\cos\left[\phi_o + \varepsilon(t) + \Phi(t)\right]\right] \tag{6.11}$$

From (6.6) it is apparent that $\Phi = k\Delta$, where k is the wave number of the interfering light. Also, let the *total perturbed phase* of the fringes be given by: $\beta(t) = \phi_o + \varepsilon(t)$ so that (6.11) may be rewritten:

$$\Phi = kMP(a^2 + r^2) + 2kMPar\cos\left[\beta(t) + \Phi(t)\right]$$

$$\Phi - B = G\cos\left(\beta(t) + \Phi(t)\right) \tag{6.12}$$

Here G $(= 2kMPar)$ is a constant relating to the closed loop gain and B $(= kMP(a^2+r^2))$ is a constant relating to the system bias.

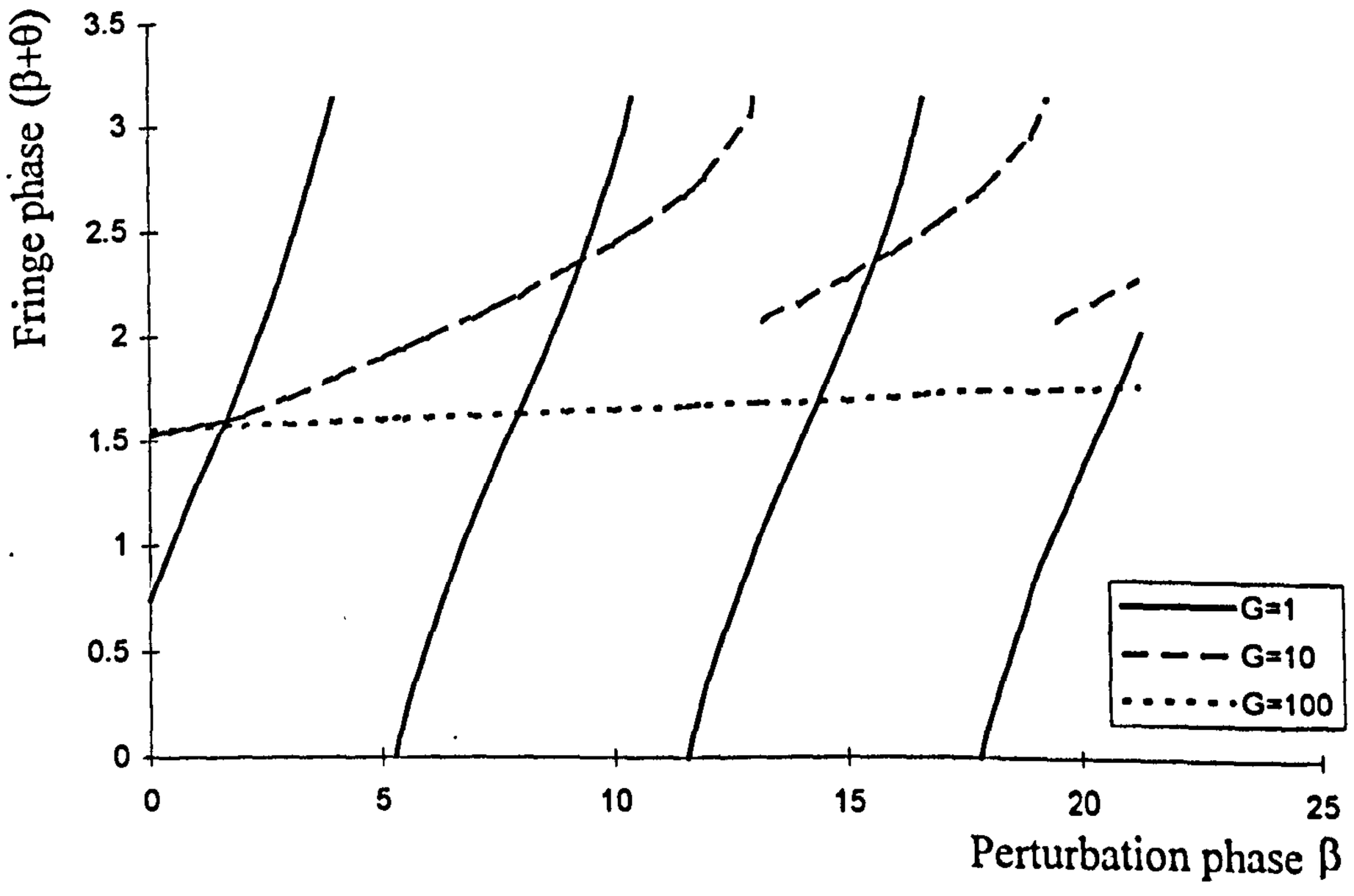

Fig. 6.5: *A graph showing the solution of the closed loop stability equation for several gain constants.*

Following [6.1] the solution to (6.12) may be analysed using a graphical method: the two sides are plotted as a function of $(\beta+\Phi)$. The right-hand side thus gives a cosinusoidal waveform and the left hand side a series of straight lines, one for each value of the perturbed fringe phase, β. Variation of β shifts the straight line and hence the $(\beta+\Phi)$ co-ordinate of the point of intersection (i.e. the solution to the equation). This yields a graph of $(\beta+\Phi)$ against β as shown in Fig. 6.5.

Physically the cosine wave represents the fringe phase of the pattern at the detector and the points of intersection with the straight lines represent the actual phase measured at the detector when the system is locking for each β.

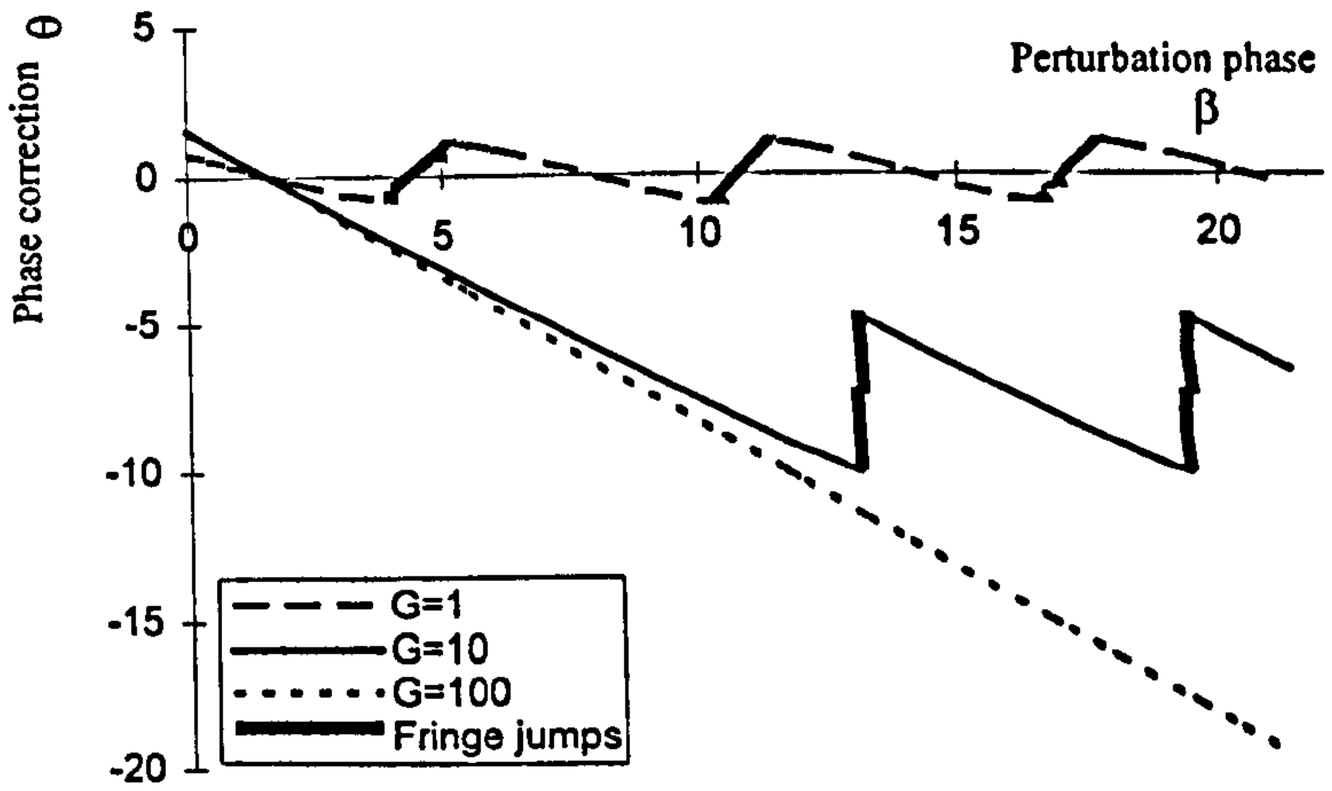

Fig. 6.6: *Showing the phase correction which the phase locker can deliver without fringe jumps for gain constants, G, of 1, 10 and 100.*

Whether this solution will lead to stable fringe locking depends on the slope at the point of intersection and the polarity of the detector amplifier response. As the fringe phase is shifted the recorded intensity will either increase or decrease and this will generate a system response which will in turn either increase or decrease the intensity. Naturally there can only be a stable solution for the case where the system tries to oppose the intensity change rather than amplify it. Thus either the positive or the negative slope will lead to a stable solution: here the positive slope has been chosen arbitrarily.

Fig. 6.5 shows the solution of the equation for values of the gain constant, *G*, of 1, 10 and 100. Fig. 6.6 shows the actual phase correction that the locker provides, θ. It is clear from

Fig. 6.5 that as G is increased the fringe phase at the detector becomes more stable. For low values of G (e.g. G=1) the fringe locking is weak; for only a small shift in β the system is taken into a region of intersect with the unstable negative fringe slope and this leads to intervals of perturbation phase for which there is no stable locking. In this case the pattern will be moved past the detector until it reaches a region of stable behaviour on the next fringe, where the weak lock will resume.

For higher gains the locking is strengthened and the system can cope with larger shifts in β without being made unstable with only a small change in the observed phase at the detector. Essentially the pattern is being pushed one way by the unwanted perturbation but this can almost all be compensated for by the phase shifter pulling the pattern back again.

6.2.3 Fringes in a Michelson interferometer

The analysis of the stability of the fringe locker described in the previous section was originally carried out for the stabilisation of quasi-linear Young's fringes. However, in this application the fringes are the circular fringes which may be observed using a Michelson interferometer as illustrated in Fig. 6.4. An interesting method of analysing the fringe formation in a Michelson interferometer [6.4] is illustrated in Fig. 6.7.

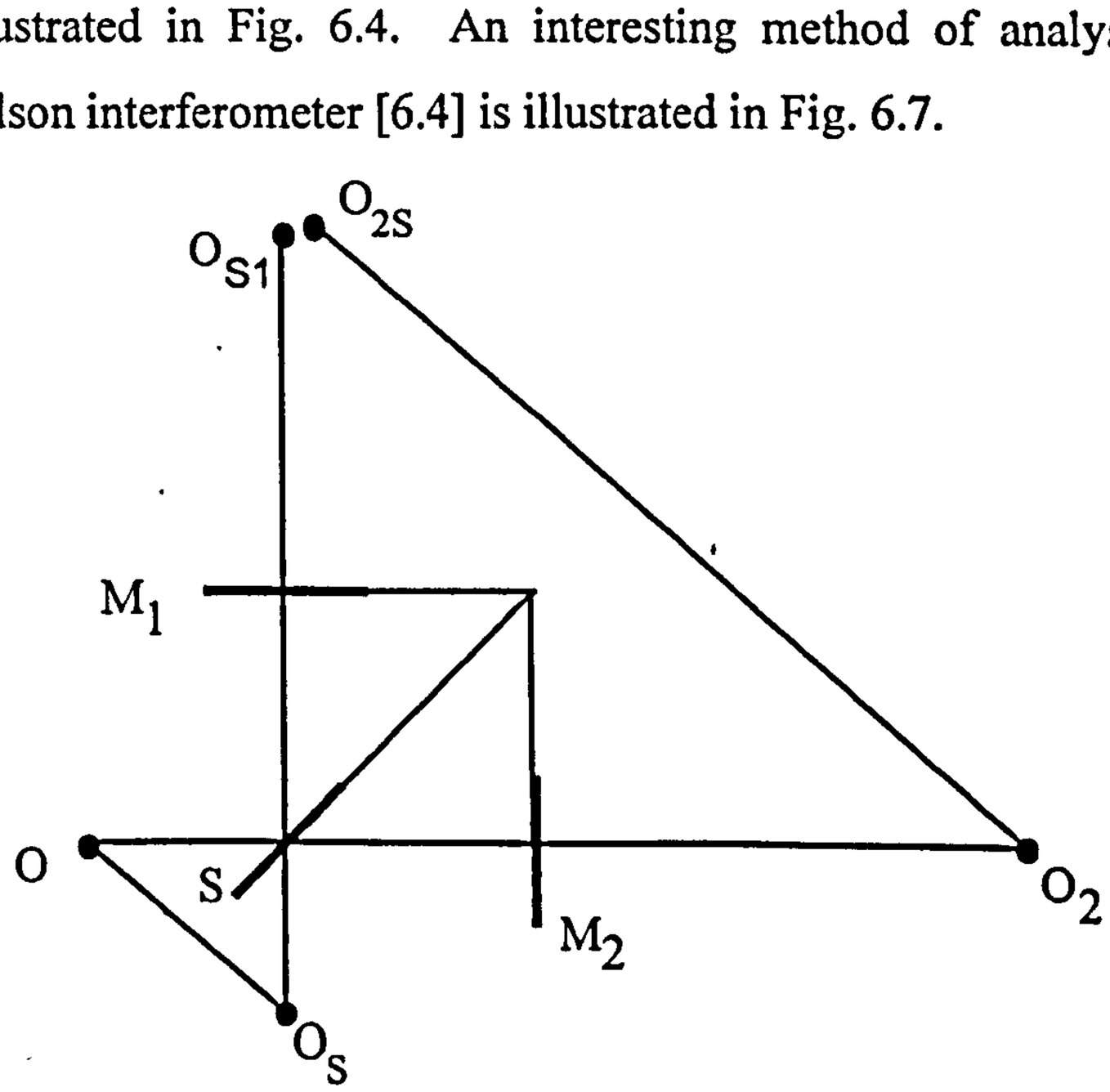

Fig. 6.7: *Showing the geometry of the source and its various images in a Michelson interferometer. [S = beam splitter and M1, M2 are mirrors.]*

The source O has an image O_S in the beamsplitter S, which in turn has an image O_{S1} in the mirror $M1$. Similarly O has an image O_2 in $M2$ which has an image O_{2S} in S. It may be considered that it is these two virtual sources O_{S1} and O_{2S} that give rise to the interference fringes. If they are adjacent to one another, then Young's fringes will be observed. However it is more common to have the two virtual sources almost collinear with the point of observation. In this case the fringes will have an approximately circular geometry according to the analysis of Fig. 6.8.

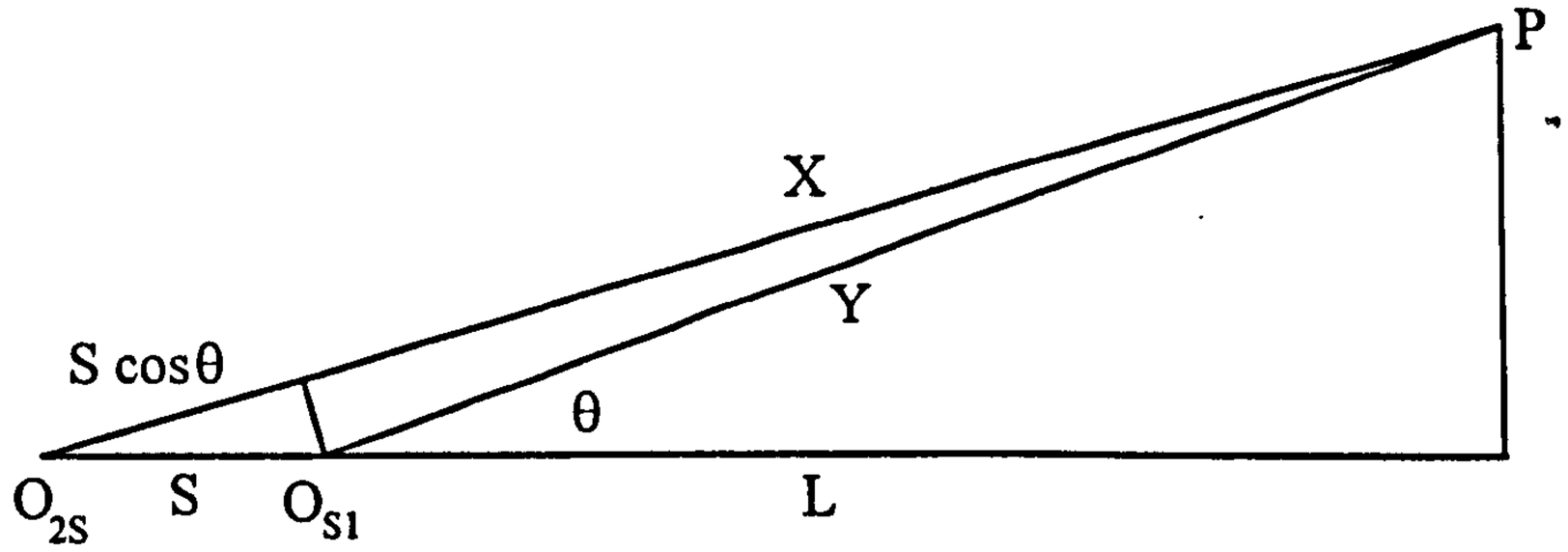

Fig. 6.8: *Showing the formation of circular fringes in a Michelson interferometer.*

If the two beams are assigned unit intensity then the amplitude of the resultant wave at P will be given by:

$$A = \exp(ikX) + \exp(ikY)$$

This may be written: $$\exp\left(ik\left[\left(\frac{X+Y}{2}\right)+\left(\frac{X-Y}{2}\right)\right]\right)+\exp\left(ik\left[\left(\frac{X+Y}{2}\right)-\left(\frac{X-Y}{2}\right)\right]\right)$$

$$\therefore A = 2\exp\left[ik\left(\frac{X+Y}{2}\right)\right]\cos\left[k\left(\frac{X-Y}{2}\right)\right] \qquad (6.13)$$

For the usual case where L »S: $(X-Y) \approx S\cos\theta$

Hence: $$I = |A|^2 \approx 4\cos^2\left(\frac{kS\cos\theta}{2}\right) = 2\left[1+\cos(kS\cos\theta)\right] \qquad (6.14)$$

Thus the pattern observed at the output of the interferometer is constant for the exit angle θ and hence the fringes are circular. The precise intensity at the centre of the pattern depends on the particular value of S. S also determines the dimensions of the fringes: as $S \to 0$ the angular radius of the central fringe increases towards infinity.

6.2.4 Theoretical analysis of fringe locking for circular fringes

Consider a fringe-locked Michelson interferometer, such as that of Fig. 6.4, aligned to give circular fringes. The particular optical path difference between the beams determines the intensity at the centre of the pattern ($\theta = 0$, $\cos\theta = 1$): from (6.14) kS must be equal to $2m_o\pi$ where m_o is an integer: the number of whole wavelengths path difference between the two interfering beams. As the angle of observation, θ, is increased, the pth bright fringe will occur at angle θ_p where:

$$kS\cos\theta_p = (m_o - p)2\pi \tag{6.15}$$

Hence, using the approximation for small angles: $\cos\alpha = 1 - \frac{1}{2}\alpha^2$

$$\theta_P = \sqrt{\frac{4p\pi}{kS}} \Rightarrow \sqrt{\frac{2p\lambda}{S}} \tag{6.16}$$

If the pattern is observed at some angle ψ then the observed intensity for two waves of amplitudes a and r will be given by [6.5]:

$$I = a^2 + r^2 + 2ar\cos[(k\cos\psi)S] \tag{6.17}$$

For a perfectly static system S is constant and so the phase of the cosine term is fixed, for a given viewing angle, at some value ϕ_o:

$$I = a^2 + r^2 + 2ar\cos\phi_o \tag{6.18}$$

If the path difference is changed, say due to the transverse movement of the recording medium, then ϕ_o will be changed by some amount ε and the micropositioner will change the phase by a further amount Φ:

$$I(t) = a^2 + r^2 + 2ar\cos[(\phi_o + \varepsilon(t) + \Phi(t)] \tag{6.19}$$

But this equation is identical to (6.8), and so the remainder of the derivation may be repeated, giving the same stability condition as for the case with Young's fringes.

6.3 PRACTICAL REALISATION OF A FRINGE–LOCKING MICHELSON INTERFEROMETER

A block diagram of the adopted fringe locker design is sketched in Fig. 6.9. The HeNe beam was brought in vertically via a fibre which filtered the beam. This vertical beam arrangement was used to give increased physical stability for the longer exposures [see section 7.1]. The reference arm uses a second piece of (unexposed) resist plate, instead of the mirror used in a traditional Michelson interferometer, in order to give better power balance between the two beams.

The workpiece itself was fixed to a piezo actuator which moved in the vertical plane. This actuator was itself mounted on a pitch and yaw adjustable mount which was levelled using the Michelson interferometer (see section 7.2) so as to reduce the demand on the locker. In the following few sub-sections the pertinent points of some of the components which required design are briefly outlined.

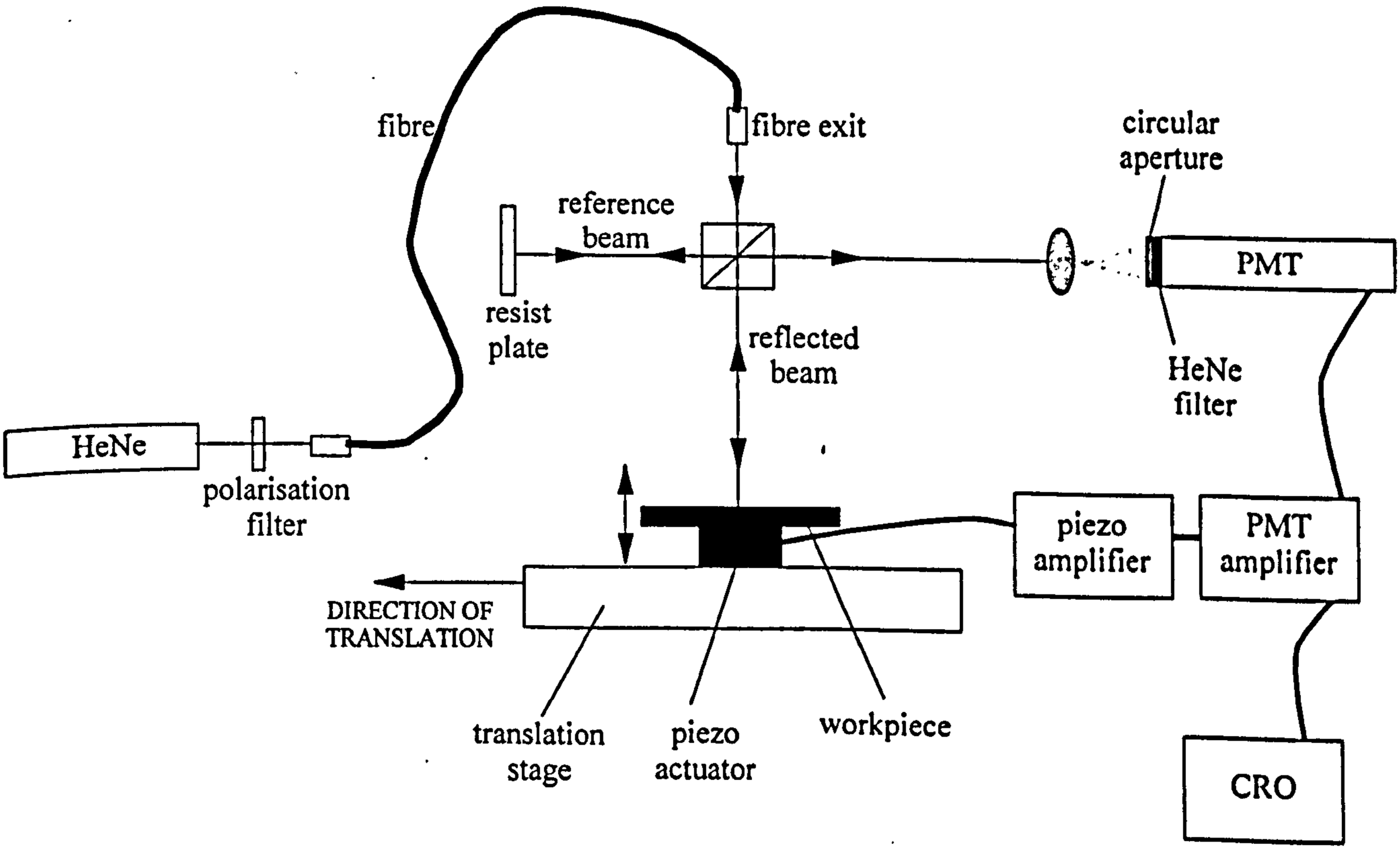

Fig. 6.9: *A block diagram of the Michelson interferometer fringe locker.*

6.3.1 Piezo electric actuator

In recent years piezoelectric actuators become widely used in applications requiring extreme high-precision positioning. They have found widespread use due to their high dynamic response and sub-nanometre resolution, coupled with the possibility of generating large forces over a large range ([6.6], [6.7]). The phenomenon of piezoelectricity occurs significantly in certain ionic solids which crystallise into structures lacking a centre of inversion, e.g. lead zirconium titanate (PZT) used in most modern actuators [6.8]. If such a solid is put under stress along certain directions, the molecules are distorted in such a way as to be polarised with the result that an electric field is observed across the crystal. Conversely if such a crystal is subjected to an electric field, its molecules will be distorted and it will change its size in one or more dimensions. It is this inverse piezo-electric effect that is exploited in piezo-electric actuators.

Of the many designs of actuator, the technique giving the highest expansion efficiency which is used in most modern piezo actuators is that of the "piezostack" which consist of a large number (typically ~ 100) of thin discs of the order of a few hundred microns thick. Each disc has an electrode connected to each of its faces and naturally the field across the material for any given voltage is dependent on the thickness of the disc. An applied voltage will result in the ends of the stack moving due to the combined longitudinal piezoelectric effect of all of the individual elements.

An important consideration in the case of dynamic applications is the capacitance of the piezostack. In essence the stack may be regarded as a set of high resistance (~10^{10} Ω) parallel plate capacitors connected in parallel. From elementary electromagnetic theory the resultant capacitance of n parallel plate capacitors with surface area A and inter-plate spacing x connected in parallel is given by [6.9]:

$$C = n\left(\frac{\varepsilon_r \varepsilon_o A}{x}\right) \tag{6.20}$$

where ε_o is the permeability of free space and ε_r is the dielectric constant of the ceramic. Naturally if the capacitance of the stack is large then in dynamic applications where high frequency oscillations may be involved there will be significant current flow and this must be considered in the design of the power supply.

When used in a vibrating dynamic situation the actuator will act as will any elastic body: as the period of oscillation approaches the time taken for a acoustic wave to travel along the actuator length, there will be a resonance [6.10]. If the stiffness of the actuator is S and assuming simple linear behaviour then the motion is simple harmonic and the resonant frequency is given by [6.11]:

$$f_{RES} = \frac{1}{2\pi}\sqrt{\frac{S}{m}} \tag{6.21}$$

Here m is the effective mass of the piezo, i.e. the mass of the actuator itself plus any preload and any external load. The value of resonant frequency for a typical short stack piezo is of the order of tens of kilohertz. Obviously the actuator will not perform reliably when the duty cycle has a frequency close to resonance.

The first fringe locking trials were attempted using a long stack (~12cm) actuator which had resonant frequencies as low as 300 Hz and since the fringe locking signal contained frequencies significantly greater than this, the resonances interfered with the fringe locker response. The result was that the locking was very weak, with many fringe jumps and the locker was easily sent into oscillation.

A new piezo was obtained: the Str-25/150/6 from ThorLabs which had a total movement of 6 μm for an applied voltage of 150 V. This actuator has a 25 mm diameter mirror mount which screws directly onto the moving barrel. This actuator was ~10mm long and the lowest resonance was at several kilohertz: safely above the high frequency response of the piezo amplifier.

One important point which was deduced from this set of trials is that although the actuator can provide a very large force along its axis, it is extremely sensitive to any forces perpendicular to this axis. Consequently the actuator is limited to a 20 g mass on the mirror mount if the piezo axis is horizontal. It was found that there was a marked improvement in performance if the axis was kept vertical. Experiments also showed that it is advantageous to avoid any form of tilting moment on the piezo i.e. any loads should be mounted symmetrically.

6.3.2 Photomultiplier tube

Photomultipliers are extremely sensitive detectors of light that provide a current which is ideally directly proportional to the incident light intensity. The incident light impinges onto a photocathode, which emits electrons as described by the photoelectric effect. These photoelectrons are accelerated by an applied field through a series of electrodes, known as dynodes, which in turn emit secondary electrons and form a cascade of electrons which provides a measurable current.

A photomultiplier may be represented by the equivalent circuit shown in Fig. 6.10 [6.12]. The photocathode may be regarded as an ideal current source in parallel with the internal resistance and capacitance of the photomultiplier itself. The output voltage *v(t)* is measured across the load resistance R_L and any capacitance associated with the measuring equipment, C_L.

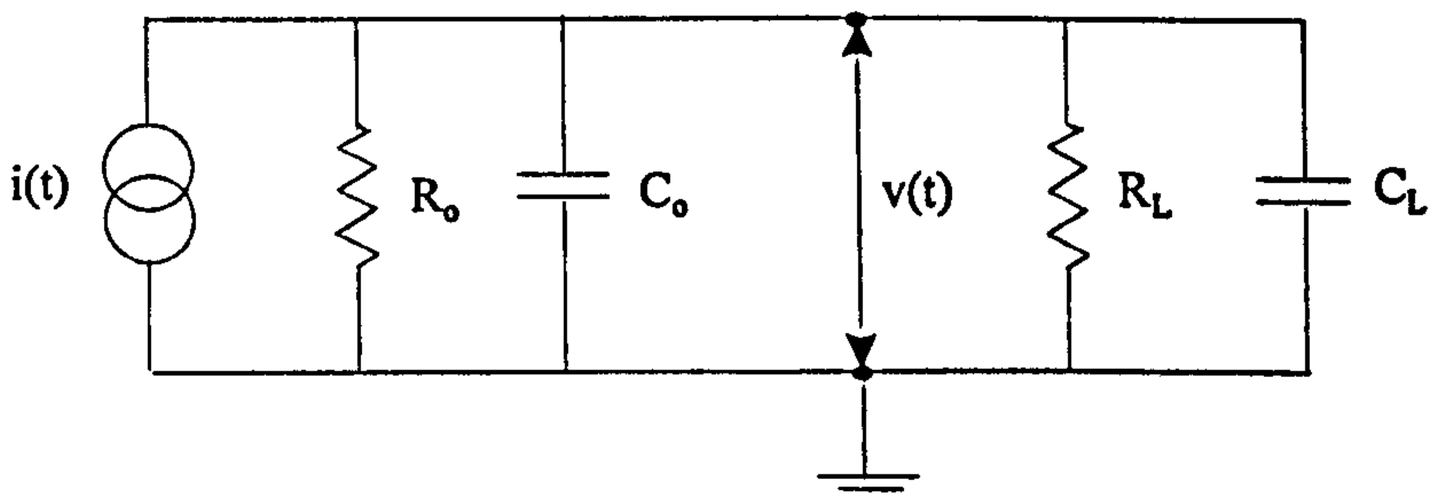

Fig. 6.10: *A sketch of the equivalent circuit of a photomultiplier.*

The time constant associated with such a circuit is given by:

$$\tau = RC \tag{6.22}$$

Where: $R = \dfrac{R_o R_L}{R_o + R_L}$ and $C = C_o + C_L$

Naturally, in order for the photomultiplier to respond faithfully to a pulse of light, the time constant associated with the pulse must be larger than τ. Similarly if the frequency of the pulses is too great, then the photomultiplier will not have sufficient time to recover between pulses, and there will be an overlap of responses. As a rule of thumb, it is usual to have τ no bigger than a quarter of the event rate to avoid these overlaps [6.12].

From the experiments with the latent image gratings it had been found that although the diffracted beam was too weak to be measured using standard laboratory light meters it was possible to observe the beam with the naked eye if the observer looked directly down the beam. In the light of these fairly modest requirements (modest considering that PMTs may used for individual photon detection) a fairly standard tube was used: Electron Tube 9124B. This eleven dynode linear focused tube has a 30 mm diameter circular bialkali (Sb-Rb-Cs) photocathode with reasonable radiant sensitivity at 632.8 nm (~12 mAW^{-1}).

The response time, or transit time is the time taken for the electrons to pass through the photomultiplier itself: from the photocathode to the anode. There is a certain amount of variation in the transit time because the electrons leaving the photocathode have a variety of energies and also because different electrons follow different paths through the tube. The transit time for the 9124B is quoted as 20 - 55 ns with a jitter of 0.5 - 1.2 ns.

6.3.3 Photomultiplier amplifier design

The amplifier design used in the fringe locker was a "resistive-T" network current to voltage converter as sketched in Fig. 6.11 [6.13].

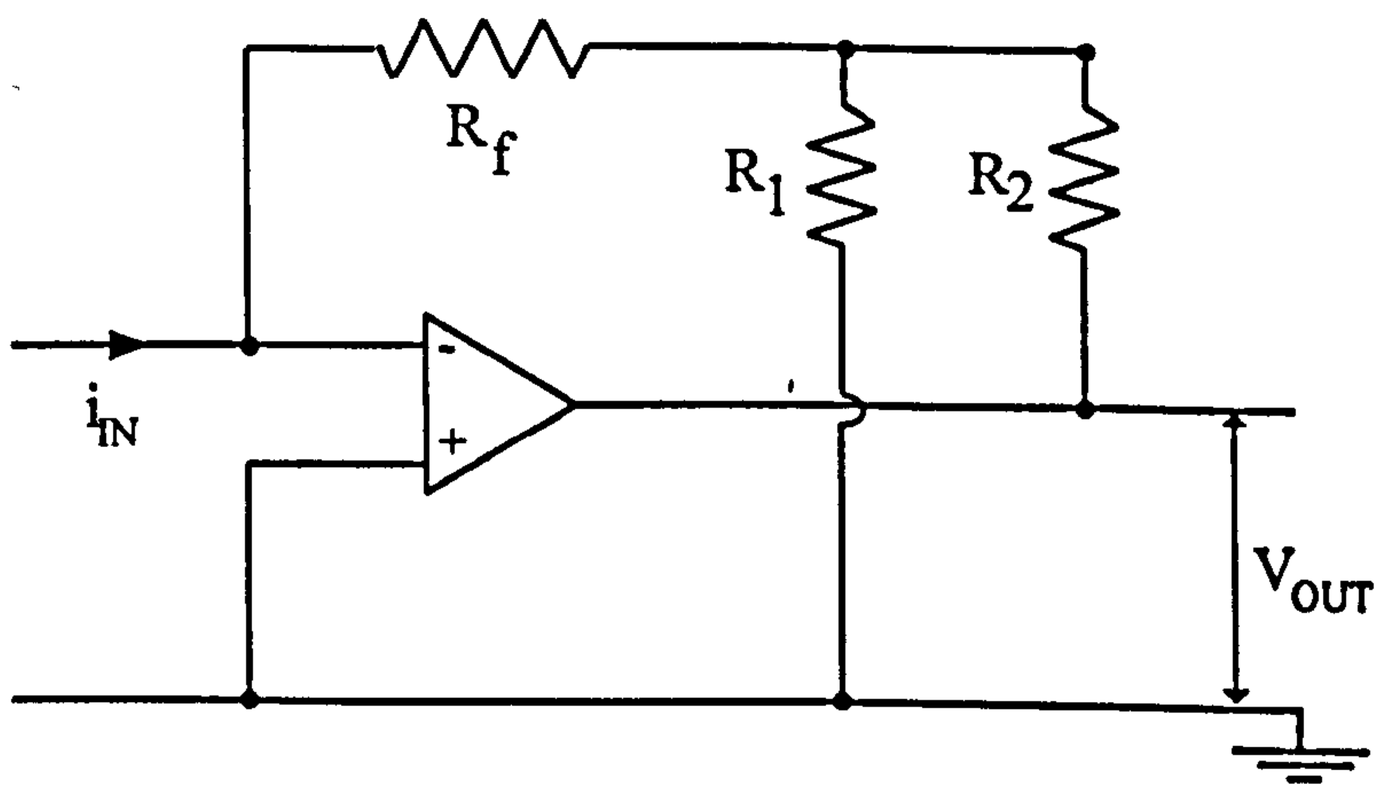

Fig. 6.11: *Showing the basic "resistive T network" current to voltage converter design.*

Because of the huge input impedance of the op-amp, essentially all of the input current from the photomultiplier is passed through the feedback resistor, R_f and so there is a voltage $-i_{IN} R_f$ across R_1.

This voltage must be equal to the voltage fed back from the potential divider formed by R_1 and R_2, hence:

$$-i_{IN} R_f = \left(\frac{R_1}{R_1 + R_2}\right) V_{OUT} \qquad \Rightarrow V_{OUT} = -i_{IN} R_f \left(1 + \frac{R_2}{R_1}\right) \tag{6.23}$$

A capacitor C_f is put across the feedback resistor R_f to counteract any elements of positive feedback from the photomultiplier internal capacitance, C_{PMT}. This capacitor also acts as a low pass filter, removing much of the unwanted high frequency noise from the signal [6.14].

There was further filtering applied to the input signal and the actual design used also incorporates an active first order low pass filter. In order to determine the cut-off frequency the response of the piezo driver amplifier for a sinusoidal input of constant amplitude was measured as a function of frequency: the results are shown in Fig. 6.12.

The piezo amplifier did not respond well to input signals of a frequency higher than ~2 kHz and so this was chosen as the cut off frequency. This filter can also provide a further gain stage: from the circuit diagram given in Fig. 6.13 it can be seen that the feedback fraction is simply given by:

$$\beta = \frac{R_A}{R_A + R_C} \tag{6.24}$$

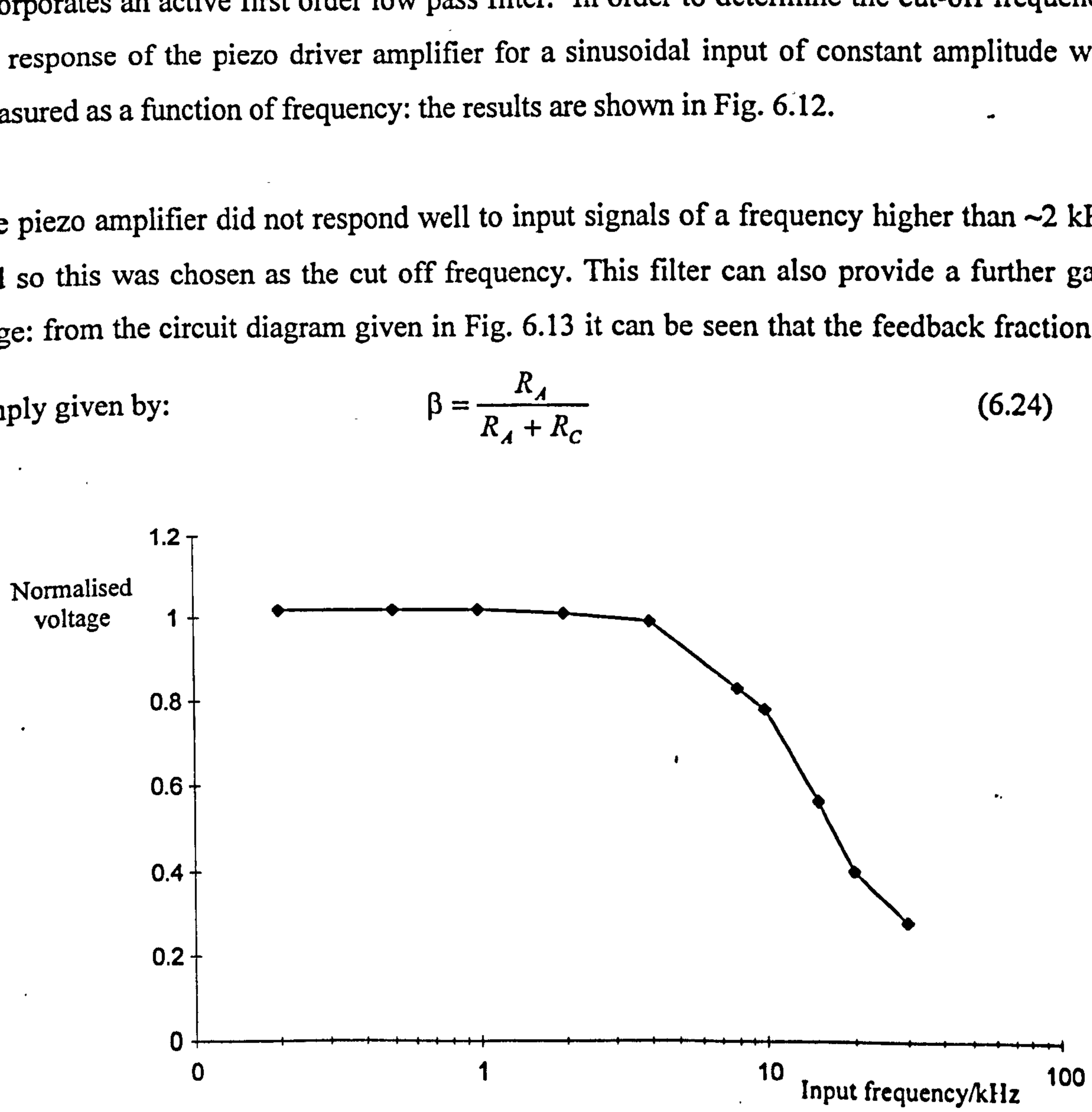

Fig. 6.12: *A graph showing the variation with frequency of the output of the piezo amplifier to a sinusoidal input of constant amplitude.*

Hence the closed loop gain, G_{CL}, for the filter is given by: $G_{CL} = \frac{1}{\beta} = \left(1 + \frac{R_C}{R_A}\right)$ (6.25)

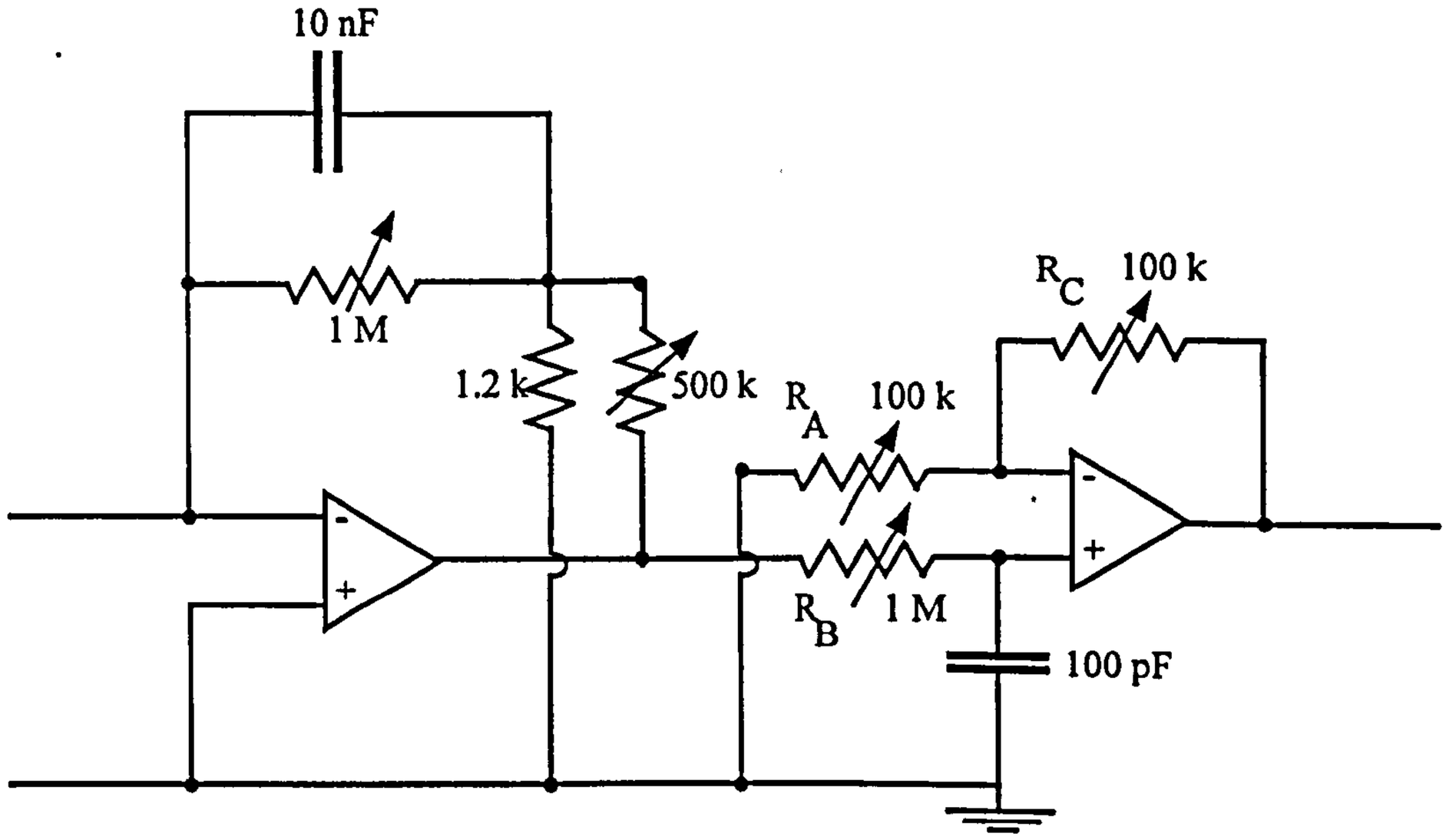

Fig. 6.13: *A circuit diagram of the amplifier and filter combination used for the fringe locker PMT.*

The cut-off frequency for the filter is due to the role of the R_B / C combination and as for any first order filter is given by [6.15]: $f_{cut-off} = \frac{1}{2\pi R_B C}$ (6.26)

Hence the total output for the signal below the cut-off frequency for the amplifier is:

$$V_{OUT} = -i_{IN} R_f \left(1 + \frac{R_2}{R_1}\right)\left(1 + \frac{R_C}{R_A}\right) \quad (6.27)$$

In order to make the amplifier more versatile, most of the resistors used were variable so that the gain and cut off frequency could be easily altered if necessary. In practice the first stage was used to do the amplification and the second gain stage was not necessary ($R_C < R_A$ so filter stage gain ~ 1). A typical set up would be $R_f \sim 1\ \text{M}\Omega$, $R_1 \sim 1.2\ \text{k}\Omega$ and $R_2 \sim 120\ \text{k}\Omega$, giving $V_{OUT} \sim -10^8 |i_{IN}|$.

6.3.4 Optical considerations

The HeNe beam from the laser was unpolarised, and so in order to obtain a linearly polarised beam it was passed thorough a polariser before entering the fibre which both filtered the beam and provided a convenient method of delivering the HeNe light vertically. The fibre was a Point Source polarisation maintaining fibre, and so the input polarisation was aligned with the

acceptance orientation of the fibre by adjusting the polarisation filter so as to obtain optimum polarisation purity at the output.

As described in section 6.2.4, in order to lock on a circular fringe, the aperture to the photomultiplier may be an annulus, or possibly a pinhole. An annular aperture was made by spraying black paint onto a microscope slide cut to size. A fine line (approximately 35 μm across, measured using a calibrated microscope) was then engraved into the paint using a scalpel and a stencil and fixed in front of the HeNe filter on the entrance aperture to the photomultiplier tube. Trials with this aperture were carried out, but it was found that better results were obtained using a small (~0.2 mm) pinhole rather than an annulus.

6.3.5 Performance of the locker

With all the components of the locker set up as described in the previous discussion, the fringe locker was very effective. With the piezo amplifier switched off, a gentle tap of the table was sufficient to send the phase of the observation point into wild oscillations as the interference fringes moved across the detector. Plate 6.1 shows two traces of the PMT output: one with the locker operating and one without. The optical table was tapped with a heavy plastic handled screwdriver at the positions indicated by the arrows and the difference in response is clear. An important demonstration of the ability of the locker is that it was possible to move the whole of the length of the micropositioner scan (2.5 cm) without a phase jump showing that the level of the plate was kept within one fringe (~300nm) over the whole distance of the travel.

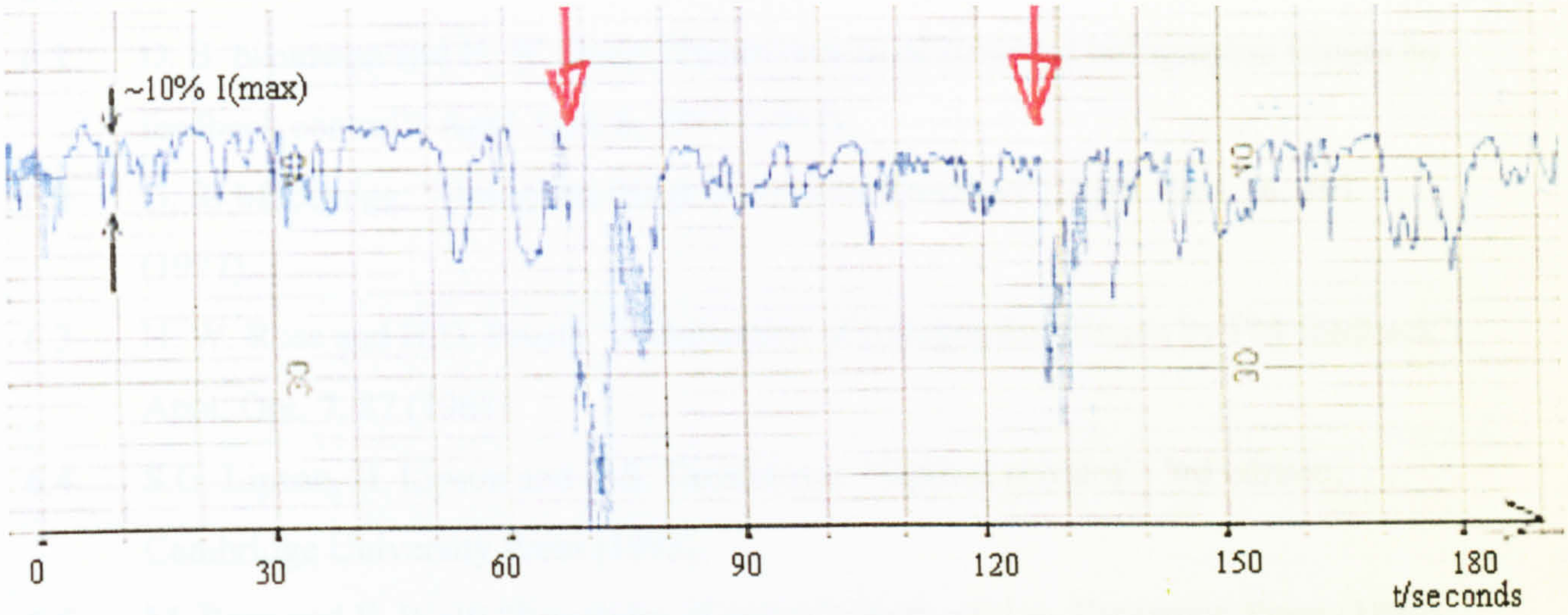

Plate 6.1b: A chart recorder trace showing the intensity of the unlocked fringe pattern with time. The red arrows indicate where the optical table was delicately agitated to show the extent of the instability.

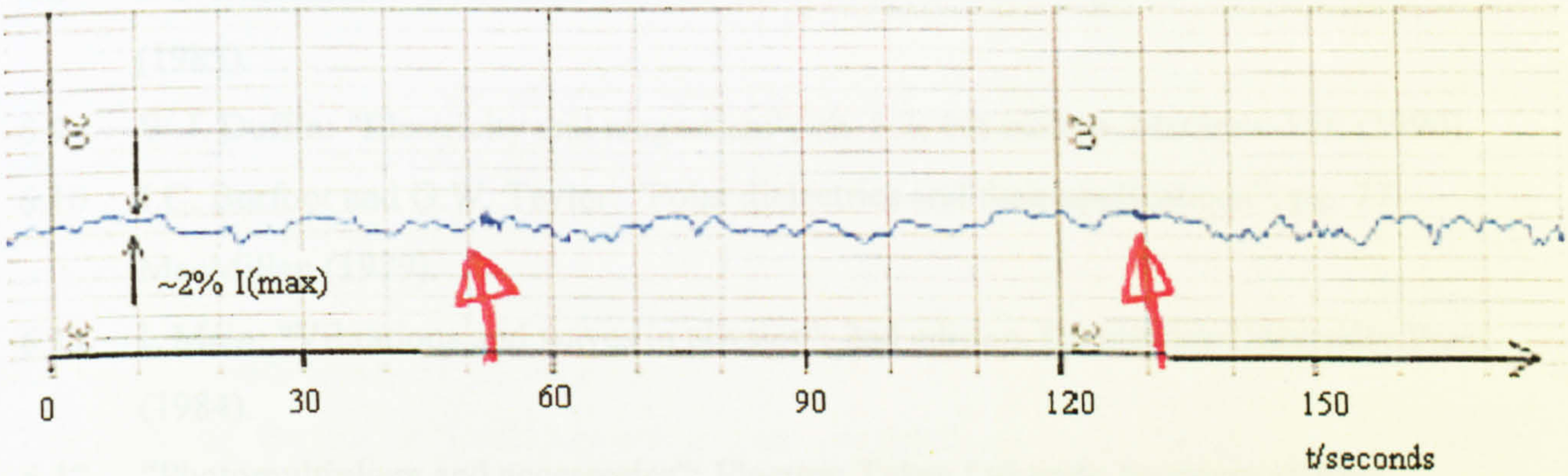

Plate 6.1b: A chart recorder trace showing the intensity of the fringe pattern with the fringe locker in operation. The red arrows indicate where the table was delicately agitated to show the extent of the instability.

Plate 6.1: Two chart recorder traces showing the intensity of the fringe pattern with and without the locker in operation. The traces are intended to be a guide only since the intensity variations were too rapid to be accurately measured by the chart recorder.

REFERENCES

6.1 D. B. Neumann and H. W. Rose: "Improvement of recorded holographic fringes by feedback control"; Appl. Opt. **6**, 1097 (1967).

6.2 D. R. MacQuigg: "Hologram fringe stabilisation method"; Appl. Opt. **16**, 291 (1977).

6.3 H. W. Rose and H.D. Pruett: "Stabilisation of holographic fringes by FM feedback"; Appl. Opt. **7**, 87 (1968).

6.4 S.G. Lipson, H. Lipson and D.S. Tannhauser: "Optical physics"; 3rd edition, Cambridge University Press (1995).

6.5 M. Born and E. Wolf: "Principles of optics"; Sixth edition, Pergamon Press (1980).

6.6 L. Pickelmann: "Piezomechanical actuators: principles and applications": Piezomechanik trade literature (1997).

6.7 "Piezoline: Theory, instruction and application": Piezosystem Jena trade literature (1997).

6.8 J. S. Blakemore: "Solid state physics"; 2nd edition, Cambridge University Press (1985).

6.9 W.J. Duffin: "Electricity and magnetism"; ch. 5.2; 4th edition, McGraw-Hill (1990).

6.10 J.C. Burfoot and G.W. Taylor: "Polar dielectrics and their applications"; pg. 77 MacMillan (1979).

6.11 I. Main: "Vibrations and waves in physics"; 2nd edition, Cambridge University Press (1984).

6.12 "Photomultipliers and accessories": Electron Tubes Ltd trade literature (1996).

6.13 G.B. Clayton: "Operational amplifiers"; ch. 4.5, 2nd edition, Butterworth Press (1979).

6.14 J. Millman and A. Grabel: "Microelectronics"; 2nd edition, Mc-Graw-Hill (1987).

6.15 J.D. Ryder: "Engineering Electronics"; pg. 279, 2nd edition, McGraw-Hill (1967).

Chapter 7

EXPERIMENTAL REALISATION OF METHOD

This chapter discusses the experimental work and the results obtained from the initial investigations into this novel method of writing continuous diffraction gratings. There are three main parts to the apparatus and these are described in detail. The experimental procedural details of the apparatus are also described and the first results are discussed.

The diffraction gratings resulting from this first stage of work are of rather low quality because of the poor calibre of some of the apparatus. Nevertheless continuous gratings over 2 cm long were written using Gaussian beams which gave a usable grating diameter of ~1 mm and electron micrographs revealed that although the grating lines themselves were somewhat scruffy the continuous process works well and the general microscopic structure of the gratings was one of good consistency. This poor uniformity of the gratings is to be expected, since intensity profiles of the writing beams reveal that they have severe distortions from a Gaussian distribution, arising due to poor quality optics and diffraction patterns imposed by the action of the acousto optic modulator.

7.1 EXPERIMENTAL APPARATUS

The bulk of the experimental apparatus was mounted on a Technical Manufacturing Corporation optical table. The optics were held in position on a variety of mounts held on 5 cm diameter, 40 cm high aluminium poles supported on large (10×5 cm^2) magnetic bases. When the method was originally conceived it was expected that the writing beams would be parallel with the plane of the optical bench and incident on a plate travelling on its edge past the point of interference. However, from the trials with the piezo actuator in the fringe locker it seemed that it would be necessary for the plate to be mounted horizontally with the actuator axis vertical. Hence a recording arrangement was devised in which the blue and the red laser beams are brought vertically onto a horizontal workpiece via optical fibres and the fringe locker is of the Michelson interferometer type. A photograph of this apparatus may be seen in Plate 7.1 on the following page.

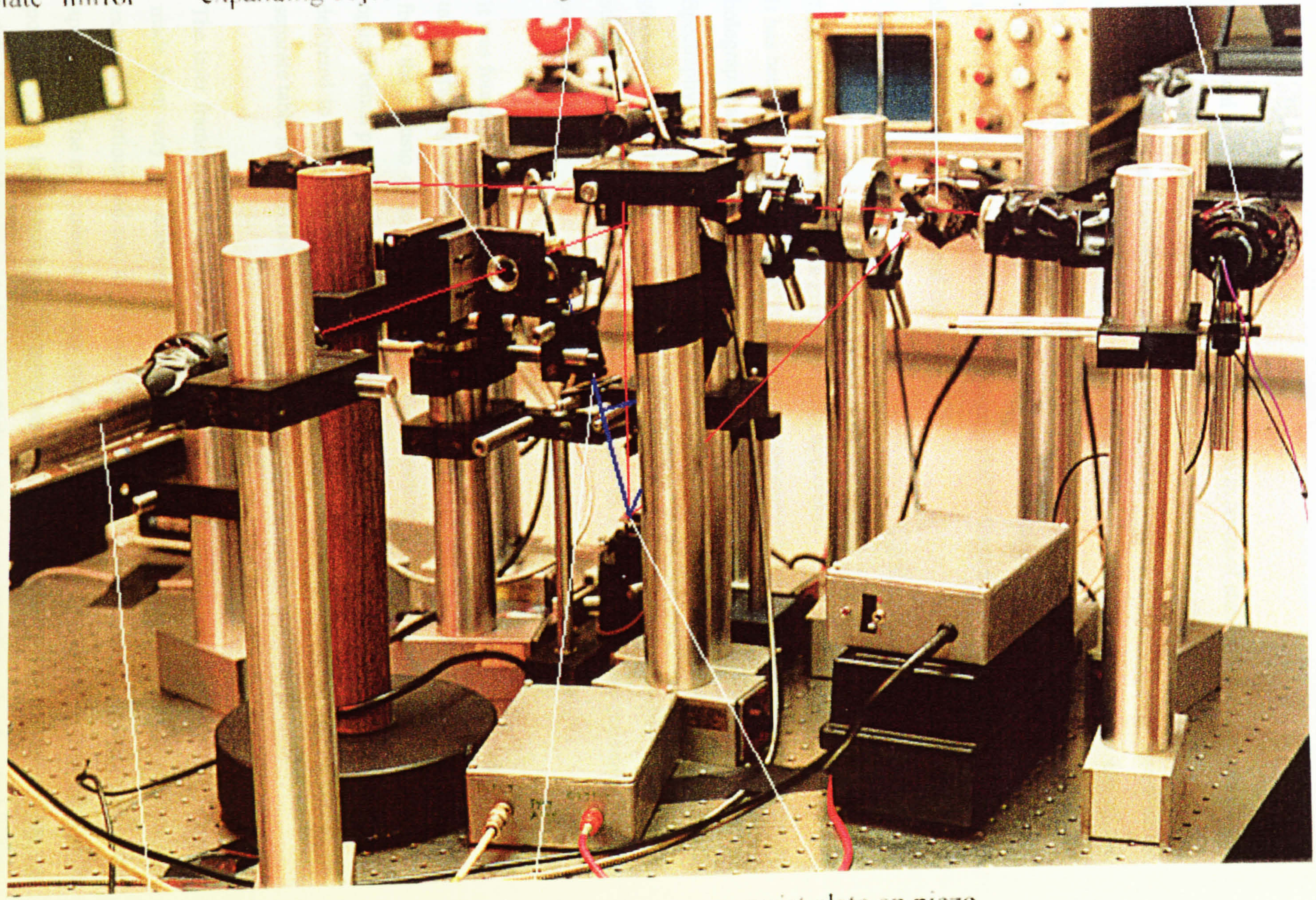

Plate 7.1: *Showing the vertical recording and interrogating beam apparatus used in these experiments.*

This vertical arrangement is generally advantageous in terms of stability: in holographic work it is considered good practice to mount the recording medium horizontally, so that gravity is "working for you and not against you". However it is stressed that in this case the geometry of the experimental design requires the various optics to be held close to the top of the mounting poles; this leads to rather poor rigidity in the set up as a whole. Fortunately the fringe locker can compensate for much of the instability caused by this feature of the rig, but it is emphasised that it is regarded as a necessary evil for these initial experimental trials in the absence of a specially designed rig.

7.1.1 Two beam holographic grating writing apparatus

It has been mentioned that there is no particular necessity that the exposure pattern be formed holographically, but that is the method which was chosen in this case. The laser used was a Spectraphysics 165 water-cooled argon ion laser with a temperature controlled etalon which gave around 60 mW at 457.9 nm for a tube current of 30 A. [This power is rather low for such a laser because the tube was nearing the end of its lifetime when these experiments were performed.]

It was found that the laser cooling water flow caused vibrations which were coupled into the table, seriously reducing the holographic fringe contrast and causing spurious trigger pulses from the acousto optic modulator. For this reason the laser was removed onto a second optical bench positioned on the floor directly underneath the main table and the laser light was delivered to the workpiece via an polarisation maintaining optical fibre. The laser on its separate table is shown in Plate 7.2 on the following page.

The laser frame itself was mounted on this lower table on legs which incorporated spheres made from very low elasticity rubber (known as "sad balls") to isolate the laser from any external vibrations and also to prevent vibrations from the laser reaching any other part of the apparatus. The main table itself was mounted above the laser table on four inner tubes each positioned on a large steel leg. The tubes were inflated sufficiently to lift the table off the top of the legs but with a pressure low enough that vibrations were efficiently absorbed and the table was well isolated.

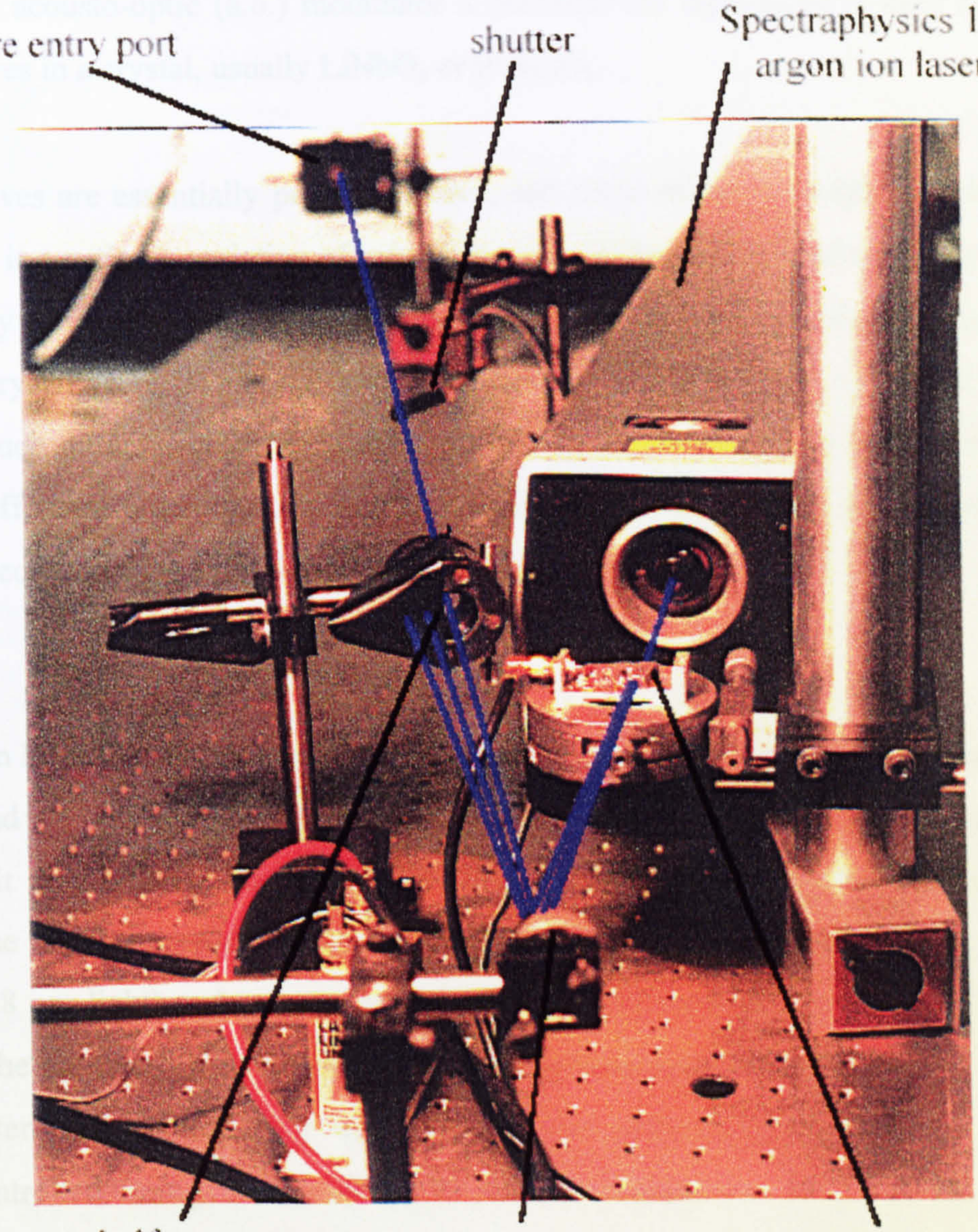

Plate 7.2: *A photograph showing the argon ion laser and a.o. modulator on the separate table.*

The key to this grating writing method is that very brief pulses are delivered at very precisely determined times. Mechanical shutters are far too slow and crude to give such precise exposure pulses, and so an acousto optic modulator was used as the method of deriving them. The acousto-optic effect describes the interaction of electromagnetic radiation with acoustic waves. In an acousto-optic (a.o.) modulator a piezoelectric transducer is used to generate ultrasonic waves in a crystal, usually $LiNbO_3$ or $PbMoO_4$.

Ultrasonic waves are essentially pressure waves, and since refractive index is a function of pressure there is a periodic variation of refractive index in the crystal leading to the formation of a temporary diffraction grating which will diffract any electromagnetic radiation passing through the crystal [7.1]. Thus the switching is under the electronic control of the piezo transducers: such modulators are capable of delivering sub-microsecond pulses of light into the several diffracted order beams. The a.o. modulator used in these experiments was an AA.MT-15 incorporating a $LiNbO_3$ crystal.

As is shown in Plate 7.2 and also in Fig. 7.1, the modulator was positioned at the output of the argon laser and the crystal aligned so as to maximise the efficiency of diffraction into the first order, since it is this beam that is used to expose the resist (~70% efficiency could be attained). The angular spread between the zeroth and first order beams is fairly small (~9 mrad with 458 nm light) and in order to prevent leakage of zeroth order light to the fibre a mirror folds the light across the length of the table and increases the separation of the beams. A relay shutter with timer facility was placed at the entrance to the fibre so as to give accurately controlled timings for the writing of the seed grating.

The first order diffracted blue light is brought to the resist plate via a polarisation maintaining optical fibre which was long enough to filter the beams reasonably effectively. This filtering is important because there was not sufficient physical space near the workpiece necessary for the more usual lens and pinhole filters to be implemented. The fibre used was a Point Source polarisation-maintaining delivery fibre: a half-wave plate was used before the fibre entry to align the argon laser beam polarisation with the acceptance polarisation of the fibre. It was

necessary to secure the fibre along its length since even small changes to its shape result in variations in tension which effect the birefringence and rotate the orientation of the output polarisation. Following the fibre exit a ×3 expanding telescope was used to magnify the size of the grating writing spot.

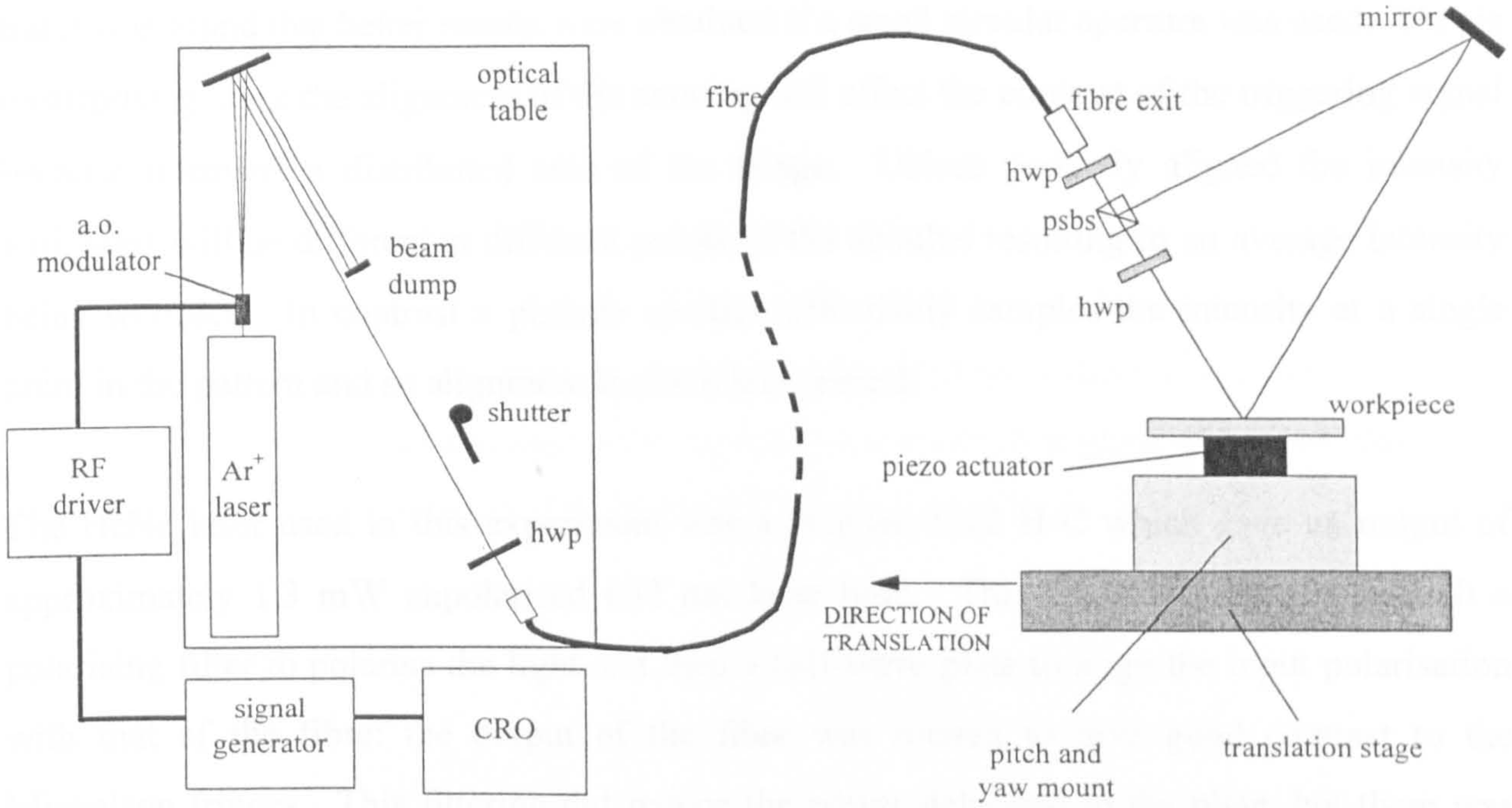

Fig. 7.1: *Schematic showing the apparatus used to write the seed gratings. [hwp: half-wave plate, psbs: polarisation sensitive beam splitter.]*

A standard method of obtaining beam power and polarisation balance was used: i.e. two half-wave plates in combination with a polarisation-sensitive beam splitter. The action of such a beamsplitter is such that the polarisation of the beam reflected from the cube is always parallel to the cut but that of the transmitted beam depends on the input polarisation. The respective power delivered to each beam is a function of input polarisation. Thus the first wave plate is used to balance the power between the reflected and transmitted beams from the beamsplitter and the second brings the polarisation of the transmitted beam back into line with that of the reflected beam. Hence the polarisations of both beams at the plate are parallel to the plate and perpendicular to the grating vector so as to give the optimum recording polarisation alignment.

7.1.2 Fringe locker apparatus

The details of the fringe locker have been described in chapter 6, and a sketch of the final design is given in Fig. 6.9. The implementation was fairly straightforward: the HeNe beam was vertically incident on the workpiece and the Michelson interferometer did not obstruct the argon beams. In the initial trials an annular aperture was used on the photomultiplier input, but it was found that better results were obtained if a small circular aperture was used. This is unsurprising since the alignment of the annulus will effect the contrast of the triggering signal because it covers a distributed area of the fringe. Unless perfectly aligned the intensity variations will be different at different points of the annulus resulting in an average intensity being recorded. In contrast a pinhole aperture effectively samples the intensity at a single point in the pattern and so alignment is much less critical.

The HeNe laser used in this experiment was a Hughes 3222 H-C which gave an output of approximately 1.3 mW unpolarised 632 nm laser light. This beam was passed through a polarising filter to polarise the light and then a half-wave plate to align the input polarisation with that of the fibre: the output of the fibre was rotated to give good contrast to the Michelson fringes. This filtering did reduce the power delivered to the plate, but there was not a requirement high HeNe intensity: the output from the fibre was typically 200 μW and this was plenty power for monitoring application. More important was the polarisation purity to yield high contrast fringes, and this was better than 0.1 %.

The signal from the photomultiplier output was monitored on a chart recorder so that the degree of transverse positional correction of the plate could be observed after the grating had been written and to check if there were any fringe jumps during the run. This chart recorder was also used to level the plate before the run. In these initial trials the small pieces of resist plate were mounted simply by sticking them to the piezo actuator base with double-sided sticky tape. This "Blue Peter" approach has yielded surprisingly good results in the past, but the reproducibility of positioning is not very good; consequently each plate must be levelled before each exposure run to reduce the demands on the fringe locker: this process is described in section 7.2.

The cutting of the quartz plates themselves was a process which required care: the resist surface was scratched even by contact with tissue paper. The procedure adopted was to raise the plate above the cutting board surface with shims and use a diamond scribe to score the quartz side of the plates. Care was taken to remove as much of the dust from the cut as possible before the actual breaking of the plate along a straightedge.

7.1.3 Exposure pulse triggering apparatus

The final part of the apparatus, sketched in Fig. 7.2 is that which measures the intensity of a point in the interference pattern formed between the diffracted beam and the locked reference beam from the fringe locker. A photograph of the apparatus is shown in Plate 7.3 on the following page. When the grating is moving this measurement leads to a sinusoidal signal and a trigger pulse is delivered each time the signal returns to its original phase (i.e. that phase measured before the movement of the grating).

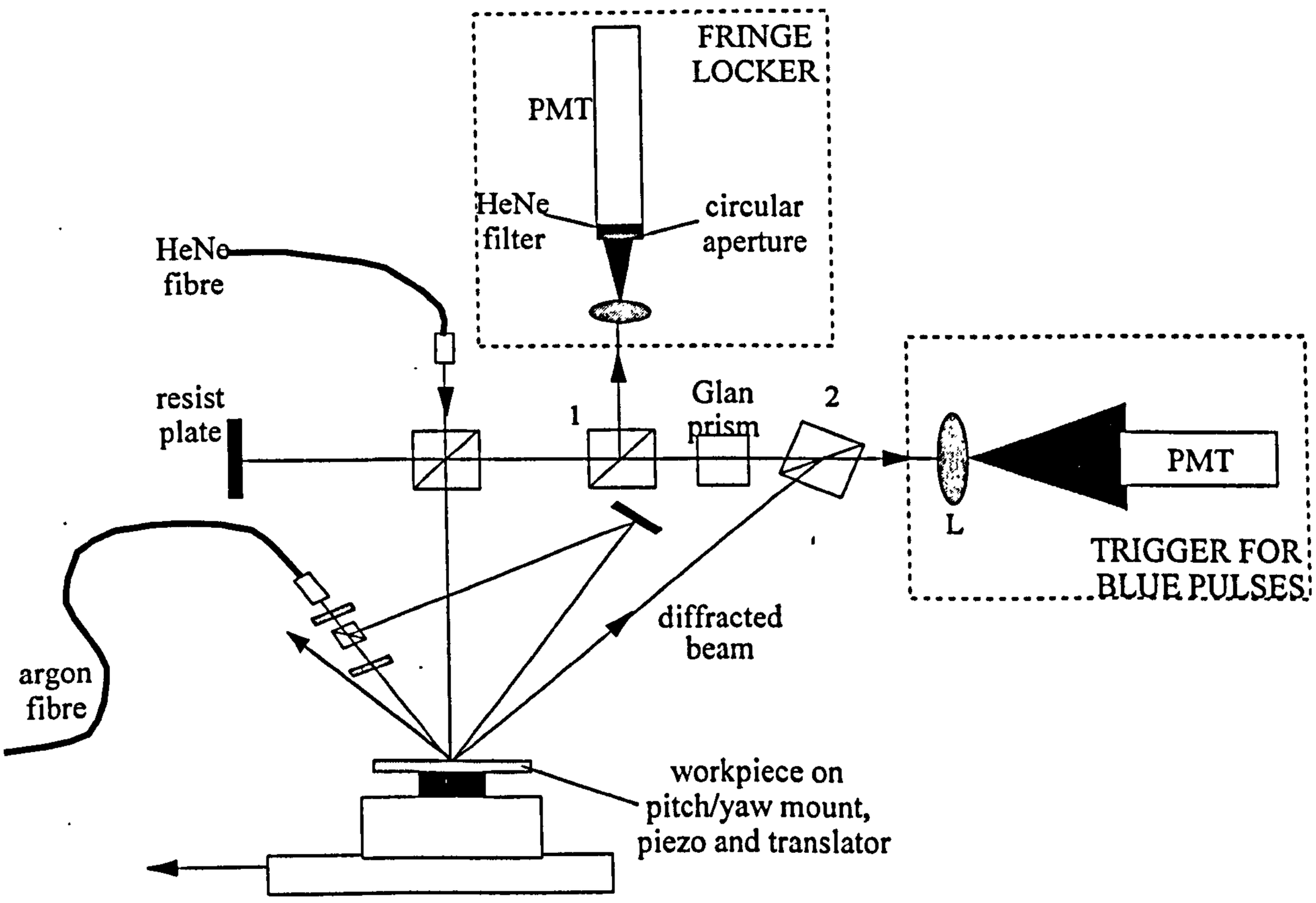

Fig. 7.2: *A diagram showing the apparatus for the monitoring of circular Michelson fringes between the locked reference and the beam diffracted from the latent image grating.*

The reference fringe from the fringe locker was several orders of magnitude more intense than the weak latent image beam and the Glan prism alone could not attenuate the locked beam sufficiently to give a 1:1 beam balance. Further attenuation was obtained by inserting a polarisation filter after the Glan prism; this gave very good intensity control on the locked beam. The polarisations of the two beams were brought back into line using a HeNe half-wave plate to adjust the polarisation of the diffracted beam. In this way good intensity and polarisation balance between the beams was obtained and high contrast fringes were observed at lens *L*.

The intensity of the central part of the central fringe of this pattern was measured using a second photomultiplier: in this case a Hamamatsu R928 side-entry broadband tube. An amplifier identical to that used in the fringe locker was made for this tube, except that the filter following the amplifier was a simple *RC* combination with a cut-off frequency of 500 kHz.

A yellow safelight was used when apparatus was being manipulated and these were extinguished during exposures in which the PMT was on. Precautions to reduce background light were taken such as using black screens where appropriate and covering unnecessary LEDs on equipment, but there was inevitable stray scattered light from the argon laser beams and from the monitoring CRO screens. The intensity of the diffracted beam was very low and so some precautions were necessary to distinguish the fringes from this background noise.

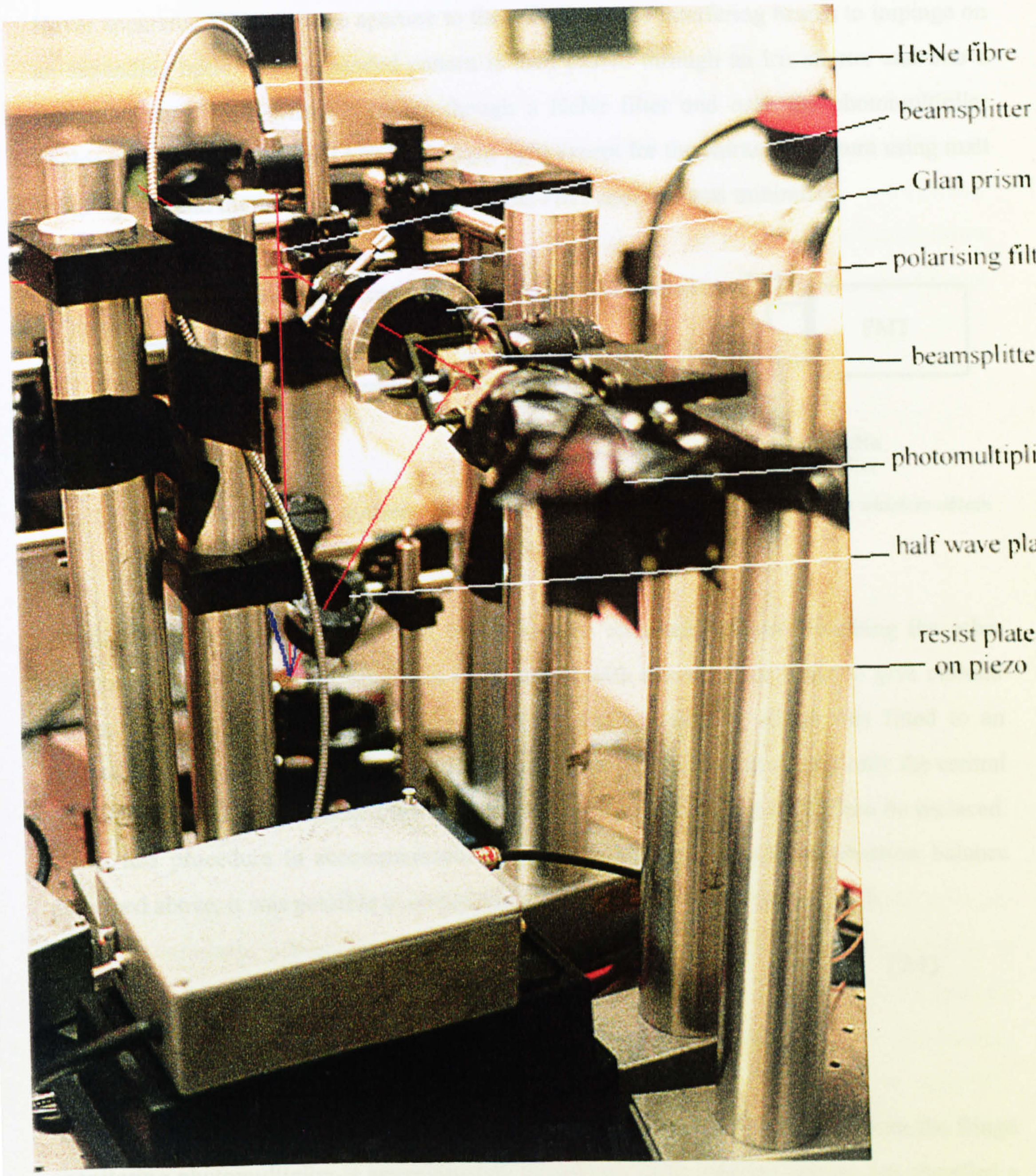

Plate 7.3: *Showing the optical rail for observation of the triggering fringes.*

In order to minimise the background light entering the tube, and so to increase the contrast of the triggering fringes, the optical rail illustrated in Fig. 7.3 was constructed using Spindler and Hoyer apparatus. The entrance aperture to the rail allows the interfering beams to impinge on an expanding optic. The expanded pattern is then passed through an iris shutter and into a further aperture from where it passes though a HeNe filter and onto the photomultiplier photocathode. The whole rail was made light tight except for the entrance aperture using matt black tape so that the solid angle subtended at the PMT aperture was minimised.

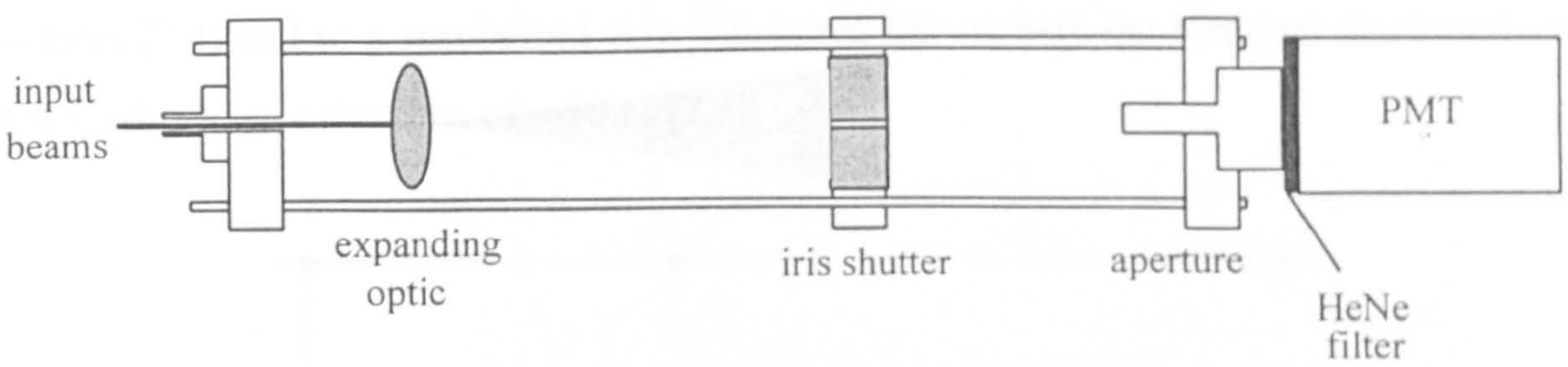

Fig. 7.3: *Showing the optical rail to observe the central region of the interference pattern from which to obtain the triggering signal.*

To align the apparatus the PMT and filter could be removed without disturbing the other components. The diffracted beam was then aligned with the reference beam to give circular fringes by adjusting beamsplitter *2* in Fig. 7.2. The iris shutter, which was fitted to an adjustable (x,y) mount was then closed to a small diameter and aligned so that only the central part of the central fringe reached the final aperture to the PMT, which could then be replaced. Using this procedure in accompaniment with the beam intensity and polarisation balance described above, it was possible to obtain fringe visibility, V, of >0.9 where [7.2]:

$$V = \frac{I_{\max} - I_{\min}}{I_{\max} + I_{\min}} \tag{7.1}$$

and where I_{max} and I_{min} are the highest and lowest intensities in the pattern.

The idea behind the triggering of the exposure pulses is as follows. The signal from the fringe monitoring photomultiplier is approximately sinusoidal: each time the grating has travelled a single pitch this wave passes through one period. When the signal returns to the same phase point an exposure pulse is delivered which reinforces the grating so building it up and extending it by one pitch. In an ideal situation it may be imagined that as the grating moves one pitch the efficiency of the illuminated grating will be decreased by a tiny fraction. If a

correctly calibrated pulse is delivered at the correct time then the grating will be reinforced back to its original intensity.

In order to give these trigger pulses the electronic device depicted in Fig. 7.4 was constructed. It is a fairly standard timing marker circuit such as that which may be found on the sweep voltage of a cathode ray oscilloscope [7.3]. The basis of the circuit is an op amp used as a comparator with a variable bias input to the non-inverting input. Conventional op-amps e.g. the industry standard 741 chip are limited in their rise times to ~ 20 μs by their relatively slow slew rates [7.4] and so a specialised chip was opted for: namely the National Semiconductor LM319, which has a rise time of ~ 80 ns [7.5].

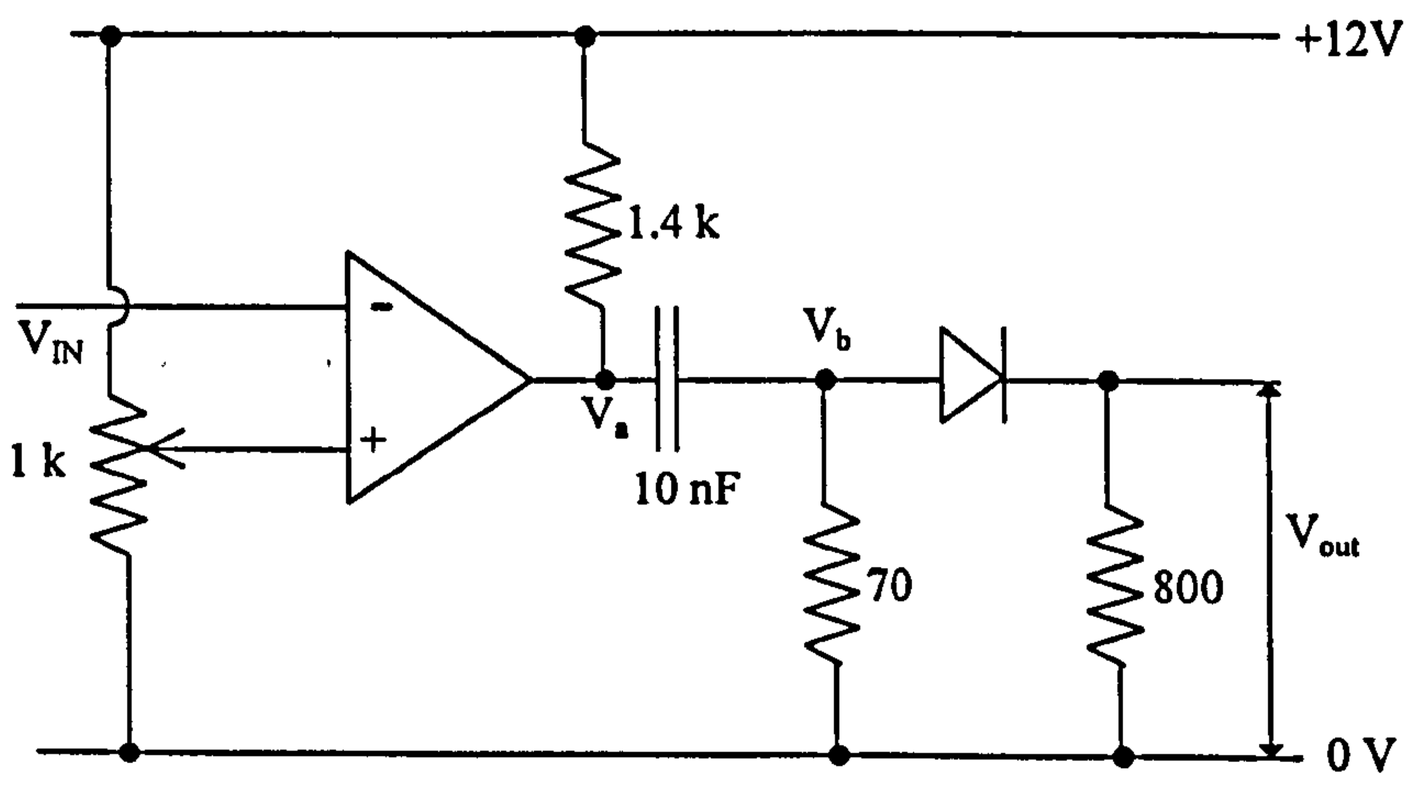

Fig. 7.4: *Circuit diagram of the trigger pulse generator.*

The circuit is fairly simple: the input voltage from the photomultiplier is compared with an adjustable reference. When the value exceeds the reference the comparator flips to give a high output, so that the near-sinusoidal PMT trace leads to a series of square edged pulses as shown in Fig. 7.5. The resistor and capacitor combination on the output of the comparator responds to these pulses, giving a series of positive and negative pulses with a decay time *RC*. Finally the diode filters out the negative pulses and leaves a train of positive spikes each triggered at a particular intensity level, which may be adjusted by changing the balance of the potentiometer at the inverting input to the comparator.

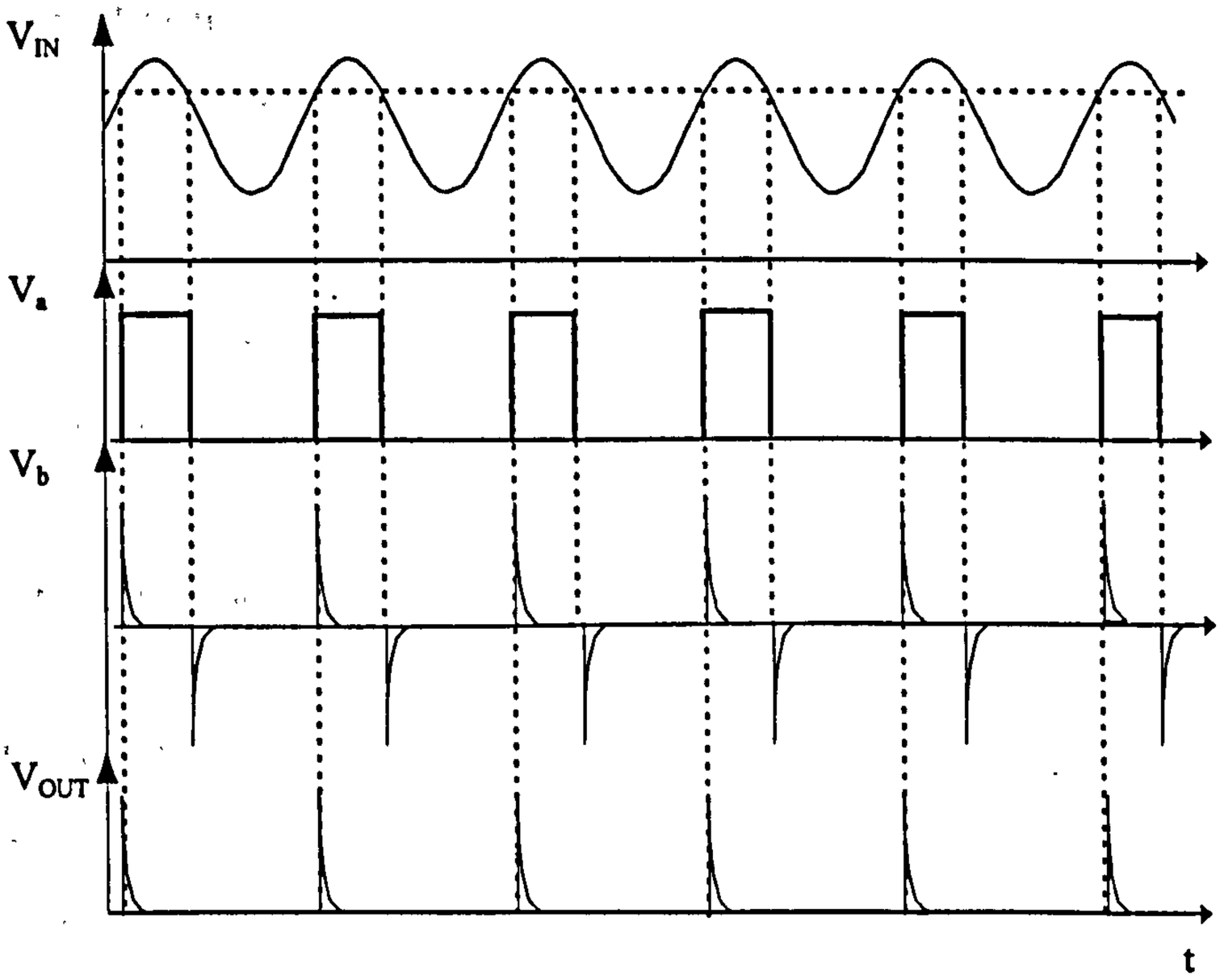

Fig. 7.5: *A sketch graph showing the voltage at each stage of the trigger generator.*

These spikes are fed into a Thurlby Thandor TG503 Pulse Generator which sends a calibrated pulse to the driver of the acousto-modulator, and hence a pulse of light of known period is delivered to the workpiece. Both the signal from the photomultiplier showing the intensity measured from the triggering pattern and the position of the triggered pulses from the signal generator are monitored on a Fluke PM3380M autoranging CRO as illustrated in Fig. 7.6.

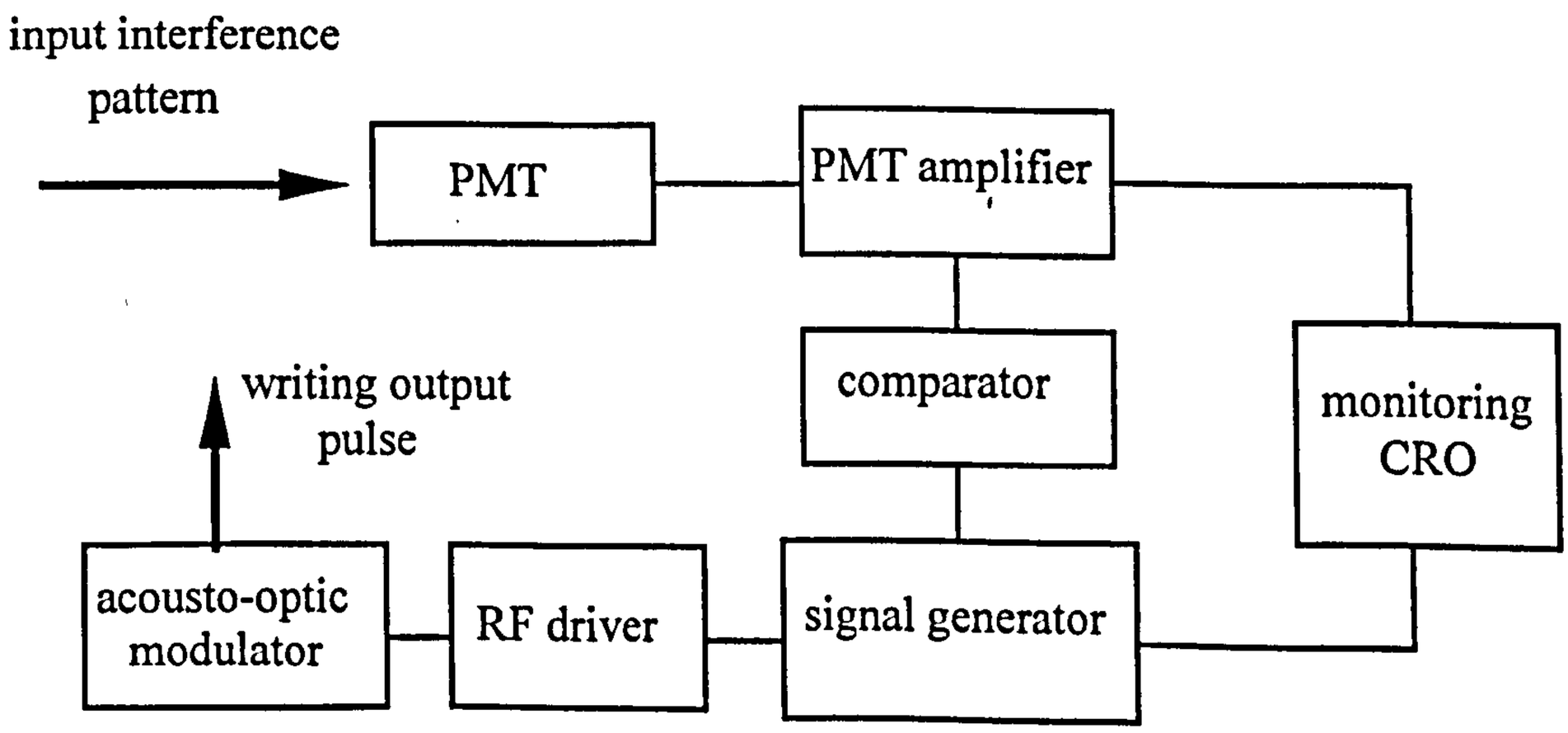

Fig. 7.6: *A block diagram of the triggering system.*

7.2 Experimental procedure

Naturally the piezo actuator has a very limited range of movement (approximately ±3μm) which puts constraints on the amount of transverse positional error that can be corrected by the fringe locker. The linearity of the micropositioner rail itself is subject to several microns error and so in order to put as small a demand on the fringe locker as possible it is necessary to level the plate with respect to the direction of movement of the micropositioner. This involves aligning the locus of the points on the resist plate illuminated by the laser so as to be parallel with the direction of translation of the micropositioner.

The method adopted for this operation was to mount the piezo actuator and resist plate onto an adjustable pitch and yaw stage: this combined assembly was itself mounted on the micropositioning device. The piezo actuator of the fringe locker was bolted onto the top of the pitch and yaw stage and the resist plate itself mounted onto the actuator stage using double sided sticky tape.

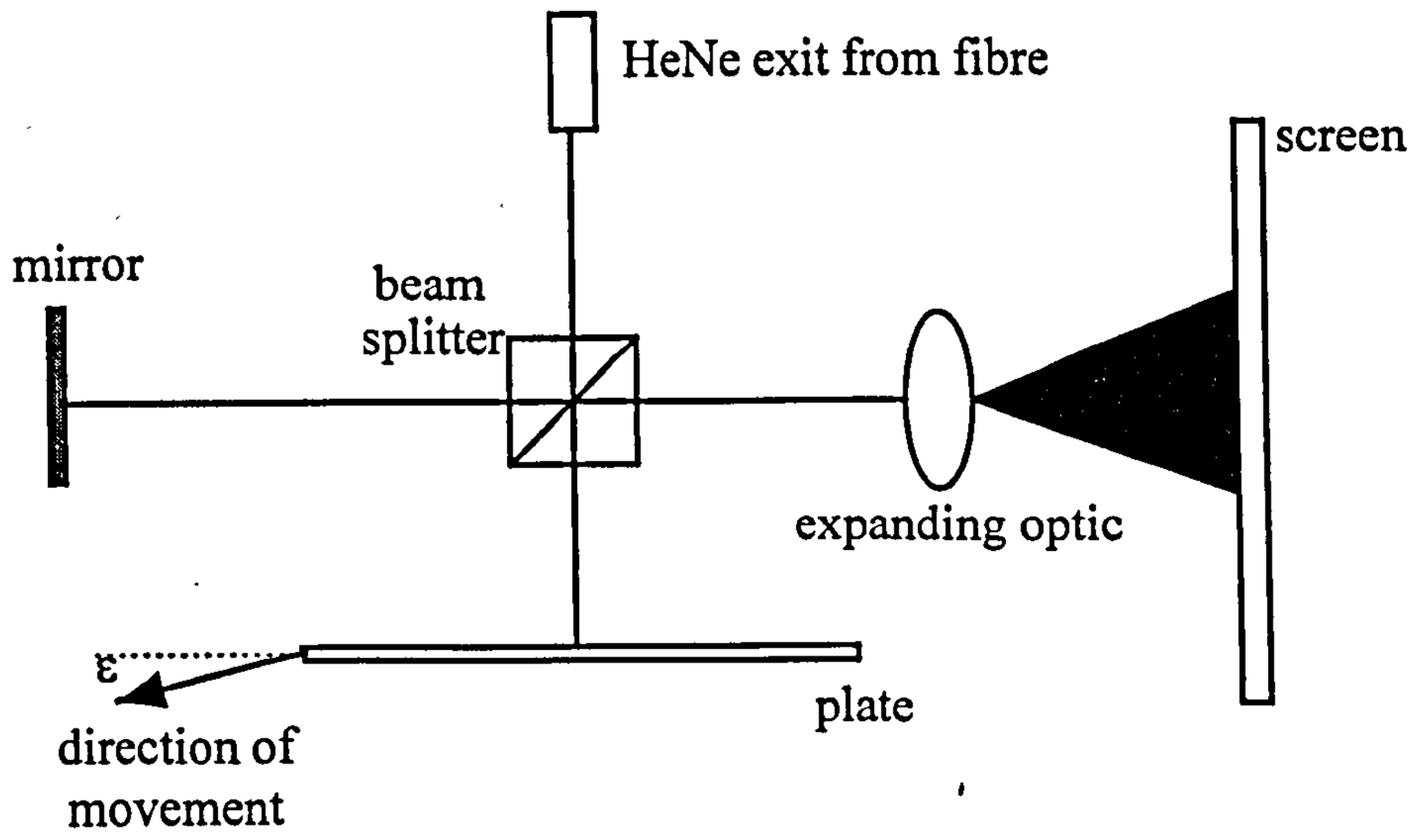

Fig. 7.7: *Showing the Michelson interferometer used for plate levelling. ε is the error angle to be minimised.*

The method adopted for the levelling of the plate utilises the Michelson interferometer of the fringe locker with the actuator switched off as shown in Fig. 7.7. The unlocked fringes are observed on a white screen placed at the PMT tube entrance aperture and the alignment of the resist plate "mirror" adjusted so as to give circular fringes on the screen. The alignment of this plate is then altered to give two or three hyperbolic fringes in order that the direction of movement of the fringes can be more easily observed. The movement of the micropositioner is commenced and the pattern observed on the screen: the fringes will move up or down the

screen due to transverse movement of the resist plate during its travel along the micropositioner bed. This transverse error consists of the combined effect of the deviations from linearity of the micropositioner screw with the transverse movement due to plate misalignment. The misalignment error is manifested by a general trend of the fringes to move up or down the screen and the micropositioner error by a random movement in the fringes which will average to zero over long movements.

The average number of fringes per millimetre travel can be deduced from these observations for a particular alignment of the plate. The mirror is adjusted to once more give circular Michelson fringes; then the alignment of the workpiece itself is adjusted up or down to give two hyperbolic fringes rather than one circular fringe on the screen. The circular fringes are restored by adjusting the mirror once more and the process is repeated. This procedure is continued so as to decrease the number of fringes per millimetre with each adjustment of the resist plate and the levelling is thus achieved by "walking in".

Using this procedure it was possible to obtain alignment within one or two fringes along the whole scan length (~2 cm) which could be compensated for by the fringe locker. A movement of the pattern by one fringe represents a transverse movement of the plate of $\lambda/2$: hence the angle of misalignment is approximately $\tan^{-1}\left(\frac{632\times10^{-9}}{0.02}\right)\sim10^{-3}\,°$. However, this value is the average value during the movement: it should be noted that due to the imperfections in the bed screw, there were movements of ±3 fringes (equivalent to approximately ± 1μm) during the travel.

Once the plate is levelled, the grating writing process begins with the writing of a small seed grating which is written before the plate movement begins. The PMT is removed from the end of the optical rail depicted in Fig. 7.3. Then the input to the pulse generator feeding the a.o. modulator is fed from a second pulse generator. The fringe locker and chart recorder are switched on so as to keep the plate level. The whole apparatus is left to settle; by monitoring the chart recorder output it can be seen when the system has stabilised. Once equilibrium is reached the plate is given a timed exposure from the automatic shutter on the first order beam from the a.o. modulator.

When the seed grating exposure is complete and the shutter closed the input to the a.o. modulator pulse generator is switched from the signal generator to the output of the PMT amplifier. By looking down the triggering optical rail and fine-tuning the position of the iris shutter, and the beamsplitter if necessary, the centre of the bullseye pattern is made incident on the PMT entrance aperture. Once alignment has been achieved the PMT is carefully put back in position, the safelights switched off, and the PMT tube voltage switched on. The signal from the PMT is observed on the CRO and the bias level on the triggering comparator is adjusted to this voltage.

Finally the movement of the resist plate is initiated, very slowly at first: less than a micron per second so that the initial phase of the pattern at the point of observation may be observed. This phase is carefully noted, then the speed of movement is increased and provided that the a.o. modulator is being triggered at the correct point in the cycle, the shutter may be opened, exposing the plate to the writing pulses.

In a crude set up such as was used in these initial experiments it is likely that during the run the contrast of the pattern observed at the PMT will vary. This is a result of several factors: for instance the efficiency of the freshly written grating may differ from that which has gone before; this will effect the intensity of the diffracted beam and hence the contrast of the interference pattern. Any errors in alignment of the optical system may result in a shift in the physical position of the fringes as the plate moves. Similarly any non-uniformities in the resist layer itself will result in variations in grating efficiency.

Such intensity and contrast variations are crucial since they will result in the intensity level of the correct trigger phase point varying during the run. Consequently it is necessary to monitor the PMT signal on the CRO. By manually varying the bias voltage on the comparator, and hence the triggering intensity level, it is possible to keep the trigger position at the same *phase point* throughout the run despite the variations in the signal intensity. When the run is complete the shutter is closed, and then the PMT and micropositioner movement may be stopped. The plate is then processed in the manner described in the Appendix.

For the writing of the initial seed grating the argon pulses were derived from a signal generator on which the pulse train was set to give a mark to space ratio of 1:10. The inter-beam angle was ~ 21.5°, designed to give a grating pitch of 1.2 μm and a first order diffraction angle of ~31° for 633 nm light at normal incidence. This particular pitch was chosen because with this set up only a narrow range of diffraction angles can be aligned without the diffracted beam being obscured by the apparatus. The average intensity at the plate was typically 700 μWcm^{-2} with this 1:10 ratio, giving an actual beam intensity of 7 $mWcm^{-2}$. The polarisation purity of the beams was approximately 1%.

The optimum exposure is awkward to calibrate precisely since the beam profile is Gaussian and the power varies across the beam; however the following analysis gives a rough guide to the exposure for a point in the centre of the grating. From (3.30) for a beam of total power P and $1/e$ radius a, the peak intensity is given by: $I_o = \frac{P}{\pi a^2}$

The characteristic exposure is taken to be at points a distance a from the centre of the beam, where the intensity is $e^{-1}I_o$. The exposure may thus be approximated by considering the beam patch to be a top hat intensity profile of this intensity and radius. Thus the effective beam width, L, is $2a$ and adding the total individual averaged exposure pulses gives a total mean exposure of approximately:

$$E = I_{average} \cdot t_{total}$$

$$E = \left(I_o e^{-1}\right)\left(\Gamma \frac{L}{\Lambda}\right) = \left(\frac{P}{\pi a^2} e^{-1}\right)\left(\Gamma \frac{2a}{\Lambda}\right)$$

$$\Rightarrow \qquad E \approx \frac{\Gamma P}{4a\Lambda} \tag{7.2}$$

where Λ is the grating pitch and Γ is the exposure pulse duration. Now the radius of the beam is approximately 1.5 mm and the total beam power measured at the plate for a 1:10 pulse train ~700μWcm^{-2}. Thus for a typical exposure (Γ~1.05 ms) the average fluence is given by:

$$E \sim \frac{1.05 \times 10^{-3}\,s \times 700.10 \mu Wcm^{-2}}{4 \times 0.15cm \times 1.2 \times 10^{-4}\,cm} \sim 100 mWcm^{-2}$$

For a blanket exposure using 458 nm light it has been found (see Appendix) that for the adopted development process a fluence of 220 $mJcm^{-2}$ gives a good result. Since the intensity at the peaks of the interference pattern will be twice the average for a perfect contrast pattern

(see (3.4)) this experimentally determined exposure is in reasonable agreement with this result.

7.3 Results and discussion

Using the method described in the previous section, gratings over 2 cm long, with a usable width of approximately 1 mm, were written; this length was the maximum distance the micropositioner could travel. Several problems which are associated with this traditional holographic grating exposure method when used with a chromoplate medium are highlighted by these gratings. Firstly the Gaussian intensity profile of the beam leads to a non-uniform transverse grating pattern and secondly the interference between the back reflection from the substrate and the incident wave causes standing waves to be set up in the resist as mentioned in section 5.2.6.

This well known effect is used to advantage in Lippmann photography, a technique originally discovered by Lippmann in 1891 using liquid mercury as a reflector of light with a low coherence length [7.6]. However, in this application, where the coherence length is much greater, these standing waves are a problem, leading to the Gaussian profile not being smoothly represented in the photoresist. Instead there are clearly a series of discrete layers in the resist: in cross-section these are observed as a set of steps, or an "aztec" profile, with each step corresponding to a node or anti-node in the standing wave pattern [7.7], [7.8].

Despite this aztec structure, with careful manipulation of the exposure parameters it was possible to obtain a properly exposed grating in the centre of the exposure area. Numerous experimental trials were performed and some of the developed gratings were examined under an electron microscope. Images from a typical grating are shown in plates 7.4, 7.5 and 7.6. Plate 7.4 shows a sample from the edge of a grating where the exposure is too small for the developer to break through to the chrome. It is clear that the grating has good uniform pitch across the sample, but that there are some ragged artefacts and significant noise in the image. Plate 7.5 shows a sample nearer to the centre of the same grating: here it can be seen that the grating is again of good uniformity but superimposed on the basic grating the noise is worse: essentially the development process has amplified the noise apparent in Plate 7.4.

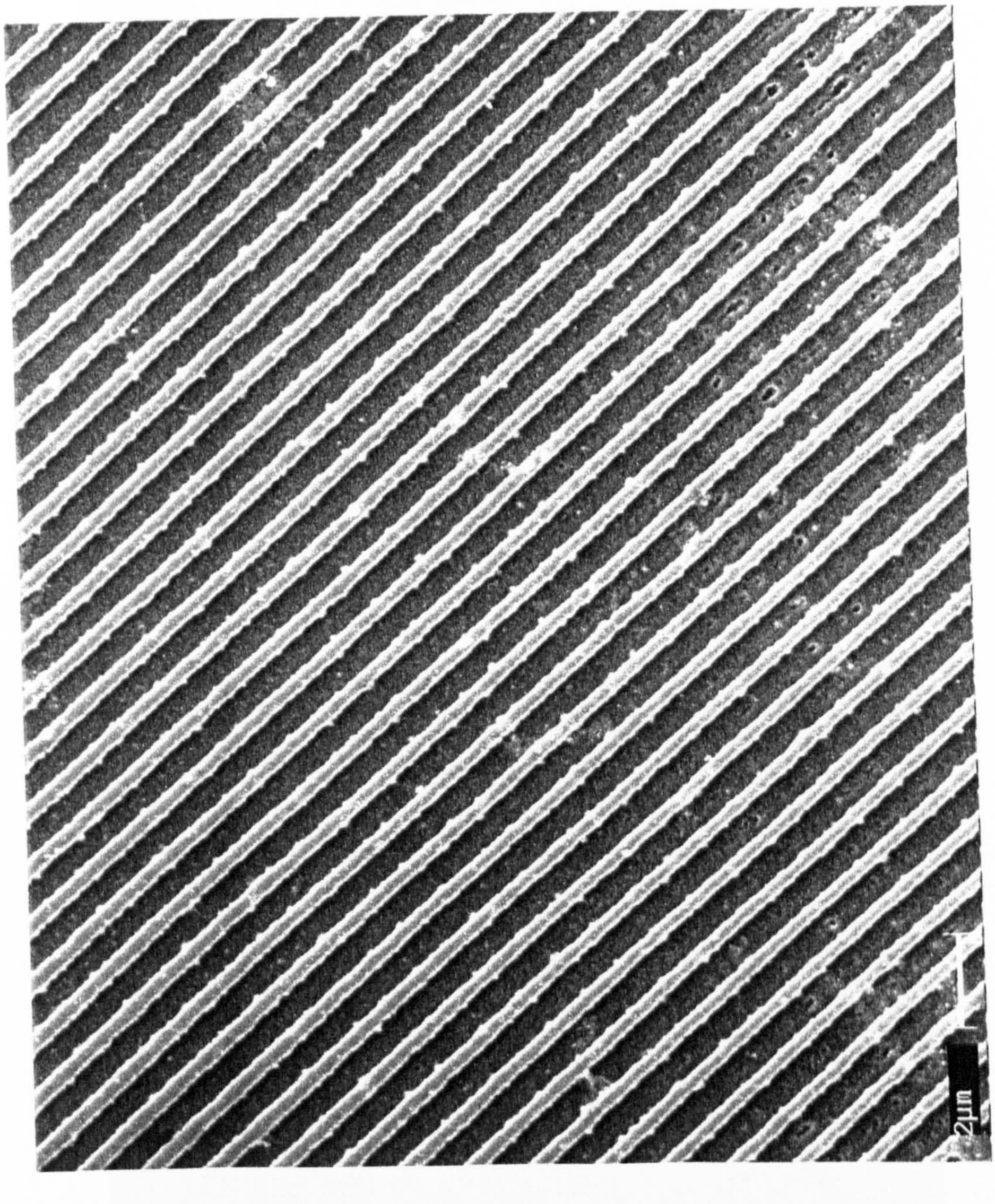

Plate 7.4: *Showing an electron micrograph of a typical section of grating made using the continuous scanning method. This section was from near the edge of the illuminated area and is somewhat underexposed. The pitch is ~1 μm, as can be seen from the scale in the bottom corner.*

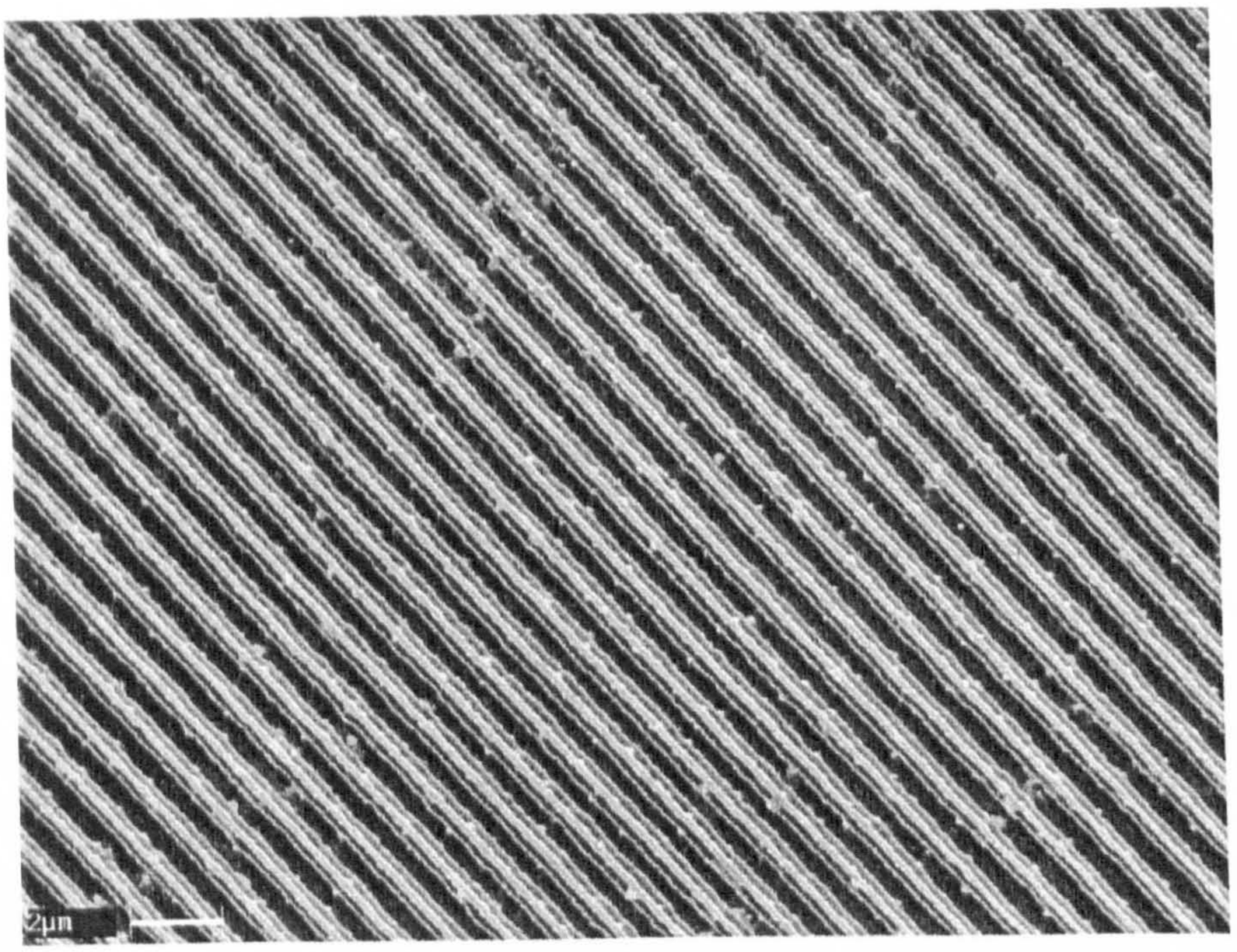

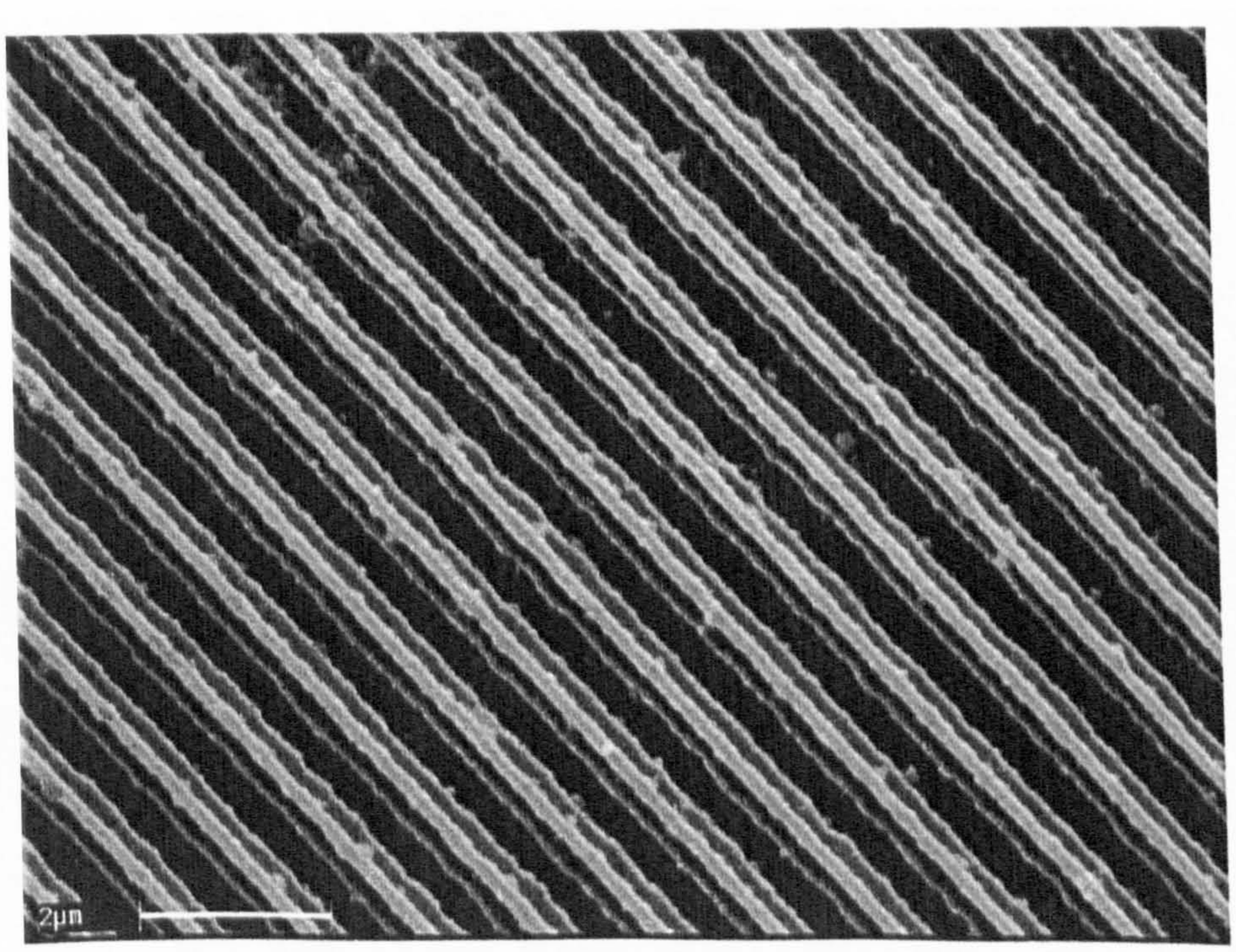

Plate 7.5: *Two electron micrographs showing a typical section of continuously written grating at two different magnifications. The aztec structure of the resist formed by the standing waves from the reflected light can clearly be seen.*

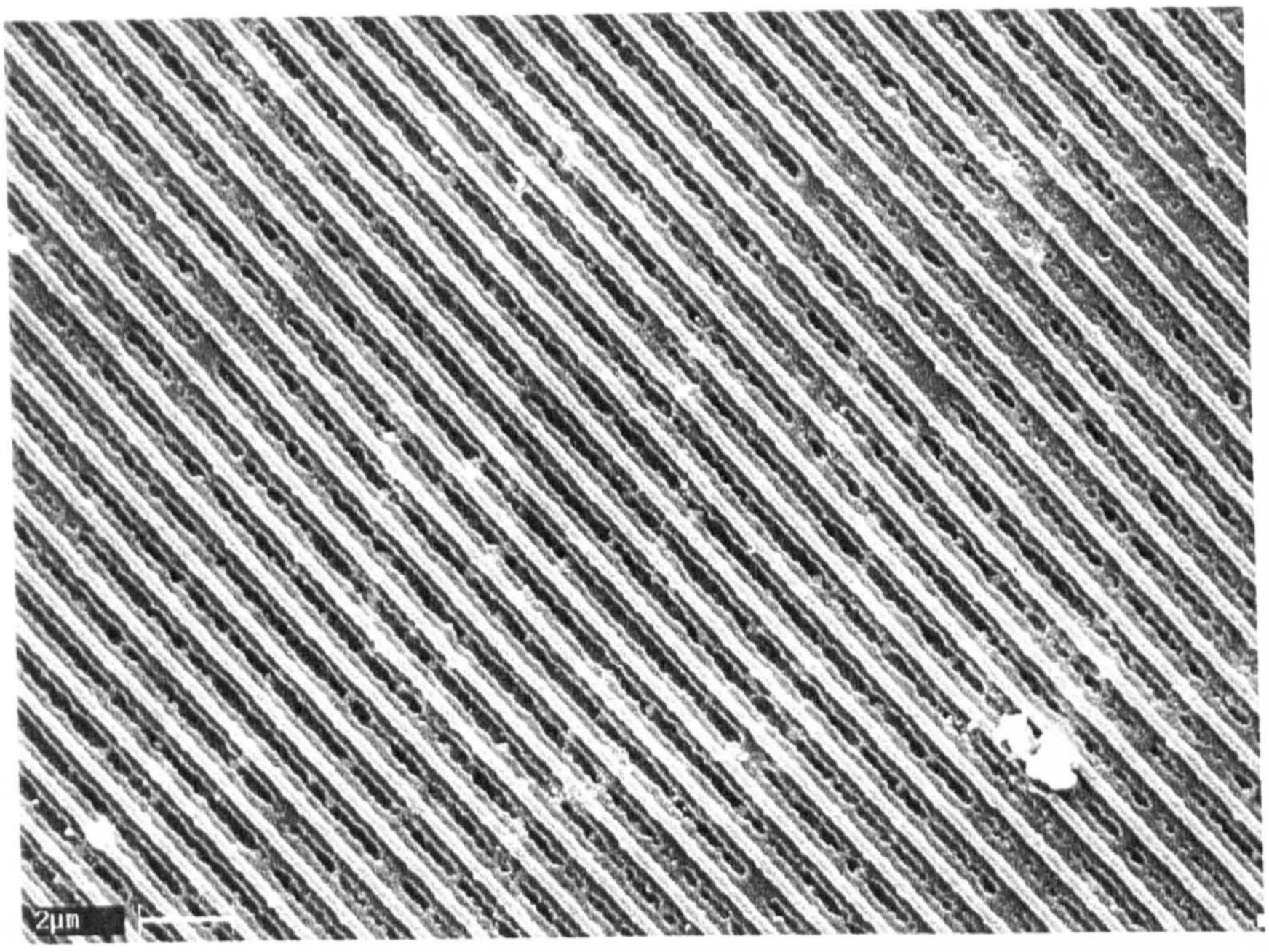

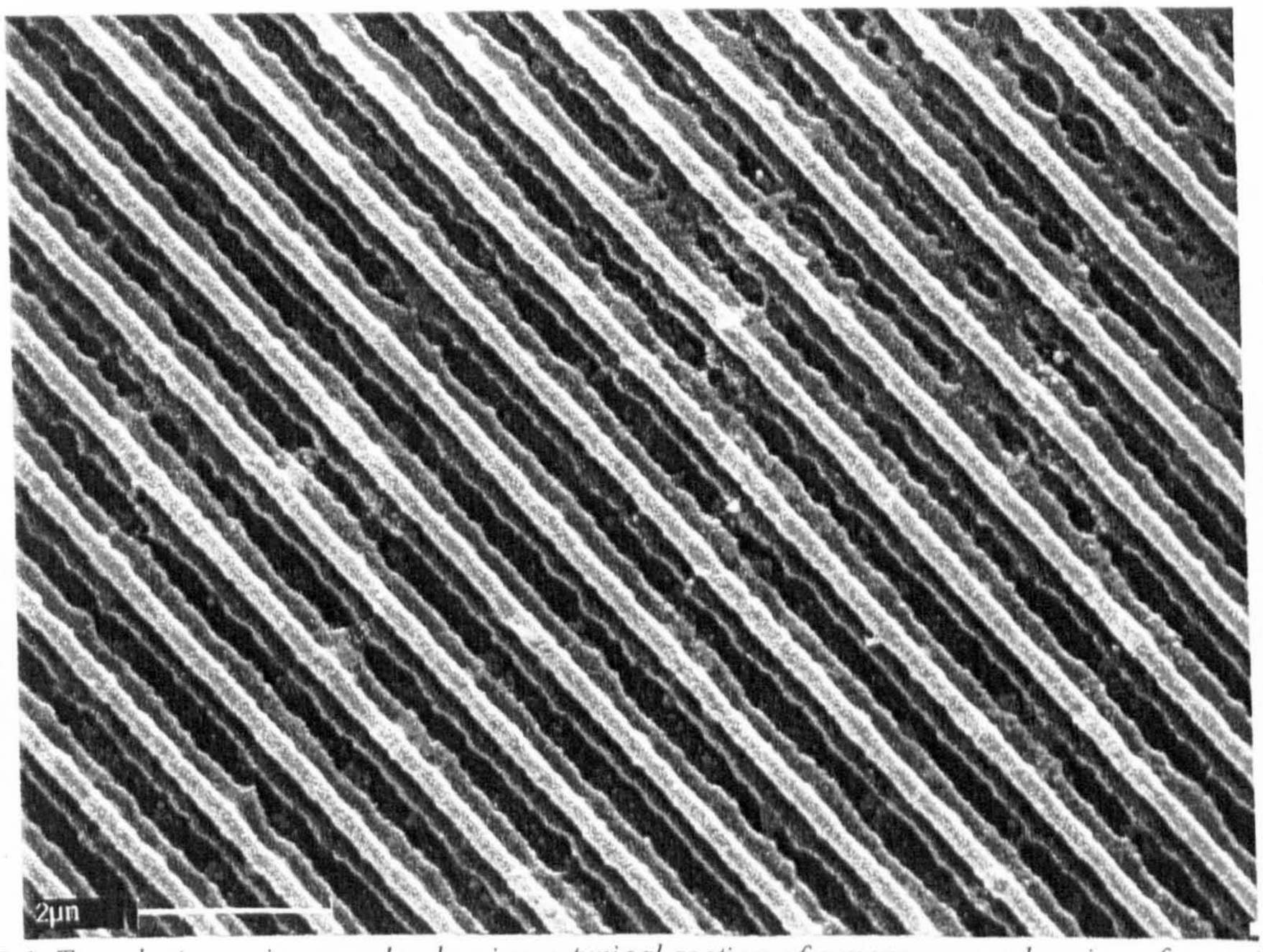

Plate 7.6: *Two electron micrographs showing a typical section of a more exposed region of a continuously written grating at two different magnifications.*

It is recognised that there are severe problems with the gratings shown in the previous electron micrographs. However, it was expected that there would be such difficulties for several reasons. One of the important rules of thumb in the holographic recording of gratings is that there should be no optics after the spatial filter so that the recording wavefronts are as near perfect as possible. Plate 7.7(a.) shows the intensity profile of the spatially filtered argon beam recorded on the table used in these experiments using a Exitech P256C Laser Beam Diagnostic System; the beautiful symmetry of the beam profile is clearly illustrated.

Plate 7.7(b.) shows an intensity profile of one of the beams used to record the gratings shown in Plates 7.4, 7.5 and 7.6. Comparing this image with the almost perfect uniformity of Plate 7.7 (a.) it is clear that the profile is terribly noisy.. This noise is attributed to several factors, one of the most important is that the filtering provided by the delivery fibre is not as effective as a good lens and pinhole filter arrangement. This is shown most clearly by the fact that there is a two dimensional diffraction pattern visible in the profile which is due to the action of the a.o. modulator crystal: the fibre is not capable of removing this pattern from the beam. Added to this serious aberration is the fact that the beams then need to pass through an expanding telescope, one or two half-wave plates (for the beam reflected or transmitted from the beamsplitter respectively) and a beamsplitter. The reflected beam is also incident on a mirror. Each of these optics will further degrade the beam profile and all these sources of noise combine to give the horrid beam profile illustrated in Plate 7.7(b.)

In addition to the aberrations to the grating caused by the poor beam uniformity, there is further noise added due to variations in the transverse position of the chromoplate during movement as a result of a rough screw thread on the micropositioner. This noise is largely removed by the fringe locker, but as was described in the previous chapter, large deviations of the actuator will affect the position of the plate. A better quality of micropositioner would lead to a far smoother run, less reliance on the fringe locker and a better grating result.

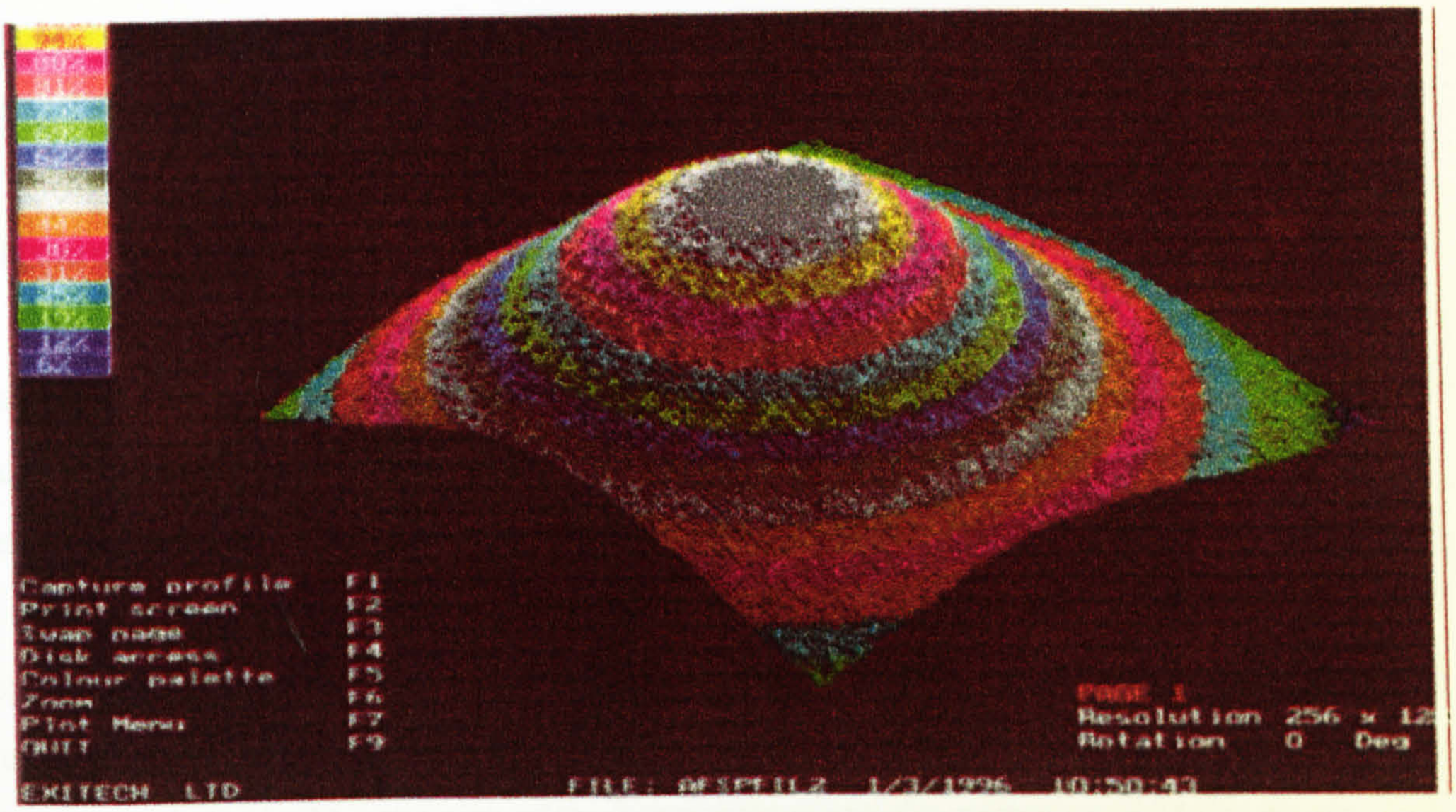

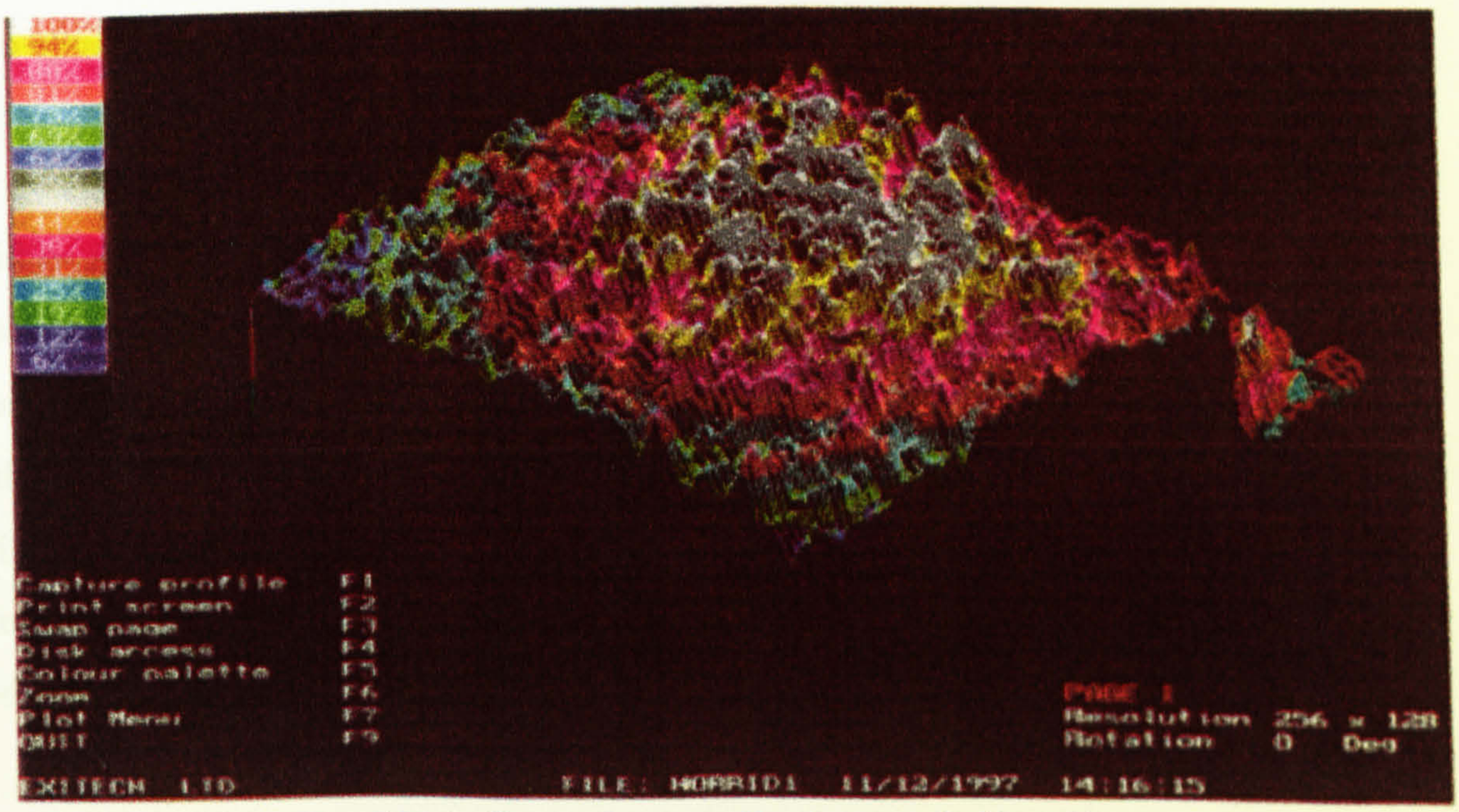

Plate 7.7(a.): *Shows a beam profile of a spatially filtered beam.*

Plate 7.7(b.): *Shows a beam profile of one of the beams used to write the gratings shown in Plates 7.4, 7.5, and 7.6.*

7.4 General conclusions and proposed future work

This thesis has been a study of several methods of writing long, in some cases unlimited, holographic diffraction gratings. This work was carried out with a view to writing in-fibre Bragg gratings which are of great current interest in the telecommunications industry, especially because of their use as dispersion compensators in long-haul routes and for wavelength-division (de-)multiplexing applications. A review of the use of fibre gratings is given in chapter 1 and chapter 2 discusses some of the ways that such gratings have been manufactured to date, together with some of the drawbacks of current techniques.

In chapter 3 it is described and shown mathematically that in certain geometries it is possible to scan two coherent laser beams across a holographic recording medium and record a single uninterrupted grating. This rather counter-intuitive phenomenon was used in this work to write continuous gratings of length over 2 cm (which was the limit of travel on the micropositioner) with a writing beams of diameter around 3 mm. The experimental procedure and results are described. Despite the elegance of this method, the length of a grating that may be written is limited by the size of the beamsplitter and the mirror used in the set up. For this reason this work was left at this development stage in favour of techniques which may be used to obtain gratings of unlimited length.

The technique which was favoured over this original scanning method involves superimposing many weak gratings with each sub-grating separated from the next by precisely one grating pitch. As the recording medium (in this case AZ-1350 photoresist) is scanned past the region of interference, the pulses are delivered from an acousto-optic modulator at times when the grating has been shifted an integral number of wavelengths from its original position. The signal from which the trigger pulses are derived are obtained by interfering the first order diffracted beam from the latent image of the photoresist with a fringe locked reference beam.

In order to more thoroughly understand the nature of the latent image and its development during the exposure, a model of its growth was formulated and the theoretical predictions were compared with experimental results. These results showed a good correlation and both the theoretical and experimental work is described in chapter 5.

In order to prevent the phase information from the interference pattern being lost amongst noise caused by imperfections in the micropositioner movement it was necessary to lock the vertical position of the workpiece using a fringe locker. The design of this piece of apparatus needed careful consideration and this successful work is discussed in chapter six.

In this seventh chapter it has been shown that the scanning technique using the interference pattern formed between the beam diffracted from the latent image in the photoresist and a stabilised reference has been successfully used to superpose many thousands of sequentially displaced identical weak diffraction gratings to form a single long grating. The experimental results from this process suffer serious cosmetic aberrations due to poor optics, spatial filtering and micropositioner imperfections.

Despite these considerations it has been shown here that a grating may be written with any length desired independent of the beam size. Although the gratings which are reported here are only 2 cm long, this limitation is imposed simply by the length of the micropositioning stage. There seems no fundamental limitation to the actual length or quality of grating which may be written. The successful results of this work have led the sponsors, Nortel, to fund further and more extensive work, which is briefly discussed below.

Here it is again stressed that these results have been obtained with a rather "hotchpotch" set of apparatus. It would seem to bode well for this technique that despite the low quality of the recording beams, the poor micropositioning device, the simplistic nature of the phase triggering during the exposure run and the poor stability of apparatus due to the lack of suitable mounts for vertical illumination, there is still a clearly recognisable single diffraction grating over the whole of the scan length. Thus it has been demonstrated that the optical feedback system operated here to trigger the fringes avoids the requirement of an ultra-precise interferometrically-controlled micropositioner (e.g. [2.71]).

Clearly if the technique is to be made into a commercially viable venture (e.g. for the writing of long diffraction gratings for use as phase masks in the manufacture of in-fibre Bragg gratings) then there is much that must be improved in the system. It is envisaged that an important first step is that a specialised solid, optically stable rig be constructed to hold all the

apparatus rigidly, rather than the separate individual poles which were used to hold the equipment for these trials.

The next important step is to dramatically improve the quality of the recording beams. This is to be achieved by designing the rig to allow sufficient space for traditional lens and pinhole filters to be used on both the transmitted and reflected beams after the 458 nm beamsplitter. It was described in section 3.1 that the spherical wavefronts from such filters will lead to holographic gratings which are linear to first order. However, in precision gratings such as those required for in-fibre gratings pitch uniformity to first order is not sufficiently precise and it is envisaged that collimating objectives will need to be used after the spatial filters.

This is a non-ideal situation, since any lens imperfections will be present in the grating recording, but if high quality optics are used then the aberrations will be less than the variation in grating pitch which would result from using spherical recording beams direct from the pinhole. A further refinement would be to improve the triggering system by incorporating a phase shifting element (e.g. a Babinet compensator or electrically-controlled waveplate) into the diffracted beam before it is brought to interference with the reference beam. By this method, the phase of the pattern observed by the PMT could be varied so as to give a phase of zero for each grating run. In addition the contrast of the triggering fringes themselves would greatly benefit from the use of a single frequency intensity-stabilised HeNe laser.

At this stage in the work it was concluded that the basic concept behind the technique is very sound, and that the method may be extended to longer gratings without any fundamental problems. Furthermore it is assumed that with a redesigned experimental rig and some investment in new optics, accompanied by several other improvements to the apparatus including a new micropositioner, long gratings of a high quality will be achievable. Such a project has already been undertaken, sponsored by Nortel, and the results will be made public in due course.

Moreover this technique is flexible with regard to the recording medium and it is proposed to adapt it to write directly into fibre. Other refinements include the expectation that it will be

possible to write chirped gratings by adjusting the inter-beam angle during scanning and hence alter the pitch gradually along the length of the grating.

REFERENCES

7.1 J. Wilson and J.F.B. Hawkes: "Optoelectronics: an introduction"; 2nd edition Prentice Hall (1989).

7.2 E. Hecht: "Optics"; 2nd edition, Addison Wesley (1987).

7.3 J. Millman and A. Grabel: "Microelectronics"; 2nd edition, McGraw-Hill (1988).

7.4 M.H. Jones: "A practical introduction to electronic circuits"; Cambridge University Press (1977).

7.5 "National operational amplifiers": National Semiconductor publication (1995).

7.6 G. Lippmann: The Photographic News, pg. 119, 13th February 1891.

7.7 L.F. Johnson, G.W. Kamlott and K.A. Ingersoll: "Generation of periodic surface corrugations"; Appl. Opt. **17**, 1165 (1978).

7.8 N.J. Phillips, H. Heyworth and T. Hare: "On Lippmann's photography"; J. Photog. Sci. **32**, 158 (1984).

Appendix

RESIST DEVELOPMENT PROCESS

The recording media used was 0.5μm AZ1350 photoresist on both Towne ferroxoplate and Hoya chromoplates (100 nm iron oxide and 100 nm chromium substrates respectively). The argon laser is not an ideal source for this medium since it is right on the edge of the resist sensitivity curve, so exposure times can be rather long, but good gratings may be written with care.

The resist manufacturer's recommended exposure process is designed for a broadband mercury source, central wavelength ~ 436 nm and not for the 457.9 nm laser radiation that was actually to be used. For a mercury source the recommended exposure is 65 mJ cm^{-2}. The development process recommended is a 70 s unagitated development in Microposit 351 Developer diluted 1:1 with de-ionised water, followed by a rinse for one minute in running water. The chrome etch is a standard formula (160 g ammonium ceric nitrate and 100 ml perchloric acid is dissolved in 1.0 l purified water and then this mixture is further diluted 1:4 in purified water) and the recommended etch time is 50 s with no agitation with a further 10 s to fully clear out all the lines if required. The plate should then be rinsed again for one minute in clean water.

This exposure and development process was adopted initially, but it was found that the window of development was very narrow: the time between a plate being underdeveloped and overdeveloped was only three or four seconds. It was also found that for such fine features the "wet etch" was not very selective and did not give good results. It was deemed necessary to adjust the method to suit the fine feature size and long exposure wavelength being used.

A number of plates were masked and blanket exposed to the blue argon light with fluences varying from 165 to 365 mJ cm^{-2}, and developed using a variety of developer concentrations. The development process eventually chosen was to immerse the plate in 1:2.5 Microposit 351 dilution for 60 s without agitation at 24.0°C (It is known that the resist development process is very sensitive to temperature, and this elevated temperature was recommended by a colleague). The plate was then washed in purified water for 60 s and then blow-dried with a mild jet of cool air.

The profile of the step on the plates was measured using a surface profilometer at Loughborough University of Technology's Manufacturing Engineering Department. The graph in Fig. A.1 shows the results obtained. The precision of the profilometer does not warrant the absolute values to be used however the general trend is clear: an exposure of >300 mJ cm^{-2} will be enough to activate this resist when this specified development process is used.

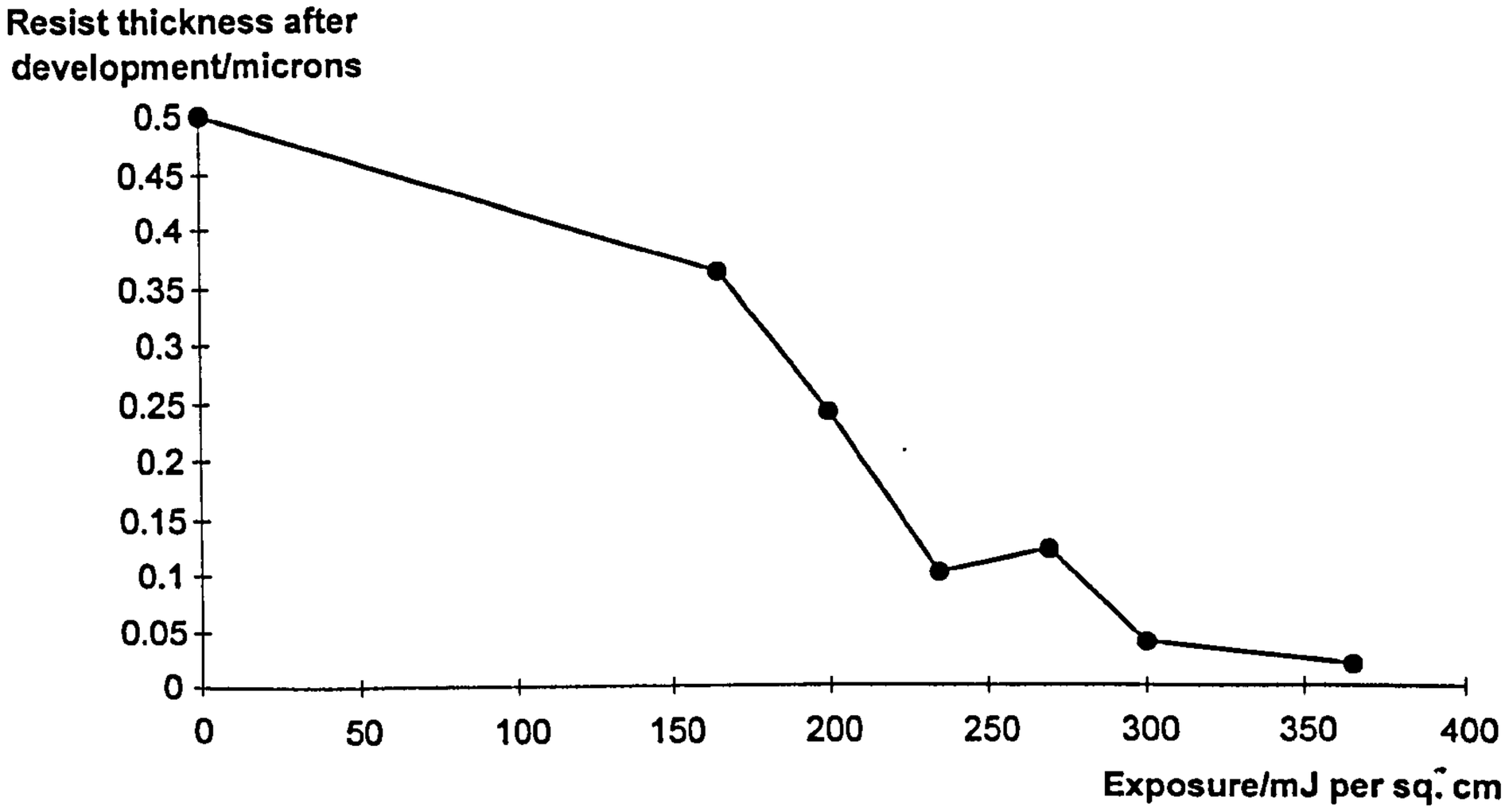

Fig. A.1: *A graph showing the etch depth against exposure for the given development process on a half micron AZ1350 Hoya chromoplate.*